Electrical and Optical Properties of Pure and Metal-Doped Single Crystals of Arsenic Triselenide

BY

A. M. AL-SAIE

A thesis submitted for the degree of Doctor of Philosophy at the University of Edinburgh.

June 1985

ABSTRACT

Pure, copper and gallium doped As_2Se_3 single crystals were grown by the open tube technique with N_2 as the carrier gas. The electrical and optical properties of the pure and doped As_2Se_3 crystal were examined and compared, between themselves and with their amorphous counterparts. It was found that in contrast to the situation in the amorphous state impurities (copper and gallium) have little effect on the electrical and optical properties of crystalline As_2Se_3. From the d.c. conductivity measurements the activation of all the samples (pure and doped) was found to be ~ 0.9 eV. An energy gap of 1.83 eV at room temperature and 2.03 eV at 0 °K was determined from optical absorption measurements and the temperature dependence of the energy gap, γ, is of the order of $8X10^{-4}$ $eV.K^{-1}$. Photoacoustic spectroscopy was also used to determine the optical gap of the As_2Se_3 crystal and these measurement were extended into the near-infrared region. From the data obtained in the near-infrared region it was possible to locate, indirectly, four energy levels in the forbidden gap of As_2Se_3 crystals, i.e. at 1.23, 0.9, 0.6 and 0.23 eV, measured from the top of the valence band. The energy level at 1.23 eV was further confirmed by thermally stimulated current measurements. Thermopower measurements indicate electron conduction but the activation energy is much lower than that calculated from the d.c. conductivity experiment. The difference in the activation energy was explained in terms of the mobility ratio of electrons and holes. Finally, by interpreting the present experimental results together

with some results from other workers, a general diagram is proposed for the structure of energy levels in the forbidden gap of crystalline As_2Se_3 which is consistent with some theoretical predictions.

ACKNOWLEDGEMENTS

I am most grateful to my supervisor Prof. A.E. Owen, for his advice and guidance during the course of this work. I would also like to thank Dr. P.J.S. Ewen for reading the manuscript.

I am indebted to Mr. C. Hampton for his help in the initial period of this project, Mr S. MacKinnon for his help in instrumentation , Mr J. Goodall for providing facility for the Scanning Electron Microscope, Miss R.E. Belford for preparing the samples , Miss S. Allan for performing the Atomic Absorption Spectroscopy and Miss J. Thompson for typing this thesis. I would also like to express my thanks to all the staff of the Department of Electrical Engineering for their help and assistance during my study.

Special thanks are also due to Mr. W.K. Choi for his help and encouragement in the process of writing this thesis. I would also like to express my gratitude to my colleagues in the amorphous group for their help.

Finally, I would like to express my sincere thanks to my wife and children for the inconveniences they endured during my Ph.D study, and my mother and my family for their moral support.

CONTENTS

1. CHAPTER 1 INTRODUCTION

Since the first demonstration of switching and memory devices based on amorphous semiconductors, the idea of using amorphous rather than carefully prepared crystalline materials in electronic devices was appealing but the lack of an adequate theoretical understanding hindered progress.

The major characteristic of a crystal is that its atoms or molecules form a pattern where they are aligned in three dimensional arrays that exhibit a long-range periodicity. As a result of this long-range periodicity, mathematical simplifications can be made in the quantum theory and hence it was possible to explain most of the physical phenomena in crystalline solids. This provided much of the impetus for the remarkable progress made in solid state electronics over the past 40-50 years.

The importance of long-range order in explaining the electrical and optical properties of solids was first challenged when Kolomiets and his co-workers [1] discovered that chalcogenide glasses (that is glasses containing a large percentage of one or more of the chalcogen elements sulfur, selenium and tellurium) can be semiconductors. This contradicts the previous notion that semiconductors can only be found in materials that exhibit long-range order. Ioffe and Regal [2] suggested that the electronic and optical properties of these semiconducting chalcogenide glasses originated from short-range order.

In chalcogenide glasses it has been found that an important key to understanding their properties in the solid state is not their periodic structure, or lack of it, but the chemical nature of their constituent atoms. Perhaps the most important concept to emerge is that electronic properties are controlled by well defined active centres (defect states). This idea was first implemented by Mott, Davis and Street (MDS) [3] and Kastner, Adler and Fritzsche (KAF) [4] who introduced simple theoretical models to explain the absence of ESR signals in chalcogenide glasses and the pinning of the Fermi level. The stimulus for the MDS and KAF models was a theoretical paper by Anderson which introduced the notion of a negative Hubbard correlation energy which could stabilise the defects. It is notable however that none of the theoretical models for defect states in chalcogenide glasses depend upon the presence of a disordered structure and the same defects should therefore occur in the corresponding crystalline elements or compounds, albeit perhaps in lower concentration [5]. The same point has also been made by Fritzsche [6] who wrote that

"Curiously, our understanding of these glasses will help us understand the corresponding crystals because the defect chemistry of these so-called lone pair materials remains essentially the same whether long-range order exists or not."

Pfister and Morgan have examined the effect of metallic impurities on amorphous As_2Se_3 [7]. They proposed a model to explain the different mechanisms introduced into the amorphous As_2Se_3 with the incorporation of different types of metallic impurities. The purpose of the present work is to study the electrical and optical properties of

pure As_2Se_3 single crystals and to examine the effect on them of copper and gallium impurities. The results for metallic dopants in As_2Se_3 single crystals are compared with those obtained by Pfister and Morgan in amorphous As_2Se_3.

In Chapter 2 the band theory of crystalline and amorphous solids is discussed together with the suggested band models for amorphous solids. The notion of defect states and the effects of metallic impurities in chalcogenides is also considered in this chapter, with particular reference to the results of Pfister and Morgan. A brief outline of the theoretical basis of the electrical and optical measurements is presented in Chapter 3. Chapter 4 illustrates various crystal growth techniques with emphasis being placed on the crystal growth method used in the present work, namely the open tube technique. The experimental set-up and the procedures for the electrical and optical measurements are described in Chapter 5. The experimental results, both electrical and optical are discussed in Chapter 6. Finally, the conclusions from Chapter 6 are considered more fully in Chapter 7 and suggestions for future work are also made.

CHAPTER 2 : ENERGY BAND THEORY OF SOLIDS

2.1.1 Energy Band Structure of Crystalline Solids

It was not until quantum theory was applied to the motion of the electrons in crystalline solids that a satisfactory theory of semiconductors emerged. In 1931 Wilson [1] first used quantum theory to provide a theoretical explanation of the difference between a metal and a semiconductor.

Following Sommerfeld [2], electrons were first assumed to move in a field-free space, the fields of force due to the atomic cores and other electrons being smoothed out except at the boundary of the solid but this gave no explanation of the vast differences between the properties of metals, semiconductors and insulators. The next step was to replace the smooth potential used by Sommerfeld with a periodic potential. The particular feature of the periodic potential is that it has the same periodicity as that of the lattice. The motion of the electrons in such a potential was considered by F. Bloch [3].

By applying quantum mechanics to crystalline solids in that way it was possible to solve the Schrodinger wave equation for long-range periodicity and two important consequences emerged: (i) there are definite energies, called band edges, at which the density of electronic states sharply decreases to zero, (ii) all the electronic wave functions in the allowed bands extend throughout the material. The uppermost empty band is known as the conduction band, while the full band below it is called the valence band. Figure (2.1) is a simple representation of

this model.

In thermal equilibrium the electrons in a solid are distributed among the allowed states (either extended or localised) according to Fermi-Dirac statistics. States in the solid are occupied according to the Pauli exclusion principle, which allows each quantum state to accept only one electron with single spin and two electrons with opposite spin. For a given state of energy E the occupation probability F (E) is defined by the Fermi-Dirac equation:

$$F(E) = \frac{1}{1+\exp[(E-E_f)/kT]} \qquad (2.1)$$

where E_f is the equilibrium Fermi energy or level (at which, when the energy E is equal to the Fermi level, the Fermi-Dirac distribution function F(E) is one half), k is Boltzmann's constant, and T is the absolute temperature.

The equilibrium distribution of electrons in the quantum states depends on the location of the Fermi level. Its position is determined by the distribution of the quantum states, the total number of electrons available and the absolute temperature of the system. The distribution of electrons in the allowed energy states n(E) is given by

$$n(E) = N(E)\ F(E) \qquad (2.2)$$

where N(E) is the number of states available in the energy range E to E+dE. The valence and conduction bands have a definite structure with an abrupt transition at the band edges, giving a well defined forbidden gap. For an intrinsic semiconductor the Fermi level is positioned

midway between the valence and conduction bands close to the centre of the forbidden gap as illustrated in Figure (2.1). At absolute zero all states below E_f are occupied, and all above are empty.

2.1.2 Band Structure of Amorphous Solids

The band theory of crystalline solids is based completely on the assumption of perfect or near-perfect long range periodicity. In amorphous solids long range periodicity is lacking. Only short range order is preserved but it is known from the experimental evidence that amorphous materials exhibit a similar range of electrical and optical properties as crystalline solids. This has led to a critical examination of the importance of long range order in band theory. It is important to note that despite the absence of long range order an amorphous solid almost always has a short range configuration which is the same as that of the corresponding crystalline solid. An important example is shown in Figure (2.2), which compares the radial distribution functions of amorphous and crystalline silicon, as determined by Moss and Braczyk [4] from electron diffraction experiments. Another similarity is demonstrated by comparing the reflectivity of amorphous and crystalline SiO_2 (hexagonal) which is shown in Figure (2.3). The band gap in both phases of SiO_2 is about 10 eV, although the first peak is suggested to be due to the formation of an exciton [5]. Nevertheless, the optical absorption edges of a wide variety of crystalline and amorphous semiconductors are very similar as illustrated in Figure (2.4) which shows the optical absorption coefficient vs. photon energy for amorphous and crystalline As_2Se_3 [5]. Another

example of the similarity in properties is the photoluminescence spectra of corresponding phases of As_2Se_3 as shown in Figure (2.5) [6]. Hence one may conclude that it is the short range order which is mainly responsible for the optical and electrical characteristics of semiconductors and other solids.

Mott [7] postulated on the basis of Anderson's theory [8] that the spatial fluctuation in the potential caused by disorder in amorphous materials may lead to the formation of localized states, producing a tail of states above and below the valence and conduction band respectively. Mott further suggested that there should be a sharp boundary between the energy ranges of extended and localized states. This leads to the existence of critical energies in each band where there is a sharp jump in mobility. These critical energies or mobility edges play the same role in amorphous materials as the band edges play in crystalline materials. The energy difference between the mobility edge of the valence band and that of the conduction band is the mobility gap (see Figure (2.6)).

2.1.3 Band Models

Several models have been suggested for the band structure of amorphous semiconductors which are almost the same, to the extent that they all use the concept of localized states in the band tails. These models have been used to interpret the experimental electrical and optical data in terms of the energy distribution of the density of states in non-crystalline semiconductors.

2.1.3.1 The Cohen, Fritzsche and Ovshinsky model

Cohen, Fritzsche and Ovshinsky (CFO) [9] supposed that in a non-crystalline structure the disorder would lead to overlapping band tails of localized states from the conduction and valence band as in Figure (2.7). The band tails of localized states originating from the conduction band would be neutral when empty while those originating from the valence band would be neutral when full. As a result of the overlapping of bands, there is a redistribution of electrons which fills the states in the conduction band tail below the Fermi level, causing them to be negatively charged. States of the valence band tail above the Fermi level are empty and therefore positively charged. This model helps to explain why the Fermi level is fixed (pinned) close to the middle of the gap, which is a feature required by the electrical properties of these materials. The other principal feature of the Cohen-Fritzsche-Ovshinsky (CFO) model is the concept of "mobility edges" at specific energies in the band tails. As mentioned earlier, these edges are identified with the critical energies separating localized from extended states in each band [10]. It is worth noting that the CFO model was proposed primarily for the multicomponent chalcogenide glasses used in switching devices. A major drawback for the CFO model was the high transparency of amorphous chalcogenides below a well-defined absorption edge.

2.1.3.2 The Mott-Davis model

An alternative idealized model for states in the gap having the form shown in Figure 2.8(a) was proposed by Mott and Davis (MD) [11].

In this picture, relatively limited tails of localized states were postulated to extend into the forbidden gap (by a few tenths of electron volts). In addition Mott and Davis proposed a band of states near the centre of the gap arising from defects in the network such as dangling bonds, vacancies, etc. The central band may be split into donor-like and acceptor-like bands, which will also pin the Fermi level (see Figure (2.8b)).

Recent experimental evidence coming mainly from luminescence, photoconductivity and drift mobility measurements indicates that various localized states are split off the tail states and are located at well-defined energies in the gap. A model which illustrates the possible bands of donor and acceptor-like states in the upper and lower halves of the mobility gap was proposed by Marshall and Owen [12], which is sometimes called the Marshall-Owen model. Figure (2.9) illustrates such a model which has been suggested for amorphous chalcogenide semiconductors. For amorphous silicon Spear and co-workers (e.g. Madan, Le Comber and Spear [13]) reached similar conclusions (Figure (2.10)). Note that the density of states in Figure (2.10) is displayed logarithmically.

2.2 Defect States

The properties of any atom are determined primarily by the number of electrons it possesses. The outermost shell normally has exactly eight possible states which are further sub-divided into two groups - two at lower energy (s-state) and six at a higher energy (p-states). To form molecules, the energy of the molecular combination must be lower

than that of the uncombined atoms. There are two ways of lowering the energy. (i) In an ionic bond the reduction in energy results from transferring one or more electrons from one atom to another, as in the case of NaCl. (ii) In covalent bonds the reduction of energy occurs when electrons in the outer shells of two adjacent atoms are shared by the two atoms. When two atoms are close enough for their outer electrons to interact, the energies of their states can be shifted by the interaction. Some of the states are reduced in energy forming "bonding" states and an equal number are increased in energy forming "antibonding" states. The bonding states are filled according to Pauli's principle (i.e. only two electrons can share the state and only if they are of opposite spin), and the antibonding states are empty. States which are unshifted in energy are called nonbonding states.

Since the separation in energy between the s and p states is usually of the same order of magnitude as the bonding energy, it is possible for one of the pair of s electrons to be moved to a p-state and then both s- and p-states combine together to form covalent bonds. For column IV elements, the configuration sp^3 gives the maximum possible number of s-p bonds, namely four. Beginning with column V (Pnictide) elements, electrons in the s-states remain paired and do not take part in bonding (they are often called a "lone pair"). In these elements only electrons in p-states form bonds i.e. there are three possible bonds. Elements of column VI (the chalcogens) have a p lone pair in addition to the s lone pair, hence elements of this group have two possible p bonds. The lone pairs play an important part in semiconductors which contain group VI elements in two-fold coordination. Examples of such semiconductors are the elements S, Se and Te, IV-VI

compounds ($GeTe_2$, GeSe, etc.), and V-VI compounds (As_2Se_3, As_2S_3, etc.), as well as many crystalline and glassy chalcogenide alloys.

From experimental observations on chalcogenide materials it has been found that they cannot be doped with impurities and the Fermi level in these materials and their compounds is found to be pinned in the middle of the forbidden gap, suggesting the existence of states in the gap. On the other hand, electron spin resonance (ESR) is not normally detectable in chalcogenide glasses, in contrast to tetrahedral elements with states in the gap, and this behaviour of the chalcogenides was a puzzle for some time.

It should be noted however that amorphous semiconductors can be subdivided into two major classes with distinctly different properties. Amorphous semiconductors made up primarily from group IV or group V elements typically have an n-type thermopower [14], exhibit variable range hopping at low temperatures, show an ESR signal, and their Fermi level can be moved by varying the electronic density. By contrast chalcogenide glasses generally have a p-type thermopower, do not exhibit variable-range hopping, do not show an ESR signal, and their Fermi level does not vary much with electronic density.

Anderson [15] put forward a proposal to explain the pinning of the Fermi energy and absence of an ESR signal. He assumed that in an amorphous semiconductor there is a strong tendency for electrons to be paired in non-bonding configurations, the coulomb repulsion between electrons at the same site being compensated by a strong electron-lattice interaction which causes a change in the local atomic structure. Street and Mott [16] and Mott, Davis and Street (MDS)[17], applied

Anderson's concepts of a negative correlation energy U_{eff} (explained later) specifically to provide a model to explain a variety of phenomena in chalcogenide glasses including some effects caused by the influence of light (discussed below). They suggest that in chalcogenide glasses there is a large number of dangling bonds. These dangling bonds behave as point defects at which the normal coordination cannot be satisfied owing to the constraints of local topography (Mott and Street [16]). Dangling bonds containing one electron are neutral defects and are designated by the symbol D^0. A transfer of an electron from a neutral defect D^0 to another D^0 will lead to the creation of two charged defects D^+ and D^-. Consider two dangling bonds at the ends of a chain as illustrated in Figure (2.11). Provided the temperature is high enough, when an electron is removed from a dangling bond at one end of the chain a D^+ is formed and the local environment around the D^+ site is distorted because lone pair p-electrons of nearby chalcogens tend to form a coordinate bond. The dangling bond at the other end of the chain will be negatively charged due to the introduction of additional electrons. Mott, Davis and Street proposed that the reaction:

$$2D^0 \rightarrow D^+ + D^- \qquad (2.3)$$

is exothermic, i.e. the total energy (electron plus lattice) associated with the pair of charged defects D^+ and D^- (both without spin since they are either empty or doubly occupied) is lower than that of two neutral defects D^0. The energy gained by the lattice distortion around the D^+ site as a result of bonding with the lone pair p-electrons on neighbouring atoms is more than the coulomb repulsion between the two electrons on the D^- site. Thus electron-phonon interactions make

electron pairing energetically favourable at defects and this is what is meant by a negative correlation energy U for the defect. The D^+ and D^- centres act as shallow donors and acceptors. They also behave as traps, capturing their respective carriers and changing their state to D^0 i.e.

$$D^- + h \rightarrow D^0 \quad \text{and} \quad D^+ + e \rightarrow D^0 \tag{2.4}$$

where h and e denote a hole or electron respectively. This model gives a good description of many of the electronic and optical properties observed in chalcogenide glasses. Equation (2.4) can be written in different ways to show the negative correlation energy which makes equation (2.3) exothermic. Let the addition of an electron from the valence band to D^+ cost an energy E_1 and the addition of an electron to the resulting D^0 an energy E_2. This can be represented in the following equations:

$$D^+ + e(+E_1) \rightarrow D^0 \tag{2.5}$$

$$D^0 + e(+E_2) \rightarrow D^- \tag{2.6}$$

Thus

$$2D^0 \rightarrow D^+ + D^- + (E_1 - E_2) \tag{2.7}$$

If the addition of the second electron to D^0 costs less energy than the first (i.e. $E_2 < E_1$), then (E_1-E_2) is positive and the total reaction is exothermic, since the creation of $2D^0$ from D^+ and D^- needs an additional energy equal to (E_1-E_2) [18,19].

Kastener, Adler and Fritzsche (KAF) developed a model similar to

that of the MDS picture but did not relate the presence of charged defect states to the topographic constraints [20]. This is a very important point, because it means that their model should also be applicable to crystalline chalcogenides. In Anderson's paper [16], he did not specifically indicate that the concept of negative correlation energy is only applicable to glasses, in fact he considered the concept is equally valid in crystalline solids [21]. In addition, Mott later indicated [21] that the concept of negative correlation is also applicable to crystalline chalcogen elements and compounds. In the KAF model D^0, D^+ and D^- are represented by C^0_3, C^+_3 and C^-_1 respectively, the subscript number corresponds to the coordination while the superscript represents the total charge. The structures and energies of several simple bonding configurations for chalcogen atoms are illustrated in Figure (2.12), as given by the KAF model. The normal bonding configuration is C^0_2; the straight lines represent the bonds (σ states), the dots are lone-pair electrons (LP), and the asterisks the antibonding (σ^* states). In C^0_2 the antibonding (σ^*) states are empty and energy relative to the LP level, is $-2E_b$. The energy to create C^0_3 is $(-2E_b + \Delta)$; it is the lowest energy neutral defect and is a more important neutral centre than the dangling bond C^0_1 [22]. The configuration C^+_3 with an energy of $-3E_b$ is the defect having the lowest energy. The energy of C^-_3 is $(-E_b + 2\Delta + U_\sigma^*)$, the positive correlation energy term U_σ^* is because of the two electrons in the antibonding state. The energy of the neutral dangling bond C^0_1 is $-E_b$. Finally, the negatively charged dangling bond C^-_1 has one electron in lone-pair states and its energy is $(-E_b + U_{LP})$, the term U_{LP} arising from the correlation energy of the LP levels.

Following the KAF model positively and negatively charged defect pairs are created in two stages [20,22]. The first reaction is

$$C^{o}_{1} + C^{o}_{2} \rightarrow C^{o}_{2} + C^{o}_{3} \qquad (2.8)$$

According to this equation the neutral dangling bond ($D^{o} = C^{o}_{1}$) interacts with the lone-pair of a neighbouring chalcogen atom to form three-fold and two-fold coordinated chalcogen atoms. Two C^{o}_{3} defects are converted into C^{+}_{3} and C^{-}_{3} by the following reaction

$$2C^{o}_{3} \rightarrow C^{+}_{3} + C^{-}_{3} \qquad (2.9)$$

The C^{-}_{3} is unstable, so it interacts with a neighbouring C^{o}_{2} lone-pair to form C^{o}_{2} and C^{-}_{1}. In this reaction C^{-}_{3} breaks one of its bonds and becomes C^{o}_{2} which converts a neighbouring C^{o}_{2} into C^{-}_{1}

$$C^{-}_{3} + C^{o}_{2} \rightarrow C^{o}_{2} + C^{-}_{1} \qquad (2.10)$$

From (2.9 and 2.10) we may write

$$2C^{o}_{3} \rightarrow C^{+}_{3} + C^{-}_{1} \qquad (2.11)$$

which is equivalent to (2.3) of the MDS model. The charged defects C^{+}_{3} and C^{-}_{1} have been called by Kastner a "valence alternation pair" (VAP). Adler and Yoffa [14] have developed a mathematical formula to illustrate the effect of positive and negative correlation energy on the position of the Fermi level.

The energy level scheme for states in the gap for a system of defect levels associated with D^{-}, D^{o} and D^{+} is illustrated in Figure

(2.13) [18,23]. The D^- is located close to the valence band. The valence band in chalcogenides is formed from the lone pair, p-electrons while the bonding states lie much deeper in energy as presented in Figure (2.14). The antibonding states form the conduction band, as in tetrahedral semiconductors [24]. However the D^- centre is a charged defect and can capture a hole from the valence band, so it behaves in a similar way to a shallow acceptor level. The D^+ site is located near the conduction band and is positively charged so it may capture electrons: it can be regarded as a shallow donor level, see Figure (2.13). When these two defects capture their respective carriers they are distorted to become D^o's. The energies are $(W^- + E^-)$ and $(W^+ + E^+)$ for D^- and D^+ respectively, where W^- and W^+ are the distortion energies associated with D^o relative to D^- and D^+ respectively.

According to Figure (2.13) there are two levels associated with D^o [18]. The upper level B corresponds to the energy required to excite an electron thermally from the valence band to D^+ (which then become D^o) and the lower B' corresponds to exciting a second electron from the valence band to the same defect (which becomes D^-), and the result of exciting the second electron is the creation of one hole in the valence band. Hence the energy to create one hole in the valence band is the average of these two energies, from which it follows that the Fermi level lies between B and B' and is effectively pinned. A similar argument can be applied to the creation of an electron in the conduction band. In this case the energy required to excite an electron from D^- to the conduction band is $[E_g - (W^- + E^-)]$ where E_g is the band gap, while the energy to take a second electron from the same defect (which is now D^o) is $(W^+ + E^+)$. Accordingly the energy per electron is $[E_g - (W^- +$

$E^-) + (W^+ + E^+)]/2$. This is equivalent to $(E_c - E_f)$ and so E_f lies midway between B and B' as for the hole.

The energy separation between B and B' is the negative correlation energy U associated with the exothermic reactions (equations (2.3) and (2.11)). Referring to equations (2.5) and (2.6) and Figure (2.13), $E_1 = [E_g - (W^+ + E^+)]$ and $E_2 = (W^- + E^-)$. Thus $(E_1 - E_2) = [E_g - (W^+ + E^+) - E + W^+)] = (B - B')$.

Group V elements (pnictides) can also undergo valence alternation [23] but the reactions are more complicated than in the case of the chalcogens because the two electrons of the non-bonding s-states are utilized for over-coordination only after hybridization.

In pnictide elements, the lowest energy defect, corresponding to D^o or C^o_3 (as in chalcogen), is considered to be P^o_4 which is formed by hybridizing the s- and p-states to create four equivalent sp^3 orbitals and then forming four bonds to nearest neighbours, with one electron left unsatisfied in the antibonding. By analogy with the chalcogens, the lowest energy defects are the charged valence alternation centres, not the neutral P^o_4. The authors [22] show that the negative correlation energy gained by transferring charge is larger in pnictides than in chalcogens, but nevertheless, the net energy gain in forming VAPs is comparable for the two groups of elements.

The creation of VAPs occurs in successive steps. Starting with two P^o_4, P^+_4 and P^-_4 defect states are created by transferring an electron from one P^o_4 to the other. This reaction requires a positive correlation energy but P^-_4 is unstable and the following reaction takes

place:

$$P^{o}_{3} + P^{-}_{4} \rightarrow P^{-}_{2} + P^{o}_{3} \qquad (2.12)$$

This involves the breaking of a bond to one of the four neighbouring P^{o}_{3}, placing the two antibonding electrons into a lone pair orbit (see Figure (2.15)), and dehybridizing the P^{o}_{4} to make it a normal P^{o}_{3}. This is illustrated in Figure (2.16). The complete exothermic reaction becomes

$$2P^{o}_{4} \rightarrow P^{+}_{4} + P^{-}_{2} \qquad (2.13)$$

the VAP P^{+}_{4} and P^{-}_{2} being equivalent to D^{+} and D^{-} in the chalcogenide case.

When both chalcogen and pnictide elements are combined in a compound such as As_2Se_3, all possible stable defects, namely P^{+}_{4}, C^{+}_{3}, P^{-}_{2} and C^{-}_{1} will be present but in different concentrations. At temperatures above the glass transition temperature (T_g), the following four reactions will be simultaneously in equilibrium.

$$2C^{o}_{3} \rightarrow C^{+}_{3} + C^{-}_{1} \qquad (2.14)$$

$$2P^{o}_{4} \rightarrow P^{+}_{4} + P^{-}_{2} \qquad (2.15)$$

$$P^{o}_{3} + C^{o}_{2} \rightarrow P^{+}_{4} + C^{-}_{1} \qquad (2.16)$$

$$C^{o}_{2} + P^{o}_{3} \rightarrow C^{+}_{3} + P^{-}_{2} \qquad (2.17)$$

Kastner and Fritzsche [22] suggest that C^{-}_{1} appears to be the dominant negative centre, but do not indicate whether the dominant positive partner is P^{+}_{4} or C^{+}_{3}. These authors also argue that under

non-equilibrium conditions (i.e. photo excitation at low temperature or rapid quenching) both C^{o}_{3} and P^{o}_{4} will be formed. Hence by allowing these defects to come to electrical equilibrium P^{+}_{4} and C^{-}_{1} will be formed. Owen and Spear [25] have isolated five defect centres in the gap of amorphous As_2Se_3.

Mott and Street [26] have suggested the possible clustering of D^{+}, D^{-} centres as a result of their coulomb attraction. The overlapping D^{+}, D^{-} pair has been called an "intimate" valence alternation pair (IVAP) [22] and is illustrated in Figure (2.17b). The IVAP is a neutral centre (actually a dipole). Kastner and Fritzsche [22] suggest that IVAPs are self-annihilating even at temperatures well below T_g. However they classified IVAPs into two types - stable and unstable. The most important IVAP is the one in which C^{+}_{3} and C^{-}_{1} are nearest neighbours. For the unstable IVAPs (figure (2.18a)) in which C^{-}_{1} and C^{+}_{3} are close together, charge transfer and bond rearrangement results in the neutral species in figure (2.18b). By breaking the bond between them, two C^{o}_{3} become two C^{o}_{2} (see figure (2.12)). The annihilation requires so little atomic rearrangement that it is likely to occur at room temperature [22]. While for the important IVAPs (Figure (2.18c)), it can be seen that charge transfer and relaxation would result in this case in a configuration as shown in Figure (2.18d), which cannot self-annihilate without the rearrangement of many atoms. Although the ratio of VAP to IVAP density is small, the density of VAPs may be sufficiently high to pin the Fermi level [22]. Kastner and Fritzsche argue that IVAPs are not likely to act as traps and their density should be independent of doping, although alloying may affect the IVAP concentration.

2.3 Predicted Effect of Doping

Mott [27] has developed theories based on the law of mass action in order to discuss the effect of impurity atoms in melt-quenched chalcogenide glasses. Mott suggests that the addition of certain elements to the chalcogenide glasses would either destroy bond centres of one sign, or form charge centres of opposite sign to the impurity which would then be compensated by a D-centre of the same sign as the impurity.

Mott predicted that the conductivity activation energy would be reduced to 2/3 of its original value. Hence the conductivity would be enhanced by exp (0.3/kT) and the Fermi level will no longer be pinned.

Most elements added to the chalcogenide material seek their lowest energy bonding configuration and thus remain relatively inactive electrically. To examine the effect of a metal additive, let v be the normal valence of the melt atom and assume that the bonding has a strong covalent component. Then the lowest energy bonding configuration is one in which the metal has v normal bonds to twofold coordinated chalcogens and 4-v coordinate bonds utilizing lone pairs on chalcogen atoms, forcing them to become threefold coordinated, as is illustrated in Figure (2.19a) where A is the additive. Such an additive in its lowest energy bonding configuration has no direct effect on the density of VAPs, because all valence electrons are utilized in bonding. The coordinated bonds are normal bonds between the additive element A and its neighbouring chalcogen. In the case of the chalcogen atom, it is clear that the energy of bonds to threefold coordinated chalcogens will

be different from those of twofold, and from those of onefold, as pointed out by Kastner, Adler and Fritzsche [20] and Kastner and Fritzsche [22].

Fritzsche et al [28] showed that the important defect pair, illustrated in Figure (2.19b), is the positively charged additive compensated by a singly coordinated negatively charged chalcogen, C^-_1, located elsewhere in the material. The other possible defect pairs are A^- (Figure (2.19c)), C^+_3 and A^{2-}, $2C^+_3$ [29]. Mott [27] suggested that negatively charged metal additives might be the common defect species. Fritzsche et al argue that negatively charged metal additives are energetically less favourable than positively charged ones.

If A^+ captures an electron it becomes neutral. This neutral centre is a defect of higher energy than the neutral A configuration illustrated in Figure (2.19a). Transformation from one into the other is not possible below the glass transition temperature [28]. The corresponding process for A^o centres, to that of an exothermic reaction for the neutral VAP centre (equation (2.14)), is shown in Figure (2.20) and may be written as:

$$2A^o_4 + C^o_2 \rightarrow A^+_4 + C^-_1 + A^o_3 \qquad (2.18)$$

This is a high energy reaction and it indicates that the positively charged additive is compensated by a C^-_1. It is only the charged additives which affect the density of the valence alternation defects, and through them the conductivity.

The assumptions applied in order to understand and predict the

influence of charged impurities are that the law of mass action determines the relative concentrations of the charged defects when the glass is prepared under equilibrium conditions at $T > T_g$ [22], the charge of ionized impurities is compensated by the intrinsic defects [26], the concentrations of the various defects is frozen-in when the glass is cooled to temperature $T < T_g$ [6], and that free holes (or electrons) are generated from the defects via the reaction $C^+_3 \rightarrow C^-_1 + 2p$ [27,29]. The relevant equations for electropositive dopants are [30]:

$$[C^+_3]\,[C^-_1] = N^2_o \tag{2.19}$$

$$np = n^2_i \tag{2.20}$$

$$n^2\,[C^-_1]/[C^+_3] = n^2_o \tag{2.21}$$

$$[C^+_3] + [A^+] + p = [C^-_1] + n \tag{2.22}$$

where N_o is the defect density in the absence of dopants (i.e. $C^-_1 = C^+_3 = N_o$), n_i is the intrinsic carrier concentration determined by the law-of-mass action for free holes p and electrons n, n_o is the free hole concentration in the absence of dopants and A^+ is the density of the fraction of positively ionized impurities. By considering a typical chalcogenide glass the equation may be simplified [30] and the total concentration of VAPs, is given by

$$N = 2(N_o^2 + \tfrac{1}{4}[A^+])^{1/2} \tag{2.23}$$

Following Kastner [31], at temperature $T < T_g$ with the total density of valence alteration centres $N = [C^+_3] + [C^-_1]$, and with the help of equation (2.11) and using equation (2.23) instead of (2.19), equation

(2.21) may be rewritten as

$$n^2 (N-[A^+]+n-p)/(N+[A^+]-n+p) = n_o^2 \qquad (2.24)$$

By considering the extreme case $[A^+] >> N_o$ and since the electron density n is enhanced by positive additives ($n \gg p$), equation (2.24) may take the form

$$n^2 (2N_o^2/[A^+] +n) = 2[A^+]n_o^2 \qquad (2.25)$$

However, only when $n >> 2 N^2_o/[A^+]$ does one obtain the solution derived by Mott [27], i.e.:

$$n = (2[A^+])^{1/3} n_o^{2/3} \qquad (2.26)$$

which leads to the reduction of the thermal activation energy to 2/3 of its original value E_o. More commonly encountered is the case at lower temperature when $n << 2 N^2_o/[A^+]$ and equation (2.25) becomes:

$$n = \frac{[A^+]}{N_o} n_o \qquad (2.27)$$

which implies that the activation energy of n retains the value E_o which it had in the absence of $[A^+]$.

Fritzsche [31] suggested that a plot of log n as a function of 1/T should have the form shown in Figure (2.21) for both doped and undoped chalcogenide materials. The conductivity is expected to be related to the carrier concentration and would display a kink at $n = 2 N^2_o/ [A^+]$ and the conductivity prefactor could increase by $[A^+]/N_o$. Fritzsche and Kastner [30] concluded that when equilibrium is permitted, the

valence alternation centres reduce the influence of foreign atoms on the conductivity in two ways: (1) they reduce the occurrence of charged additives, and (2) they increase in number such that their concentration always exceeds that of the charged additives. Consequently, the VAPs remain the source of charge carriers. They did not find a decrease in the activation energy to 2/3 of its original value, except under specific conditions. Instead they found an increase in the conductivity prefactor and no change in the activation energy. In the non-equilibrium condition, if the concentration of charged additives exceeds that of VAPs, the chalcogenide glass behaves similarly to a partially compensated semiconductor in which the charged additives act either as shallow acceptor or donors depending on their charge.

2.4 Experimental Results

Several workers have studied the effect of doping amorphous As_2Se_3 with various metallic and non-metallic impurities. In undoped a-As_2Se_3 at 120 C, Kolomiets and co-workers [32] found that the addition of Ag and Cu up to about 10^{19} atoms/cm^3 causes a decrease in the hole mobility and a slight increase in the activation energy, while a further increase of concentration of these impurities results in an increase in mobility and a decrease of activation energy. The reduction in the activation energies at high dopant concentration was considered to indicate a decrease in the effective trap depth. For lower impurity concentrations the decrease in mobility and increase in activation energy was suggested to be due to scattering by the impurities or by lattice imperfections caused by the dopant. Several workers

[33,34,35,36 and 37] studied Cu-As_2Se_3 and Ag-As_2Se_3 alloys with much larger concentrations of the metal.

Pfister, Morgan and Liang [38] and Pfister and Morgan [39] studied both transit time and d.c. resistivity in evaporated As_2Se_3 films doped with electropositive metals [Cu, Ge, Ga, In, k, Li, Mn, Na, Ni, Tl and Zn] prepared by co-evaporation onto Al substrates maintained at a temperature close to the glass transition temperature (T_g) of As_2Se_3. They did not observe any electron transport whatever the concentration, which is puzzling since these impurities only enhance the negative defects C^-_1 (or D^-) which trap hole carriers. From their observation on the effect of impurities on the transit time and dc resistivity, Pfister and Morgan [39] classified the impurities into three groups of dopants.

In the first group, namely Mn, Fe, Ni and Cu the transport properties of a-As_2Se_3 show similar behaviour in many respects. On doping with Fe, Mn and Ni (10^{17} - 10^{18} atoms/cm^2) the hole transit time and its associated activation energy increased linearly with increasing dopant concentration, although for Cu it had to exceed 10^{19} atoms/cm^3 to show such effect. Typical results are shown in Figure (2.22a,b). The d.c. resistivity behaves somewhat differently, although it does increase with concentration but not in a similar manner. The combination of both a large increase in the hole transit time with an associated increase in activation energy led Pfister and Morgan to suggest that Mn, F, Ni and Cu generate traps at energies extending from the intrinsic trapping level located 0.6 eV above the hole transport states to the middle of the bandgap (see Figure (2.23a)). For Cu concentrations less

than 10^{19} atoms/cm^3 only the hole mobility is reduced and there is no effect on the activation energy. They interpret this behaviour as due to the creation of hole traps at 0.6 eV. Although these dopants enter as positively ionized impurities they should decrease the electron trap density, but no electron transients were observed. McNeil [40] has reported electron transients in crystalline As_2Se_3 doped with Cu and pure (undoped) As_2Se_3.

The second group consists of Zn, Ga and In. Their influence on electronic transport in a-As_2Se_3 is completely different. Ga and In cause a significant increase in both transient and d.c. transport for concentrations in excess of 10^{18} atoms/cm^3 but for Zn there is a much smaller increase. The lower part of Figures (2.24 and 2.25) shows the resistivity and transit time as a function of concentration respectively. Both Ga and In increase the hole mobility and d.c. transport in a similar manner. The transit time almost follows the resistivity, as a function of dopant concentration, and also the activation energy for both processes, through the range 10^{18} - 10^{19} atoms/cm^3 (Figures (2.24, 2.25 and 2.26)). For concentrations in the range 2×10^{19} - 2×10^{20} atoms/cm^3 no decrease of activation energy was observed but both transit time and dc resistivity continue to decrease. The authors attributed the decrease in transit time and d.c. resistivity, with a decrease in their respective activation energy by 0.1 eV, to a build up of additional localized valence states 0.01 V above the hole transport channel, rather than to a shift in the Fermi level (Figure (2.23b)). This interpretation is supported by absorption edge measurements which show a red shift with increasing dopant concentrations (Lezal et al [41], Kolomiets et al [42]). The red shift

is of the same magnitude as the decrease of the transport activation energy. The localized states resulting from the addition of impurities which lower the activation energy by 0.1 eV are thought to be associated with neutral bonding configurations, which the author suggests are most likely fourfold coordinated Ga and In.

The third group of elements are Tl, Li, Na and K. The d.c. transport in a-As_2Se_3 doped with Tl has been studied by several authors [39,41,42,43 and 44]. The results confirm that the resistivity increases to a maximum of 3 - 4 x 10^{13} ohm cm, and then decreases rather steeply as the concentration approaches the "alloy" range (see Figure (2.24)). The transit time also shows a maximum as a function of concentration, as is illustrated in the upper part of Figure (2.25). For concentrations exceeding 1 x 10^{19} Tl/cm^3, the transit time and activation energy exhibit similar features to Ga and In doped samples, the difference being that for the latter dopants a decrease of the transit time sets in for concentrations about one order of magnitude lower (Figures (2.26 and 2.27)). In the range of concentration below the maximum transit time, its features are similar to those of samples doped with the first group of metals (Mn, Ni and Cu).

Results for Na-doped a-As_2Se_3 [39] are similar to those for Tl impurities, the differences being as follows: (1) The transit time starts to increase only when the Na concentration exceeds 10^{18} atoms/cm^3, which is about two orders of magnitude higher than for Tl (see Figure (2.25)). (2) The rate of increase in transit time with concentration is higher than for Tl (Figure (2.25)). (3) Na shows an increase in the activation energy for transport by 0.06 eV with

concentration, while Tl shows a very slight increase and then a steplike decrease to a value of 0.52 eV for impurity concentrations exceeding 1 x 10^{20} Tl/cm^3, see Figure 2.27. (4) The d.c. resistivity follows more closely the concentration dependence of the transit time (Figure (2.24a)). Only when the concentration exceeds the transit time maximum do the transit times for Na, K and Tl doped As_2Se_3 approach the same values and exhibit a similar concentration dependence as that for d.c. resistivity.

Pfister and Morgan suggest that for low concentration the impurities increase the density of intrinsic traps N_t (10^{16} cm^{-3}) rather than affecting the hole trap population N_h (10^{18} - 10^{19} cm^3), since the effect of Tl becomes noticeable for concentrations much less than N_h and just above N_t. The decrease of transit time for high concentration is thought to be caused by an increase in the concentration of states which are the same as those proposed for Ga and In. Figure (2.23c) illustrates the proposed model for the third group. The build up of states above the band edges is also confirmed by the absorption measurements of Lezal et al [41], who reported a red shift of the absorption edge of As_2Se_3 which depended on the presence of group III A elements.

1. CHAPTER 3 : ELECTRICAL AND OPTICAL PROPERTIES

3.1 D.C. Conductivity

The essential feature of the Mott and Davis (MD) model [1] discussed in Chapter 2, is the concept of a "mobility gap" which separates two types of states in the conduction and valence bands of a non-crystalline material. States above the mobility gap in the conduction band, and below the mobility gap in the valence band are extended states, while states in the tails are localized. Apart from the mobility gap idea, the MD model and Marshall and Owen's model [2] also suggested the existence of localized states in the middle of the gap. The introduction of the mobility gap and localized levels in the gap leads to four possible conduction mechanisms which will affect the d.c. conductivity measurements in different temperature regimes [3]. Starting at high temperature, as the temperature decreases, the four processes are as follows:

1. Extended State Conduction

Consider the case of electron conduction. The conductivity due to electrons excited beyond the mobility edge (E_c) into the extended states can be expressed as:

$$\sigma = eN(E_c)kT\mu_c\exp[-(E_c-E_F)/kT] \qquad (3.1)$$

where $N(E_c)$ is the density of states in the conduction band, e is the electron charge, k is Boltzmann's constant and μ_c is the mobility. In order to explain the concept of a mobility edge, we follow Mott's

treatment [3]. Mott introduced the concept of minimum metallic conduction (σ_{min}). He defined σ_{min} as the smallest non-zero value the conductivity can have at absolute zero temperature, i.e. at E_c. He derived the expression:

$$\sigma_{min} = \text{const. } 2\pi e^2/ha \qquad (3.2)$$

where h is Plank's constant and a is the interatomic distance. The constant has the value of 0.026 [4]. From (3.2) one may obtain an expression for μ_c at E_c as [2]

$$\mu_c = 0.078\ 2\pi e a^2 B/hkT \qquad (3.3)$$

where B is the width of the band. Taking a = 2 °A and B = 2.5 eV then μ_c= 10 $cm^2V^{-1}s^{-1}$ at room temperature. Cohen [5] derived a similar expression for the variation of μ with kT as in equation (3.3) (i.e.μ_c (pt1/kT). Equation (3.1) may be written therefore as

$$\sigma = \sigma_o \exp[-(E_c-E_F)/kT] \qquad (3.4)$$

which is represented in Figure (6.1) by section "a" of the line.

Optical measurements on amorphous semiconductors usually show that the band gap decreases approximately linearly with temperature, i.e.

$$(E_c-E_F) = E(0)-\gamma'T \qquad (3.5)$$

where E(o) is the value of $(E_c- E_F)$ at T = 0 °K and γ' is the temperature coefficient. Then equation (3.4) becomes

$$\sigma = \sigma_o \exp(\gamma'/k) \exp[-E(0)/kT]$$

which can be written in the form:

$$\sigma = C_o \exp[-E(0)/kT] \tag{3.6}$$

where

$$C_o = eN(E_c)kT\mu_c \exp(\gamma'/kT) \tag{3.7}$$

Since $\mu_c \propto 1/T$ the pre-exponential factor C_o is temperature independent. An estimate of γ' can be obtained from the temperature dependence of the optical gap. For a chalcogenide γ (the temperature coefficient of the optical gap) has a value between 4×10^{-4} and 8×10^{-4} eV K^{-1}. In chalcogenide glasses E_F is normally situated near the middle of the gap, and hence the value of γ' is approximately half the value of γ. As a result exp (γ'/k) should be in the range of 10-100 [6].

2. Conduction in Localized States in Band Tails

The wave function of states in the band tails are localized, and conduction can only occur by thermally activated hopping. The mobility will have a thermally activated nature, given by:

$$\mu_{hop} = \mu_o \exp[-W(E)/kT] \tag{3.8}$$

where W(E) is the hopping energy, and

$$\mu_o = \frac{1}{6} \nu_{ph} eR^2/kT$$

ν_{ph} being the phonon frequency and R the distance covered in one hop. For a phonon frequency $\nu_{ph} = 10^{13}$ s^{-1} and $W \simeq kT$ Equation (3.8) yields a mobility of the order of $10^{-2} cm^2 v^{-1} s^{-1}$ at room temperature and hence there is an abrupt drop in its value compared to μ_c in the extended states. The conductivity in this case is given by:

$$\sigma = C_1 \exp[-(E_A - E_F + W_1)/kT] \qquad (3.9)$$

where W_1 is the activated energy for hopping, E_A is the energy at which the band tail in the conduction band starts (or E_B in the case of the valence band). The constant C_1 is difficult to estimate [2,4], but the lower mobility and the lower density of states near E_A as compared to E_c will make C_1 several decades smaller than C_o. Equation (3.9) is represented by section "b" in figure 3.1.

3. Conduction in Localized States at the Fermi Level

If there exist a finite density of states at the Fermi level, then at low temperatures there will be a contribution to the conductivity by carriers with energies near E_F, due to hopping between localized states. Following Mott's estimation [7] for the temperature dependence of the hopping conduction at E_F, we can consider the energy difference between the states as W_2, then the probability p that an electron will jump from one state to another is determined by three factors:

(i) The probability of finding a phonon with an excitation energy equal to W_2, which is given by the Boltzmann expression $[\exp(-W_2/kT)]$.

(ii) An attempt frequency ν_{ph} in the range $(10^{12}\text{-}10^{13}\ s^{-1})$.

(iii) The probability of electron transfer from one state to another which is expressed as $[\exp(-2\alpha R)]$, where R is the jumping distance, which at high temperature is equal to the interatomic spacing, and α is a quantity which is representitive for the rate of fall-off of the

wavefunction at a site.

The probability p that an electron will jump is then given by:

$$p = \nu_{ph} \exp(-2\alpha R - W_2/kT) \tag{3.10}$$

This leads to the following expression for the conductivity:

$$\sigma = \frac{1}{6} e^2 R^2 \nu_{ph} N(E_F) \exp(-2\alpha R) \exp(-W_2/kT) \tag{3.11}$$

where $N(E_F)$ is the density of states at the Fermi level. Equation (3.11) can be written in the form:

$$\sigma = C_2 \exp(-W_2/kT) \tag{3.12}$$

This equation is indicated as section "c" in Figure (3.1).

4. Conduction Due to Variable Range Hopping

As the temperature is further lowered, carriers will tend to hop larger distances in order to find sites which lie energetically closer than the nearest- neighbour site. This mechanism is called variable range hopping. Mott shows that the hopping probability in this case is:

$$p = \nu_{ph} \exp(-B/T^{1/4}) \tag{3.13}$$

where

$$B = 2.1 \, [\alpha^3/kN(E_F)]^{1/4} \tag{3.14}$$

Equation (3.13) leads to a temperature dependence for the conductivity of the form:

$$\sigma = \frac{1}{6} e^2 R^2 \nu_{ph} N(E_F) \exp(-B/T^{1/4}) \qquad (3.15)$$

or

$$\sigma = \sigma_o(T) \exp(-B/T^{1/4}) \qquad (3.16)$$

where

$$R = 3^{1/4}/(2\pi\alpha N(E_F)kT)^{1/4} \qquad (3.17)$$

Equation (3.16) will have the form of section "d" in Figure (3.1).

In chalcogenide crystals the principal conduction mechanism is considered to be via extended states, i.e.

$$\sigma = \sigma_o \exp[(E_c - E_F)/kT] \qquad (3.18)$$

which is similar to equation (3.4) for the non-crystalline case.

All of the above arguments were derived by Mott and others with specific reference to the amorphous state of semiconductors such as the chalcogenide compounds. It should be noted however, that even in pure chalcogenide crystals, there still is the possibility of intrinsic defect states in the gap, as discussed in Chapter 2 (i.e. D^+,D^- and D^o) and in addition there may be other defects such as voids, dislocations, etc. Thus these materials should not be considered as purely intrinsic semiconductors, even though $(E_c - E_F)$ has a value close to $E_{g/2}$ ($E_g = E_c - E_v$). Indeed values of $(E_c - E_F) < E_{g/2}$ have been reported by Brunst and Weiser [8].

3.2 Thermopower

Two materials denoted by a and b, forming a circuit containing two junctions A and B as shown in Figure (3.2) at temperatures T_2 and T_1 respectively, develop a voltage V_o across the contacts C (which are assumed to be at a uniform temperature T_o), given by

$$V_o = \int_{T_1}^{T_2} S(T)\, dT \tag{3.19}$$

If $T_2 = T_1 + \Delta T$, where ΔT is small then

$$V_o = S\, \Delta T$$

or:

$$S = V_o/\Delta T \tag{3.20}$$

where S is the thermoelectric power or Seebeck coefficient. The sign of the thermoelectric power gives a direct indication of the type of carrier responsible for the electronic transport in the material, a negative sign for electron transport i.e. n-type material and a positive sign for hole transport i.e. p-type material. For a p-type crystalline semiconductor S is given by:

$$S = \frac{k}{e}\,[(E_F - E_v)/kT + A] \tag{3.21}$$

where k is Boltzmann's constant, e the electronic charge, E_F the Fermi energy, E_v the energy of the valence band edge, and A is a constant. The value of A depends on the nature of the scattering process and is normally a constant between 1 and 2 [3]. In extended states, A is

expected to be equal to unity [3], and makes only a small contribution to S when (E_c-E_F) or $(E_F-E_v) \gg kT$.

Uphoff and Healy [9] reported on the thermopower measurements on As_2Se_3 at temperature between 325°C and 380°C, and found the Seebeck coefficient to be positive but decreasing linearly with increasing temperature. According to Uphoff and Healy the thermopower activation energy (E_s) is 0.6 eV, which is less than the conduction activation energy (E_o). Seager and Quinn [10] reported a value of thermopower activation energy $E_s = 0.6 \pm 0.07$ eV and conduction activation energy (E_o) = 0.91 eV. Arnoldussen et al [11] reported similar results for $As_2(Se_{1/3}Te_{2/3})_3$, where the value of E_s was found to be 0.15 eV less than the activation energy measured from dc conductivity experiments. While Hurts and Davis [12] report that the activation energy for both E_s and E_σ are identical for As_2Se_3 glass (Owen [6] suggested similar arguments for As_2Se_3). Measurement of thermopower suggest that amorphous materials are always found to be p-type.

The explanations which have been suggested to describe such behaviour[3], are

1. That conduction is at E_b (the top of the valence band which is thought to be unlikely.

2. That the carriers are polarons, and the different (E_o-E_s) is the polaron hopping energy W_H [13].

3. That there are fairly long-range inhomogeneities in the potential at the top of the valence band.

4. That all measurements have been made in the transition region between hopping transport at the band edge and transport in an extended band, which was proposed by Nagels et al [14], and further developed by Mott, Davis and Street [15]. The model used [3] to explain such behaviour can be understood with the help of Figure (3.3). It is assumed that there is no temperature variation of E_C, E_A or E_F relative to each other. At temperatures above T_C, conduction is predominantly by carriers at E_C and below T_C by carriers at E_A. In the temperature range marked A both the conduction and the thermopower are activated with an energy equal to E_C-E_F. While in B the conductivity is activated with energy $E_A-E_F + w(T)$, where $w(T)$ is the hopping energy. For no hopping energy contribution to thermopower, the slope of S in the corresponding range of temperature is of the form E_A-E_F. Since for both ranges A and B the thermopowers extrapolated to $(1/T) = 0$ are similar[3], S in the transition region can take several forms depending on the sharpness of the transition in σ. The total thermopower for parallel conduction mechanisms is simply the sum of the individual thermopowers weighted according to the contribution each mechanism makes to the conductivity [3]. This implies that E_S is less than E_σ.

3.3 Thermally Stimulated Current

In a thermally stimulated process (TSP) the sample is heated in a controlled manner and a certain physical property is continuously monitored. This definition covers several phenomena, for some of which

the effect of interest appears only when the sample has been excited or treated in a certain manner prior to its heating.

If the varying parameter is measured and recorded as a function of time or the sample temperature, the resulting curve may provide information concerning the processes which take place in the sample during heating. There are many types of thermally stimulated measurement. In each case a physical quantity related to the sample is recorded while the sample temperature is raised in a predetermined manner from a certain low temperature T_o. The result of the measurement is a curve which describes the measured parameter as a function of time or temperature (f(t) or f(T)). This curve is often called a glow or heating curve, or thermogram. Despite the fact that the various TSP's are due to different mechanisms, their thermograms are often similar. Typical thermograms consists of one or more "peaks", or steps, each connected with a certain thermally activated microscopic process. The parameters of these microscopic processes can be determined from the number, shape and position of the peaks (steps), and from the dependence of the whole curve on the heating rate, the excitation of the sample before heating, etc. Chen and Kirsh [16] suggested that for certain TSP's one can use methods which have been developed for other TSP's as both the curves and the basic equations of the various thermally stimulated phenomena are similar.

3.3.1 Mathematical Description of TSP's

Although different thermally stimulated phenomena are due to quite different microscopic processes, the thermogram and the equations

describing the variables as a function of temperature are similar [16] as described above. This mathematical similarity enables the use of methods developed for a specific TSP for the analysis of others. A mathematical model for thermoluminesence will be considered as an example.

Thermoluminesence (TL) appears when a solid sample (insulator or semiconductor) is heated after being irradiated at a low temperature, T_o, by some kind of radiation (X or γ rays, particle beams, UV light, etc.). Part of the energy absorbed by the sample in the course of the radiation may be released during the heating in the form of light. Most of the excited electrons return to the valence band after a short time giving rise to luminescence. Some of the electrons, however, are trapped in local trapping levels within the forbidden gap. Each trapped electron leaves a hole in the valence band which is soon trapped in a hole-trap (or recombines with a trapped electron). However, a trapped electron (or hole) can be thermally raised to the conduction (valence) band, and move in the crystal, and then finally recombine with a trapped charge carrier of the opposite sign. The site of a possible recombination is referred to as a recombination centre. If those recombinations are radiative, and take place during the heating of the sample, TL is observed.

If we assume that the TL is caused by the thermal release of electrons from a single type of trap, at a depth E beneath the conduction band, the escape probability of a single electron per second is [s.exp(E/kT)] [16], where s is the frequency factor, E the depth of the trap (activation energy), k is the Boltzmann constant and T the

absolute temperature. If the trap is deep enough, it will be inactive at T_o , but will release electrons in considerable numbers at elevated temperatures. For example if E = 0.5 eV and s = 10^{12} sec^{-1}, the escape probability is 3 x 10^{-20} sec^{-1} at 80 °K, 10^{-9} sec^{-1} at 120 °K and about 10^{-4} sec^{-1} at 160 °K. As the temperature of the sample is raised, electrons are released, then, after reaching a maximum it falls down as the traps (or recombination centres) are depleted. Thus the resulting TL curve is a single peak as shown in Figure (3.4).

The first theoretical treatment for a single trap TL peak was given by Randall and Wilkins [17]. They assumed that the TL intensity is proportional to the rate at which trapped charge carriers are thermally released, and that this rate is proportional at any instant to the population of trapped carriers.

$$I = -C\left(\frac{dn}{dt}\right) = Csn \exp\left(\frac{-E}{kT}\right) \qquad (3.22)$$

where I is the TL intensity (or some other quantity depending on the process), n the concentration of trapped electrons, T the absolute temperature, k Boltzmann's constant, E the activation energy, and s the frequency factor. C is a proportionality factor which can be set to unity without loss of generality.

In the case of constant heating rate β ($T = To + \beta t$), the solution of equation (3.22) is

$$I(T) = n_o s \exp\left(\frac{-E}{kT}\right) \exp\left[-(s/\beta) \int_{T_o}^{T} \exp\left(\frac{-E}{kT'}\right) dT'\right] \qquad (3.23)$$

where T_o and n_o are the initial temperature and concentration of trapped

charge carriers respectively. Equation (3.23) is known as the first order kinetics equation. Garlick and Gibson [18] assumed strong retrapping probability, and suggested another equation

$$I = -dn/dt = s'n^2 \exp(\frac{-E}{kT}) \qquad (3.24)$$

which is known as the second order kinetics differential equation. Here the pre-exponential factor s' is constant with dimensions of cm^3 sec^{-1}. The solution of the last equation for a constant heating rate β is

$$I(T) = n_o^2 s' \exp(\frac{-E}{kT})[1+(n_o s'/\beta) \int_{T_o}^{T} \exp(\frac{-E}{kT'}) dT']^{-2} \qquad (3.25)$$

In both the first and second order cases I plotted as a function of T will show a peak-shaped curve whose temperature at the point of maximum intensity (T_m) depends mainly on E (the higher E, the higher T_m) and to a lesser extent on s (or s') and on β (and also on n_o in the second-order case). By equating to zero the derivative of equation (3.23) with respect to T_o, it can be shown that in a first order TL peak the condition for the maximum intensity temperature is

$$\beta E/(kT_m^2) = s \exp(\frac{-E}{kT}) \qquad (3.26)$$

This equation can be used for evaluating E when s is known or, vice versa, finding s when E is given. Typical peaks for first and second order kinetics which correspond to (3.23) and (3.25) appear in Figure (3.5). Equations (3.22) and (3.24) do not cover all single-trap single recombination centre TL peaks. A more general model for single-trap single recombination centre TL processes was given by Italperin and

Braner [19]. They found that if the thermal release of electrons (or holes) is to the conduction (valence) band, then in a wide range of cases a good approximation to the TL intensity is given by

$$I = dm/dt = sn \exp(\frac{-E}{kT}).A_m m/[A_m m + A_n(N-n)] \qquad (3.27)$$

where N is the concentration of traps, n the concentration of electrons in traps, m the concentration of holes in recombination centres, and A_m and A_n the recombination and retrapping probability respectively. A general solution of equation (3.27) is possible by numerical methods if a certain relationship between m and n is assumed. A useful equation can be assumed for TL peaks [16] which is neither first nor second order kinetic differential equation:

$$I = -dn/dt = s'' \, n^b \exp(\frac{-E}{kT}) \qquad (3.28)$$

where b (the kinetic order) is an empirically determined parameter which can have values other than 1 or 2, and s'' is a pre-exponential factor of dimensions $sec^{-1} \, cm^{3(b-1)}$. The solution of equation (3.28) for b = 1 is

$$I = s''n_o \exp(\frac{-E}{kT})[(b-1)s''/\beta_{T_o} \int^T (\frac{-E}{kT'})dT' + 1]^{-b/(b-1)} \qquad (3.29)$$

where s'' is defined by

$$s'' = s \, n_o^{b-1}$$

By differentiating equation (3.29) and equating to zero one gets:

$$[(b-1)s''/\beta] \, _{T_o}\int^{T_m} \exp(\frac{-E}{kT})dT + 1 = (s''bkT_m^2/\beta E) \exp(\frac{-E}{kT}) \qquad (3.30)$$

which is the equivalent to equation (3.26) for a general order peak.

In thermally stimulated current measurements, the procedure consists of cooling the system to a temperature which is below the minimum temperature required to prevent thermal activation of the trap level occupants. A voltage is then applied across the sample. After applying the voltage, the system is heated up, and as a result of this, a dielectric relaxation current (relative to the current prior to the establishment of a steady-state conduction [17]) occurs which depends on the thermal activation of carriers from trap levels. As the traps deplete, the current will drop and a steady state current will be established. This phenomenon introduces a peak in the current temperature relationship similar to that occuring in thermoluminescence. Therefore it is possible to obtain certain information about trapping levels in semiconductors or insulators by using this method. It is worth pointing out here that the dielectric relaxation current described is a purely thermally stimulated process as compared with other similar processes which require a pre-excitation of carriers [18]. Simmon and co-workers [20,21,22,23 and 24] have examined thermally stimulated current and developed an expression to determine the depth of the trap level in terms of T_m (where T_m is the temperature at which the maximum current occurs):

$$\beta \Delta E / kT_m^2 = e_n = \nu \exp -\frac{\Delta E}{kT_m} \qquad (3.31)$$

where ΔE is the depth of the trapping level below the bottom of the conduction band, e_n is the emission coefficient for the trap, $\nu (= 10^{11} s^{-1})$ is the escape frequency. Simmon and Nadkarni [20]show

that equation (3.31) can be expressed analytically as follows:

$$\Delta E = T_m[1.92\times10^{-4} \log_{10}(\nu/\beta) + 3.2\times10^{-4}] - 0.15 \qquad (3.32)$$

By substituting the values of T_m, ν and β one can calculate ΔE directly from equation (3.32).

3.4 Absorption Coefficient

Many semiconductors are almost indistinguishable in appearance from metals, having the characteristics of polished metals; the reason for this is their high reflectivity. In the visible region of the spectrum, light is generally absorbed strongly, that is, the coefficient of absorption is high. The characteristic feature of all semiconductors, in the pure state, is that at a certain wavelength (generally in the near or intermediate infra-red), the absorption coefficient drops rapidly so that the material becomes fairly transparent at larger wavelengths. This marked drop in absorption is called the fundamental absorption edge. The wavelength and frequency corresponding to the fundamental absorption edge are given approximately by the equation

$$hc/\lambda = h\nu = E_g \qquad (3.24)$$

where E_g is the forbidden energy gap, since E_g is the energy required to excite an electron from the top of the valence band to the bottom of the conduction band. This transition, however, is not always possible without involving other parameters, so equation (3.24) has to be

modified. In order to obtain an accurate value of the position of the absorption edge, specimens of the highest purity should be used. They should also be high-quality single crystals, since strains tend to blur the edge [25].

Near the absorption edge the absorption coefficient can be expressed as [25 and 26]

$$\alpha = C\ (h\nu - E_g)^{\gamma} \qquad (3.25)$$

where $h\nu$ is the photon energy, E_g is the optical band gap, and γ is a constant. γ can take the value 1/2 or 3/2 depending on whether there is an allowed direct transition or forbidden direct transition respectively (with $k_{min} = k_{max}$ as transitions (a) and (b) shown in Figure (3.6)). In the indirect transition (transition (c) shown in Figure (3.6)) γ is 2. All possible transitions whether indirect or direct for the cases of $k_{min} \neq k_{max}$ or $k_{min} = k_{max}$ are discussed by Smith [25].

To calculate the optical absorption coefficient α from the measured transmission data (T) for each wavelength the following model (Figure (3.7)) was used to derive an expression for α in terms of T.

$$T = (1-R)(1-R')\ e^{-\alpha d} + (1-R)(1-R')R'^{2}e^{-3\alpha d} + (1-R)(1-R')R'^{4}e^{-5\alpha d} + \ldots\ldots$$

$$T = (1-R)(1-R')\ e^{-2\alpha d}\ (1 + R'^{2}e^{-2\alpha d} + R'^{4}e^{-4\alpha d} + \ldots\ldots \qquad (3.26)$$

where T is the transmission, α is the optical absorption coefficient, d is the sample thickness, and R and R' are the reflectances at the air-

film and film-air interfaces respectively. Since R < 1, the geometrical series in parenthesis has a finite sum equal to $1/(1-R'^2 e^{-2\alpha d})$ so equation (3.26) becomes

$$T = (1-R)(1-R')e^{-\alpha d} / (1-R'^2 e^{-2\alpha d}) \qquad (3.27)$$

R and R' are calculated from the formula for reflectance at the interface between two media A and B, as:

$$R_{AB} = (n_B - n_A)^2 / (n_B + n_A)^2 \qquad (3.28)$$

where n_A and n_B are the relevant refraction indices. In the present study the refractive index of the material was determined by examining the interference fringes, which appeared in the high transmission region. The condition for maximum transmission is defined by the following equation:

$$2\,nd = m\lambda \qquad (3.29)$$

and for minimum transmission the equation is

$$2\,nd = (m + 1/2)\lambda \qquad (3.30)$$

where d is the sample thickness, m is the integer denoting the order of the fringe, and λ is the free space wavelength of the incident light. By eliminating m from equation (3.29) and (3.30) and using the data of transmission measurement for successive maximum and minimum transmission, the refractive index can then be easily calculated. The sample thickness was measured with the help of electron microscopy.

Figure (3.8) illustrates the maximum and minimum transmission of one of the samples in the IR spectrum.

CHAPTER 4: CRYSTAL GROWTH

4.1 General Background to Crystal Growth

In nature materials commonly occur in one of the three phases, solid, liquid or vapour, and crystal growth basically involves the control of a phase change. Crystal growth methods can be broadly divided into three main categories.

(i) Solid growth - processes involving solid-solid phase transitions.

(ii) Liquid growth - processes involving liquid-solid phase transitions.

(iii) Vapour growth - processes involving gas-solid phase transitions.

A fourth category (strictly already included in the above definitions) is growth from a solution, because solution growth differs from the methods used for pure melt growth. Solution growth may be from an aqueous or non-aqueous solution (non-aqueous solutions include e.g. solutes dissolved in melts). So we have four main categories of crystal growth techniques.

Solid-solid processes are rarely used except for certain metals where strain annealing is effective and certain cases where a change in crystal structure occurs between the melting point and room temperature. Liquid-solid processes can be achieved by several well-known techniques

e.g. the normal (or directional) freezing technique, zone refining (although that is a solid-liquid-solid process), and crystal growth from solution. Vapour-solid processes include sublimation (even though it is a solid-vapour-solid process) and vapour phase reactions which are used in the epitaxial growth of semiconductors. The gaseous phase may be pure or contain deliberately added gases which act as transporting agents.

Crystal growth techniques will be briefly described within the first three categories.

4.1.1 Solid Growth Processes

4.1.1.1 Annealing or sintering

If a rod or compressed powder of polycrystalline material is held at a temperature close to its melting point for many hours, some grains grow at the expense of others. This method is not ideal for growing large single crystals.

4.1.1.2 Deformation growth

In some cases it is possible to enhance the growth of a large grain by deformation i.e. by rolling or hammering.

4.1.1.3 Polymorphic phase transitions

Allotropic elements such as iron or zirconium, or compounds like CuCl, are polymorphic. They have a transitional temperature at which one phase transforms into another. Accordingly, crystal growth may be

achieved by allowing a temperature gradient to travel through a rod of the material.

4.1.2 Crystal Growth from a Melt

4.1.2.1 Normal or directional freezing

When an ingot is gradually frozen from one end to the other, it is said to have frozen normally or directionally (Figure (4.1)). This process is achieved by placing the ingot in a temperature gradient and then lowering the temperature so that the solid-liquid interface travels progressively from the cold to the hot end of the ingot. Starting with a pure material a large single-crystal region is produced in the resulting ingot.

A single crystal ingot is not always the result of a normal freezing process unless a seed crystal is introduced to the melt. The seed is allowed to touch the melt which is just at the melting temperature, then as the freezing interface moves the seed grows and the whole material will solidify as a single crystal. This method is known as the Kyropoulus method.

4.1.2.2 Crystal pulling method

A more common and well developed technique for growing large single crystals from the melt is the Czochralski or crystal pulling method, illustrated in Figure (4.2). In this technique the melt is kept just above the melting temperature in a crucible of a suitable refractory material (e.g. graphite or quartz) which does not contaminate the

resulting crystal. A seed crystal with desired orientation is dipped into the melt which is then pulled at a slow steady rate to form an ingot which is often a single crystal. During pulling the seed is rotated at a constant speed to maintain a uniform crystal growth which is cylindrical in shape.

The pulling method is a very flexible technique in growing single crystals and by altering the heater power it is possible to control the diameter of the crystal. If the power is increased the diameter of the ingot is decreased and a neck can be produced (Figure 4.2). Necking is used to produce a single crystal from a polycrystalline seed, or it can be used to reduce the dislocation density in the growing crystal so that a dislocation free crystal can be grown.

With certain modifications it is possible to grow successfully a crystal such as GaAs with volatile components. It is even possible to grow crystals of any predetermined cross-section by the pulling method [1,2].

4.1.2.3 Zone refining

Zone refining is not an ideal method of growing single crystals, but by starting with a seed crystal at the start of a zone's run it is possible to produce a single crystal ingot. The principle of zone refining is the passing of a molten zone down an ingot. Many impurities prefer to stay in the melt and hence the solid is purified by successive passages of the molten zone. Figure (4.3) illustrates the basic features of zone refining for a compound with volatile components such as GaAs. The material to be refined is kept in a boat inside a tube at

a suitable ambient temperature so that there is no net tendency for the volatile component to evaporate from the molten zone. A moveable heater melts the molten zone and passes down the ingot.

In float zone refining the zone is passed vertically up through the ingot, and no crucible is used to support it. Only surface tension forces support the molten zone. This method is widely used in industry to produce dislocation free crystals of high purity for integrated circuits (Figure (4.3b)).

4.1.2.4 Flame fusion techniques

Flame techniques, or the Verneuil method, are similar to float zone refining but with the advantage of not requiring a crucible. Basically in this method a seed crystal, the top of which is molten, is fed with molten drops of a source material, fed usually as a powder through a flame or plasma, as illustrated in Figure (4.4).

4.1.2.5 Arc fusion techniques

Arc fusion methods are variants of the flame fusion technique. The arc is struck between a nickel cathode, for example, and a NiO anode the top of which is kept molten by the heat of the arc. Nickel is transported from cathode to anode and is oxidized in the process. The method is restricted to a few oxides (Co, Fe, Te, U) and some ferrites.

High melting point oxides such as Mgo, CaO, etc., may be grown as single crystals inside a charge of their own powders. Here the arc electrodes are buried in the charge which melts near their tips. When

the melt is allowed to freeze slowly, large crystal volumes are frequently found. This is also a crucibleless normal freezing method [3].

4.1.3 Solution Growth Methods

The distinction between the solution growth and melt growth techniques is that in melt growth the solvent (major component) freezes whereas in solution growth it is the solute which crystallizes, usually well below its melting point (assuming it even has one, since some decompose before melting).

Solution growth is a slow process, being generally an order of magnitude slower than melt growth, and also results in less pure crystals. However, high purity materials for the electronics and optical industries are produced from solution [4].

Solution growth can be classified simply into two categories: (a) low temperature solution growth and (b) high temperature solution growth. A more useful classification is into three groups depending on the method of obtaining supersaturation [5]:

(i) Temperature change i.e. by cooling (or in rare cases, heating) the solution.

(ii) Solvent extraction i.e. usually by evaporation.

(iii) Circulation, a two-temperature system in which the solvent passes nutrient from source to seed.

4.1.4 Vapour Growth Processes

Vapour growth processes may be subdivided into three main categories:

(a) Sublimation

(b) Vapour transport

(c) Gas phase reactions

4.1.4.1 Sublimation

In sublimation the vapour of a solid is passed down a temperature gradient and crystals grow from the vapour phase at the cold end. Figure (4.5) illustrates the phase diagram for some elements (e.g. iodine). It shows that for such materials, it is possible to pass directly from solid to vapour phase and back again due to temperature change alone. For these materials, the triple point T is above 1 bar in pressure. Such materials may be grown as crystals directly from the vapour phase in vacuum or in an inert gas at atmospheric pressure. Materials with a triple point below 1 bar (i.e. they transfer to the intermediate liquid phase before reaching the vapour phase) may still be sublimed but at reduced pressure.

4.1.4.2 Vapour transport

The vapour transport process is similar to sublimation except that a gas flow is present to help transport the vapour from the source zone to the crystal growth zone. This process has been used to grow the As_2Se_3 crystals under examination in this project and will be discussed later.

4.1.4.3 Gas phase reaction

In a sense iodine transport is an example of a gas-phase reaction method of crystal growth. Here the iodine acts as a kind of catalyst, transporting the compound, but it is not finally involved in the process. This process is widely used in integrated circuit technology where a new layer of silicon is grown onto an existing polished, etched, slice of crystalline silicon. A typical reaction would be

$$SiHCl_3 + H_2 \rightarrow Si + 3\ HCl$$

4.2 The Structure and Growth of Single Crystals of As_2Se_3

4.2.1 The Crystal Structure of As_2Se_3

Arsenic triselenide (As_2Se_3) forms a layered crystal which is isomorphous [6] with the orpiment structure of As_2S_3 [7] but both As_2Se_3 and As_2S_3 differ in several respects from many other layered crystal structures. The two dimensional extended network which forms the molecular building block in these crystals is held together by virtually pure covalent bonds although within the layer structure, unlike graphite (with its π-bonding), the bonding is entirely σ-type [8]. Also, unlike the transition-metal dichalcogenides (with their complicating d electrons), only s and p valence electrons are involved, and unlike the gallium chalcogenides (with their Ga-Ga bonds between the two halves of the layer), only a single bond type occurs. Thus from a chemical bonding and bonding-topology point of view, the arsenic chalcogenides are probably the simplest type of layered crystals. Nevertheless, crystalographically they are more complex than the other cases

mentioned. Their layer and crystal symmetries are low and their unit cells contain relatively many atoms.

Zachariasen [9] presented a figure using a hypothetical A_2 B_3 compound to provide a two-dimensional analogy for his ideas on the relationship between crystalline and amorphous solids. The A atoms were regarded as bonded to three nearest-neighbour B atoms, the B atoms to two nearest-neighbour A atoms. This structure, in its crystalline form, is illustrated diagrammatically in Figure (4.6). The situation is identical to crystals formed from atoms of column 5 and 6 of the periodic table, as might be expected from the simple (8-n) rule for σ type covalent bonding (n is the number of s and p valence electrons, (8-n) the anticipated coordination). The interlayer bonding in As_2Se_3 and As_2S_3 is highly covalent and the 3,2 coordination follows. Thus the bonding topology is accurately represented by Figure (4.6), although the actual structure is non-coplanar and much less symmetric than that shown in the figure. Photographs of a model representing the As_2Se_3 structure are shown in Figures (4.7a,b). Figure (4.7a) is a view of the layers from above and Figure (4.7b) shows an edgewise view of the adjacent layers demonstrating the thickness of the two-dimensionally extended network and the interlayer separation.

The stacking of layers in the orpiment structure is determined by the geometry associated with providing the closest possible packing. From Figure (4.8b) the thick portions of one layer tend to fit over the thin portions of the next. This is the usual situation in layered crystals, but due to the low symmetry of the individual layers in arsenic chalcogenides, the isolated layer does not allow a multiplicity

of equivalent layer-layer configurations, implying a unique stacking arrangement for optimum packing. Hence the arsenic chalcogenides do not exhibit extensive polytypism which means that the many possible stacking sequences of layer-layer close-packed arrangements found in other layered structures do not occur (for example PbI_2 has at least thirty polymorphic variations [10]). In As_2Se_3 there are no stacking arrangements, other than that shown in Figure (4.7b).

The arsenic selenide unit cell is monoclinic containing ten atoms in each layer, i.e. with a total of twenty atoms in the unit cell, equivalent to four formula units. The unit cell is illustrated in Figure (4.8b). There are five inequivalent sites unrelated by symmetry to one another, two As and three Se sites denoted in Figure (4.9) by (i, ii, iii, iv, v) for clarity.

The As_2Se_3 crystal can be regarded as a molecular crystal in which the molecular unit is macroscopically extended in a two dimensional network such that the molecular unit itself possesses translational periodicity in the network. Thus the single layer can be viewed as a diperiodic molecule with ten atoms in an orthorhombic unit cell consisting of two chains linked by bonds similar in strength to those in the chain.

According to Kitao et al [12] the dimensions of the monoclinic unit cell of As_2Se_3 are a = 11.98 ± 0.011 °A, b = 9.91 ± 0.01 °A, c = 4.28 ± 0.01 °A and = 90 23' 5" while values of a = 12.053 °A, b = 9.890 °A, c = 4.277 °A and B = 90 28' are reported by Dembovskii and Vaipolin [6]. These were measured on single crystal samples and have been confirmed by Crevecover and De Wit [13]. Renninger and Averbach [14] have determined

slightly different cell dimensions and detailed structures using powdered polycrystalline samples of As_2Se_3 and justify their result by comparison of X-ray density [15]. Using the results of Dembovskii and Vaipolin [6] and Vaipolin [16], the agreement is less good. The cell dimensions determined by Mullen and Nowacki [17] are a = 11.475 °A, b = 9.577 °A, c = 4.256 °A and B = 90 41' which are close to those measured by Dembovskii and Vaipolin.

The internal structure of the layer is a consequence of the conformational requirements of the covalent bonding between nearest neighbours. The electron configuration of atomic Se is 4s2, 4p4 and hence it is two-fold co-ordinated while As atoms with an electron configuration 4s2, 4p3 are three fold co-ordinated. The orpiment structure (Zallen and Blossey) [8] is made up of superimposed As_2Se_3 layers in which each As atom is surrounded by three Se atoms and each Se atom is shared by two As atoms. In the layers, the atoms are arranged in the order Se-As-Se-As and form a spiral which, when given a translation parallel to the spiral axis, produces a chain. Such spiral chains run parallel to one another and to the c-axis, while the extra bond of the As atoms produces a bridge between chains by covalent bonds involving a Se atom in the middle of the bridge. The layers are linked to each other by weak Van der Waals forces, so that there is a perfect cleavage normal to the b-axis. The nature of the weak intermolecular forces which act between the layers and which hold the two dimensional network together is poorly understood, although the assumption of Van der Waals forces is widely made (Zallen, Slade and Ward [11], Zallen and Blossey [8]).

4.2.2 The Crystal Growth of As_2Se_3

4.2.2.1 Introduction

The solidification of molten As_2Se_3 under natural cooling usually results in a glassy solid, while under carefully controlled cooling a polycrystalline mass can be produced. This has generally precluded the use of melt growth techniques, although in a few instances [11,13] single crystals of As_2Se_3 have been prepared from the melt by seeding with small single crystals. Single crystals of As_2Se_3 of reasonable size for electrical and optical measurements have so far been prepared by transport in the vapour phase, mainly using a closed tube technique in which a small amount of As_2Se_3 in its glassy form is heated inside a sealed ampoule in a suitable temperature gradient. The technique has been modified by a number of workers to improve the growth rate and size of crystals and the results of these experiments are summarized in the following section.

4.2.2.2 The closed tube technique

It is known that at temperatures around 300 °C As_2Se_3 is a volatile substance which can be sublimed with negligible decomposition [18,19], and Dembovskii and Vaipolin [6] were the first to report a successful attempt to grow As_2Se_3 crystals using vacuum sublimation. They carried out an investigation of the rate of crystallization at two temperatures and showed that the rate at 330 °C is two orders of magnitude higher than at 240 °C. Dembovskii and Vaipolin [6] grew As_2Se_3 crystals in evacuated quartz capsules placed in a furnace at a temperature of 330 °C

and with a temperature gradient of 10-15 °C between the hot zone, containing the initial As_2Se_3, and the cold zone of the capsule. Crystal growth by this method is a very slow process requiring periods varying from two weeks to several months [6]. The resulting crystals are great in number, but of small size with the largest only about 4 x 1.5 x 0.2 mm.

In an attempt to improve and speed up the growth Kitao et al separated the process into two stages, (i) nucleation, and (ii) growth process [12]. They made certain assumptions about the temperature dependence of the rates of nucleation and growth, based upon their observations of supercooling in the melt [12,20]. At temperatures of 300 °C or below the rate of nucleation is relatively high and dominant compared to the growth rate of the crystals. On the other hand at temperatures just below the melting point of As_2Se_3 the rate of growth is high while nucleation is unlikely to take place. Hence Kitao et al started their experiments at a temperature of about 300 °C for the nucleation to take place, and then followed with a growth stage at temperatures of about 350 °C. They were able to grow crystals by vacuum sublimation in a few days, but the crystals were still relatively small in size (4 x 1 x 0.1 mm).

Crevecoeur and De Wit [13] have used a different method; they used a vapour transport agent such as hydrogen or iodine to grow As_2Se_3 crystals in closed tubes. When iodine was used as a transport agent, a small amount of iodine (one percent by weight) was included with the As_2Se_3 glass source before sealing the ampoule. This gave a low partial pressure of iodine vapour in the tube at the growth temperature (330

-400 °C).

When hydrogen was used the tube was first evacuated and then refilled with hydrogen to a pressure of 10 cm Hg at room temperature. Crevecoeur and De Wit also separated the nucleation and growth stages after cleaning the growth zone by heating it to 400 °C. It is thought that iodine assists the vapourization of the As_2Se_3 by forming relatively volatile iodine compounds at the hot zone where the As_2Se_3 source is placed, which decompose to form As_2Se_3 at the cooler growth zone of the tube, the iodine returning to complex again with more As_2Se_3 from the source zone but the precise role of the transporting gas is not clearly defined. With iodine as a transport agent, thick samples were produced (1 mm), in one or two weeks, while with hydrogen thin sheets or needles which extended from wall to wall were obtained in a few days. Growth in the direction perpendicular to the sheets was observed only after a prolonged time.

Smith et al and Street et al [20,21] have also used closed tube techniques to grow As_2Se_3 single crystals although the work of Smith et al was aimed primarily at studying the growth of crystals of mixed compounds of arsenic sulphide and selenide $As_2(S,Se)_3$ using argon as a transport gas. They were able to grow crystals of dimensions up to 20 x 10 x 0.2 mm in a few days. Smith et al [20] believe that the main function of the ambient gas pressure (argon, iodine or hydrogen) is to restrict the flow of the As_2Se_3 vapour to the growing crystal, allowing the growth to occur at relatively slow rates and at higher temperature.

In addition to the experiments of Dembovskii and Vaipolin [6], Kitao et al [12], Crevecoeur and De Wit [13] and Smith et al [20],

several other workers have also used close tube techniques to provide samples of crystalline As_2Se_3 [8,11,22,23,24,25].

4.2.2.2 Growth from the melt

Very limited efforts have been directed to study the growth of As_2Se_3 crystals from the melt. It is well known that during the stage of nucleation a large number of nucleation centres are formed which in turn cause a mass of small crystallites to grow. Nevertheless, Crevecoeur and De Wit [13] report the successful growth of As_2Se_3 crystals from melt. They seeded the transported As-Se (-I) liquid present during the growth of crystals in the cold compartment of the tube. The growth zone was held at 375 °C and the seed crystal grew into the liquid without the necessity of a temperature difference between the liquid and the crystal.

Zallen et al [11] have reported the growth of nearly single crystal ingots of As_2Se_3 by a vertical Bridgman technique from a thallium doped melt. The material grown consisted of lamellar crystals of parallel orientation which could be cleaved to produce single crystal samples.

4.2.3 Growth by Open Tube Techniques

The use of open tube techniques for the growth of single crystals of As_2Se_3 has been reported by two workers. The first report was by Turnbull [26] who examined the growth of As_2Se_3 under a low flow of Ar gas in an open tube system and obtained a few very small platelets at a growth temperature of 325 °C. On the basis of recrystallization studies on evaporated As_2Se_3 thin films, Turnbull concluded that the

optimum growth temperature is 330 °C which is in agreement with the conclusions of Dembovskii [27], but rather lower than found by some other workers [12,13] who have reported that for growth in a closed tube the optimum temperature range is 360-370 °C. Hampton et al [28] have also reported an open tube technique and a similar method, with only slight modification in the gas flow system, has been used by the author in the present research. A photograph of the crystal growth reactor and the associated apparatus is shown in Figure (4.9). Figure (4.10) shows the gas flow arrangement for the open tube reactor system which is shown in more detail in Figure (4.11). The furnace consists of three separate electrical resistance heated zones, which are independently controlled, with provision for two gas inlets (A and B in Figure (4.10)). The furnace was constructed from two concentric transparent fused-silica tubes. The turns of the electrical resistance heater were wound as close together as possible to reduce the possibility of having a significant temperature drop between each pair of windings around the inner tube, but without neglecting electrical isolation. The diameter of the inner tube is 5.5 cm and its length is 81 cm. It is surrounded with an outer transparent fused silica tube of diameter 7.9 cm and length 81 cm, which is concentric with the inner tube. The outer tube carries a jacket of reflective commercial aluminium foil, wrapped in such a way that two windows 2 cm in width run along opposite sides of the length of the furance to allow continuous visual observation of both source and growth zones. The heaters are independently controlled by proportional controllers and chromel/alumel thermocouples which give stability of the furnace temperature to within ±0.5 C [28,29].

The heater tube (inner) as well as the reflecting tube (outer) are

held in place at their ends by two aluminium plates to each of which is fixed an aluminium ring of appropriate dimensions such that the heater tube lies inside the ring while the reflecting tube is supported by the outer surface of the ring. In designing the end plate and rings the different expansion coefficients of the fused silica glassware and the aluminium were taken into consideration. A scale marked in centimetres, shown in Figure (4.9) is placed along the outer tube; this scale helps to give a spatial reference for the arrangement of the glassware within the furnace and the positioning of the source material, and in addition was used by the designer [28,29] to plot the temperature profile of the furnace. Figure (4.10) shows the arrangement of the fused silica tubes which are placed within the furnace and in which the crystal growth takes place. The main work tube is 4.7 cm in diameter and 89 cm long, and extends the full length of the furnace. At the gas inlet end of the furnace a "source" tube is inserted into the work tube which is held in position by an aluminium end cap. There are two gas inlets to the furnace, one feeding the source tube while the other feeds the work tube. At the other end of the furnace (the gas outlet end), a similar tube called the "receiver" tube is inserted into the work tube and situated in the third zone of the furnace. It is here that the nucleation and crystal growth processes take place. With this arrangement of the receiver tube it is possible to remove crystals from the apparatus at the end of each growth experiment.

On the inlet side the gas line is divided into two independent lines fitted with flowmeters and needle control valves to regulate and monitor the flow of gas to the source chambers. The gas outlet passes through a trap of quartz wool and a molecular sieve designed to filter

out fine particles of As_2Se_3 or Se dust leaving the furance. Exhaust gases pass through a bubbler gas trap filled with rotary pump oil, to eliminate back diffusion of oxygen, before being vented to the fume exhaust system of the laboratory. A rotary pump is included for preliminary evacuation and flushing through with the carrier gas. This is connected to the exhaust side of the apparatus via an absorption filter trap (to eliminate contamination by rotary pump oil vapour). The pressure is monitored by a Pirani guage during evacuation to check for leaks. Bypass valves are also included to reduce the pump-down time which would otherwise be long because of the length and relative narrowness of the various tubes making up the reactor.

The design of the reactor did not allow the temperature inside the system to be monitored directly during the actual growth of the crystals, as the presence of a thermocouple might have had an unwanted effect on the growth [29]. The temperatures measured by the control thermocouples are different from the actual temperatures inside the source and growth zones because of the way in which the control thermocouples are positioned. This is an unavoidable consequence of the design of the apparatus. It is possible that the control thermocouple, which gradually shifts in its mounting away from the heater, may introduce an error in the furnace temperature. Since the temperature inside the furnace during the crystal growth could not be measured directly, a series of experiments was carried out by Hampton [29] to draw a temperature profile of the furnace. A typical temperature profile is shown in Figure (4.10). These temperature profiles were used to estimate the source and growth temperatures for the crystal growth experiments.

Nitrogen (N_2) was used exclusively as carrier gas during all the experiments. An inert carrier gas was considered desirable to ensure that no effects due to incorporation of the gas as an active impurity were likely to occur.

CHAPTER 5 EXPERIMENTAL TECHNIQUES

5.1 Sample Preparation

Vitreous As_2Se_3 was used as the source material used to grow the As_2Se_3 crystals. It was prepared from the elements arsenic and selenium (5N purity) together with copper and gallium for the doped crystals. A program was written in "Applesoft" basic to calculate the necessary amount of arsenic, selenium and dopant to produce the desired atomic concentration for the crystal growth. In this program, one first chooses the number of impurity atoms per cubic centimetre, then the type of impurity element and finally the desired total weight. The program is listed in Appendix 1. The results of the calculations were printed out in terms of the amount of arsenic, selenium and impurity in grams. The elements were weighed to an accuracy of 0.01% or, in the case of the impurity, 0.001% to make a total charge of 10 or 20 g. Appendix 2 lists another program which calculates the actual number of impurity atoms per cubic centimetre of the actual weight of each element as input.

The elements were placed in a fused quartz tube under a continuous N_2 gas flow. The tube was first carefully cleaned by ultrasonic agitation in Decon 90 solution followed by rinsing in de-ionised water for at least thirty minutes. It was then baked at 100 °C for several hours to remove all trace of water before being loaded with source materials. The tube was then fitted with a loosely fitting fused quartz stopper and evacuated by diffusion pump to 10^{-5} torr. The stopper was fused into the tubes neck by heating with a gas torch. The tube chosen was of sufficient length to ensure that the charge it contained was not

close to the neck during sealing, in order to minimize the amount of material lost by evaporation during sealing.

The tube was heated in a rocking furnace to fuse the constituent materials. The rocking furnace is illustrated schematically in fig.(5.1). A chromium-aluminium thermocouple was ~~inbeded~~ embedded near the tube to insure the correct furnace temperature was reached. The control of furnace temperature was via a Eurotherm temperature controller. Because of the high vapour pressure of arsenic, the tube was first heated at 550 °C for several hours as a safety measure. Then the temperature of the furnace was increased to 850-1000 °C and held there for 24 hours.

The rocking motion of the furnace ensured good mixing of the melt. After 24 hours the tube was quenched by immersing it in water. The resulting glass was visually homogeneous and suitable as source material for crystal growth. The impurity content was determined by atomic absorption spectroscopy. This provides a quick and straightforward method of determining impurity concentrations down to 0.001 atomic percent and the analysis was performed on both the glass source and crystal samples.

Before each growth the apparatus for crystal growth (work tube, source tube, receiver tube and the rod) were soaked in concentrated sodium hypochlorite solution for several hours to dissolve any remaining traces of chalcogenide compounds from the previous run. The tubes were then rinsed in de-ionised water and soaked in Decon 90 solution (10-20%) for several hours. Decon 90 is a surface active agent which removes Na^+ ions. The tubes were finally thoroughly rinsed in de-ionised water again and allowed to dry in a clean cabinet to minimise contamination.

The set up for the crystal-growth reactor was described in detail in Chapter 4.

5.2 D.C. Conductivity

The d.c. conductivity was measured as a function of temperature in an Oxford Instrument DN1704 variable temperature liquid nitrogen cryostat, Figure (5.2). The cryostat operates on the principle of a controlled continuous flow of liquid nitrogen from a reservoir to a heat exchanger which surrounds the sample space. The sample is top loaded and is cooled by a static column of exchange gas which thermally links the sample to a heat exchanger which is positioned at the lower end of the tube and is connected to a liquid nitrogen supply to allow continuous operation for about four hours. The coolant flows from the nitrogen reservoir down the feed capillary and into the copper heat exchanger. It leaves the heat exchanger by a tube and passes through a capillary before exhausting through a valve at the top plate. A platinum temperature sensor and a non-inductively wound heater are fitted to the heat exchanger. Electrical connections to the heater and temperature sensors are made via a 10-pin feed-through on the top plate of the cryostat. An activated charcoal filter located in the vacuum space allows self-pumping of the vacuum space surrounding the nitrogen reservoir and the heat exchanger when the system is cooled. The sample space and the vacuum insulation space are both provided with relief valves which are set to open if the internal absolute pressure exceeds 1.4 bar.

It was possible to cover a temperature range from 77 to 500 °K

using an Oxford Instrument DTC2 digital temperature controller, with temperature resolution of 0.1 °K, in conjunction with the cryostat.

The conductance of the sample was measured with a Cary 410 vibrating-reed electrometer. This instrument has an input impedance of 10^{17} ohm making it suitable for highly resistive materials. The voltage, supplied by a constant voltage source (Fluke model 412B),was connected to a voltage divider and then applied across the sample. A voltmeter was connected across the voltage divider to monitor the actual applied voltage across the sample under investigation. The circuit is shown schematically in Figure (5.3). the entire system was carefully screened and earthed through one point in order to avoid pick up from stray electromagnetic fields and earth loops.

A sandwich cell configuration was used for d.c. measurements with gold electrodes evaporated onto the crystal platelet surfaces. Therefore d.c. measurements were made in the (010) or b direction (i.e. perpendicular to the plane of the platelets). A standard circular mask of 1 mm diameter was used to define the electrodes. This is small enough to avoid striae that occur on the sample surfaces, otherwise larger dimensions would mean that the mask could cover several striae on the surface and this would introduce a problem in deciding the actual sample thickness under the electrodes. After evaporation of Au electrodes a very thin silver "Dag" track was made from the lower electrode to the edge of the sample which was then firmly adhered to a thin glass substrate. With the aid of silicon grease the glass substrate was firmly adhered to the sample holder. Once again, silver "Dag" contacts were then drawn from both the upper and lower electrodes

onto glass substrates well clear of the sample, this enables electrical contacts to be removed without damage to the fragile crystals. Figure (5.4) illustrates the specimen assembly.

With electrical contacts made, each sample was raised to the maximum temperature (400 °K) and a voltage was applied across the sample and then cycled several times from several tens of volts to zero volts. With the sample at the maximum temperature several volts were applied to the sample overnight. This procedure was found to improve the formation of the electrodes.

5.3 Thermoelectric Power

For thermoelectric power measurements as a function of temperature the specially designed sample holder illustrated in Figure (5.5) was used [1]. After gold contacts were evaporated on the sample surface a small piece of tin wire was pressed on the gold electrode to ensure good thermal contact for the electrode area, since the surface of the As_2Se_3 crystals are not completely smooth. The sample was held between large copper electrodes (Figure (5.6)), which had been ground and lapped to remove any oxide layer in order to give a good thermal and electrical contact to the sample. Each copper electrode was fitted with a copper-constantan thermocouple inserted into a hole in the electrode which was filled with silver "Dag" in order to hold the thermocouple firmly in place and to provide good thermal and electrical contact between the thermocouple and the copper electrode. Each electrode was also provided with a heater in addition to th thermocouple. The top electrode was a copper bar which was insulated from the heater coil by

overwound P.T.F.E. tape. The heated coil of constantan wire was embedded in epoxy resin. The bottom electrode was fixed to an aluminium block, electrically insulated from it by P.T.F.E. sheet. Similar heater elements, embedded in epoxy resin were wound around the block. The aluminium block was attached to a copper flange which was cooled to liquid nitrogen temperature through four small heat transfer washers (Figure (5.5)). The flange was coupled to a liquid nitrogen reservoir by a hollow vacuum jacket copper pipe. Due to the high resistivity of the As_2Se_3 crystals, thermoelectric power measurements at low temperatures were not attempted. The whole assembly was placed in a brass box and evacuated with a rotary pump.

The thermoelectric power of the sample was measured across the copper branch of the thermocouples, with the copper branch of the bottom thermocouple connected to the electrometer "Hi" input while the copper branch of the top thermocouple was connected to the electrometer input earth (Figure (5.6)). The thermocouples were run with a common reference junction at 0 °C in ice-water, and a common output to a Keithley 616 electrometer. The two junctions mounted in the copper electrodes were selected by means of a double-pole change over configuration of reed relays. These relays were chosen because of their high insulation resistance in the off-state. A Keithley multimeter was used to read the temperature from the thermocouple. It normally read the temperature of the top electrode and only when it was necessary to take a reading of the temperature of the bottom electrode were the reed relays energised. With this arrangement it was possible to avoid pick-up interference which would result if the reference junction was connected permanently to the electrometer high terminal

[1]. The temperature gradient $\Delta T = (T_1 - T_2)$ along the sample was kept relatively very small compared to the average temperature $T_{ave} = [(T_1 + T_2/2]$ i.e. $\Delta T \ll T_{ave}$, and it was assumed that the temperature gradient across the sample is linear. By maintaining a small value of ΔT it is possible to minimise errors in measuring the average temperature.

5.4 Thermally Stimulated Current

The thermally stimulated current technique was employed to investigate trapping levels in the crystals. The basis of this technique is to apply a linear temperature ramp to the sample and observe the output current. It was necessary to modify the temperature controller (Oxford DTC2) to provide a temperature ramping facility. The DTC2 was provided with facilities for remote control, which could be achieved by disconnecting the internal set point link on the motherboard of the DTC2. A signal in the range 0 to 5 volts was then connected to the external set point of the temperature controller. A linear sweep generator made by Chemical Electronic Co. was used as a source of ramp voltage. The modified DTC2 temperature controller was used in conjunction with the cryostat described earlier (Oxford Instrument DN1704). Over the range of 120 to 360 °K the temperature increased linearly, and could be read directly from the temperature controller. In the range 360-400 °K the temperature ramp became non-linear and took longer to reach the external temperature set point which was supplied by the ramp voltage from the linear sweep generator.

The procedure for the thermally stimulated current experiments was as follows. The sample was mounted in the cryostat which was filled

with nitrogen gas. The gas acts as a heat exchanger which helps to transfer heat from the heater of the cryostat to the sample, as described earlier in the section on d.c. conductivity measurements. The sample was cooled rapidly from room temperature down to about 150 °K with zero bias and allowed to stabilise. A voltage was then applied to the sample and heating started. The heating was carried out at a known constant rate, typically 4.5 °K/min, with the current monitored concurrently. The heating process was stopped at 400 °K. A Cary 410 vibrating reed electrometer connected to a Vitatio chart recorder was used to measure and log the current. The circuit diagram for the thermally stimulated current experiment is identical to that for the d.c. conductivity experiment (Figure (5.3)). Figure (5.7) illustrates the stages of the thermally stimulated current experiment.

5.5 Optical Absorption

5.5.1 Optical Transmission

Measurement of the optical transmission, T, of As_2Se_3 crystals allows the determination of their optical absorption constant and refractive index. These measurements were carried out on crystals with thicknesses ranging between 1-4 μm, using a Pye Unicam SP500 series 2 Spectrophotometer. The SP500 spectrophotometer is designed to carry out measurements with a single beam within the wavelength range 186-1000 nm. A photometric accuracy of about ± 0.3% T and reproducibility of about ± 0.1% T could be achieved using the "null balance" mode. All measurements were obtained using a tungsten lamp. Three temperatures (80, 150 and 293 °K) were chosen at which to measure the

optical gap for all the samples. The Oxford Instrument DN1704 variable temperature liquid nitrogen cryostat and Oxford Instrument DTC2 digital temperature controller described earlier were used for this experiment. A special sample holder was designed to be fixed to the arm of the cryostat (see Figure (5.8)): the solid cylinder of brass which was used for its construction is shown in cross-section in the upper part of the figure. Holes were drilled in each surface perpendicular to each other and in such a position that the axes passing through the centre of the hole met at a point on the axis of the cylinder. The sample holder was then fixed to the cryostat arm with a screw. The cryostat has a facility for optical measurements because the sample tube in it is fitted with up to five windows made of synthetic sapphire. Four of them are radial and one axial (dia. = 17 mm). The windows in the outer vacuum case have a clear diameter of 35 mm. The sample was placed over one of the holes by first mounting it on a piece of black paper which was then glued to the sample holder. The whole cryostat was placed in the sample compartment of the spectrometer, which was shielded from any extraneous light with a black cloth. After the sample had reached the desired temperature, it was allowed to stay at that temperature for at least two hours.

To measure the transmission, the arm of the cyostat with the sample holder fixed to it was turned in order to position the reference hole (i.e. the uncovered hole) in the path of the incident light so that the null balance of the instrument could be set to 100% transmission for that particular wavelength. Then the cryostat arm was turned 90° so that the sample was in the light path, and a reading of the transmitted light from the sample was taken. This process was repeated for each

wavelength.

5.5.2 Photoacoustic Spectroscopy

An EDT photoacoustic spectrometer (PAS) model OAS400 was used for optical absorption measurements to determine the optical gap of the sample, and it has been extended to cover the near-infrared region of the spectra, where the sample becomes nearly transparent to the incident light. In such ranges, where the sample becomes optically transparent the PAS revealed important features about localized levels in the energy gap of the sample; such information is impossible to obtain with optical transmission methods for thin samples, since the transmission oscillation that occur in the transparent regions will be superimposed on any features that might occur there.

The OAS400 can either be run manually or under PET computer control with appropriate softwear supplied by EDT. The OAS400 system employs a 300 W, high pressure, short-arc Xe continuous source with integral parabolic reflector and a 25 mm diameter sapphire window mounted within a fan-cooled housing. The light source is powered from a separate supply unit with variable lamp current (Figure (5.9)).

Radiation from the Xe source is focussed onto the plane of rotation of a variable speed rotating sector (chopper) which allows source modulation at preset frequencies of 10, 20, 40, 80, 160 and 240 Hz and which is placed adjacent to the entrance slit of the f/4 monochromator as illustrated in Figure (5.9). The monochromator employs two gratings, one for each of the two range 280-800 nm and 900-2.5 μm in the UV/visible and near-infrared respectively. The monochromator scan-rate

is selected from 5 speeds between 10 and 200 nm/min in the UV/visible and between 0.04 and 0.8 nm/min in the IR. A fast forward/reverse facility is also provided. During spectral scans with either grating order, sorting filters mounted at the exit slit of the monochromator are selected automatically to prevent transmission of unwanted radiation to the sample cell; the wavelength scan is inhibited during filter change over.

At the monochromator exit slit, a fraction of the dispersed radiation is reflected onto a pyroelectric detector (Figure (5.9)). This provides a reference signal for correction of the photoacoustic signal for either variation in source intensity with wavelength or fluctuation in source intensity with time. The greater part of the dispersed radiation emerging from the exit slit is focussed directly onto the PAS cell containing the sample to be examined. The OAS400 system employs an aluminium PAS cell with a transparent fused silica window. An aluminium sample tray accommodates solid or liquid samples of up to 2 mm depth, 5 mm width and 15 mm length (Figure (5.10)). The cell contains a sensitive microphone transducer, the diaphram of which forms part of the internal wall of the cell, and an integral preamplifier system.

The signals from the PAS cell and the pyroelectric reference detector are lead to two separate lock-in amplifiers, the reference signals for the phase sensitive detectors in these amplifies being provided by the rotating sector source modulator as illustrated in Figure (5.9). The sensitivity control of the PAS signal channel may be selected between 10 V and 300 mV full scale detection in a 1-3-10

sequence.

The phase angle at which the PAS signal is monitored relative to the reference waveform from the rotating sector may be continuously varied over 360°. The PAS and pyroelectric detector (reference) signals are taken to a ratiometer unit whose output then provides corrected spectral data.

The data stored in the PET computer were normalized with carbon black data, and could then be plotted on an X-Y recorder which is part of the system. The computer also provides a facility for smoothing the data. The results of the measurements can be obtained in two forms, either as numerical data or a graphic plot of signal vs. wavelength. A program was written for a HP9836 mini-computer which gathers the numerical data from the PET computer and plots them out as PAS signal vs. photon energy. This program is listed in Appendix 3.

CHAPTER 6 : RESULTS AND DISCUSSION

6.1 Arsenic Triselenide Single Crystal

Figures (6.1-3) show some typical crystals grown by the open tube technique. All the crystals grew initially in the form of whiskers. Details of crystal growth have been discussed in chapter 4.

Most of the lath-like crystals were found to have striations on at least one of their surfaces. The striations were parallel to the longitudinal axis and can be narrowly or widely separated. They are often much more pronounced on one side of the crystal, and the number of striations vary from crystal to crystal. The existence of striations has also been found in other crystals grown from the vapour, such as Sb_2Te_3 [1] and chalcopyrites [2]. The striations were often most marked near the end of the crystal where the growth began decreasing in size and number towards the other end. It was also noted that the striations were more pronounced on the surface which was facing the direction of the gas flow. Paorici et al [2] report similar observation on the growth of chalcopyrite crystals with iodine as a transport agent. Reed and La Fleur suggested that the striations may be due to constitutional undercooling which causes an instablitiy in the growth conditions [3]. Constitutional undercooling appears as the result of both large supersaturations and the presence of mass convection in the vapour.

Shaw [4] has shown that the striae revealed by etching can be deliberately introduced into epitaxial GaAs films by modulating the temperature of the wafer by about 10 °C, although spontaneous

temperature fluctuations are not likely to occur in typical resistance heated GaAs vapour growth systems using H_2 as a carrier gas [5]. Experimentally it has been proved and accepted that hydrogen and helium are found to provide very much more stable growth conditions than argon or nitrogen under equivalent circumstances [5,6 and 7].

By the use of interference holography Giling [7] has shown that it is possible to visualize gas flow patterns and temperature profiles. In both water-cooled horizontal reactor cells and air-cooled cells with H_2 or He as carrier gas, dynamically stable laminar flow profiles were obtained throughout the reactor. In contrast to the stable flow characteristic of H_2 and He, the flow of N_2, and Ar was always unstable. Giling [7] argues that the instability may be due to : (i) the possibility of turbulence, (ii) instability due to convection, and (iii) instability due to what Giling calls "entrance effects" (i.e. the effect of the distance and position of the gas entrance from the sample). The contribution of these three separate effects to the final flow pattern will depend on the process parameters such as cell design, flow velocities, nature of the gases, temperature, etc.

In Giling's experiments, a flow of gas was passed over a hot susceptor held at a constant temperature. The reactor used in this study to grow As_2Se_3 crystals is more complicated in terms of temperature profile inside the furnace and design complexity. Hence, although Giling's work was based on a different reactor design, a comparative discussion still has some validity, bearing in mind that the reactor used in this project is more complex. Figure (6.4) is a schematic diagram of Giling's reactor which was used to study the

pattern of flow of H_2, He, N_2 and Ar, using holographic techniques. This figure is to be compared with Figure (4.10) which shows the design of the furnace that has been used in the present work.

The combination of flow instability of the gas (in the case of N_2), and the configuration of the tubes can cause a severe structural defect in the crystals grown in this project. Figure (6.5-12) depicts a series of photographs of the cross-section of As_2Se_3 crystals, obtained using a scanning electron microscope (SEM). The cross section of the sample was obtained by cutting it perpendicularly with a new sharp scalpel. These photographs show that there may be gaps between the layers of As_2Se_3 crystals in the range from less than 0.5 μm to more than 40 μm, as illustrated clearly in Figure (6.5 and 6). Figure (6.7) shows the edge of a striae which grew through the crystal. It is clear that layers from these striae may be loosely attached to the crystal. One may regard these striae layers as themselves, layers of a single crystal grown on top of another crystal which were demonstrated by Figure (6.6 and 7). The Figures (6.6 and 7) are of the same crystal and it may be concluded therefore that this As_2Se_3 crystal consists of several single crystals within one unit.

Evidence which proves the unstable conditions in the growth zone is illustrated by Figures (6.8 and 9). In Figure (6.8) two sections of growth can be seen on the surface of the crystal; i.e. the crystalline layer growth which is the smooth gray shade in the photograph, and a glassy island at the edge.

The formation of the glass structure (glassy island) on the crystal layer is probably due to the fluctuation in temperature at the growth

zone which in turn might be due to the unstable transport gas (N_2) and the complexity of the reactor design as discussed previously. Furthermore, it is worth emphasising that the layer with the glassy island was obtained after peeling off the single crystal, i.e. a layer in the middle of the crystal. Figure (6.9) shows another type of surface of an As_2Se_3 crystal. To understand Figure (6.10) it is better to divide the photograph into three sections: (a) the bright flat part, (b) the gray part and (c) the part which shows the trace of the sharp blade. Figure (6.11) is a schematic representation of the cross-section at the edge of the crystal shown in Figure (6.10) and like Figure (6.10) it can again be divided into three sections (a, b and c). Section (a) illustrates the layer structure of As_2Se_3 away from the edge, for both the photograph and the diagram. Here the layers are parallel to each other with a space between the layers. Near the edge of the crystal, the layers start to bend as they reach the edge (section (b) in Figure (6.11)). The bending of the plates was created as the sharp razor was forced through the sample and the layers are pressed closer together until they form a compact structure. Section (c) in Figure (6.10) shows the trace of the razor at the edge of the crystal. This is clearly demonstrated in Figure (6.12), where it can be seen that the striae on the surface of the crystal are bent. If it is assumed that the sample thickness at c is the total thickness of the sample, then the spacing in the crystal can be measured directly by measuring x and y as labelled in Figure (6.11). From Figures (6.10,12 and 13) it was found that the value of x/y is different for one sample to another. From Figures (6.10,12 and 13) the gap shown in the cross-section of these crystals has not been eliminated even under the pressure applied

when cutting the samples, demonstrating that these gaps are structurally formed. Figures (6.14 and 15) on the other hand, show no trace of bending in the crystals suggesting that the layers are closer together and hence these crystals are of better quality for electrical measurements. Figure (6.16) is a picture of a surface of another sample which is again indicative of the unstable conditions in the growth zone.

Further evidence illustrating the difficulties with many of the crystals grown by the open-tube method comes from experimental results, such as I-V measurements and optical transmission measurements. Figure (6.17) illustrates the I-V measurements of one of the crystals. The I-V characteristic labelled (I) represents I-V measurements taken before the sample was used for thermally stimulated current measurements, while (II) was obtained after thermally stimulated current measurements. It can be seen from (I) and (II) in Figure (6.17) that there is a dramatic change in the I-V characteristic. This change may be attributed to structural defects in the samples. Good samples did not show any change, as illustrated in Figure (6.18). This argument is further supported by the calculation of refractive index from the optical transmission measurements (see Table 6.1). Such variations in the values of refractive index can only be related to the presence of gaps between the layers of the crystal which resembles a multilayer structure. Bearing these problems in mind it was extremely difficult to select good samples for electrical measurements but the results discussed in the next section were obtained after many trials with many samples.

6.2 D.C. Conductivity

The d.c. measurements were carried out in a direction parallel to the b axis (i.e. perpendicular to the plane of the crystal). Although in principle the d.c. conductivity is easy to measure, it is often very difficult to acquire reliable results on very resistive samples. Two methods of measurement were employed in the present work. The first involved simply reading the current directly at selected temperature intervals with a fixed applied voltage. In the second method complete current-voltage (I-V) measurements were first carried out at different temperatures.

6.2.1 D.C. Conductivity Results by the 1st Method

This first method required that two I-V measurements were made at two different temperatures as widely separated as possible. The I-V characteristic was plotted, at each temperature on a log-log scale and attention focussed on the overlap of the ohmic regions of the two I-V plots. A voltage (V) was selected in the region of overlap and with this fixed voltage applied, d.c. conductivity measurements were made by measuring the current through the sample as the temperature was varied. The sample conductance was obtained from the ratio (I/V) with V constant throughout.

Figures (6.19,20 and 21) show the results of d.c. measurements using the first method. The first two figures are for pure As_2Se_3 crystals while the third is for a crystal of composition $Cu_{0.1}(As_{0.4}Se_{0.6})_{99.9}$. The activation energy E_o from these results are

listed in Table (6.2).

The first method was, in fact, not suitable for many of the samples studied. One difficulty in applying it was that sometimes no overlapping ohmic region occured in the I-V plots, and an example is shown in Figure (6.22). On other occasions there was no ohmic region at all. It was thought initially that these problems might be related to electrical contact effects and hence some experiments were carried out with different metals, namely Nb, Al as well as Au which was normally used. The problems with the I-V characteristic still persisted however.

As pointed out in section (6.1), the instability of growth conditions associated with the open-tube technique of crystal growth probably causes macroscopic structural defects in the sample. It is possible that behaviour of certain samples which have no ohmic region in their I-V plot can be accounted for by these defects. Accordingly, the second method was adopted for all samples which did exhibit ohmic behaviour, irrespective of whether overlapping ohmic regions existed or not.

6.2.2 Results Obtained by the 2nd Method

As mentioned previously, complete I-V measurements were carried out at different temperatures, and the temperature range covered was normally 340 - 400 °K, but in some cases 330 - 460 °K. The conductance was obtained from the slope of the ohmic portion of the I-V curves and where no ohmic region was found the data was neglected.

Results for all the various samples are shown in Figure (6.23-27). In most cases there are two I-V plots for two different samples of the same kind and the corresponding figures are labelled (a) and (b); in these cases the figures labelled (c) are graphs of log σ vs. (1/T) for the two samples. In other cases there is only one sample and the I-V characteristic is labelled (a) with (b) the corresponding log σ vs. (1/T) plot. Only in the case of pure As_2Se_3 the figure labelled (c) corresponds to conductance vs. (1/T). All the results are also tabulated in Table (6.3). A list of the activation energy, E_σ obtained from the log σ vs. (1/T) results are given in Table (6.4). Two immediate conclusions can be drawn. First, the thermal activation energies obtained from different samples of the same type are almost the same, with at most 0.03 eV deviation. Recall from Table (6.2), that the deviation of the activation energy obtained from the first method is about 0.11 eV for samples of the same type (i.e. pure As_2Se_3 crystals). This high deviation in E_σ with the first method is due to the fact that the selected voltage (V) is inappropriately chosen, as shown in Figure (6.28) for some samples. The second conclusion from Table (6.4) is that the introduction of impurities does not have any appreciable effect on the activation energy for conduction. This is in contrast to Pfister and Morgan's [8] results, where they report a change in activation energy of amorphous As_2Se_3 samples with the introduction of Ga impurity, while Cu shows no effect on the activation energy. In their paper, they report that the activation energy decreases with the addition of Ga impurity.

Wood and Owen [9] reported an activation energy of 0.95 eV and 1.1 eV from d.c. measurement for As_2Se_3 single crystals grown in closed

tubes with H_2 and I_2 as vapour transport agents respectively. Marshall [10] also used crystals grown in closed tubes with hydrogen, as the transport agent and reported thermal activation energies between 0.94 - 1.05 eV. Brunst and Weiser [11] measured an activation energy of 0.77 eV, but their crystals were grown by using iodine as a transport agent and argon as a carrier gas. Hampton, Owen and Dryburgh [12] reported a value of 0.95 eV for crystals grown under the same conditions and with the same crystal growth reactor as used in this project. From these different activation energies reported by different workers using different crystal growth techniques, it seems that the ambient gas under which crystal growth takes place has an effect on the electronic properties of the crystals. Results from the literature and the present work are summarized in Table (6.5). Similar observation was reported by Owen et al [13] on the growth of single crystals of anthracene in He, Xe, Ne and vacuum and he observed consistent change in E_o depending on the gas used.

6.3 Thermally Stimulated Current

The experimental arrangement was described in section (5.4) and results of the thermally stimulated current (TSC) measurements are presented in Figures (6.29 and 30). Measurements were carried out perpendicular to the plane of the sample. Only one sample showed a reproducible peak with this technique. In both Figures (6.29 and 30), the only difference of experimental condition is the applied voltage. In Figure (6.29) it was 10 V while in Figure (6.30) it was 20 V. From both measurements it was found that the temperatures T_m at which the current reaches its maximum value was the same and equal to 284 °K. The

constant temperature rate β in both measurements was approximately 0.80 degree/sec. By substituting the values of T_m and β into equation (3.32) (which is rewritten below) the trap activation energy can be calculated:

$$\Delta E = T_m[1.92X10^{-4} \log_{10} \frac{\nu}{\beta} + 3.2X10^{-4}] - 0.15 \qquad (6.1)$$

$$\Delta E = 0.6 \text{ eV}$$

where ν is the escape frequency ($\nu = 10^{11}$). This value of ΔE is the same as the activation energy which Shaw et al derived from their photoconductivity measurement on As_2Se_3 crystals [14]. They associated this activation energy with the presence of a donor level 0.6 eV below the conduction band. This energy level is also found to fit well with the interpretation of the photoacoustic peaks in the near-infrared region, which is discussed later in section (6.5.2).

As discussed earlier in section (3.4), in the thermally stimulated process (TSP) there are three kinetic orders (first, second and general order). From the symmetry of the peak shape, it is possible to determine the kinetic order from the form factor (μ_g), where μ_g is defined as (δ/ω) with $\omega = (T_2-T_1)$, $\delta = (T_2-T_m)$ and T_1 and T_2 are the half intensity temperatures at the low and high temperature side of the peak, as illustrated in Figure (6.31) [15].

For a first order peak, Halperin and Braner [15] numericaly determined a value for μ_g equal to 0.42 and for second order peak μ_g is equal to 0.52. For intermediate values of μ_g, the kinetic order (b) has a value $1<b<2$, but if $\mu_g>0.52$ then $b>2$ and if $\mu_g<0.42$, $b<1$ [16]. Values of b other than 1 or 2 are referred to as being of general order,

and several workers report such values [17,18,19,20 and 21]. Takuchi et al [22] reported a thermoluminescnce peak in iron-doped MgO which was of second order at low concentrations of iron, and generaly changed to about 1.3 at higher concentrations. Figure (6.32 and 33) are a plot of the same results of Figure (6.29 and 30). but with I vs. T. The form factor μ_g was found to be 0.7 and 0.51 from Figure (6.32 and 33) respectively. They should of course be the same, since they are from the same sample and they should have the same kinetic order. The reason for the difference could be due to the initial rise in the TSC being (i.e. the section of the peak at which T<Tm) field dependent, and this is supported by the following argument. According to Simmons and Taylor [23] and Chen and Kirsh [16] from the plot of ln I vs. (1/T) (as in Figures (6.29 and 30)) for I<Im should yield a straight line with the slope equal to (-ΔE/kT), thus enabling the immediate evaluation of ΔE, which should be equal to ΔE calculated from equation (6.1), i.e. ΔE=0.6 eV. The values of ΔE measured from the shape of Figure (6.29), for which the applied voltage was 10 V, is 0.74 eV, while from Figure (6.30), in which case 20 V was applied, is 1.4 eV. Note that, except for the applied voltage, the condition for the experiments leading to the results in Figure (6.29 and 30) were exactly the same and this observation strongly supports the suggestion that the slope of the initial rise is voltage (field) dependent. Accordingly, it is not possible to determine the kinetic order of the thermally stimulated process from the form factor μ_g.

6.4 Thermoelectric Power

The apparatus described in section (5.3) was used to make

thermopower measurements on samples of $Cu_{0.1}(As_{0.4}Se_{0.6})_{99.9}$ $Cu_{0.17}(As_{0.4}Se_{0.6})_{99.83}$ and pure crystalline As_2Se_3. Thermoelectric power measurements were made along the b axis. When the temperature gradient across the sample is reduced to zero, there should be no thermovoltage across the specimen, but this was not the case, and with zero gradient a small "offset" voltage was still detected. Thus several measurements of thermovoltage (i.e. V vs. ΔT) were made with the same mean temperature T, but with different temperature gradients across the sample. Figures (6.34,35 and 36) are plots of thermovoltage V against ΔT for different mean temperature T (with the value of T held constant) for doped and pure As_2Se_3 crystals. The Seeback coefficient is obtained from the slope of the straight line in the figures for each mean temperature and these slopes were calculated using the linear regression method. In the apparatus used (see section (5.3)) there was a significant separation between the thermocouples and the sample and it is to be expected therefore that a slight difference exists beween the actual and the measured sample temperature. This in turn could account for the offset voltage, or it could be due to instrumentation factors.

Figures (6.37,38 and 39) show the measured thermopower as a function of reciprocal temperature for samples of $Cu_{0.1}(As_{0.4}Se_{0.6})_{99.9}$ $Cu_{0.17}(As_{0.4}Se_{0.6})_{99.83}$ and As_2Se_3. From Figures (6.38 and 39) it is clear that there is a substantial scatter in the data for the doped samples, which makes it difficult to draw any conclusions. This could be due to the macroscopic structural defect discussed earlier in section (6.1). On the other hand, consistent thermopower measurements were obtained with undoped As_2Se_3 crystals and results plotted in the form of Seeback coefficient (S) vs. (1/T) are shown in Figure (6.39). The

measured thermoelectric activation energy (E_s) from this figure is 0.14 eV and thus is much smaller than the thermal activation from the d.c. conductivity experiments ($E\sigma$=0.9 eV see section (6.2)). By contrast, Brunst and Weiser [11] reported 0.7 eV for both E_s and E_σ from their measurements on As_2Se_3 single crystals.

There are two possibilities which may explain the difference of E_s and E_σ in our case. The first is based on the proposition by Newman [24], that in compounds it is always possible to cover a wide range of donor and acceptor concentrations without altering the stoichiometry on the concentration of foreign impurities. Newman considers a semiconductor in which the band gap does not change with temperature and assumes also that it contains a small fixed number of acceptors but the number of donors can increase with temperature. Then the variation of the Fermi level relative to band edges will have the form as illustrated in Figure (6.40). Although the variation of Fermi level with temperature depends on the concentration of imperfections, one may assume for simplicity, linear variation with temperature. If thermoelectric power measurements were carried out on such compounds, then the results will be of the form as shown in Figure (6.41). This prediction has been observed with compound semiconductors [25,26,27 and 28]. It seems unlikely however that this hypothesis is applicable to the present results. The reason is that, from Figure (6.41), one would expect E_s to remain the same for the same type of sample in similar ranges of temperature; E_s will change only if the temperature range is different. It is pertinent therefore to compare results from various sources and Figure (6.42) is a plot of Seeback coefficient (S) vs. (1/T) for amorphous As_2Se_3 (line 1) [29], the results on single crystal As_2Se_3

from the present work (line 2) and from Brunst and Weiser (line 3) [11]. Over similar temperature ranges the slopes are very different in each case and there is a difference in sign between amorphous and crystalline As_2Se_3. This does not seem consistent with Newman's hypothesis. An alternative explanation in terms of the mobility ratio of electrons and holes (μ_e/μ_h) was adopted.

From simple semiconductor physics, it can be shown that in the case of an intrinsic or nearly intrinsic material, with both electrons and holes contributing to the transport of charge (energy) the Seeback coefficient is given by [30 and 31]

$$S = -\frac{k}{e}\left(\frac{b-1}{b+1}\right)\left[\left(E_g/2kT\right) + A\right] \qquad (6.2)$$

where $b=(\mu_e/\mu_h)$ and A is a constant associated with the scattering mechanisms. The slope of (S) vs. (1/T) is then given by:

$$\text{Slope} = \left(-E_g/2e\right)\left(\frac{b-1}{b+1}\right) = 0.14\text{eV} \qquad (6.3)$$

If $\mu_e \gg \mu_h$ the material appears to be n-type and the slope is negative and vice-versa for a $\mu_h \gg \mu_e$. When $\mu_e = \mu_h$ the slope is zero.

From d.c. measurements a thermal activation energy (E_o) of 0.9 eV was obtained (section (6.2)) and optical absorption measurements give an energy gap for the As_2Se_3 crystals equal to 1.83 eV at room temperature (see later section (6.5)). Thus, the Fermi level is almost exactly in the middle of the gap as in an intrinsic semiconductor. Interpreting the data in this spirit (i.e. applying equation (6.3)) results in a mobility ratio:

$$b = \mu_e/\mu_h = 1.9$$

It is relevant to note therefore that in a [illegible] study (in this laboratory) of drift mobility of carriers in As_2Se_3 [illegible] crystals grown by the open tube technique, McNeil [32] observed approximately equal electron and hole mobility each ($\simeq 2$ $cm^2V^{-1}s^{-1}$), and this is consistent with the above interpretation. The results of Brunst and Weiser (E_o and energy gap equal to 0.7 eV and 1.85 eV respectively) imply that their samples are n-type and the slope of (S) vs. (1/T) should be close to E_o.

The question arises, of course, why the present results should be so different in this report from those of Brunst and Weiser. It should be recalled however (section (6.2)) that Brunst and Weiser grew their crystals by a closed tube technique using iodine as transport agent and argon as a carrier gas and it has already been pointed out (section (6.2)) that different growth conditions (e.g. carrier gases) do seem to result in crystals with rather different electrical properties. The crystals used in this present work were grown in an open-tube reactor and one speculative interpretation of the differences noted here is that this technique produces crystals closer to stoichiometry (and hence essentially intrinsic) with N_2 as carrier gas, than the closed-tube technique.

Finally, it is also significant to note that in Figure (6.42) the three lines (one for amorphous and two for crystalline As_2Se_3) extrapolate to essentially the same point of intersection (i.e. the same value of $(\frac{b-1}{b+1})\frac{Ak}{e}$ in this work and $\frac{Ak}{e}$ in Brunst and Weiser case) equal to

0.15 mV K^{-1}).

6.5.1 Optical Absorption and the Optical Energy Gap

Optical transmission measurements were made on thin samples (2-4 μm) at three selected temperatures i.e. 295, 150 and 80 °K and Table (6.6) tabulates the results for doped and undoped samples at different temperatures. The thicknesses of the samples were measured by scanning electron microscope and by taking the wavelengths at which maximum and minimum transmission occur, it was possible to calculate the refractive index, as described in Chapter 3. The calculated refractive index was found to vary considerably from sample to sample (see Table (6.1)) and as mentioned earlier in section (6.1) this could be due to gaps between the crystal layers. In order to examine the effect of the difference in refractive index on optical absorption coefficient, the two extreme values were taken for one of the samples. The result is shown in Figure (6.49), which clearly indicates that even this maximum difference has a very small effect on a plot of optical absorption coefficient against hν (photon energy).

Given a value for the refractive index (n), it is possible to calculate the optical absorption coefficient for each photon energy from the transmission data by applying equation (3.27). As pointed out by Shaw et al [14] , Althans et al [33] and Sussmann et al [34], As_2Se_3 crystals have indirect electronic transition and hence the optical gap was obtained by plotting $\alpha^{1/2}$ vs. hν [30]. Table (6.7) lists the optical gaps for all the samples, at different temperatures.

The optical gaps (E_{opt}) of all samples at the three different

temperatures are plotted linearly against temperature in Figure (6.50) from which E_{opt} at absolute zero ($E_{opt}(0)$), and the bandgap temperature dependent coefficients of the optical energy gap are obtained, i.e.(γ):

$$E_{opt} = E_{opt}(0) - \gamma T \qquad (6.4)$$

The value of $E_{opt}(0)$ and γ obtained from Figure (6.50) are listed in Table (6.8), and also included are results of other workers [14,33,34,35 and 36]. From Table (6.8) it is obvious that $E_{opt}(0)$ is almost unchanged with doping, although the value of E_{opt} at higher temperature does not show the same tendency as $E_{opt}(0)$, but the values of E_{opt} are close together in comparison to the results of the other workers [14,33,34,35 and 36]. From the slope of Figure (6.50) the value of γ was found to be in the range $7\text{-}9\times10^{-4}$ eV K^{-1}, with an average value of 8×10^{-4} eV K^{-1}, which is close to the value γ reported by Kolomiets et al [37] of 7×10^{-4} eV K^{-1}.

6.5.2 Photoacoustic Spectroscopy

Measurements of optical absorption using the photoacoustic spectroscopy (PAS) technique were carried out in two regions of the spectrum namely (a) in the visible region and (b) in the near-infrared and this section considers the two in turn.

6.5.2.1 Visible region

The use of PAS to determine the optical gap is a simple procedure which did not involve any special arrangement or design of a special sample holder. The PAS experiments in the visible region were carried out at 40 Hz chopping rate, and the results are shown in Figure (6.51-57) where the PAS signal is plotted on an arbitrary linear scale vs. photon energy. Table (6.9) tabulates the optical gap (E_{opt}) obtained from these results and it is again clearly demonstrated that for the levels of concentration used here neither copper nor gallium impurities have any effect on the optical gap. Lezal et al [38] and Kolomiets et al [39] reported from their measurements of the absorption edge of amorphous As_2Se_3 that there is a red shift with increasing concentrations of gallium impurity (0.5 to 10%) and the shift was found to be of the same magnitude as the decrease in the transport activation energies reported by Pfister and Morgan [8]. On the other hand there seems to be no report on changes in the gap on doping with copper. Thus, the role of gallium impurities in amorphous and crystalline As_2Se_3 is presumably different but the situation with copper is not clear.

6.5.2.2 Near-infrared region

In this range of the spectrum, two sets of experimental conditions were tried to optimise the PAS signal, i.e. chopping rates of 40 Hz and 10 Hz. The results are illustrated in Figures (6.58a and b) respectively from which it is obvious that the lower chopping rate improved the PAS output signal considerably. Therefore 10 Hz was used for all subsequent experiments in the near-infrared.

A list summarising the figures for all the samples is give in Table (6.10). The PAS spectra for all samples show two distinct peaks. The first occurs at a photon energy equal to 0.9 eV and the second is located at 0.67 eV.

To understand the origin of these two peaks, it is necessary to consider all three possible electronic excitations, as follows:

1. Band-to-band excitation: electrons are excited from the valence band to the conduction band. This occurs with photons having energies higher than or equal to the optical gap.

2. Band-to-localized level excitation: electrons are excited from the valence band to localized states in the forbidden gap.

3. Localized-to-localized excitation: this involves electron excitation between localized level in the forbidden gap.

Figure (6.58b) shows that there is an absorption peak at 0.9 eV which is almost identical (in energy) with the d.c. activation energy and it possibly corresponds therefore to a level in the middle of the energy gap implying an electronic excitation of the second type described above.

The second peak in Figure (6.58b), at an energy of 0.67 eV, probably involves a rather complicated electron excitation, but examination shows that it is a result of two super-imposed peaks. To interpret the origin of multiple peaks it is necessary to consider the

energy band model for As_2Se_3 crystal in Figure (6.65) which is based on the results of this project and several other workers [10,14,40 and 41] (The construction of Figure (6.65) is described in more detail in Chapter 7.) In Figure (6.65) the levels relevant to the multiple PAS peaks are probably those designated E_3, E_4, E_5 and E_6. The energy difference between E_3 and E_5, and E_4 and E_6 respectively are:

$$E_3 - E_5 = 1.23 - 0.6 = 0.63 \text{ eV} \quad (6.5)$$

$$E_4 - E_6 = 0.9 - 0.23 = 0.67 \text{ eV} \quad (6.6)$$

Referring back to Figure (6.58b) there is evidence that the multiple peak is a combination of one at 0.67 eV and another at 0.64 eV. The energy at which the peaks occur cannot be directly related to localized levels at 0.67 eV and 0.64 eV above the valence band however, since they are below the Fermi level and would normally be full (see Chapter 2), precluding the possibility of excitation from the valence band to those levels. Thus the multiple peak at an energy lower than the activation energy (0.9 eV) can only be explained in terms of electron excitation between levels in the band gap, i.e. type 3 electron excitation. On comparing the values of the energy where the multiple peak occurs with the values calculated from equation (6.5 and 6.6), it seems clear that the multiple peak is the result of electron excitation between localized levels, i.e. between E_3 and E_5 for 0.64 eV peak and between E_4 and E_6 for the 0.67 eV peak.

The peaks at 0.64 eV and 0.67 eV are also indirect proof of the presence of the energy levels E_3, E_4, E_5 and E_6. An important point to be stressed here is the absence of any distinct peaks at energies higher

than 0.9 eV. The reason for this is mainly due to the instrument limitation in covering certain ranges of wavelength.

To examine the effect of impurities, all the results are plotted in Figure (6.66) after normalization and from this figure it is clear that impurities have no effect on the location of the peaks, i.e. there is no displacement in the position of the peaks in any of the samples. The only effect is a change in the height of the peaks on the addition of impurities. Figure (6.67) illustrates the influence of impurity concentration on the peak height with the addition of copper and gallium. Both impurities have a similar effect with the peak height going through a minimum as the impurity concentration increases from 0.02 - 0.17 at. % for Cu and 0.01 - 0.8 at. % for Ga. The minimum peak height occurs at 0.1 at. % and 0.12 at. % for Cu and Ga respectively. Another notable feature is the relative height of the peaks at 0.9 eV and 0.67 eV. This is tabulated in Table (6.11) and the results suggest that electronic transition between localized levels can exceed excitation from the valence band to localized levels in the forbidden gap.

CHAPTER 7 : CONCLUSION AND FURTHER WORK

7.1 Crystal Growth

In the previous chapter (section 6.1) it was shown that sometimes there are macroscopic structural defects present in As_2Se_3 crystals grown by the open tube technique using N_2 as the carrier gas. These defects are clearly revealed by scanning electron microscopy on cleaved samples. Samples with such macroscopic defects almost certainly give unreliable results in experiments such as d.c. conductivity, thermopower and thermally stimulated current. The influence of these defects was perhaps most clearly noticeable in the optical absorption measurements, where the calculated refractive indices for different samples differ substantially (see table (6.1)).

As indicated earlier in section 6.1, several other workers [1, 2 and 3] considered that N_2 and Ar are less suitable as gas transport agents for crystal growth than He and H_2. They found that He and H_2 were stable and gave a laminar flow throughout the reactor, which are essential properties for maintaining stable conditions in the growth zone. Furthermore, it was pointed out that (section 6.2) the type of gas used as transport agent for crystal growth has an indirect effect on the electronic properties of the crystal. This observation is supported by a similar study on anthracene crystals grown in different ambients (vacuum, N_2, Ar, He and H_2) [4], which shows a change in the electronic properties of the crystals.

The reason for such macroscopic defects could be associated with

instabilities in the gas flow in the growth zone of the reactor caused by using N_2 as transport agent. In future work it may be desirable to use He or H_2 as the carrier gas instead of N_2. In addition, the use of H_2, in particular, would provide a direct comparison with the crystal grown by the closed tube technique using the same carrier gas. It would also be possible to examine the effect of carrier gas on the electronic properties of the crystal, by comparing the results of this project and that of crystals grown with H_2 or He as transport agent.

7.2 Electronic Transport Properties and Band Structure of Crystalline As_2Se_3

7.2.1 D.C. Conductivity

From the results of d.c. conductivity measurements on pure, copper- and gallium-doped As_2Se_3 crystals (Table 6.4), it is concluded that doping has no significant effect on the activation energy of crystalline As_2Se_3. Brunst and Weiser [5] come to the same conclusion from their experiments on the doping of As_2Se_3 crystals with sodium and telurium, but the doping levels in their case were relatively low (e.g. a maximum concentration of Na ~ 10^{16} cm^{-3}). These observations are in marked contrast to those reported by Pfister and Morgan [6] and Pfister and Taylor [7] on doped amorphous As_2Se_3 (see section 2.4)with comparable impurity levels.

In the present work activation energies for the doped and pure As_2Se_3 crystal were found to be approximately 0.9 eV with an optical

absorption gap of about 2.03 eV at 0 °K (see section 6.5), implying that the Fermi level lies near the middle of the gap. Brunst and Weiser reported an activation energy of 0.77 eV, which together with the thermopower data (i.e. n-type) they interpreted as suggesting that their crystals were more like n-type extrinsic semiconductors. It should be noted however, that their samples were grown using the closed tube technique with iodine as the transport agent and argon as a carrier gas, and as mentioned earlier (in section 6.2 and 7.1) Owen et al [4] pointed out that the carrier gas also has an influence on the electronic properties of the grown crystals. Thus the different activation energy reported by Brunst and Weiser could be considered as a result of using a different carrier gas in the crystal growth process. Different values of the activation energy have also been reported by other workers (see Table 6.5). For example, Wood and Owen [8] reported a value of 1.1 eV and 0.95-0.93 eV for crystals grown in a closed tube with iodine and hydrogen as the transport agent respectively. Hampton et al [9] reported a value of 0.95 eV for crystals grown by the open tube technique with nitrogen as the carrier gas. It seems, therefore, that the activation energies for crystals grown with H_2 or N_2 as the carrier gas are close to each other, while the activation energies of crystals grown with iodine and a mixture of iodine and argon are significantly different.

All of this indicates that the method of crystal growth (i.e. closed or open-tube techniques and the type of carrier and/or transport gas used) has a significant influence on the nature of the crystal in terms of its structure, stoichiometry, impurity content etc. and can noticeably affect its electronic properties.

7.2.2 Thermally Stimulated Current

The results of the thermally stimulated measurements indicate a trapping level of 0.6 eV below the conduction band edge, assuming that electrons are the majority carrier, and this is in agreement with the conclusions of Shaw et al [10] from their photoconductivity measurement on the As_2Se_3 crystals. Evidence for this level was also obtained, indirectly, from the photo-acoustic spectroscopy experiment (see section 6.5.2.2). From the glow curve of the thermally stimulated process, Kolomiets and Mazets [11] and Brunst [12] reported deep traps for majority carriers near 0.55 eV and 0.5 eV respectively. It should be noted that the trap level reported by Kolomiets and Mazets is reasonably close to the value obtained in the present work. The difference in the values of the trap level energy between Brunst (0.4 eV) and Kolomiets and Mazets and this work (0.55 - 0.6 eV) could be due to differences in the method of growing the crystals (i.e. the transport agent).

It is suggested that the initial rise in the plot of ln I vs (1/T) is field dependent (see section 6.3). In future work it would be worth while to examine the effect of the applied field on the initial rise, to derive a field-dependent expression in the "initial rise regime" and hence determine the trap activation energy from the initial rise.

7.2.3 Thermoelectric Power

The activation energy obtained from the thermoelectric power measurement was 0.14 eV which is much smaller than the d.c. conductivity result of 0.9 eV. The only other available data on the thermoelectric power of As_2Se_3 single crystals was reported by Brunst and Weiser [5]. They obtained a value of 0.77 eV which is exactly the same as their dc. conductivity result. The difference between the result of this project and that of Brunst and Weiser is interpreted in terms of the mobility ratio (see section 6.4). It is notable, however, that despite the differences in magnitude and slope, the intercept of the S vs (1/T) straight line with the S axis (i.e. S_o at 1/T = 0) yields a value of 0.15 mV K^{-1} for both the present results and those of Brunst and Weiser. This value is also very close to the value of S_o (S_o = 0.19 mV K^{-1}) for the amorphous p-type As_2Se_3 as derived from the result of Seager and Quinn [13] (see Figure 6.42). From the value of S_o, Brunst and Weiser used the following expression to calculate the coefficient of the Fermi level shift (δ or γ')

$$S_o = -\left(\frac{\delta}{e} + \frac{k}{e}\right)A \qquad (7.1)$$

With A = 2, for scattering by acoustic phonons, they derived a value of δ = -0.32 m eV K^{-1}. In fact this value is found to be incorrect for either A = 1 or 2. Using the same expression the correct values of δ are as follows

For A = 1 $\qquad \delta = -0.24$ meVK^{-1}

For A = 2 $\qquad \delta = -0.16$ meVK^{-1}

In the present case, with the introduction of the mobility ratio as discussed in section 6.4, equation (7.1) will have the form:

$$S_o = -\left(\frac{\delta}{e} + \left(\frac{b-1}{b+1}\right)\frac{k}{e}\right)A \qquad (7.2)$$

Hence the following values of δ are obtained

For A= 1 $\quad \delta = -0.31\ \text{meVK}^{-1}$

For A= 2 $\quad \delta = -0.24\ \text{meVK}^{-1}$

7.2.4 Optical Absorption

Crystalline As_2Se_3 has an indirect electronic transition, as pointed out by Shaw et al [10], Kolomiets et al [14] and Sussmann et al [15]. As mentioned earlier, the macroscopic structure defect in some of the open-tube grown crystals has an effect on the transmission measurements which causes a large scatter in the calculated refractive index (n) (see Table 6.1), but the optical gaps (E_{opt}) derived from the plots of absorption coefficient vs. hν for the two extreme values of n vary only slightly ($\Delta E \sim 0.04$ eV). Taking ΔE into consideration, doping has no effect on the optical absorption gap of crystalline As_2Se_3. A similar conclusion can be drawn from the results of the photoacoustic spectroscopy measurements. Once again these findings are in contrast with those obtained with amorphous As_2Se_3. For instance, Lezel et al [16] and Kolomiets et al [17] report a red shift for amorphous As_2Se_3 doped with gallium impurity for comparable impurity concentrations.

The photoacoustic spectroscopy experiments in the near-infrared region where the As_2Se_3 crystals become transparent, have revealed

interesting features from which it was possible to identify four levels in the gap of As_2Se_3 crystals (see section 6.5.2.2). In addition, the PAS results shows that on adding impurities (either copper or gallium) the density of the various states (levels) first increases, then goes through a maximum at about 0.01 at.%, followed by a minimum at about 0.1 at.%. If these trends are significant and not simply due to experimental fluctuations, they suggest that impurity atoms go into the crystal in different ways, or even different sites, as the concentration increases.

It would be extremely interesting therefore to investigate the impurity dependence of the PAS signal in much more detail

7.2.5 Band Structure

It is possible to construct the energy band diagram for single crystals of As_2Se_3 shown in Figure (6.65). Four of the levels, namely E_3, E_4, E_5 and E_6 were determined in this project and the others were obtained from the results of other workers. The four levels (E_3-E_6) are located at 1.23 eV, 0.9 eV, 0.6 eV and 0.23 eV from the valence band. The first level (1.23 eV) was determined from the thermally stimulated current measurements, and by Shaw et al [10] from photoconductivity. The second level is suggested by the PAS peak at 0.9 eV in the near-infrared region, and is almost identical to the measured d.c. activation energy. The third is also proposed by Brunst [12] from his photoconductivity and is also derived indirectly from the PAS signal in the near-infrared region. Finally the fourth level was again derived indirectly from the PAS measurement in the near-infrared

region; a level at the same energy was also reported by Street et al [18] based on their photoluminescence measurement.

7.3 Defect States

The defect models of Mott, Davis and Street(MDS) [19] and Kastner, Adler and Fritzsche (KAF) [20] have successfully explained the Fermi level pinning, and other unusual features of the electronic properties of chalcogenide glasses, by the interconversion of defects from one charge state to another. From theoretical considerations, Vanderbilt and Joannopoulos (VJ) [21], proposed simlar models, but their theories are also applicable to the crystalline material. According to VJ, levels in the forbidden gap are due to defects from wrongly coordinated atoms (mal-coordinated atoms MCAs in their terminology) and bonds between equivalent (or "like") atoms (like atom bonds LABs). They have calculated the influence of these defects on the density-of- states. In a crystal the number of defects would be reduced, as compared to the glass, by the requirement that the crystal structure should be maintained. In the following the notation of VJ is adopted. Pnictide atoms (such as As) are denoted by P and the chalcogen atom (e.g. Se) by C; the subscript gives the coordination and the number of primes is the number of LABs. For example, C_3''' is a threefold coordinated chalcogen linked to three other chalcogens. Figure 7.1 illustrates the defects in amorphous As_2Se_3 postulated by VJ. They estimated theoretically the energy levels for each defect within a total energy gap of 2.61 eV which is, note, high compared with that obtained experimentally (it is typically 2 eV). The possible defects proposed by VJ for glassy As_2Se_3

with energy levels within the gap are listed in the upper part of Table (7.1), together with the results of Joannopoulos [22]. It must be noted that Joannopoulos estimated a band gap of 1.67 eV, which is lower than the experimental value, but does not comment on the reasons for this difference ! For the purpose of an empirical comparison, therefore the estimated energies in Table (7.1) are scaled to an energy of 2.03 eV (the optical energy gap at 0 °K obtained in the present work for crystalline As_2Se_3) and listed in column (3) of the table. That theoretical data is to be compared with the experimental data derived from the band diagram in Figure (6.65); tentatively, the experimental levels may be related to the theoretical predictions as follows:

Energy Level	Energy eV	Possible Defect State
E_1	1.66	P_2, P_1 (1)
E_2	1.53	C_3'''
E_3	1.23	P_1 (2), C_3
E_4	0.9	P_2''(1), C_2'
E_5	0.6	P_3', P_2' (1)
E_6	0.23	P_2', P_3''', P_2'' (2)

It is also interesting to compare the predictions of Table (7.1) with the band model of amorphous As_2Se_3 suggested by Owen and Spear[23]. Some of the states which they proposed agree closely with levels in Figure (7.2) i.e E_2, E_3 and E_5.

The $P_2'C_3''$ defect resembles a superposition of the C_3''' and P_2'', with the difference that the degenerate orbitals have been split by the

lowered symmetry. This defect is neutral when the As NBO (non-bonding orbital) near midgap (i.e. at 1.3 eV compared with VJ 2.6 eV) contains two electrons. The presence of the lower coordinated pnictides P_1 and P_2 is considered less likely in As_2Se_3 [21,24 and 25] since, as pointed out by Adler [24], the coulombic force U for creating P_2' (or P_2') involves placing two electrons (or holes) in a highly localized orbital, which requires energy larger than the creation of C_1^- and C_3^+. In addition VJ [21] argued that the lower coordinated pnictides (P_1, P_2) are positively charged. In their discussion of possible defects in As_2Se_3. Kastner and Fritzsche (KF) [25] favour the P_4^+ defect over C_3^+, while VJ agree with Adler [24] in considering that P_4^+ are relatively unfavoured due to the large s-p promotion energy required.

Thus, it seems that neither the low nor high coordinated pnictide defects are favoured in As_2Se_3. An alternative possibility, proposed here, is that, a combination of $P_3''C_1^-$ and $C_3'^+$ defects can be responsible for the pinning of the Fermi level, as well as other related features associated with the electronic properties of chalcogenide glasses and crystals. These suggested defects are shown in Figure (7.3). The two possible defects $P_3''C_1^-$ and $C_3'^+$ are shown in Figure (7.3a)and (7.3c) respectively. If an electron/hole pair is generated by any form of excitation (e.g. photons) the $P_3''C_1^-$ centre will capture the hole to form the neutral defect $P_3''C_1^0$, as illustrated in Figure (7.3b). However, this defect is unstable and will seek to capture another hole and so become the positively charged centre $C_3'^+$, as illustrated in Figure (7.3c). According to VJ [21] for any reaction to occur the same "chalcogen excess" must be maintained (they defined the chalcogen excess as the number of Se atoms, say, over and above the

usual As_2Se_3 ratio, introduced by the defects). For $P_3''C_1^-$, the chalcogen excess is 1/2 and the resulting defect (i.e. $C_3'^+$) also has a chalcogen excess of 1/2. The neutral defects (C_1^o and/or $C_3'^o$) will interact directly with each other and transform back to their previous charged state, in this case the reaction is

$$P_3''C_1^o + C_3'^o \rightarrow P_3''C_1^- + C_3'^+ \qquad (7.3a)$$

or

$$2\ P_3''C_1^o \rightarrow P_3''C_1^- + C_3'^+ \qquad (7.3b)$$

or

$$2\ C_3^o \rightarrow P_3''C_1^- + C_3'^+ \qquad (7.5c)$$

The same argument can be used for the capturing of an electron by $C_3'^+$. Thus the proposed combination of defects would pin the Fermi level, and at the same time satisfy the postulates of both Adler [24] and VJ [21] regarding favourable and unfavourable defects in the As_2Se_3 material.

It is recognised that these are very qualitative proposals but it is not possible, at the present time, to estimate the energy involved for quantitative calculations.

REFERENCES

Chapter 1:

1. N.A., Goryunova and Kolomiets B.T., Zh. Tekh Fiz., vol.25, p.984, (1955).

2. A.F., Ioffe and Regel A.R., Prog. Semicond., vol. 4, p. 237, (1960).

3. N.F., Mott, Davis E.A., and Street R.A., Phys. Rev. Lett., vol. 32, 32, p. 961, (1975).

4. M., Kastner, Adler D., and Fritzsche H., Phys. Rev. Lett., vol. 37, p. 1504, (1976).

5. A.E., Owen. Private Communication

6. H., Fritzsche, In Proc.7th Int. Conf. Amrphous and Liquid Semiconductors, (1977). Ed: Spear W.E. (CICL Edinburgh, U.K.)

7. G., Pfister and Morgan M., Phil. Mag. B, vol. 41, p. 209, (1980).

Chapter 2:

1. A.H., Wilson, Proc. Roy. Soc. A, vol. 133,134, p. 458,277, (1931).

2. A., Sommerfeld, Z. Phys., vol. 47, p. 1, (1928).

3. F., Bloch, Z. Phys., vol. 52, p. 555, (1928).

4. S.C., Moss and Braczyk J.F., Proc. Tenth Intern. Conf. Phys. Semicond. (U.SA. E.C. Washington), p. 658, (1970).

5. N.F., Mott, and Davis E.A., "Electronic Processes in Non-Crystaline Material", (1979), Oxford Press.

6. R.A., Street, Adv. Phys., vol. 25, p. 397, (1976).

7. N.F., Mott, Phil. Mag., vol. 22, p. 7, (1970).

8. P.W., Anderson, Phys. Rev., vol. 109, p. 1429, (1958).

9. M.H., Cohen, Fritzsche H., and Ovshinsky S.R., Phys. Rev. Lett., vol. 22, p. 1065, (1969).

10. N.F., Mott, Phil. Mag., vol. 13, p. 989, (1966).

11. N.F., Mott and Davis E.A., Phil. Mag., vol. **22**, p. 903, (1970).

12. J.M., Marshall and Owen A.E., Phil. Mag., vol. **24**, p. 1281, (1971).

13. A., Madan, Le Comber P.G., and Spear W.E., J. Non-Cryst. Sol., vol. **10**, p. 239, (1976).

14. D., Adler and Yoffa E.J., Phys. Rev. Lett., vol. **36**, p. 1197, (1976).

15. P.W., Anderson, Phys. Rev. Lett., vol. **34**, p. 953, (1975).

16. R.A., Street and Mott N.F., Phys. Rev. Lett., vol. **35**, p. 1293, (1975).

17. N.F., Mott, Davis E.A., and Street R.A., Phil. Mag., vol. **32**, p. 1293, (1975).

18. E.A., Davis, "Amorphous Semiconductors," In Topics in Applied Physics, ed. Brodsky M., vol. **36**, p. 41, (1980).

19. R.A., Street, Phil. Mag. B, vol. **38**, p. 191, (1978).

20. M., Kastner, Adler D., and Fritsche H., Phys. Rev. Lett., vol.**37**, p. 1504, (1976).

21. Owen A.E. Private Communication.

22. M., Kastner and Fritsche H., Phil. Mag. B, vol. **37**, p. 199, (1978).

23. M., Kastner, Phys. Rev. Lett., vol. **28**, p. 355, (1972).

24. M., Kastner and Fritzsche H., Phil. Mag. B, vol. **37**, p. 285, (1978).

25. A.E., Owen and Spear W, Phys. and Chem. of Glass, vol. **17**, p. 174, (1976).

26. N.F., Mott and Street R.A., Phil. Mag. B, vol. **36**, p. 33, (1977).

27. N.F., Mott, Phil. Mag. B, vol. **34**, p. 1101, (1976).

28. H., Fritzsche, Graczi P.J., and Kastner M., Phil. Mag. B, vol.**37**, p. 593, (1978).

29. G., Pfister and Morgan M., Phil. Mag. B, vol. **41**, p. 209, (1980).

30. M., Kastner, Phil. Mag. B, vol. **37**, p. 127, (1978).

31. H., Fritzsche, 1977. Proc. Int. Conf. on Amorphous and Liquid Semiconductors. C.I.C.L., Edinburgh.

32. B.T., Kolomiets, Rukhlyadev Y.Y., and Shilo V.P., J. Non-Cryst. Sol., vol. 5, p. 389, (1971).

33. K.S., Liang, 1973. Thesis, Stanford University

34. A.V., Danilove and Myuller R.L., Zh. Prikl. Khim, vol. 35, p. 2012, (1962).

35. A.V., Danilove and El Mosli, Fiz. Tverd. Tela., vol. 5, p. 2105, (1963).

36. J., Petursson, 1975. Thesis, University of Edinburgh.

37. M., Frazer, 1984. Thesis, University of Edinburgh.

38. G., Pfister, Morgan M., and Liang K.S., Sol. Stat. Comm., vol. 30, p. 277, (1979).

39. G., Pfister and Morgan M., Phil. Mag. B, vol. 41, p. 209, (1980).

40. J., Mc. Neil, 1980. M.Sc., Thesis, University of Edinburgh.

41. D., Lezal, Trkal V., Srb I., Dokoupil S., Smid V., and Rosicka V., Phys. Stat. Sol. (a), vol. 12, p. K39, (1972).

42. B.T. Kolomiets, Rukhlyadev Yu. V. and Shilo V.P., J. Non-Cryst. Sol., vol. 5, p. 402, (1971).

43. E., Mariani, Trnocova T., and Lezel E., Phys. Stat. Sol. (a), vol. 16, p. K51, (1973).

44. R., Strunk, J. Non-Cryst. Sol., vol. 12, p. 168, (1973).

Chapter 3:

1. N.F., Mott and Davis E.A., Phil. Mag., vol. 13, p. 989, (1966).

2. J.M., Marshall and Owen A.E., Phil. Mag., vol. 24, p. 1281, (1971).

3. N.F., Mott and Davis E.A., Electronic Processes in Non-Crystalline Solids.

4. P., Nagel, "Electronic Transport in Amorphous Seimconductors." Amorphous Semiconductor. Topics in Applied Physics, vol. 36, ed. M. Brodsky (1980).

5. M.H., Cohen, J. Non-Cryst. Sol., vol. 4, p. 391, (1970).

6. A.E., Owen., "Coherence and Energy Transfer in Glass", Nato conf. Series VI: Material Science, ed. Fleury P.A. and Golding B., vol **9**, p.243, Plenum Press.

7. N.F., Mott, Phil. Mag., vol. **19**, p. 835, (1969).

8. G. Brunst and Weiser G., Phil. Mag. B, vol **51**, p. 67, (1985).

9. H.L., Uphoff and Healy J.H., J. Appl. Phys., vol. **32**, p. 950, (1961).

10. C.H., Seager and Quinn R.K., J. Non-Cryst. Sol., vol. **17**, p. 386, (1975).

11. T.C., Arnoldussen, Menezes C.A., Nakagawa Y., and Bure R.H., Phys. Rev. B, vol. **9**, p. 3377, (1974).

12. C.H., Hurst and Davis E.A., J. Non-Cryst. Sol., vol. **16**, p. 343, (1974).

13. D., Emin, Seager C.H., and Quinn R.K., Phys. Rev. Lett., vol. 28, p. 813, (1972).

14. P., Nagal, Callaerts R., and Denayer M., Garmisch, p. 867, (1974).

15. N.F., Mott, Davis E.A., and Street R.A., Phil. Mag., vol. 32, p. 961, (1975).

16. R., Chen and Kirsh Y., in Analysis of Thermally Stimulated Processes, vol. **15**. Scince of the Solid State, Pergamon Press.

17. J.T Randall and Wilkens M.H.F., Proc. Roy. Soc.(London), vol. **A184**, p. 36, (1945).

18. G.F.J., Catrlik and Gibson A.F., Proc. Phy. Soc., vol. **60**, p. 574, (1948).

19. A., Halperin and Braner A.A., Phys. Rev. , vol. **117**, p. 408, (1961).

20. J.G., Simmon and Nadkarni G.S., Phys. Rev. B, vol. **6**, p. 4815, (1972).

21. G.S., Nadkarni and Simmon .J.G., J. Appl. Phys., vol. **43**, p. 3650, (1972).

22. J.G., Simmon and Taylor G.S., Phys. Rev. B, vol. **7**, p. 1619, (1972).

23. G.S., Nadkarni and Simmon J.G., Phys. Rev. B, vol. **7**, p. 3719, (1973).

24. J.G., Simmon and Taylor G.W., Phys. Rev. B, vol. 6, p. 4804, (1972).

25. R., Smith, "Semiconductor", (1968). Cambridge Press

26. C., Main, 1977. Ph. D. Thesis University of Edinburgh.

Chapter 4:

1. B., Chalmers, La Belle H.E., and Mlausky, A.T., J. Crystal Growth, vol. 14, p. 84, (1972).

2. A.V., Stepanov, p. 1775, (1969). Bull Acad. Sci., USSR 33.

3. J.R., Drabble and Palmer A.W., J. Appl. Phys., vol. 37, (1966).

4. L.J., Schupp, Electrochem. Tech., vol. 36, p. 542, (1968).

5. B.R. Pamplin, "Crystal Growth", Pergamon Press.

6. S.A., Dembovskii and Vaipolin A.A., Sov. Phys. Sol. Stat., vol. 6, p. 1388, (1964).

7. N., Morimoto and Miner J. , 1, p. 160, (1954)

8. R., Zallen and Blossey P.F., "Optical and Electrical Properties", ed. Lee P.A., pp. 231-272, (1976). P. Reidel Publishing Co.

9. W.H., Zachariasen, J. Am. Chem. Soc., vol. 54, p. 3841, (1932).

10. J.I., Hanoka, Vedam K., and Heniscn H.K., J. Phys. Chem. Sol., p. 389, (1967) Supplement.

11. R., Zallen, Slade M.L., and Ward A.T., Phys. Rev. B, vol. 3, p. 4257, (1971).

12. M., Kitao, Asakura N., and Yamada J., J. Appl. Phys., vol. fB8, p. 499, (1968).

13. C., Crevecoeur and De Wit H.J., Crystal Growth, vol. 12, p. 334, (1972).

14. A.L., Renninger and Averbach B.L., Acta. Cryst. B, vol. 29, p. 1583, (1973).

15. A.P., Chernov, Dembovskii S.A., and Chistov S.F., 4, p. 1658, (1968). Izov. Akad. Nauk. SSSR, Neorg. Mater.

16. A.A., Vaipolin, Sov. Phys. Crystallogr., vol. **10**, p. 509, (1966).

17. D.J.R., Mullen and Nowacki W., Kristallogr. Kristallgeom, vol. **136**, p. 48, (1972).

18. S.I., Gorbov and Krestovnikon A.N., Zh. Neorgan. Khimii, vol. 13, p. 136, (1972).

19. Y.E., Orlov, Karasik S.D., Darashkevitch V.R., Malyukov B.A., and Federova C.A., A., Inorg. Mater., vol. **13**, p. 784, (1977).

20. B.A., Smith, Cowlam N., and Sharmah A.M., Phil. Mag. B, vol. **39**, p. 111, (1979).

21. R.A., Street, Austin I.C., Searle T.M., and Smith B.A., J. Phys. C, vol. **4**, p. 4185, (1974).

22. R.F., Shaw, Liang W.Y., and Yoffe A.D., J. Non-Cryst. Sol., vol. **4**, p. 29, (1970).

23. B.T., Kolomiets, Mazets T.E., and Efendiv Sh.M, Sov. Phys. Semicond., vol. **4**, p. 34, (1970).

24. H.L., Althaus and Wieser C., Phys. Stat. Sol. (b), vol. **99**, p. 537, (1980).

25. G., Brunst, (1981), Diploma Thesis, Der Philipps Universitat Marburg.

26. J.G., Turnbull. Report on the Growth of Crystalline As_2Se_3, Honours Report, Electrical Engineering Depatment, University of Edinburgh, (1972), [unpublished].

27. S.A., Dembovskii, Zh. Neorgan. Khim., vol. 8, p. 1534, (1963).

28. C., Hampton, Owen A.E., and Dryburgh P.M., Unpublished.

29. C., Hampton. Private communication.

Chapter 5:

1. B., Flynn, (1977). Ph.D. Thesis, University of Edinburgh.

Chapter 6:

1. I., Sommer, J. Cryst. Growth, vol. **19**, p. 259, (1972).

2. C., Paorei, Zanotti L., and Zucalli G., J. Cryst. Growth, vol. **43**, p. 705, (1978).

3. T.B., Reed and La Fleur W.J., Appl. Phys. Lett., vol. **5**, p. 191, (1964).

4. D.W., Shaw, Electrochemical Society Meeting, Oct.(1971). News Paper No. 194, Cleveland, Ohio

5. B.J., Curtis and Dismukes J.P., J. Cryst. Growth, vol. **17**, p. 128, (1972).

6. B.J. Curtis and Dismukes J.P., Chemical Vapour Disposition, Fourth International Conference, p. 218, (1972).

7. L.J., Giling, J. Electrochem. Soc., vol. **129**, p. 634, (1982).

8. G., Pfister and Morgan M., Phil. Mag. B, vol. **41**, p. 209, (1980).

9. C., Wood and Owen A.E., Sol. Stat. Comm., vol. **20**, p. 329, (1976).

10. J.M., Marshall, J. Phys. C, vol. **10**, p. 1283, (1977).

11. G., Brunst and Weiser G., Phil. Mag. B, vol. **51**, p. 67, (1985).

12. C., Hampton, Owen A.E. and Dryburgh P. Unpublished

13. G.P., Owen, Thomas J.M., Williams D.F., and Williams J.O., J. Chem. Soc. Faraday II, vol. **70**, p. 853, (1974).

14. R.F., Shaw, Liang W.Y., and Yoff A., J. Non-Cryst. Sol., vol. **4**, p. 29, (1970).

15. A., Halperin and Braner A.A., Phys. Rev., vol. **117**, p. 408, (1960).

16. R., Chen and Kirsh Y., "Anaylsis of Thermally Stimulated Processes," in International Series on the Science of the Solid State, vol. **15**, Pergamon Press

17. C., Mountoni, Rucci A., and Serpi P., Ricerca Sci., vol. **38**, p. 762, (1968).

18. R., Chen, J. Electochem. Soc., vol. **116**, p. 1254, (1969).

19. V., Ausin and Al varez-Rivas J.L., J. Phys. C, vol. **5**, p. 82, (1972).

20. P., Macuotta-Serpi, Russi A., and Serpi A., J. Lumin, vol. **9**, p. 488, (1975).

21. R.W., Ward and Whippey P.W., Canad. J. Phys., vol. **50**, p. 1409, (1971).

22. N., Takeuchi, Inabe K., and Nanto H., Sol. Stat. Comm., vol. **17**, p. 1267, (1975).

23. J.G., Simmon and Taylor G.W., Phys. Rev. B, vol. **6**, p. 4804, (1972).

24. P.C., Newman, Proc. Phys. Soc., vol. **79**, p. 1299, (1962).

25. A.S., Epstein, Fritsche H., and Lark-Horvitz K., Phys. Rev., vol. **107**, p. 412, (1957).

26. J., Blanc and Weisberg L.R., Nature, vol. **192**, p. 155, (1961).

27. J., Apple and Kurnick S.W., J. Appl. Phys., vol. 32, p. 2206, (1961).

28. E., Miller, Komarek K., and Cadoff I., J. Appl. Phys., vol. **32**, p. 2457, (1961).

29. C.H., Seager and Quinn R.K., J. Non-Cryst. Sol., vol. **17**, p. 386, (1975).

30. R., Smith, "Semiconductor". Cambridge Press

31. K.C., Kao and Hwang W., "Electrical Transport in Solids," in International Series in the Science of the Solid State, vol. **14**, Pergamon Press.

32. J., McNail, in Thesis, University of Edinburgh, (1980).

33. H.L., Althaus, Weiser G., and Nagel S., Phys. Stat. Sol. (b), vol. **87**, p. 117, (1978).

34. R.S., Sussmann, Searle T.M., and Austin I.G., Phil. Mag. B, vol. **44**, p. 665, (1981).

35. B.T., Kolomiets, Mamontova T.N., and Babaev A.A., J. Non-Cryst. Sol., vol. **4**, p. 289, (1970).

36. R., Zallen, Drews R.E., Emerald R.L., and Slade M.L., Phys. Rev. Lett., vol. **26**, p. 1564, (1971).

37. B.T., Kolomiets, Sarsembinov S.S., Efendiev S.M., Lusis A.R., and Langsdens Y.L., J. Non-Cryst. Sol., vol. **8-10**, p. 1010, (1972).

38. D., Lezal, Trakal V., Srb I., Dokoupil S., Smid V., and Rosicka V., Phys. Stat. Sol. (a), vol. **12**, p. K39, (1972).

39. B.T., Kolomiets, Rukhlyadev Yu. V., and Shilo V.P., J. Non-Cryst. Sol., vol. **5**, p. 402, (1971).

40. R.A., Street, Austin I.G., Searl T.M., and Smith B.A., J. Phys. C, vol. **4**, p. 4185, (1974).

41. G., Brunst, Thesis Der Philipps_Universitat Marburg, (1981).

Chapter 7:

1. B.J., Curtis and Dismukes J.P., J. Cryst. Growth, vol. **17**, p. 128, (1972).

2. B.J., Curtis and Dismukes J.P., Chemical Vapour Deposition, Fourth Intr. Conf., p. 218.

3. L.J., Giling, J. Electrochem Soc., vol. **129**, p. 634, (1982).

4. G.P., Owen, Thomas J.M., Williams D.F., and Williams J.O., J. Chem. Soc. Faraday II, vol. **70**, p. 853, (1974).

5. G., Brunst and Weiser G., Phil. Mag. B, vol. **51**, p. 67, (1985).

6. G., Pfister and Morgan M., Phil. Mag. B, vol. **41**, p. 209, (1980).

7. G., Pfister and Taylor P.C., J. Non-Cryst. Sol., vol. **35**, p. 793, (1980).

8. C, Wood and Owen A.E., Sol. Stat. Comm., vol. **20**, p. 329, (1976).

9. C., Hampton, Owen A.E., and Dryburgh P., Unpublished

10. R.F., Shaw, Liang W.Y., and Yoff A., J. Non-Cryst. Sol., vol. **4**, p. 29, (1970).

11. B.T., Kolomiets and Mazets T.F., J. Non-Cryst. Sol., vol. 3, p. 46, (1970).

12. G., Brunst, (1980). M.Sc. Thesis, Der Philipps-Universitat Marburg.

13. C.H., Seager and Quinn R.K., J. Non-Cryst. Sol., vol. **17**, p. 386, (1975).

14. B.T., Kolomiets, Sarsembinov S.S., Efendiev S.M., Lusis A.R., and Langsdens Y.L., J. Non-Cryst. Sol., vol. **8-10**, p. 1010, (1972).

15. R.S., Sussman, Searle T.M., and Austin I.G., Phil. Mag. B, vol. **44**, p. 665, (1981).

16. D., Lezel, Trkal V., Srb I., Dokoupil S., Smid M., and Rosicka V., Phys. Stat. Sol. (a), vol. **12**, p. K39, (1972).

17. B.T., Kolomiets, Rukhlyadev Yu.V., and Shilo V.P., J. Non-Cryst. Sol., vol. **5**, p. 402, (1971).

18. R.A., Street, Autin I.G., Searl T.M., and Smith B.A., J. Phys. C, vol. **4**, p. 4185, (1974).

19. N.F., Mott, Davis E.A., and Street R.A., Phys. Rev. Lett., vol. **32**, p. 961, (1975).

20. M., Kastner, Adler D., and Fritzsche H., Phys. Rev. Lett., vol. **37**, p. 1504, (1976).

21. D., Vanderbilt and Joannopoulos J.D., Phys. Rev. B, vol. **23**, p. 2596, (1981).

22. J.D., Joannopoulos, J. Non-Cryst. Sol., vol. **35-36**, p. 781, (1980).

23. A.E. Owen and Spear W., Phys. and Chem. of Glass, vol. **17**, p. 174, (1976).

24. D., Adler, J. Non-Cryst. Sol., vol. **35-36**, p. 819, (1980).

25 M., Kastner and Fritzsche H., Phil. Mag. B, vol. **37**, p. 199, (1978).

APPENDIX 1

```
1  PRINT "IMPURITY CONTENT IN CUBIC CENTEMETER IN AS-2 SE-3"
2  PRINT : PRINT
10  REM  WEIGHT OF AS = WAS
12  PRINT "TYPE THE WEIGHT OF AS AFTER QUESITION MARCK,"
14  INPUT "WHAT IS THE WEGIHT OF AS?";WAS
20  REM  WEIGHT OF SE = WSE
22  PRINT "TYPE THE WEIGHT OF SE AFTER QUESITION MARCK,"
24  INPUT "WHAT IS THE WEIGHT OF SE?";WSE
30  REM  WEIGHT OF IMPURITY = WE
32  PRINT "TYPE THE WEIGHT OF IMPURITY AFTER QUESITION MARCK,"
34  INPUT "WHAT IS THE WEIGHT OF IMPUROTY?";WE
40  REM  A$ = "I,CU,GA"
41  PRINT "TYPE IMPURITY YOU LIKE AFTER QUESITION MARCK,": INPUT "WHAT IMP
     URITY YOU LIKE?";A$
42  IF A$ = "I" THEN  GOTO 50
44  IF A$ = "CU" THEN  GOTO 52
46  IF A$ = "GA" THEN  GOTO 54
50 AD = WE * 4.93: GOTO 60
52 AD = WE * 8.92: GOTO 60
54 AD = WE * 5.904: GOTO 60
60  REM     THE WEIGHT OF THE COMPOSITION = W
62 W = WAS + WSE + WE
64  PRINT "COMPOSITION WEIGHT = ";W
70  REM      AVERAGE DENSITY = D
72 D = (AD + ((WAS + WSE) * 4.7)) / W
74  PRINT "AVERAGE DENSITY = ";D
80  REM     VOLUME OF COMPOSITION = V
82 V = (WAS + WSE + WE) / D
84  PRINT "VOLUME OF COMPOSITION = ";V
90  REM   NUMBER OF IMPURITY MOLES = M
92  IF A$ = "I" THEN  GOTO 100
94  IF A$ = "CU" THEN  GOTO 102
96  IF A$ = "GA" THEN  GOTO 104
100 M = WE / 126.9044: GOTO 110
102 M = WE / 63.546: GOTO 110
104 M = WE / 69.72: GOTO 110
110  REM  NUMBER OF IMPURITY ATOMS = N
112 N = M * 6.022E + 23
120  REM     NUMBER OF IMPURITY ATOMS IN CUBIC CENTEMETER = R
122 R = N / V
124  PRINT : PRINT "NUMBER OF IMUPURITY ATOMS IN CUBIC CENTEMETER = ";R
126  END
```

APPENDIX 2

```
1  PRINT "IMPURITY CONTENT IN CUBIC CENTEMETER IN AS-2 SE-3"
2  PRINT : PRINT
10  REM  IMPURITY (%) = X
12  PRINT : PRINT "TYPE THE IMPURITY (%) YOU LIKE AFTER THE QUESITION MARC
    K,"
14  PRINT
16  INPUT "WHAT (%) YOU LIKE?";X
20  REM  AS-2 SE-3 (%) = C
22 C = 100 - X
24  PRINT : PRINT "AS-2 SE-3 (%) = ";C
30  REM  THE WEIGHT OF THE COMPOSITION = W
32  PRINT : PRINT "TYPE THE WEIGHT OF COMPOSITION AFTER THE QUESITION MARC
    K,"
34  PRINT : INPUT "WHAT WEIGHT YOU LIKE? ";W
40  REM  A$ = "I,CU,GA"
42  PRINT : PRINT "TYPE THE IMPURITY YOU LIKE AFTER THE QUESITION MARCK,"
44  PRINT : INPUT "WHAT IMPURITY YOU LIKE? ";A$
50  IF A$ = "I" THEN  GOTO 60
52  IF A$ = "CU" THEN  GOTO 62
54  IF A$ = "GA" THEN  GOTO 64
60 E = X * 126.9044: GOTO 70
62 E = X * 63.546: GOTO 70
64 E = X * 69.72: GOTO 70
70 AS = C * 0.4 * 74.9218
72 SE = C * 0.6 * 78.96
80 T = AS + SE + E
90 PAS = AS / T
92 PSE = SE / T
94 PE = E / T
100 WAS = PAS * W
102  PRINT "AS WEIGHT = ";WAS
104 WSE = PSE * W
106  PRINT "SE WEIGHT = ";WSE
108 WE = PE * W
110  IF A$ = "I" THEN  GOTO 120
112  IF A$ = "CU" THEN  GOTO 122
114  IF A$ = "GA" THEN  GOTO 124
120  PRINT "I WEIGHT = ";WE: GOTO 130
122  PRINT "CU WEIGHT = ";WE: GOTO 130
124  PRINT "GA WEIGHT = ";WE: GOTO 130
130 ASSE = WAS + WSE
132  PRINT "AS-2 SE-3 WEIGHT = ";ASSE
140  IF A$ = "I" THEN  GOTO 150
142  IF A$ = "CU" THEN  GOTO 152
144  IF A$ = "GA" THEN  GOTO 154
150 AD = WE * 4.93: GOTO 160
152 AD = WE * 8.92: GOTO 160
154 AD = WE * 5.904: GOTO 160
160  REM   AVERAGE DENSITY = D
162 D = (AD + (ASSE * 4.7)) / W
164  PRINT "AVERAGE DENSITY = ";D
170  REM  VOLUME OF COMPOSITION = V
172 V = (ASSE + WE) / D
174  PRINT "VOLUME OF COMPOSITION = ";V
180  REM  NUMBER OF IMPURITY MOLES = M
182  IF A$ = "I" THEN  GOTO 190
184  IF A$ = "CU" THEN  GOTO 192
186  IF A$ = "GA" THEN  GOTO 194
190 M = WE / 126.9044: GOTO 200
192 M = WE / 63.546: GOTO 200
194 M = WE / 69.72: GOTO 200
200  REM  NUMBER OF IMPURITY ATOM = N
202 N = M * 6.022E + 23
210  REM   NUMBER OF IMPURITY ATOM IN CUBIC CENTEMETER = R
212 R = N / V
214  PRINT : PRINT "NUMBER OF IMURITY ATOMS IN CUBIC CENTEMETER = ";R
216  END
```

APPENDIX 3

```
10    ! DATA OF THE PHOTO ACOUSTIC ABSORPTION FOR Ga.12(As2 Se3)99.88 IR GLASS
20    COM X(500),Y(500),N,Id
30    INPUT "NUMBER OF YOUR DATA IS 158. PLESE TYPE 158 NOW",N
40    FOR Id=1 TO N
50      READ X(Id),Y(Id)
60    NEXT Id
70    DATA .86,1.25,.87,1.09,.88,.908,.89,1.03,.9,1.26,.91,1.25,.92,1.10
80    DATA .93,1.02,.94,1.02,.95,1.01,.96,.986,.97,.978,.98,.980,.99,.973
90    DATA 1,.964,1.01,.964,1.02,.965,1.03,.959,1.04,.954,1.05,.954,1.06,.958
100   DATA 1.07,.963,1.08,.968,1.09,.969,1.1,.966,1.11,.964,1.12,.960,1.13,.957
110   DATA 1.14,.959,1.15,.952,1.16,.938,1.17,.941,1.18,.960,1.19,.977,1.2,.986
120   DATA 1.21,.981,1.22,.966,1.23,.954,1.24,.956,1.25,.965,1.26,.971,1.27,.971
130   DATA 1.28,.976,1.29,.984,1.3,.983,1.31,.971,1.32,.962,1.33,.962,1.34,.964
140   DATA 1.35,.963,1.36,.967,1.37,.984,1.38,1.01,1.39,1.02,1.4,1.03,1.41,1.02
150   DATA 1.42,1.02,1.43,1.03,1.44,1.04,1.45,1.02,1.46,.982,1.47,1.01,1.53,.962
160   DATA 1.54,.980,1.55,.981,1.56,.982,1.57,.986,1.58,.989,1.59,.987,1.6,.979
170   DATA 1.61,.970,1.62,.965,1.63,.965,1.64,.964,1.65,.963,1.66,.969,1.67,.979
180   DATA 1.68,.984,1.69,.986,1.7,.985,1.71,.977,1.72,.971,1.73,.980,1.74,.991
190   DATA 1.75,.987,1.76,.978,1.77,.980,1.78,.989,1.79,.993,1.8,.993,1.81,.993
200   DATA 1.82,.993,1.83,.995,1.84,1.01,1.85,1.03,1.86,1.06,1.87,1.07,1.88,1.07
210   DATA 1.89,1.07,1.9,1.08,1.91,1.07,1.92,1.06,1.93,1.07,1.94,1.08,1.95,1.07
220   DATA 1.96,1.05,1.97,1.04,1.98,1.03,1.99,1.02,2,1.02,2.01,1.02,2.02,1.02
230   DATA 2.03,1.03,2.04,1.04,2.05,1.03,2.06,1.03,2.07,1.03,2.08,1.04,2.09,1.05
240   DATA 2.1,1.05,2.11,1.04,2.12,1.03,2.13,1.04,2.14,1.05,2.15,1.05,2.16,1.05
250   DATA 2.17,1.06,2.18,1.08,2.19,1.09,2.2,1.08,2.21,1.07,2.22,1.07,2.23,1.10
260   DATA 2.24,1.13,2.25,1.13,2.26,1.13,2.27,1.15,2.28,1.17,2.29,1.17,2.3,1.14
270   DATA 2.31,1.10,2.32,1.09,2.33,1.09,2.34,1.09,2.35,1.11,2.36,1.14,2.37,1.14
280   DATA 2.38,1.13,2.39,1.12,2.4,1.12,2.41,1.11,2.42,1.10,2.43,1.11,2.44,1.11
290   DATA 2.45,1.10,2.46,1.09,2.47,1.09,2.48,1.10,2.49,1.05,2.5,.772
300   GET "PAS_1",1000,1000
1000  !********** PROGRAM TO PLOT PHOTO ACUSTIC SPECTRIUM DATA **********
1010  GOSUB Sort_max
1020  PRINT "MAXIMUM ABSORPTION IS",Max
1030  INPUT "DO YOU WANT TO CHANGE? Y/N",Sor$
1040  IF Sor$="Y" THEN
1050    INPUT "TYPE MAXIMUM VALUE",Max
1060  ELSE
1070    IF Sor$<>"N" THEN GOTO 1030
1080  END IF
1090   GINIT
1100   GRAPHICS ON
1110  GOSUB Write_fig_cap   !************** ROUTINE TO WRITE FIGURE CAPTION ***
1120  INPUT "DO YOU WANT TO PLOT ON SCREEN? Y/N",Scr$
1130  IF Scr$="N" THEN
1140    PLOTTER IS 705,"HPGL"
1150  ELSE
1160    IF Scr$="Y" THEN
1170      PLOTTER IS 3,"INTERNAL"
1180    ELSE
1190      GOTO 1120
1200    END IF
1210  END IF
1220  INPUT "DO YOU WANT TO LABEL AND MARK THE AXES? Y/N",Mark$
1230  IF Mark$<>"Y" AND Mark$<>"N" THEN
1240    GOTO 1220
1250  END IF
1260   GRAPHICS ON
1270   IF Mark$="N" THEN GOTO 1360
1280   CSIZE 2.5
```

```
1290    MOVE 78,100
1300    LORG 6
1310    LABEL "PAS-SIGNAL"
1320    MOVE 18,50
1330    DEG
1340    LDIR 270
1350    LABEL "PHOTON ENERGY eV"
1360    GOSUB Figure_caption    !***************** FIGURE CAPTION ****************
1370    VIEWPORT 26,123,5,90
1380    PEN 2
1390    FRAME
1400    INPUT "ARE YOUR DATA IN THE UV RANGE? Y/N",Range$
1410    IF Range$="Y" THEN
1420      GOSUB Uv_range       !TICKING X AXES ********************
1430      GOSUB Uv_x_axes      !LABELING X AXES ********************
1440    ELSE
1450      IF Range$="N" THEN
1460        GOSUB Ir_range     !TICKING X AXES ********************
1470        GOSUB Ir_x_axes    !LABELING X AXES ********************
1480      ELSE
1490        GOTO 1400
1500      END IF
1510    END IF
1520    GOTO Plot_data
1530  Ir_range: !_____________________________________________
1540    IF Mark$="N" THEN RETURN
1550    WINDOW 0,Max,1500,500
1560    FOR Xa=750 TO 1250 STEP 250
1570      Ya=0
1580      Yb=.01
1590      MOVE Ya,Xa
1600      DRAW Yb,Xa
1610    NEXT Xa
1620    RETURN
1630  Uv_range: !_____________________________________________
1640    IF Mark$="N" THEN RETURN
1650    WINDOW 0,Max,2500,1250
1660    FOR Xa=1500 TO 2250 STEP 250
1670      Ya=0
1680       Yb=.01
1690        MOVE Ya,Xa
1700      DRAW Yb,Xa
1710     NEXT Xa
1720    RETURN
1730  Ir_x_axes: !ROUTIN TO LABEL X AXES _____________________________
1740    IF Mark$="N" THEN RETURN
1750    PEN 1
1760    CLIP OFF
1770    CSIZE 2
1780    DEG
1790    LDIR 270
1800    LORG 5
1810    Ly=-.03
1820    FOR Lx=500 TO 1500 STEP 250
1830      MOVE Ly,Lx
1840      LABEL Lx/1000
1850    NEXT Lx
1860    RETURN
1870  Uv_x_axes: !ROUTINE TO LABEL X_AXES _____________________________
1880    IF Mark$="N" THEN RETURN
1890    PEN 1
1900    CLIP OFF
1910    CSIZE 2
```

```
1920    DEG
1930    LDIR 270
1940    LORG 5
1950    Ly=-.03
1960    FOR Lx=1250 TO 2250 STEP 250
1970      MOVE Ly,Lx
1980      LABEL Lx/1000
1990    NEXT Lx
2000     RETURN
2010 Figure_caption:  !_____________________________________________
2020    IF P$="N" THEN GOTO 2110
2030    DEG
2040    LDIR 270
2050    LORG 6
2060    CSIZE 3
2070    MOVE 12,50
2080     LABEL USING "K";Q$
2090     MOVE 9,50
2100     LABEL USING "K";W$
2110     RETURN
2120 Write_fig_cap:   !_____________________________________________
2130      DIM W$[60],Q$[60] ! ** EACH STRING REPRESENT ONE LINE IN THE FIGURE CAP
TION
2140      INPUT "IS THERE A FIGURE CAPTION ? Y/N",P$
2150      IF P$="N" THEN RETURN
2160        IF P$="Y" THEN
2170          INPUT "TYPE FIRST LINE OF YOUR FIGURE CAPTION",Q$
2180          INPUT "TYPE NEXT LINE OF YOUR FIGURE CAPTION",W$
2190        ELSE
2200          GOTO 2140
2210        END IF
2220      RETURN
2230 Sort_max:    !SORTING MAXIMUM VALUE OF Y_____________________________
2240          Max=Y(1)                          !INITIALIZING MAXIMUM VALUE
2250          I=1
2260          WHILE I<=N                        !START SORTING
2270            IF Max<=Y(I) THEN
2280              Max=Y(I)
2290            END IF
2300            I=I+1
2310          END WHILE
2320      RETURN
2330 Plot_data: !ROUTIN TO PLOT DATA_____________________________________
2340     INPUT "TYPE ANY NUMBER FROM 3 TO 6 FOR PEN COLOR",Pen
2350     PEN Pen
2360     CLIP ON
2370     IF Range$="Y" THEN
2380       WINDOW 0,Max,2500,1250
2390       Id=1
2400       MOVE Y(Id),1240000/X(Id)
2410       REPEAT
2420         X(Id)=1240000/X(Id)
2430         DRAW Y(Id),X(Id)
2440         Id=Id+1
2450       UNTIL Id>N
2460     ELSE
2470       WINDOW 0,Max,1500,500
2480        Id=1
2490        MOVE Y(Id),1240/X(Id)



2500         REPEAT
2510           X(Id)=1240/X(Id)
2520           DRAW Y(Id),X(Id)
2530           Id=Id+1
2540         UNTIL Id>N
2550     END IF
2560         END
```

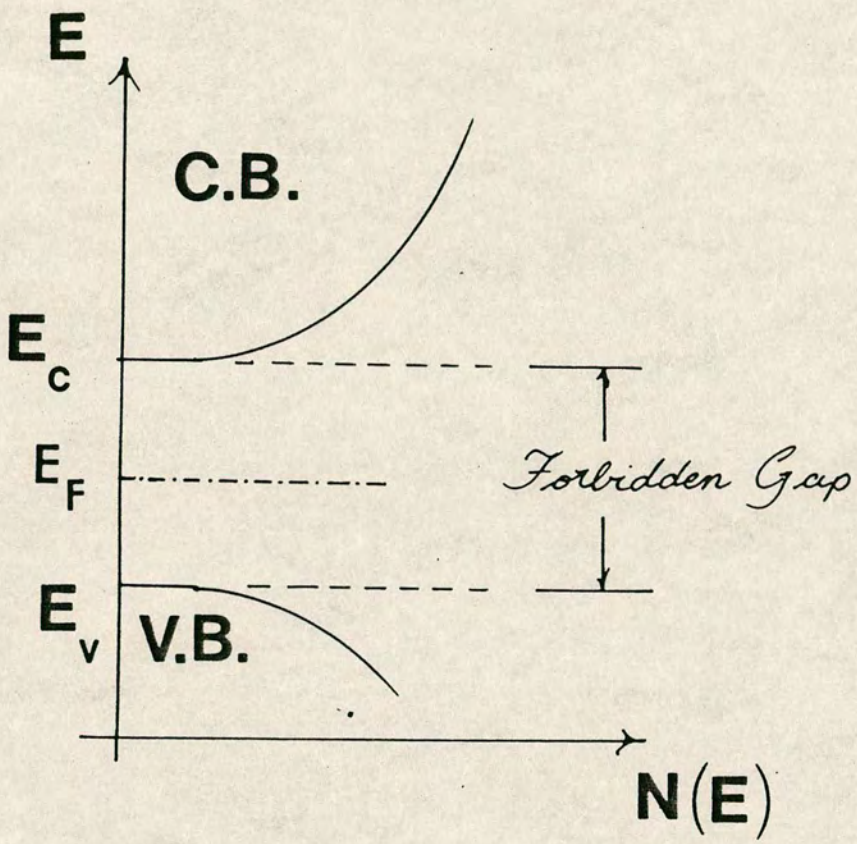

FIG. 2_1

Density of states function for crystalline materials

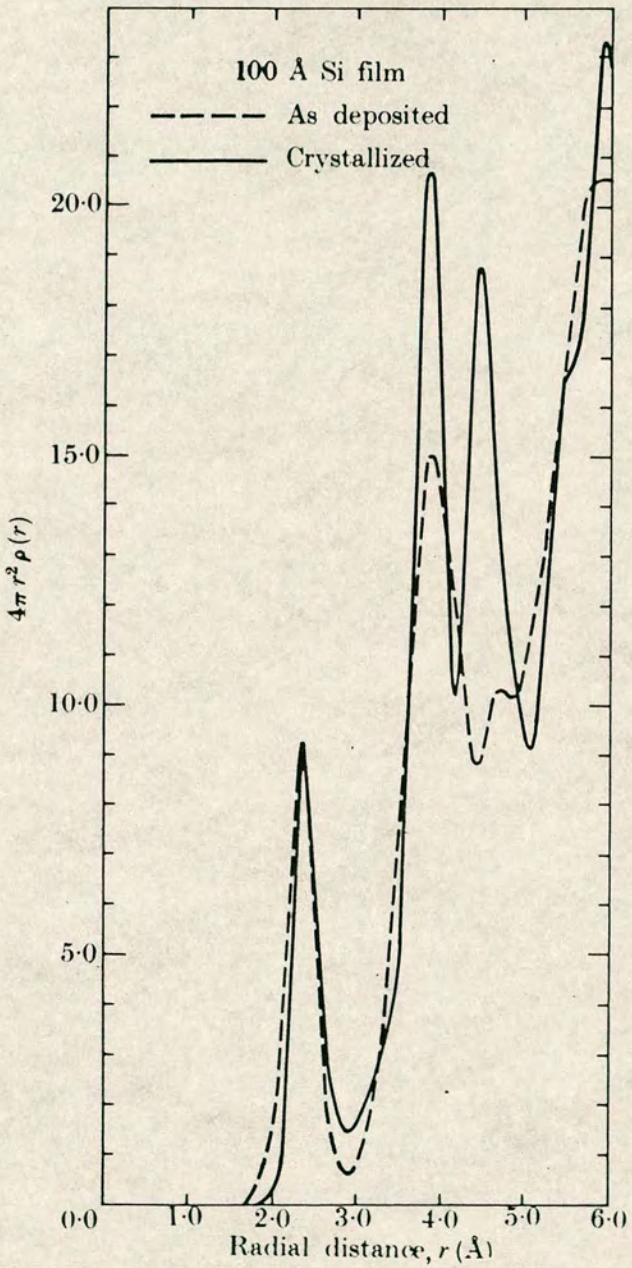

Radial distribution function (RDF) of amorphous (evaporated) and crystalline silicon as determined from analysis of electron diffration data. (From Moss and Graczyk 1970.)

FIG.[2.2]

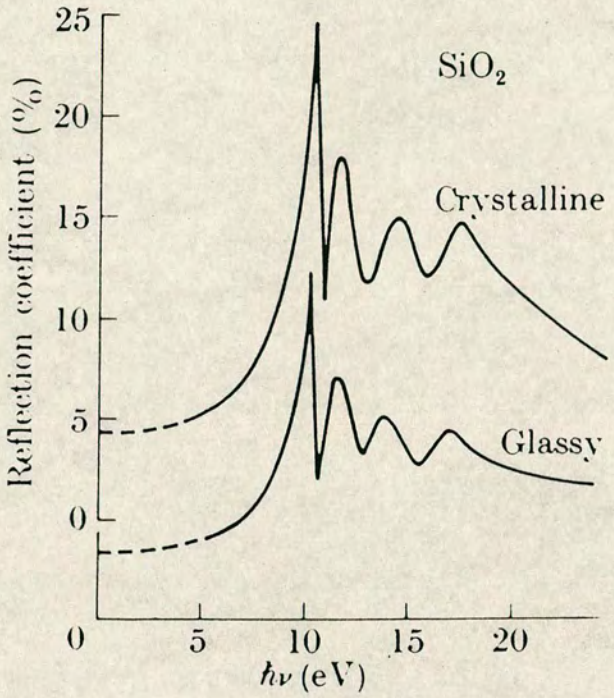

Reflectivity of crystalline and glassy SiO_2. (From Phillip 1972.)

FIG. [2.3]

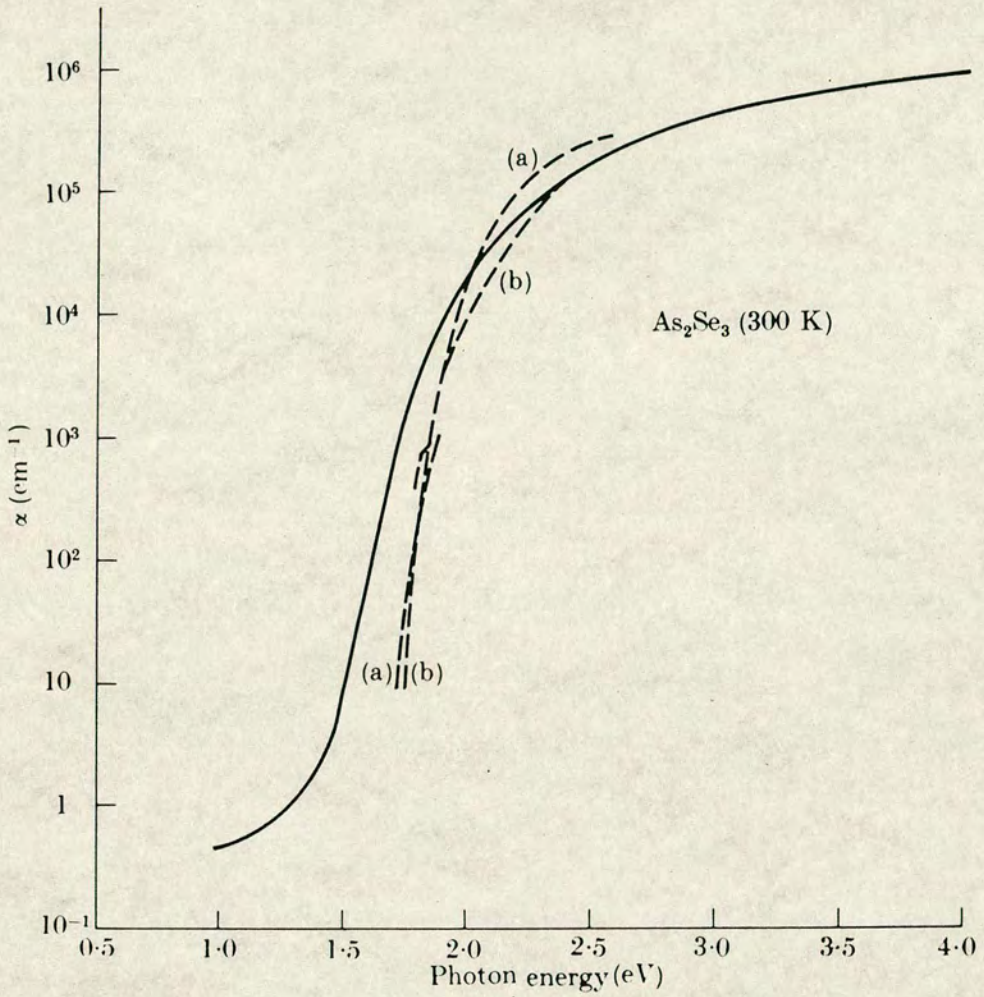

Room-temperature optical absorption edges in amorphous (solid curve) and crystalline As_2Se_3 (broken curves); electric vector (a) parallel and (b) perpendicular to the *a* axis. Data for the amorphous material from Felty and Myers (private communication) and Edmond (1966), and for the crystalline material from Shaw *et al.* (1970) and Zallen *et al.* (1971*a*.)

FIG. [2.4]

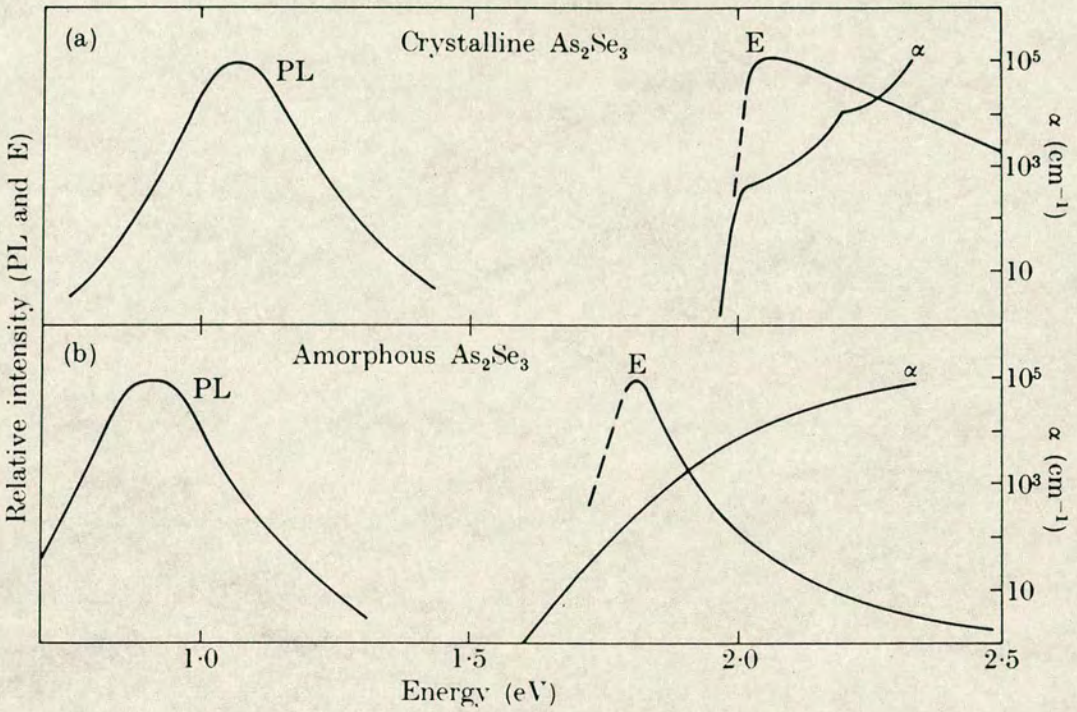

Excitation and photoluminescence spectra and absorption coefficient of crystalline and amorphous As_2Se_3. (From Street 1976.)

FIG.[2.5]

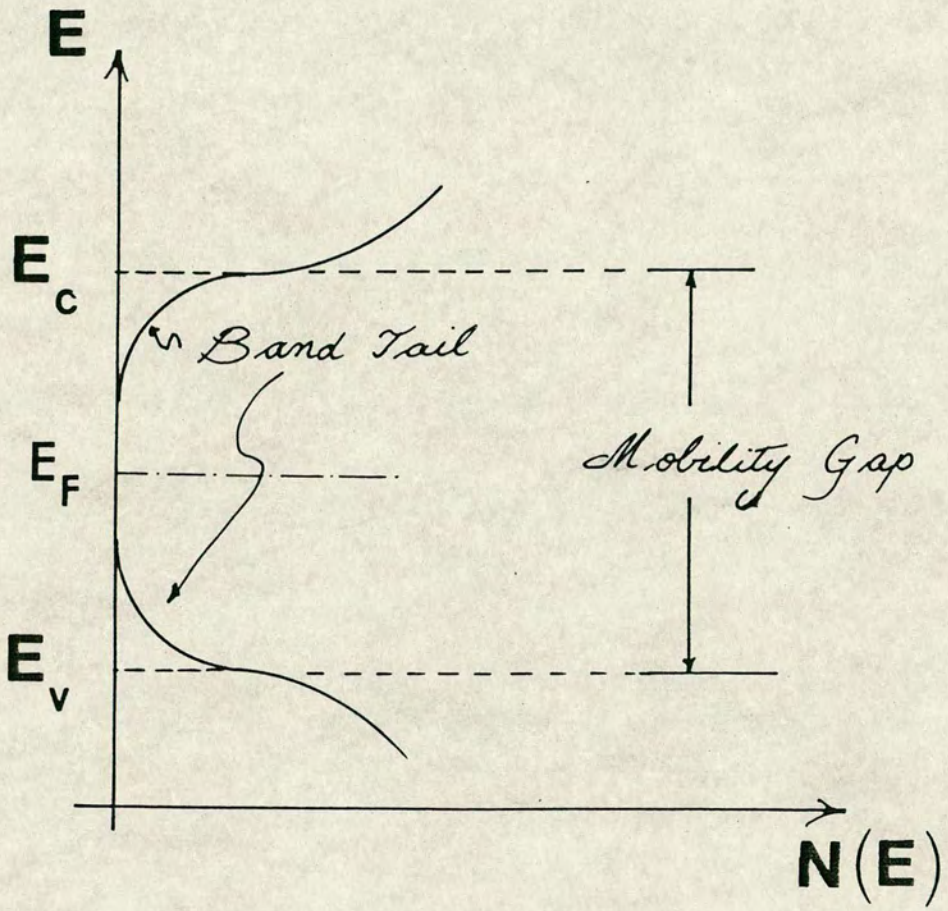

FIG. 2.6

Density of state function for amorphous material

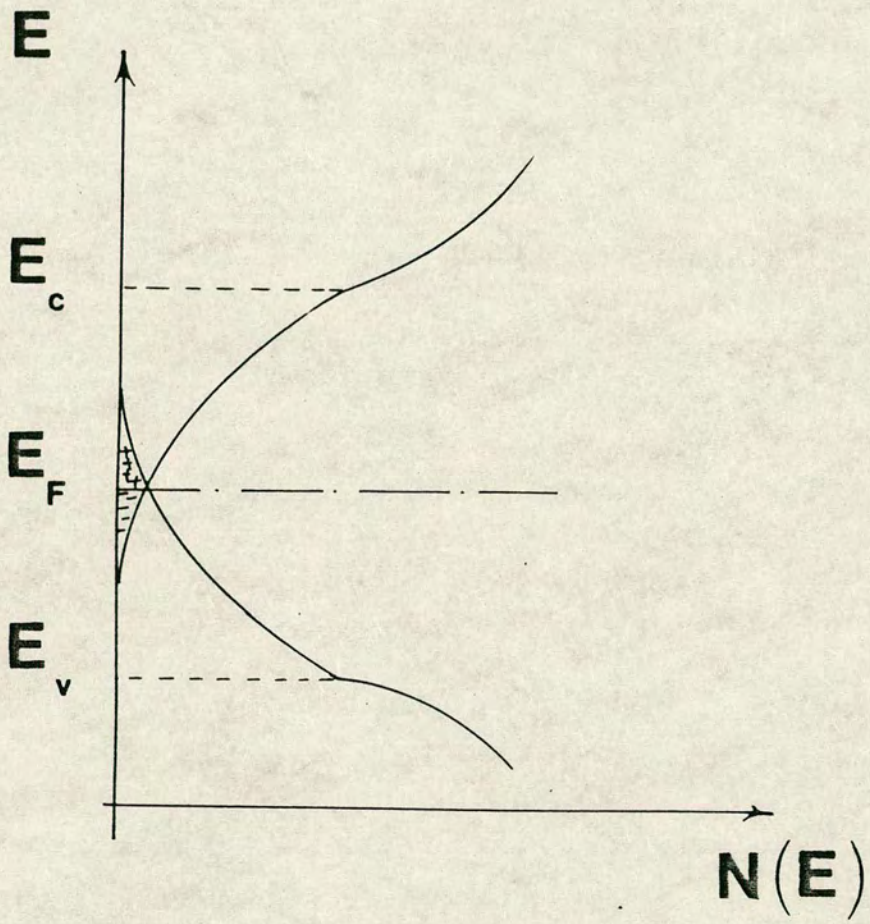

FIG. 2.7

CFO model for amorphous solids

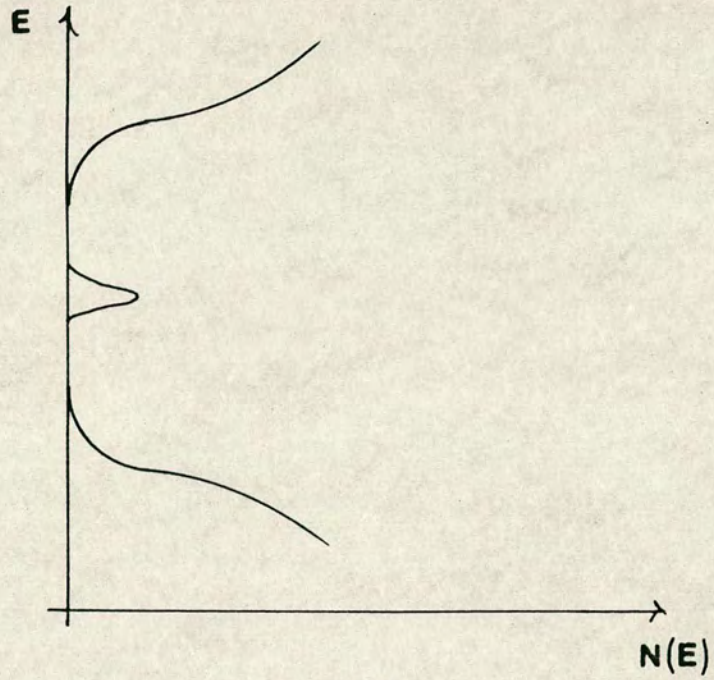

(a)

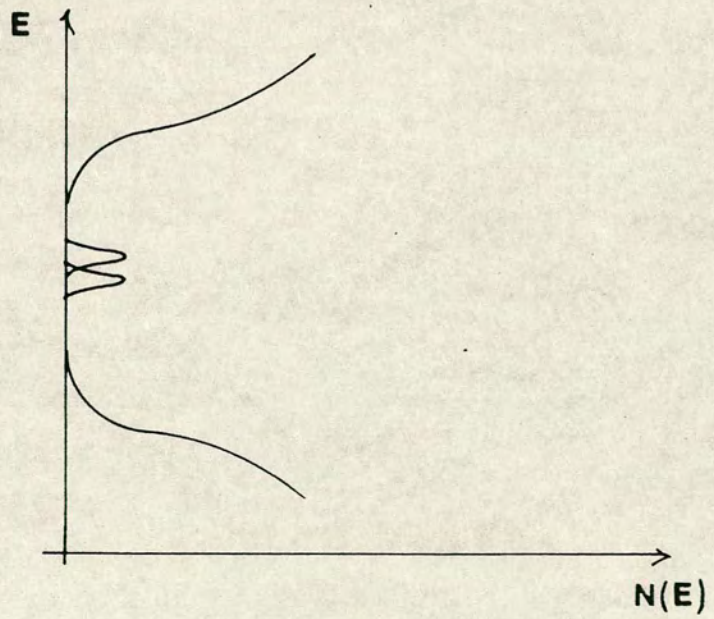

(b)

FIG. 2.8

MD model for amorphous solids

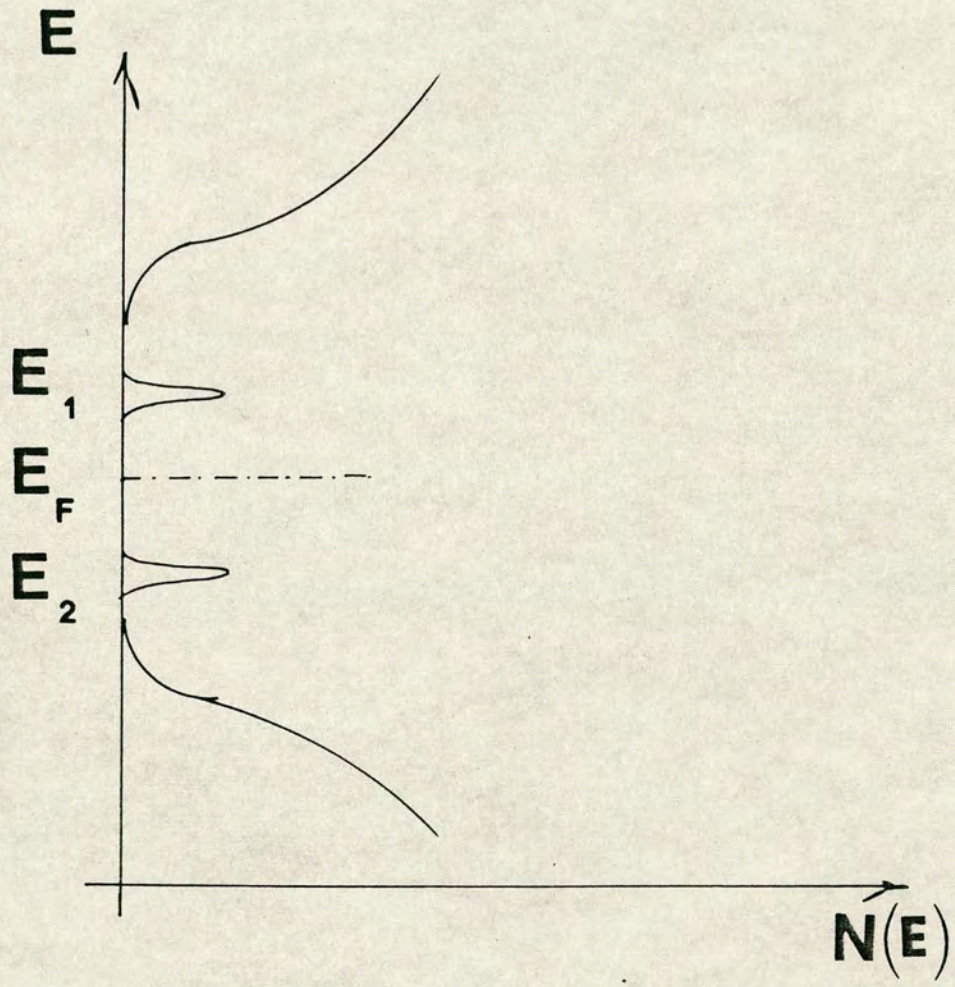

FIG. 2.9

Marshall-Owen model with acceptor and donor like states

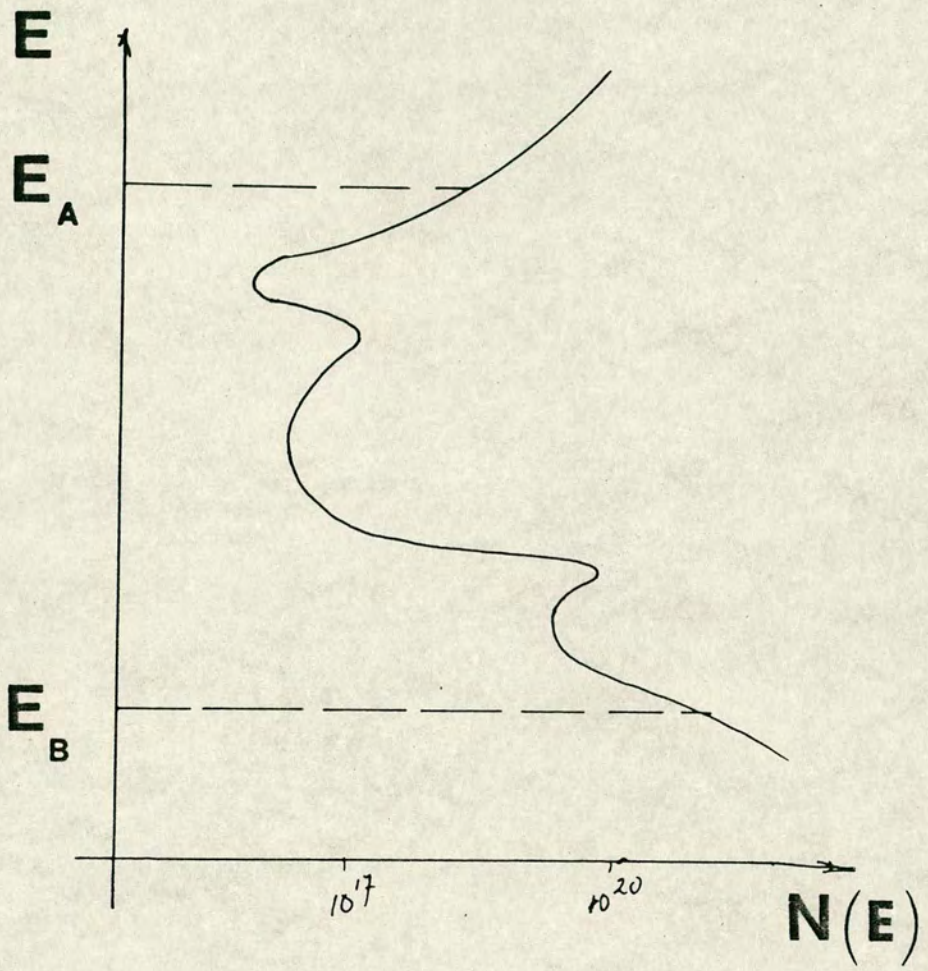

FIG. 2.10

Band diagram of amorphous Si

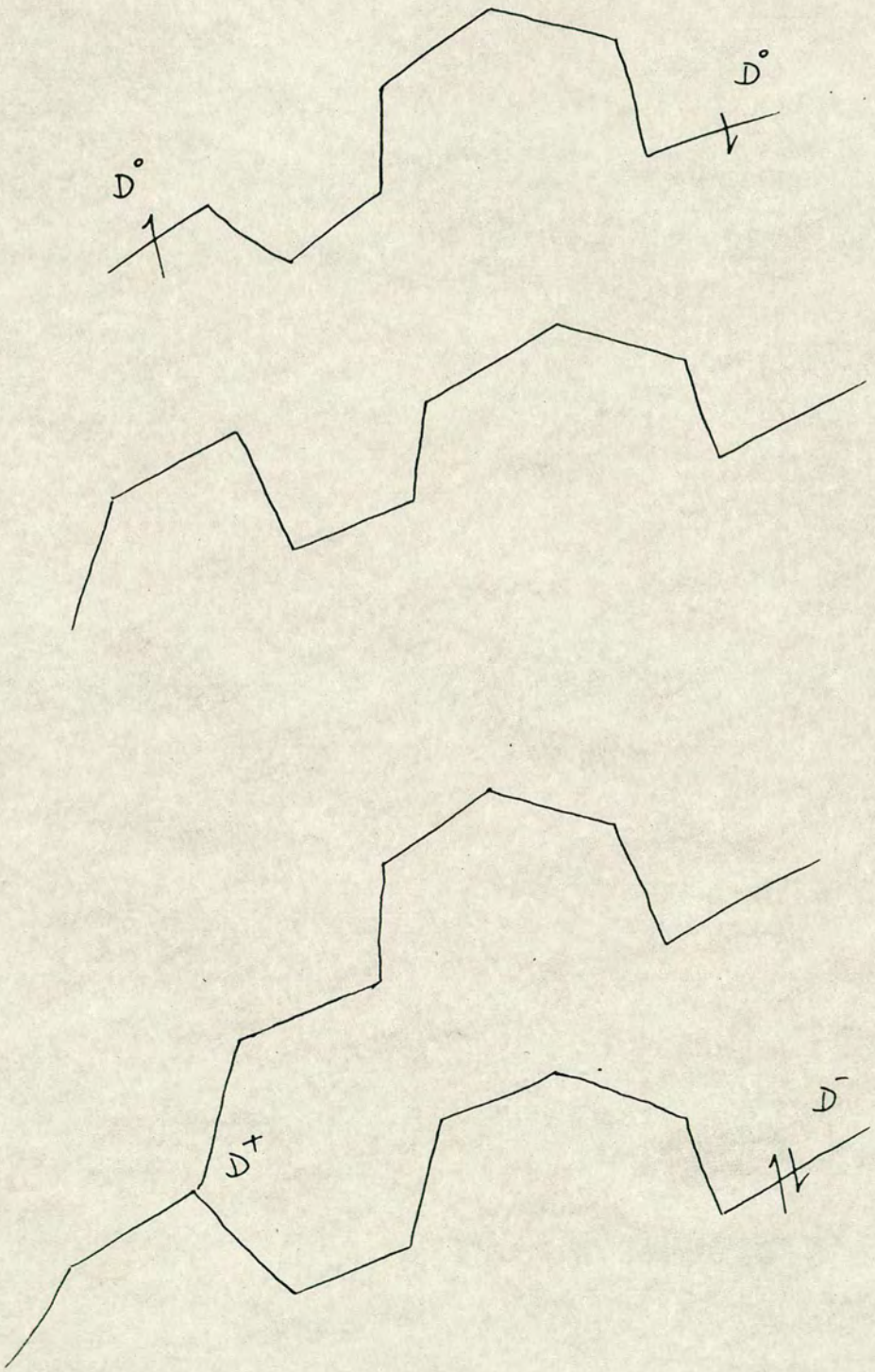

FIG. 2.11

The formation of D^+ and D^- from the two dangling bond D^o defects

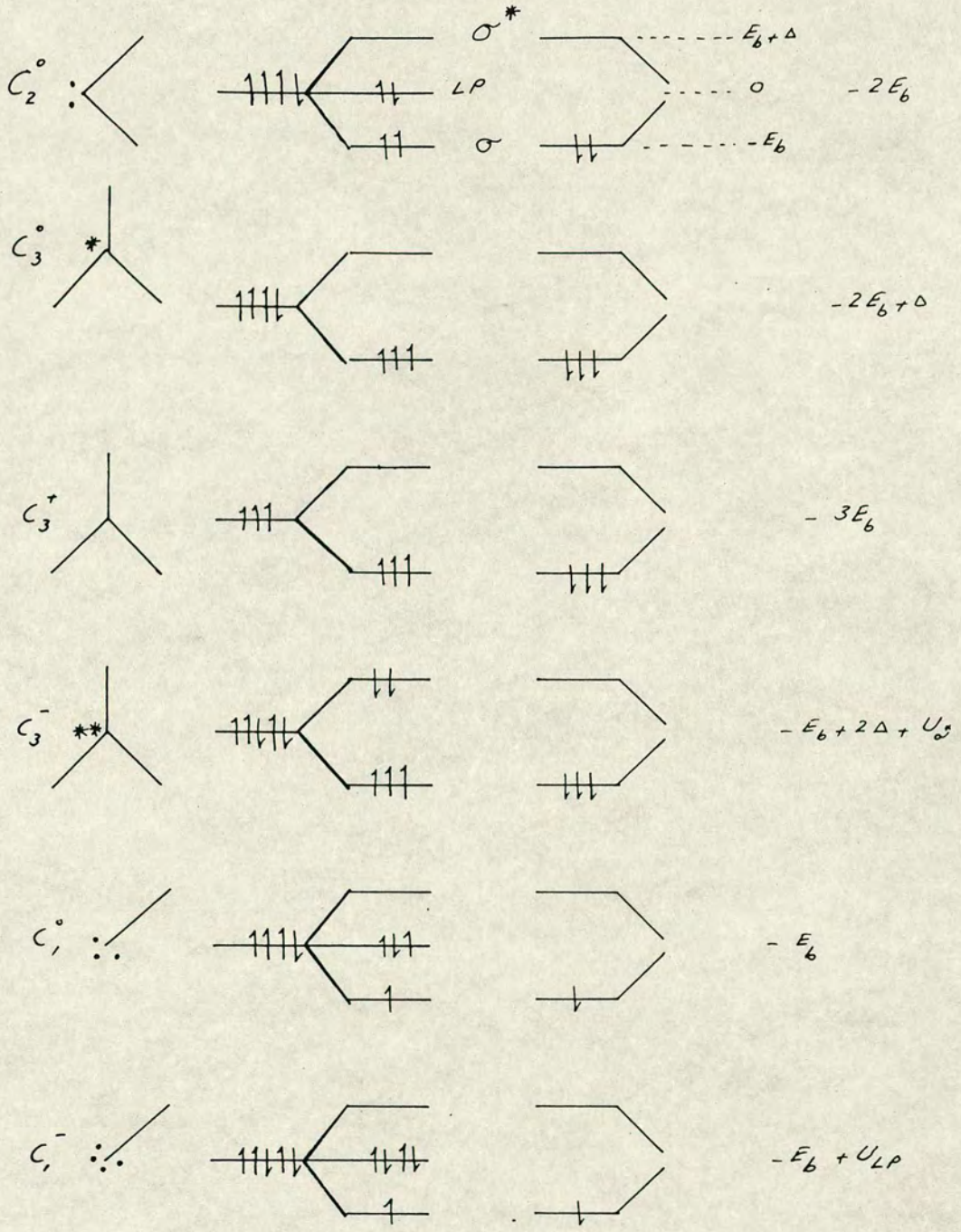

FIG. 2.12

The structure and energy of several simple bonding configurations of chalcogen atoms

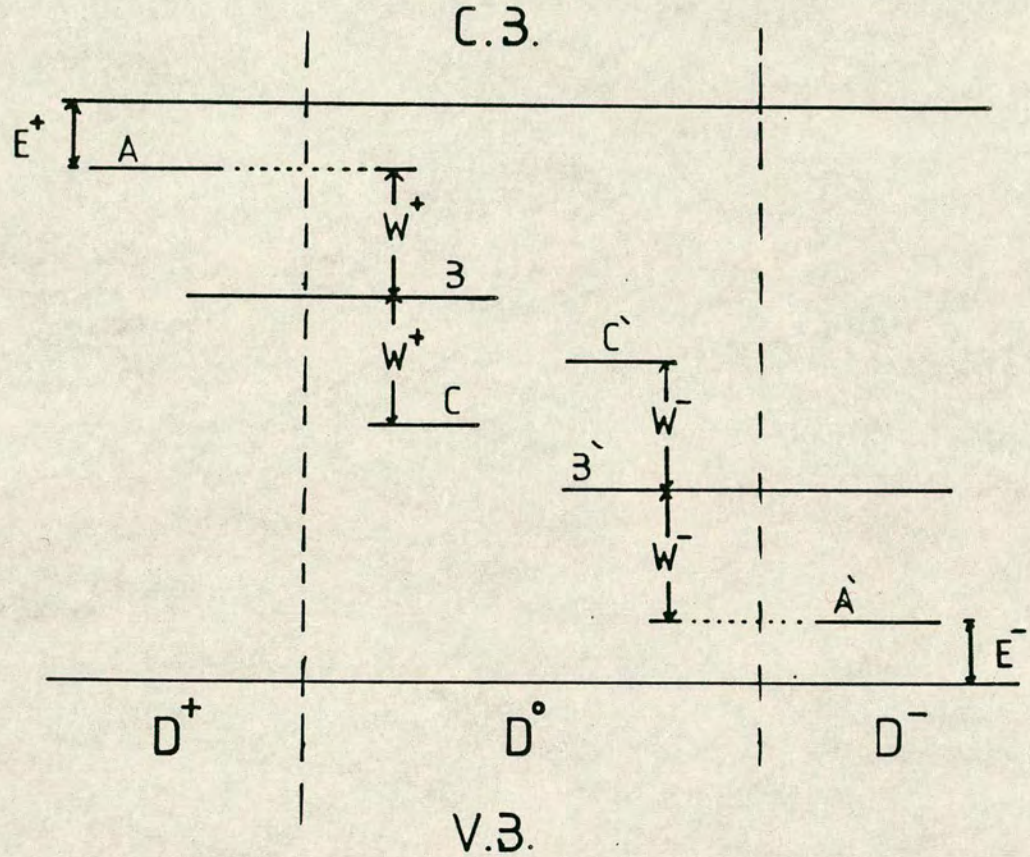

FIG. 2.13

Energy levels associated with D^+, D^o and D^-

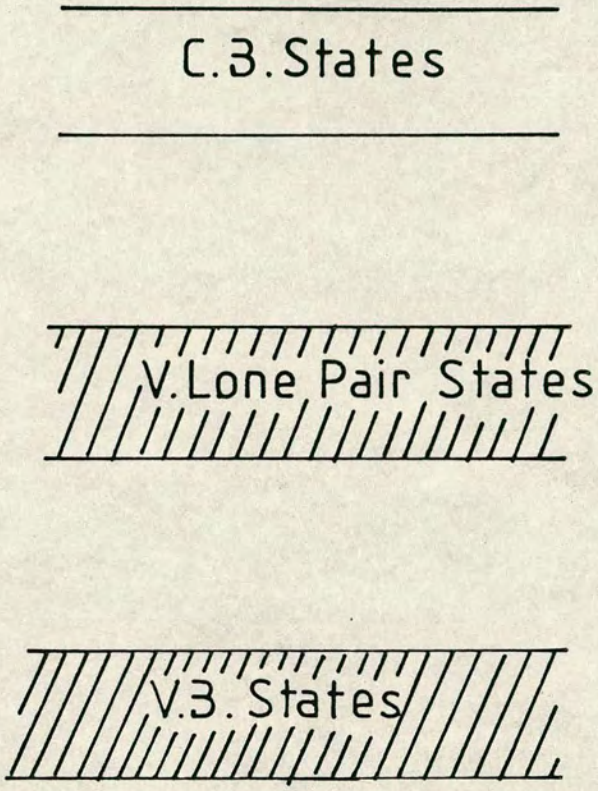

FIG. 2.14

Energy band diagram for chalogonide material

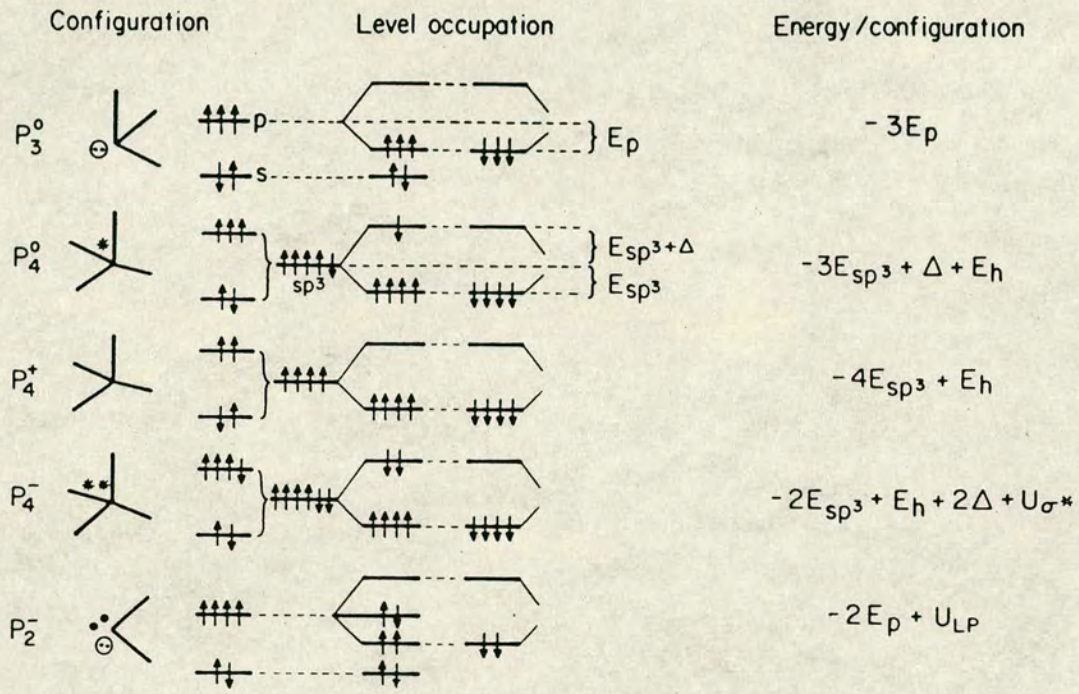

Structure and energy of simple bonding configurations for group V elements. In configurations, straight lines represent bonds (σ states), asterisks the antibonding (σ^*) electrons, dots the p lone pairs and dots in circle the s lone pairs. The zero of energy is chosen at that of the atomic configuration with two s and three p electrons. Hybridization yields five electrons in sp^3 states and raises the total configurational energy by E_h. Electron in σ is always paired with one from a nearest neighbour atom as shown. Configurational energies are computed neglecting change of energy of electrons on nearest neighbours.

FIG. [2.15]

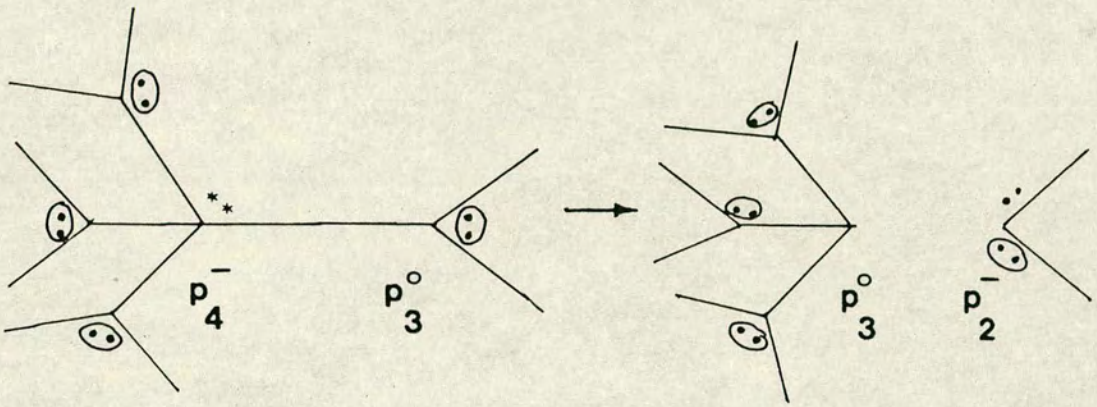

FIG.2.16

The formation of P^-_2 from P^-_4 and P^o_3

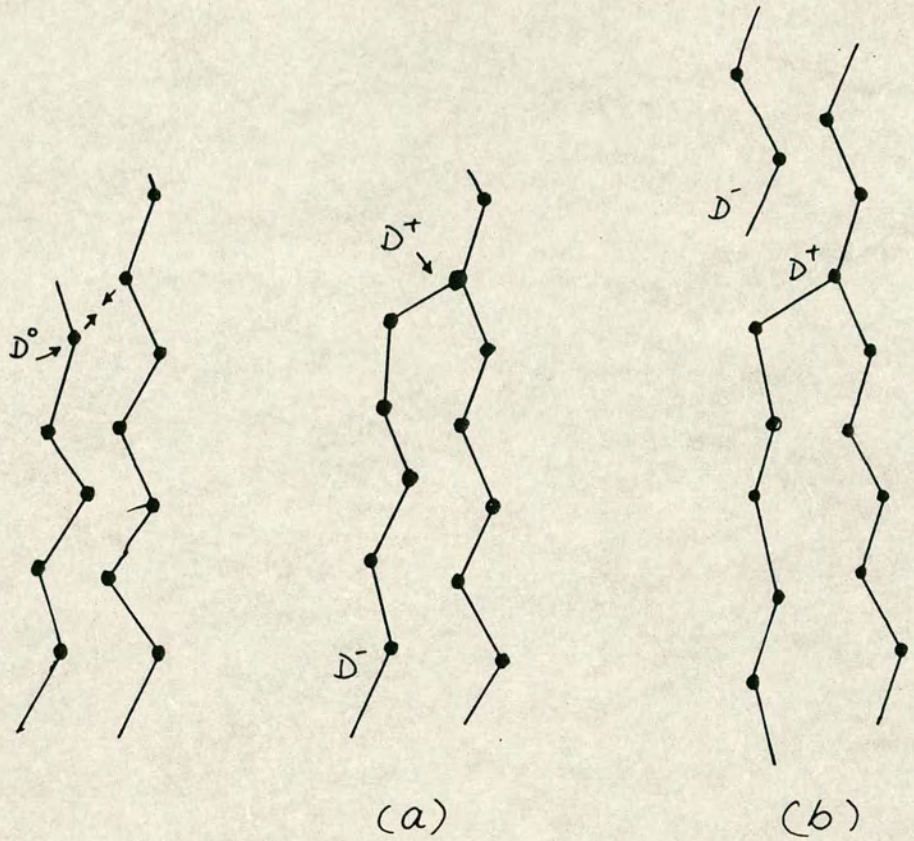

FIG. 2.17

(a) D^+ and D^- centres formed from two D^0 centre at the ends of a chain
(b) Intimate valence alternation pair

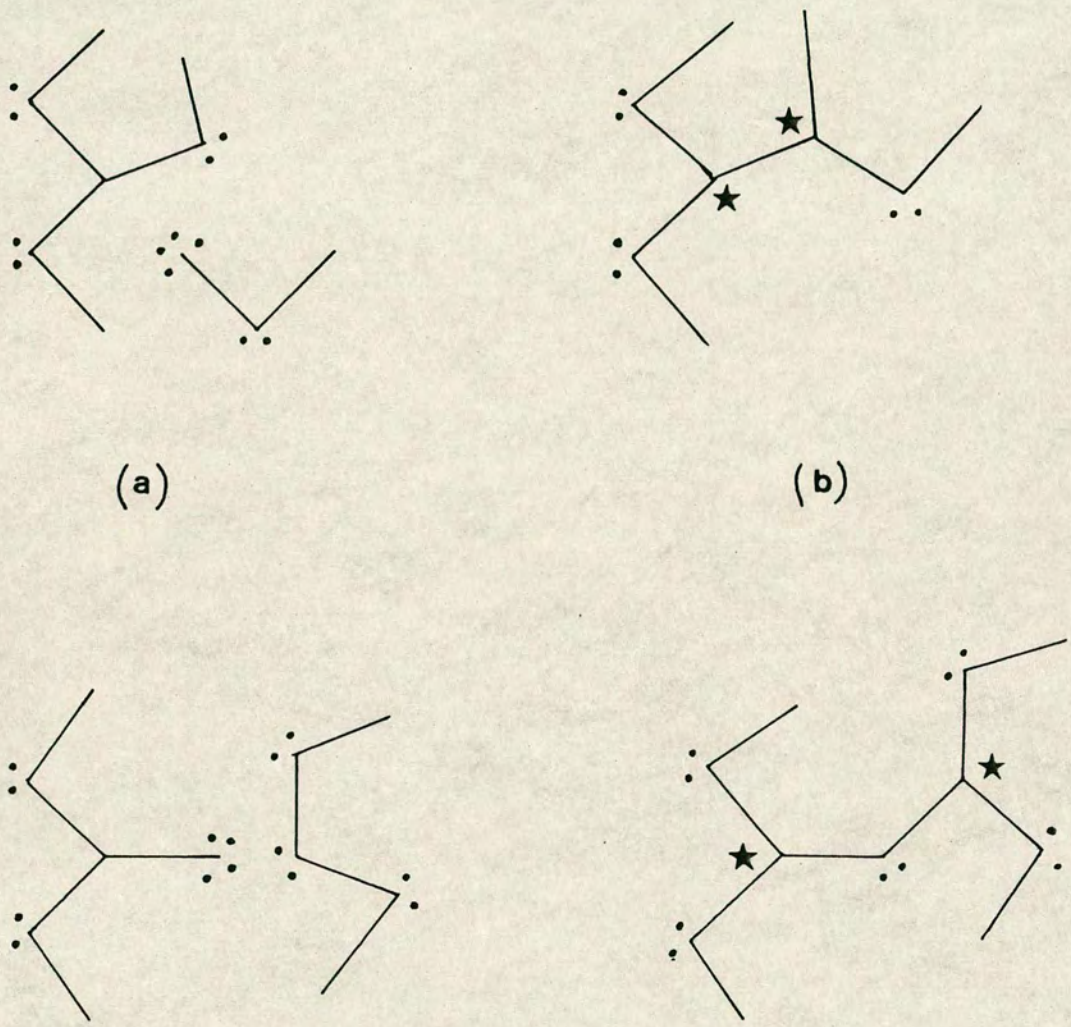

FIG. 2.18

The two types of IVAP [unstable (a,b) and stable (c,d)]

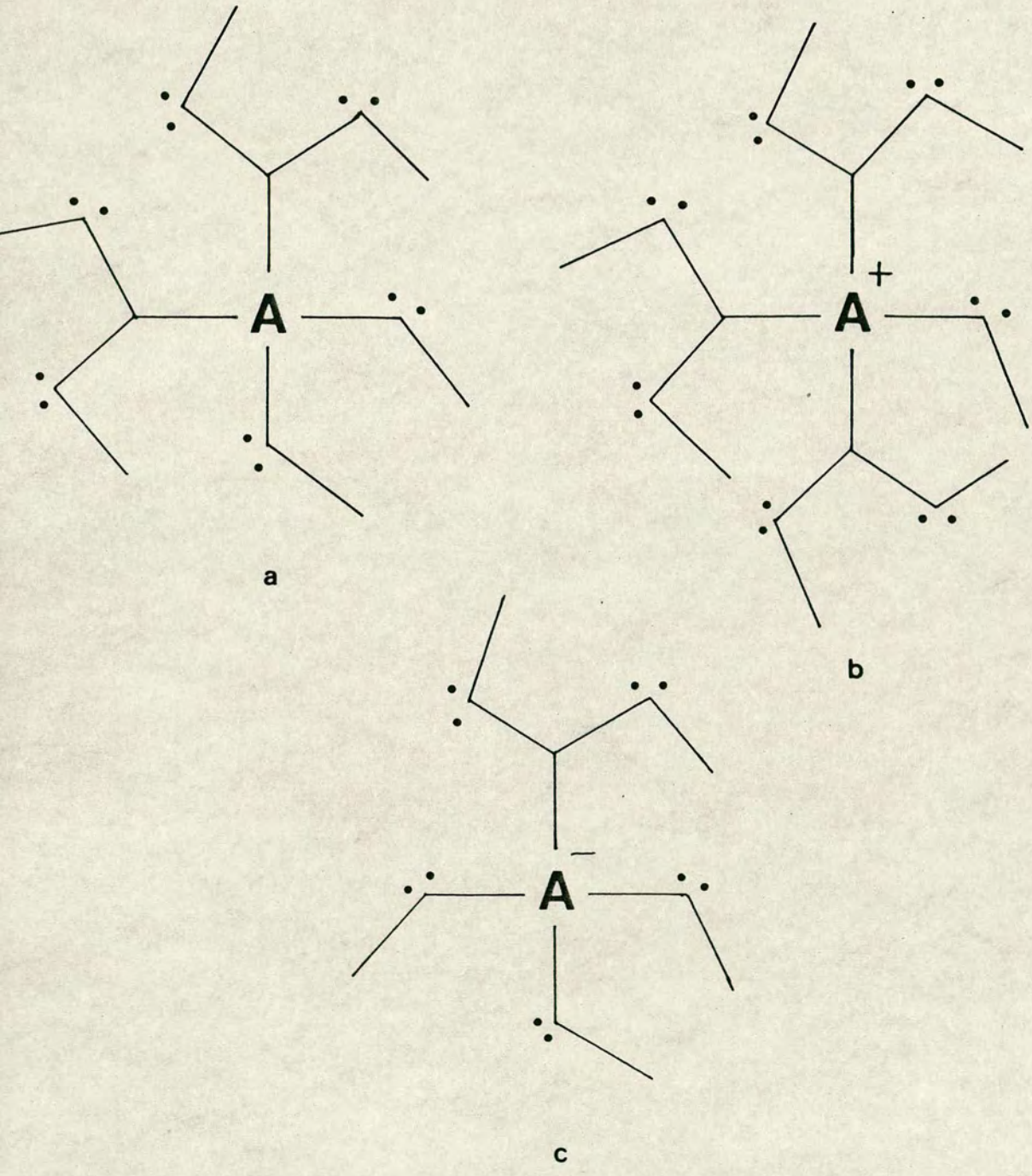

FIG. 2.19

The type of configuration that the metal additive may possess

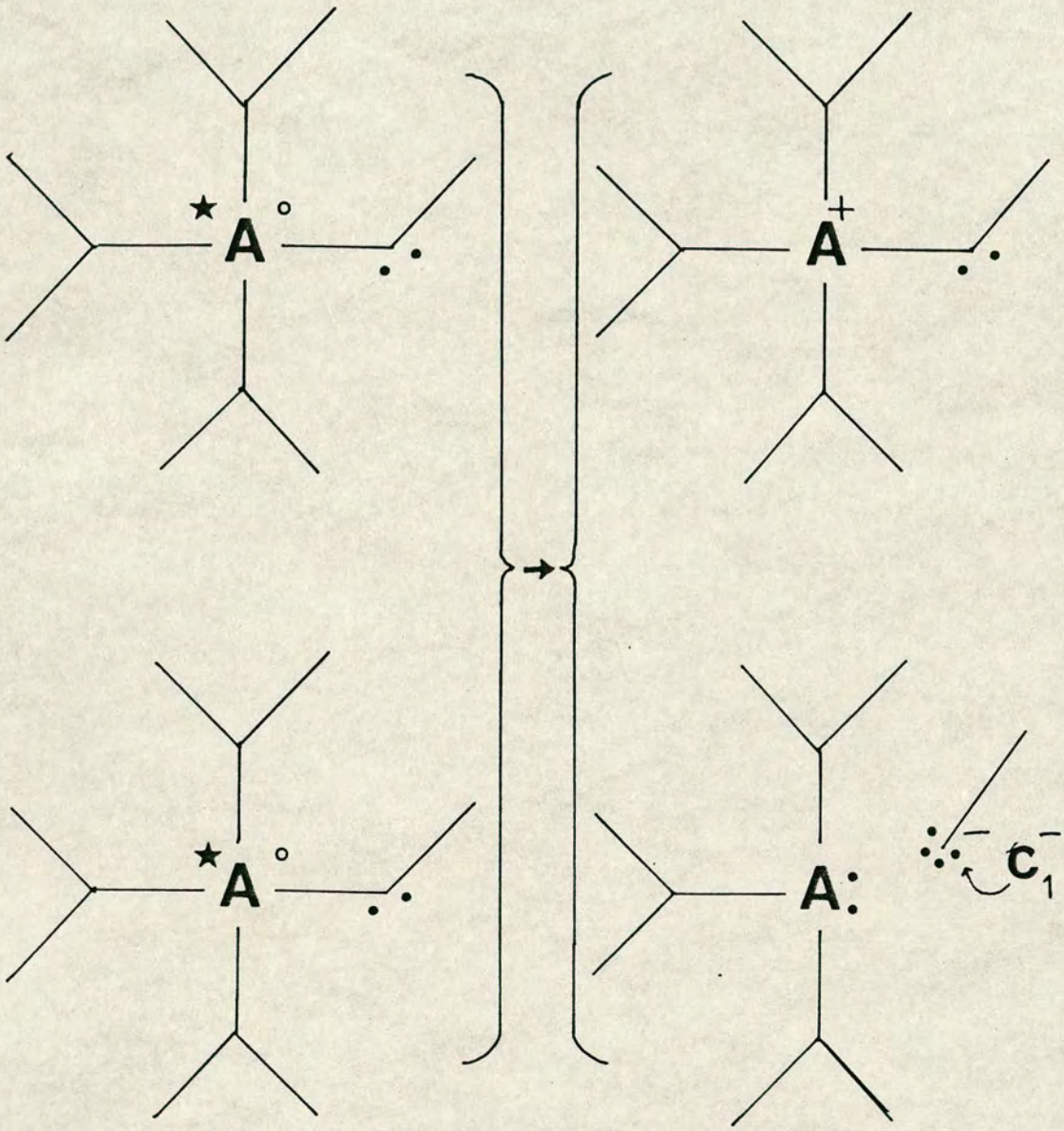

FIG. 2.20

The corresponding process for A^{o} centre to that of exothermic reaction for the neutral VAP centre

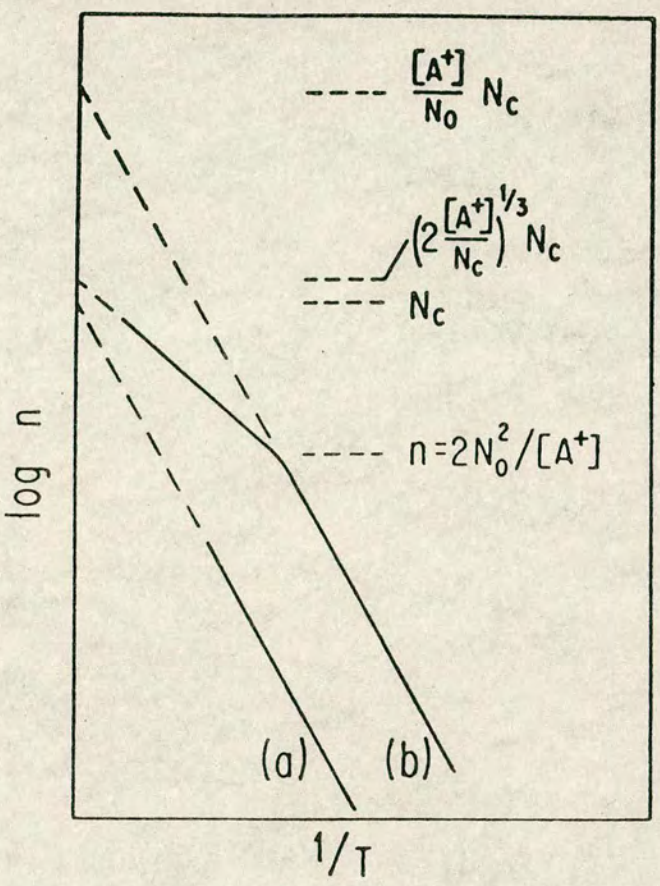

Electron concentration log n, as a function of $1/T$ of chalcogenide material (a) undoped and (b) containing a concentration $[A^+]$ of positively charged additives. The concentrations for the $1/T = 0$ intercepts and for the position of the kink are given. The conductivity is expected to be proportional to the carrier concentration.

FIG. [2.21]

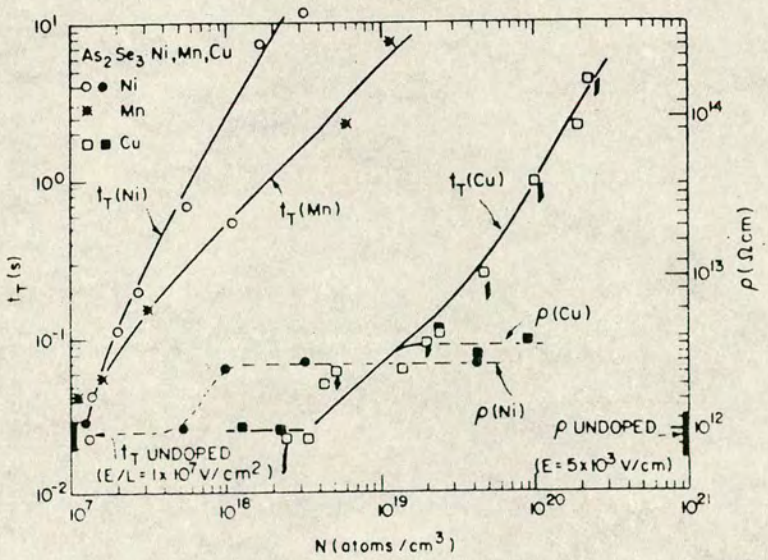

log plot of t_T (left ordinate) and ρ (right ordinate) versus the concentration N of Ni, Mn and Cu doped As_2Se_3. $T = 296$ K. The transit-time data were plotted for fixed $E/L = 1 \times 10^7$ V/cm^2 The d.c. resistivity data were measured at $E = 5 \times 10^3$ V/cm.

FIG. [2.22 a]

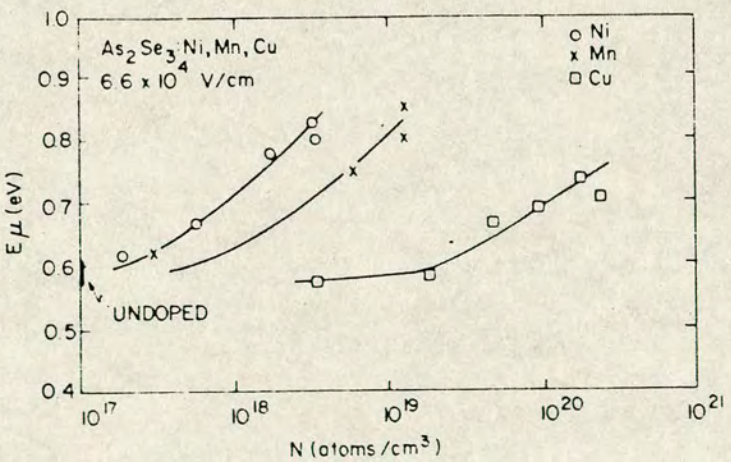

Concentration dependence of transit-time activation energy for Ni-, Mn- and Cu-doped As_2Se_3 measured at $E = 6{\cdot}6 \times 10^4$ V/cm.

FIG. [2.22 b]

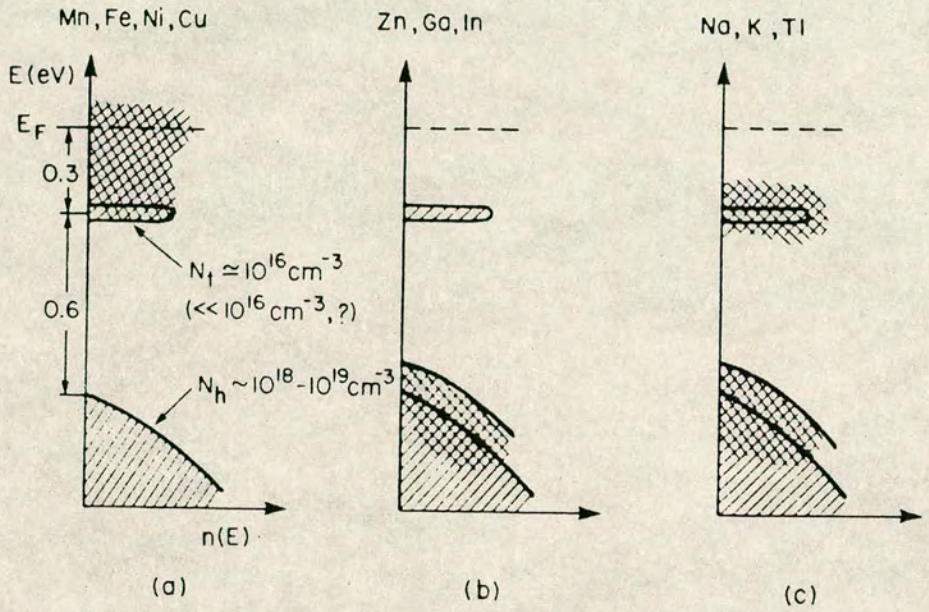

Schematic energy level diagrams for As_2Se_3 doped with (*a*) Mn, Fe, Ni, Cu, (*b*) Zn, Ga, In and (*c*) Na, K, Tl.

FIG. [2.23]

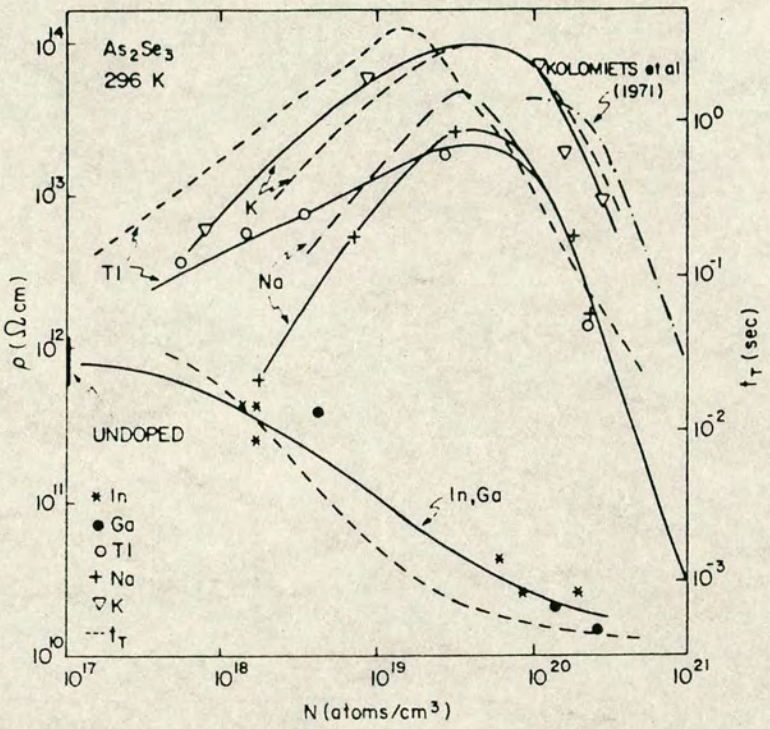

Log–log plot of ρ versus concentration N of Tl-, Na-, K-, In- and Ga-doped As_2Se_3 measured at $E = 5 \times 10^3$ V/cm. $T = 296$ K. The dashed lines indicate the concentration dependence of the transit time shown in fig. 7. The dash-dotted line represents data obtained by Kolomiets *et al.* (1971).

FIG. [2.24]

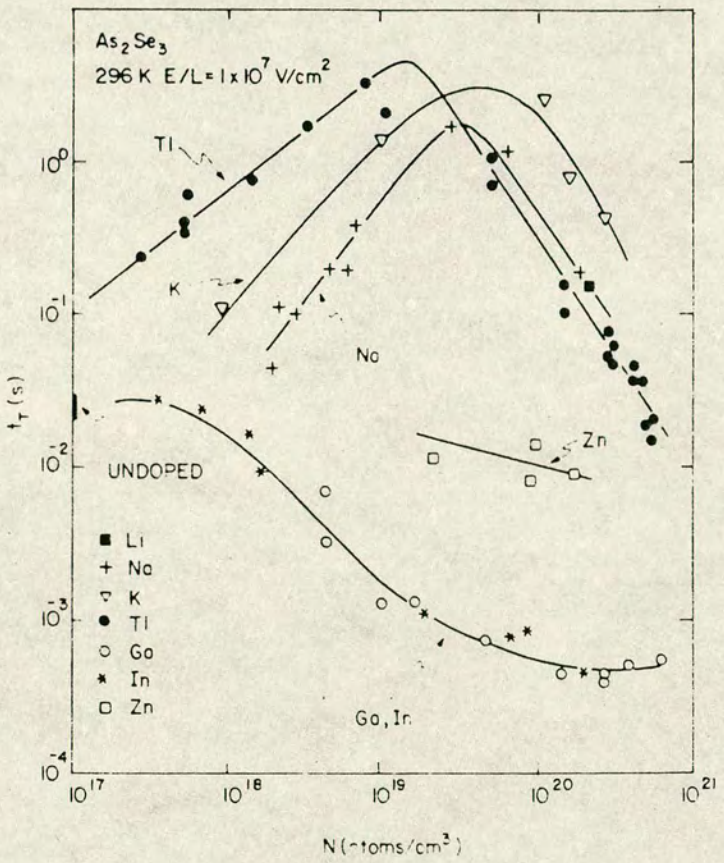

Log–log plot of t_T versus the concentration N of Tl-, Na-, K-, Ga-, In- and Zn-doped As_2Se_3. $T = 296$ K. The transit-time data were plotted for fixed $E/L = 1 \times 10^7$ V/cm^2

FIG. [2.25]

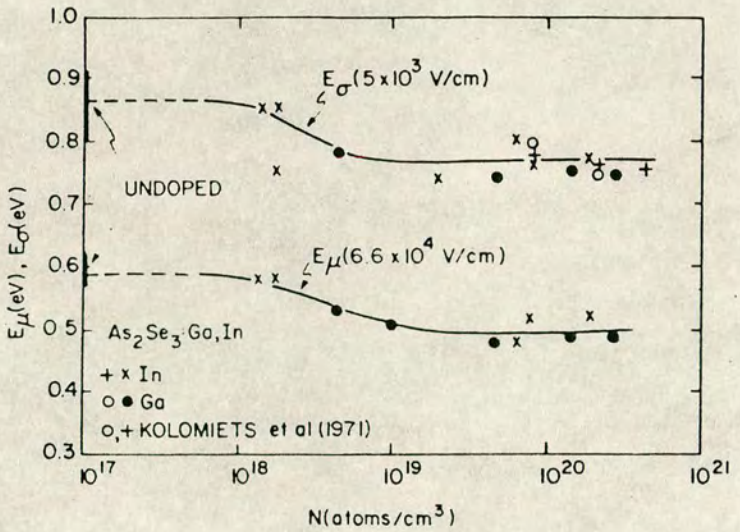

Concentration dependence of activation energies of transit time (E_μ) and d.c. resistivity (E_σ) for Ga- and In-doped As_2Se_3. E_μ was measured at $E = 6{\cdot}6 \times 10^4$ V/cm and E_σ at 5×10^3 V/cm. Included are E_σ values obtained by Kolomiets *et al.* (1971).

FIG. [2.26]

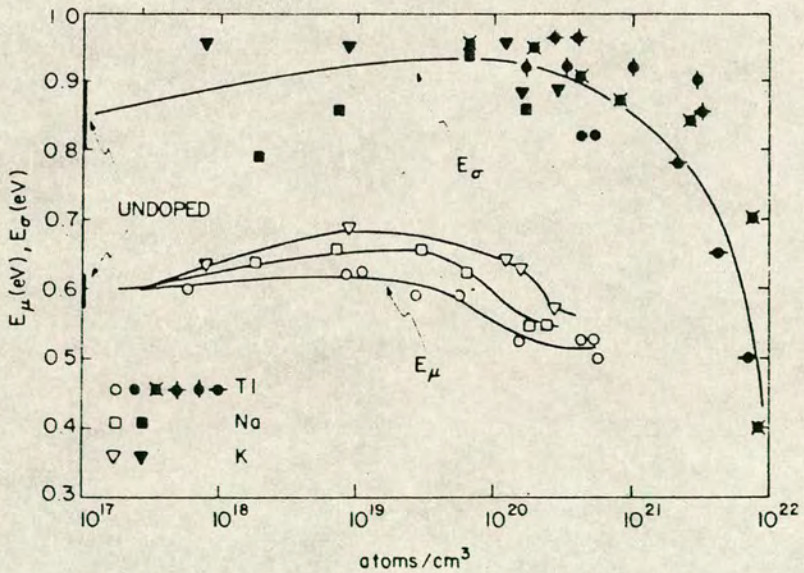

Concentration dependence of activation energies of transit time (E_μ) and d.c. resistivity (E_σ) for Tl-, Na- and K-doped As_2Se_3. E_μ was measured at $6{\cdot}6 \times 10^4$ V/cm, E_σ was measured at 5×10^3 V/cm. Included are values for E_σ obtained by Kolomiets *et al.* (1971) ✖, Lezal *et al.* (1972) ◆, Mariani *et al.* (1973) ◆ and Strunk (1973) ◆.

FIG. [2.27]

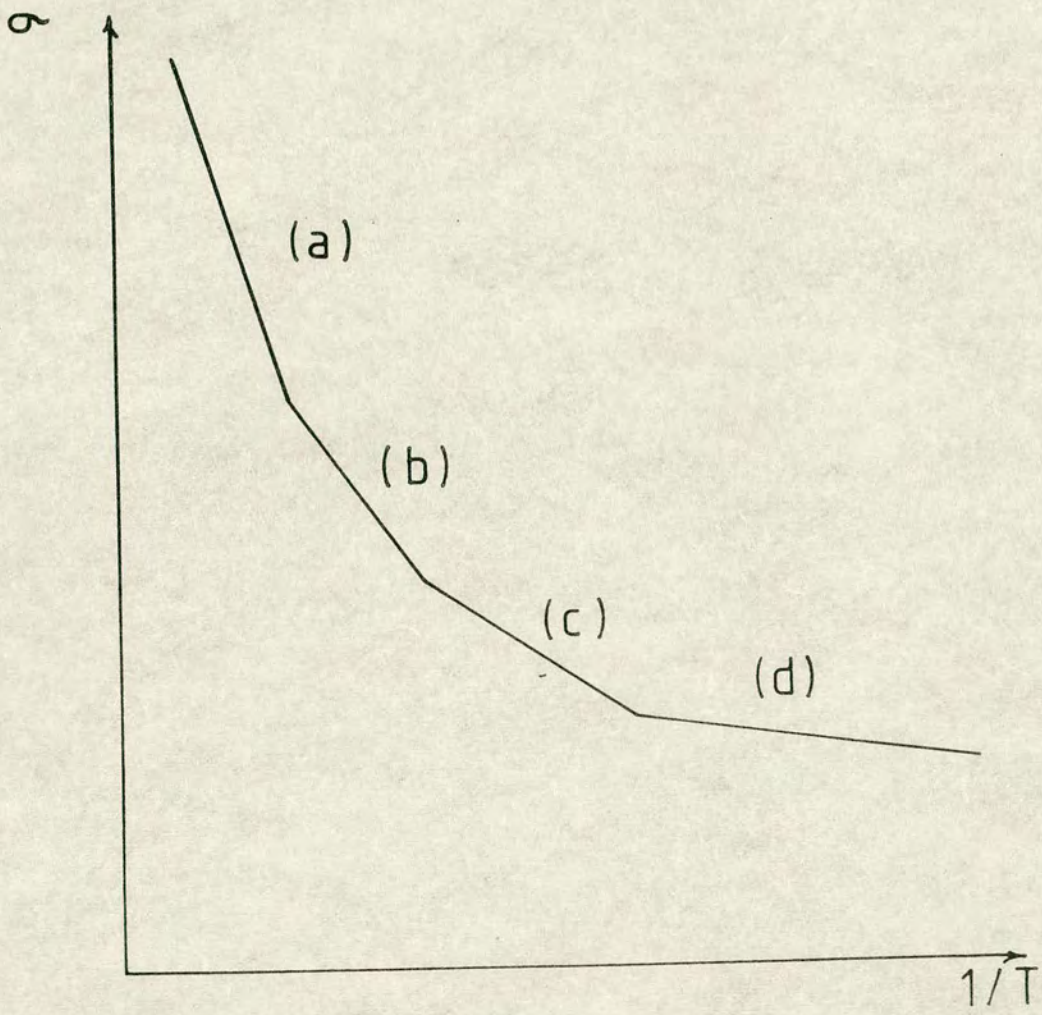

FIG. (3.1)

Illustration of the activation energies associated with various conduction mechanisms

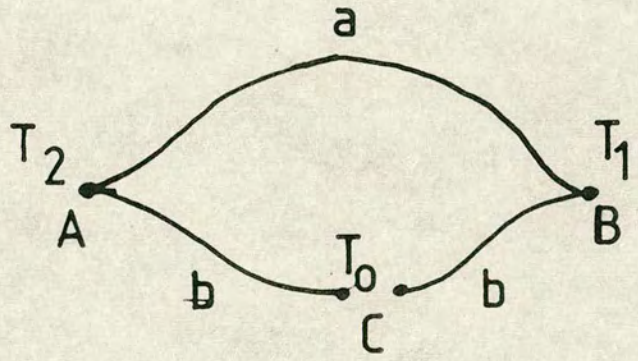

FIG.[3.2]

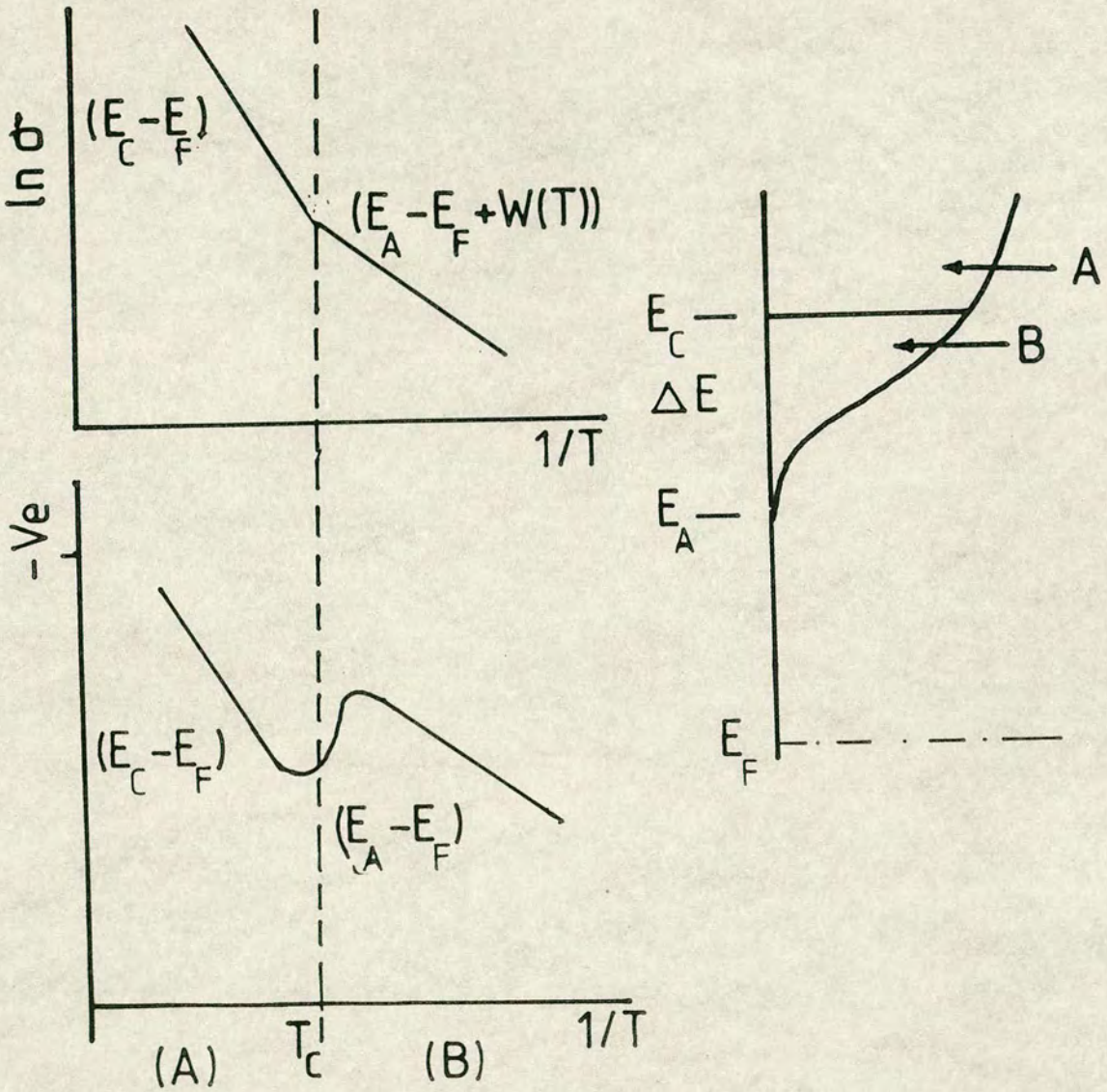

FIG.[3.3]

Schematic representation of temperature dependence of d.c. conductivity σ and thermopower S for carriersin a band with a mobility edge as shown on the right

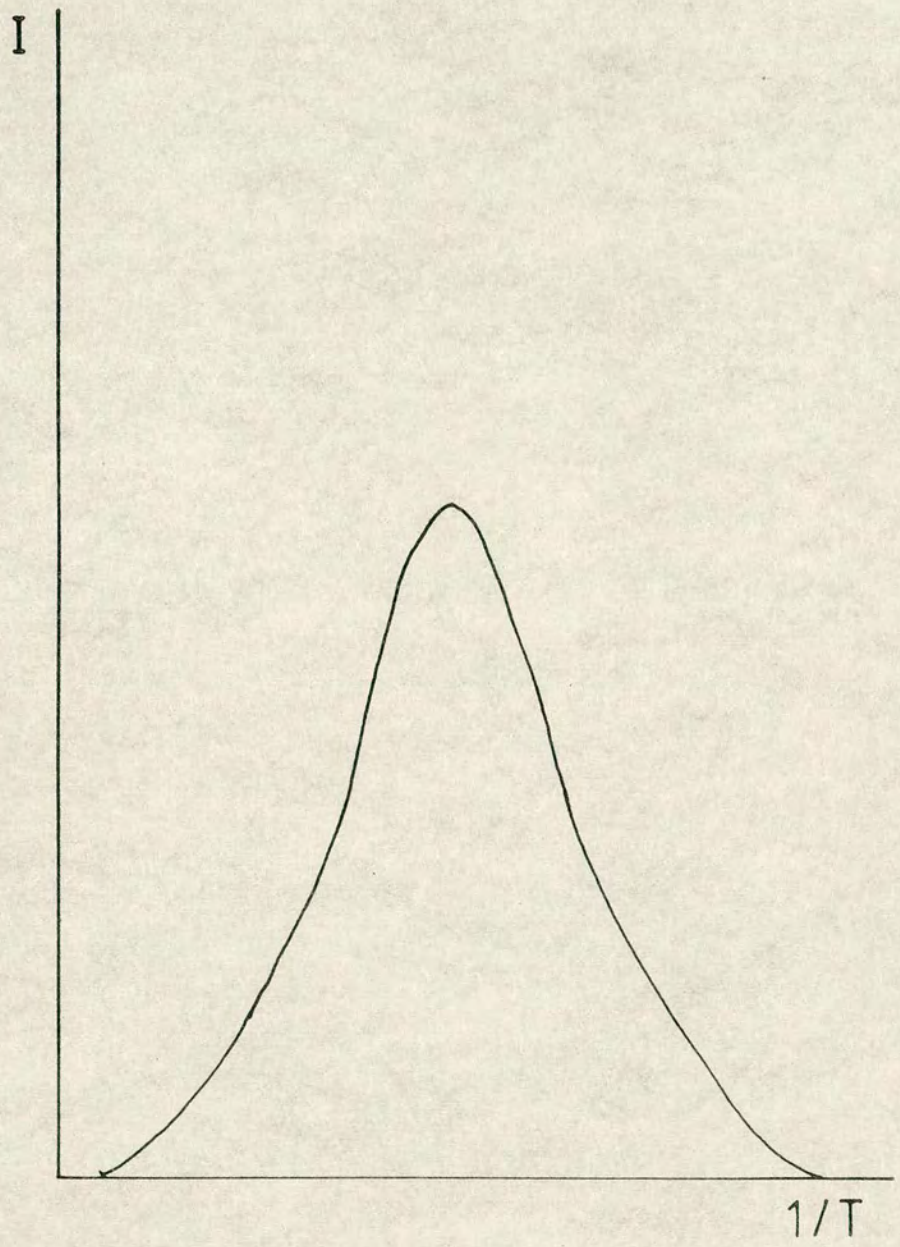

FIG.[3.4]

Thermoluminescence peak

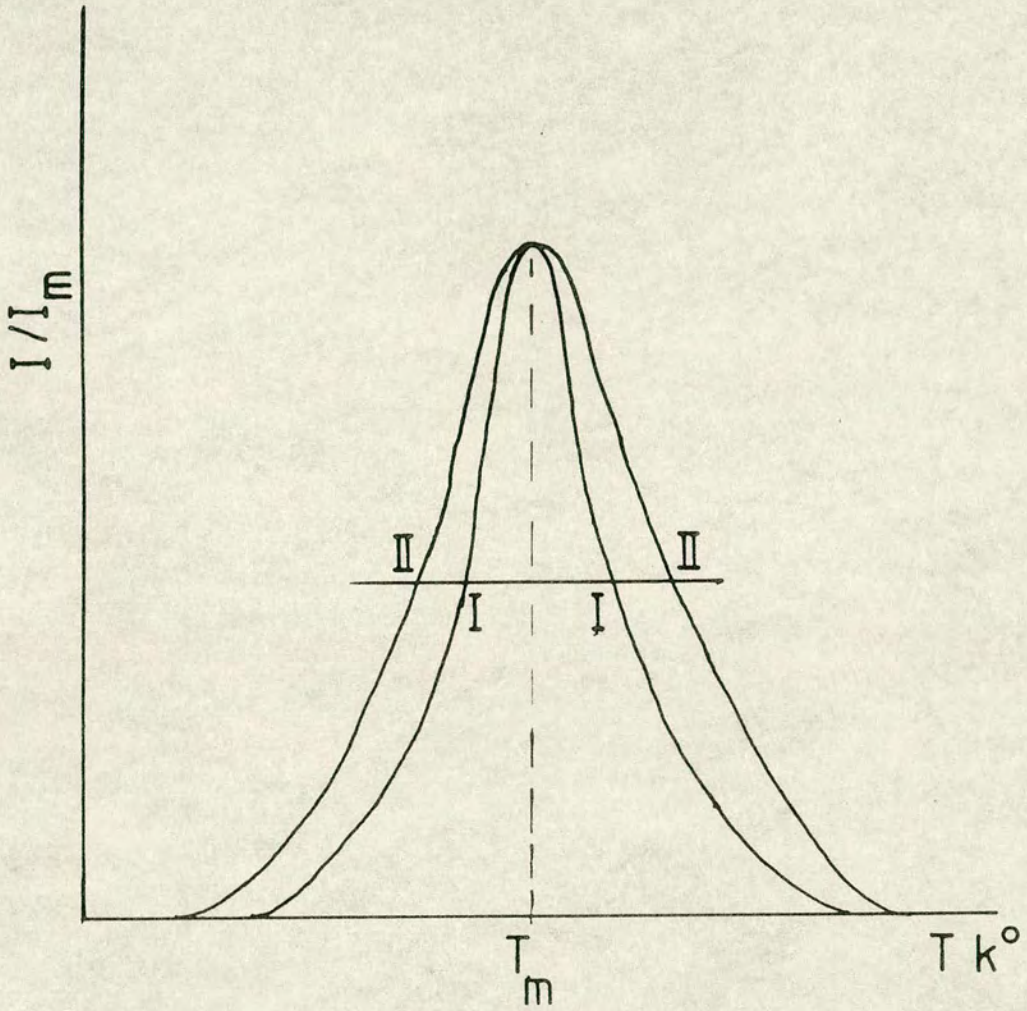

FIG.[3.5]

Thermoluminescence peaks of first (I) and second (II) order kinetics

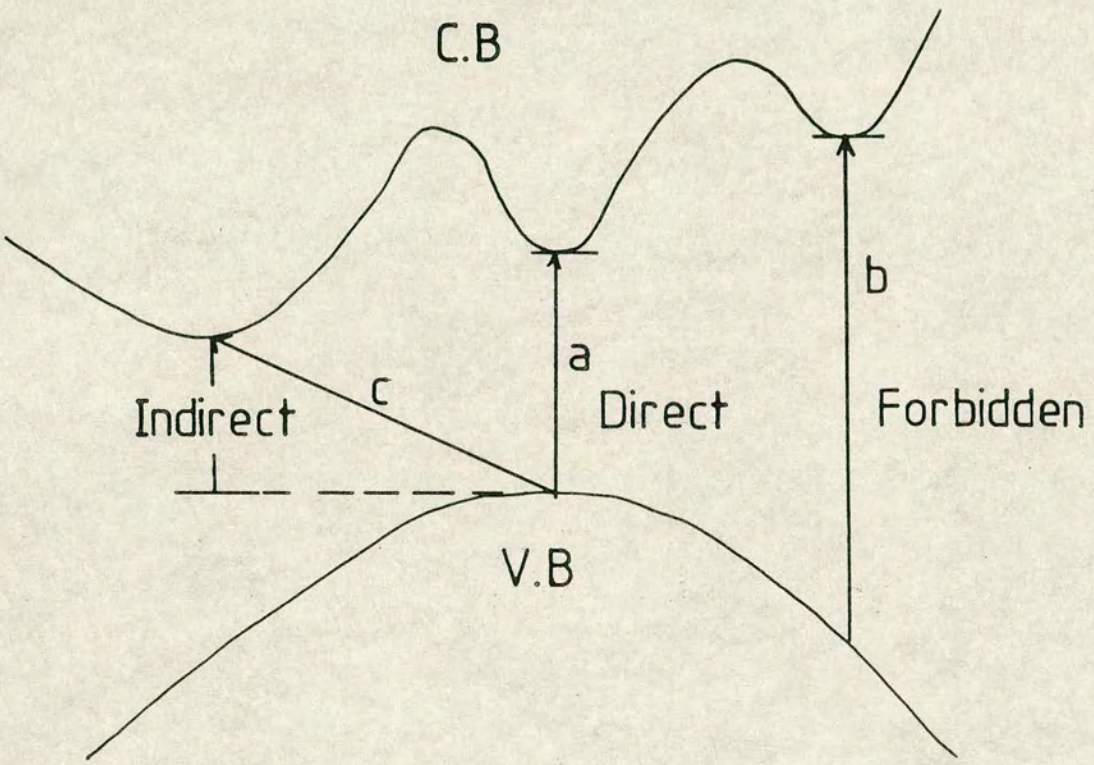

FIG.[3.6]

Illustrate the different types of transtion

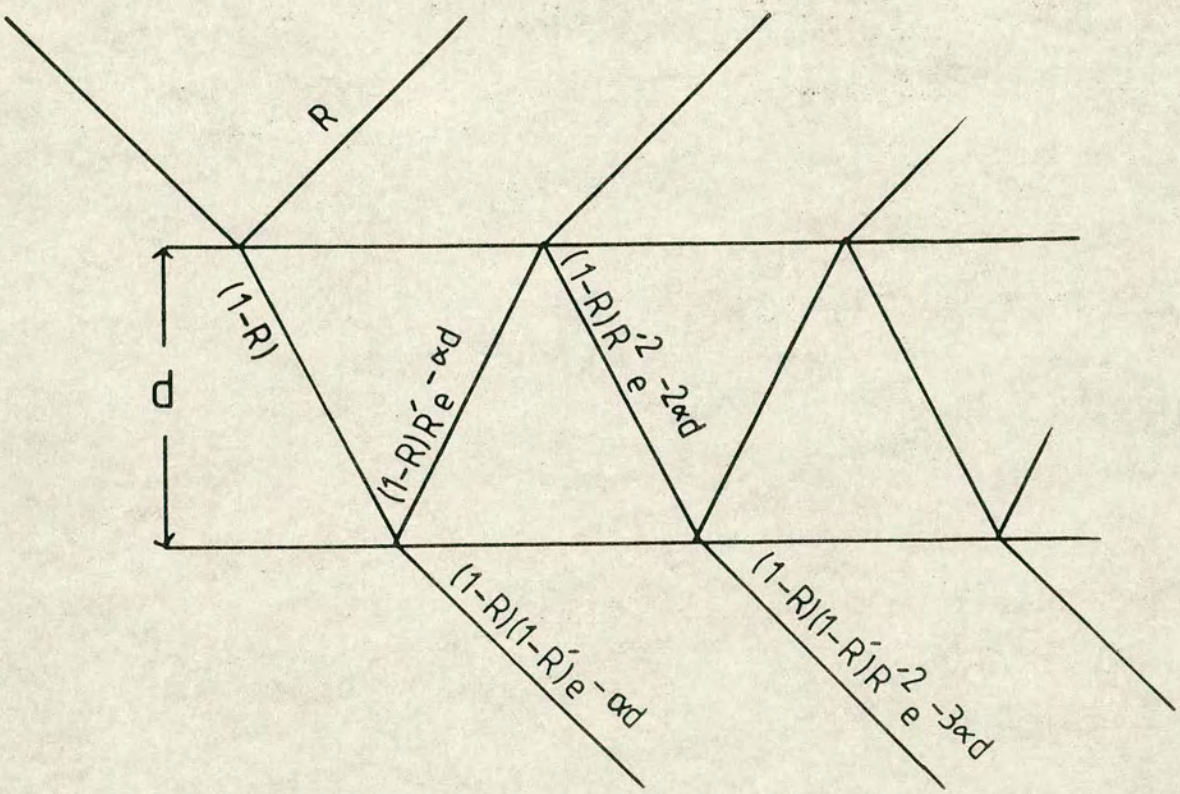

FIG. [3.7]

Amplitudes of successive rays in multiple reflection

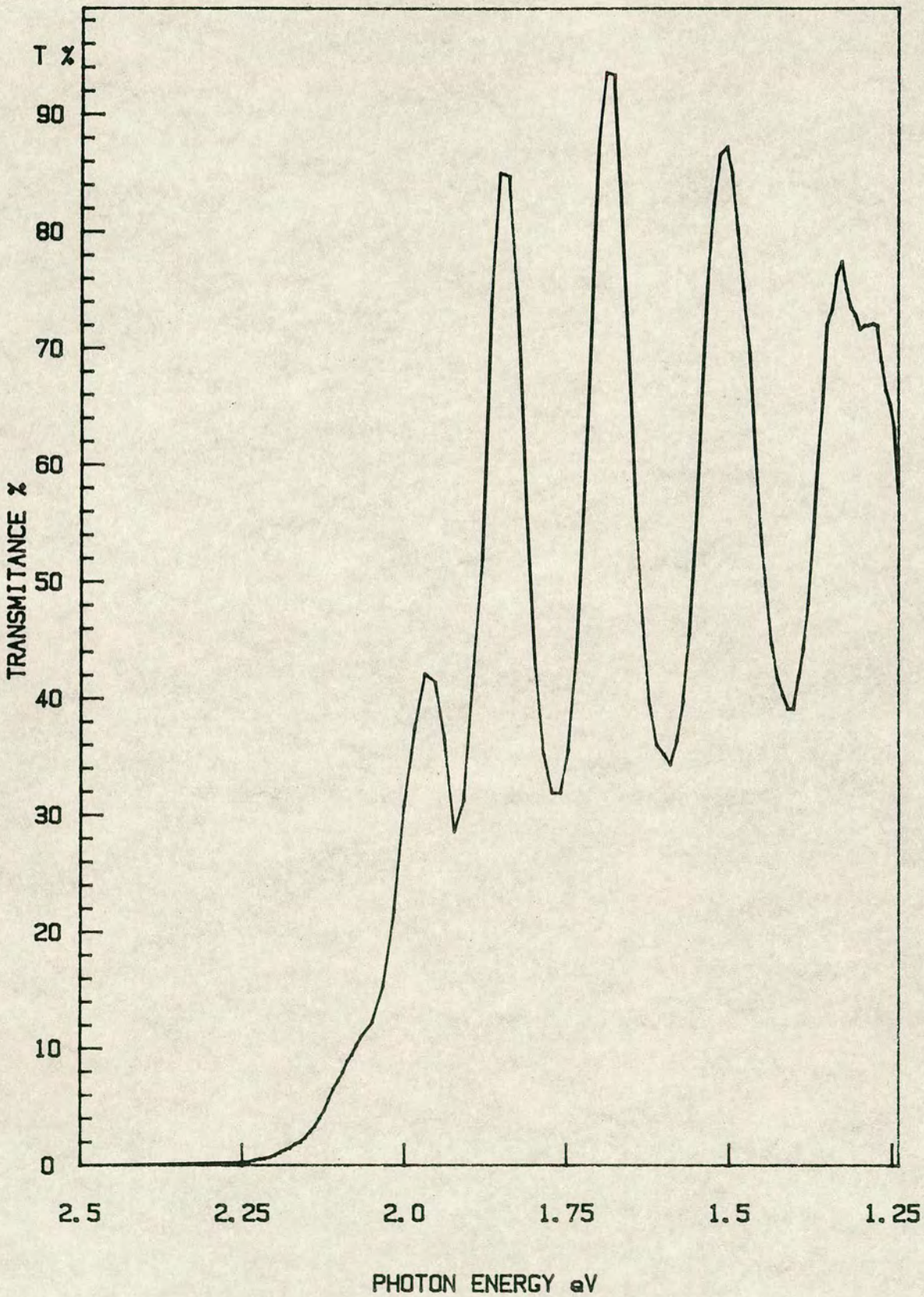

FIG.[3.8]

Illustration of the maximum and minimum transmission in the transparent region

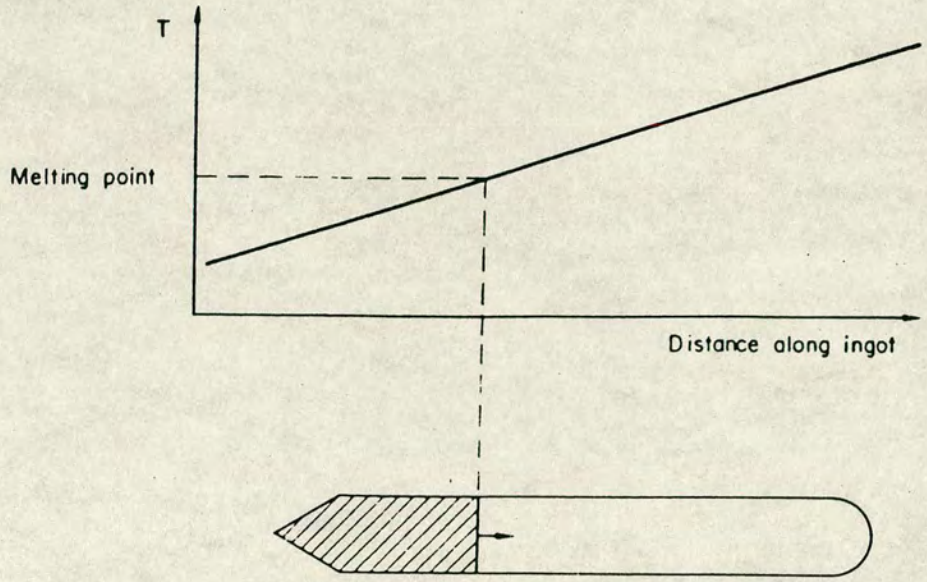

Fig.4.1. Normal freezing, also called directional freezing.

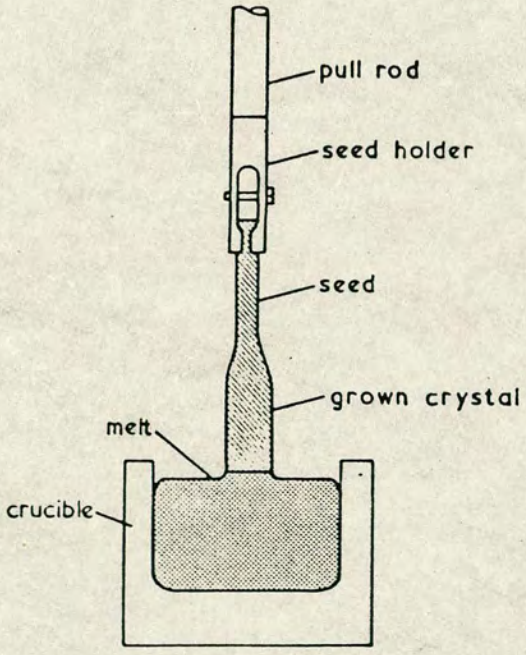

Figure 4.2. Crystal pulling (or Czochralski method). The single crystal is rotated and slowly withdrawn from the melt.

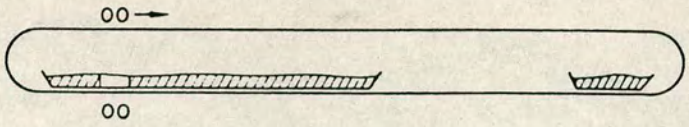

(A)

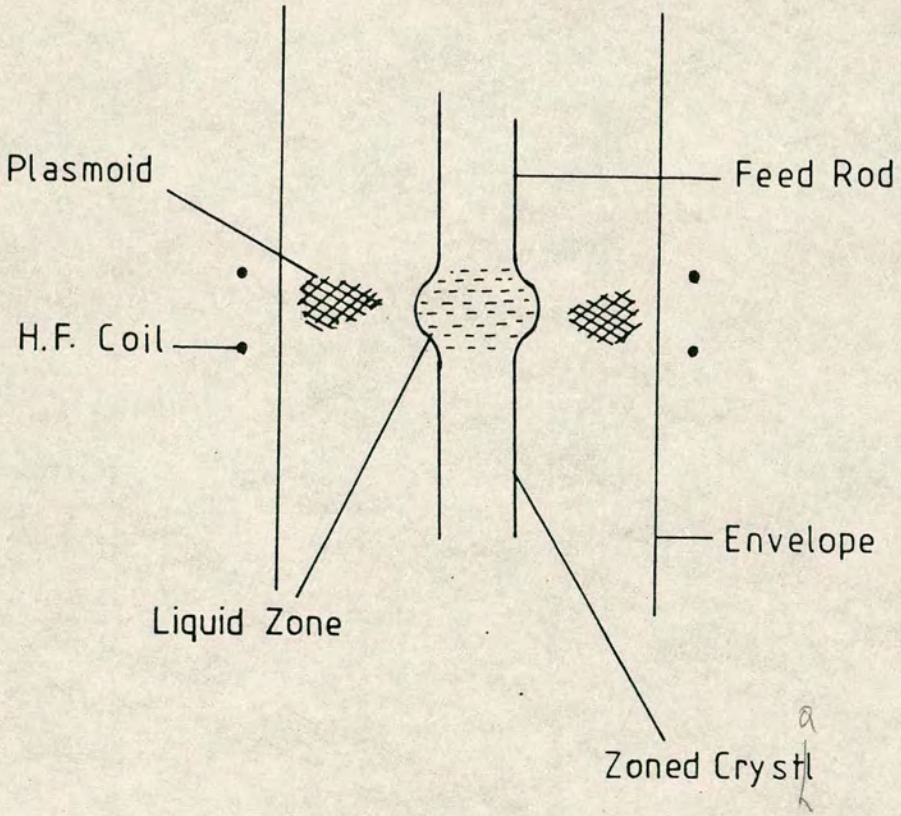

(B)

FIG.[4.3]

(A) Zone refining. The molten zone, shown here heated by r.f. induction, is moved along the ingot. The separate boat at a lower temperature contains a volatile component and the temperatures are adjusted to prevent any transport to or from the molten zone. (B) A zone melting arrangement using a stationary r.f. plasma.

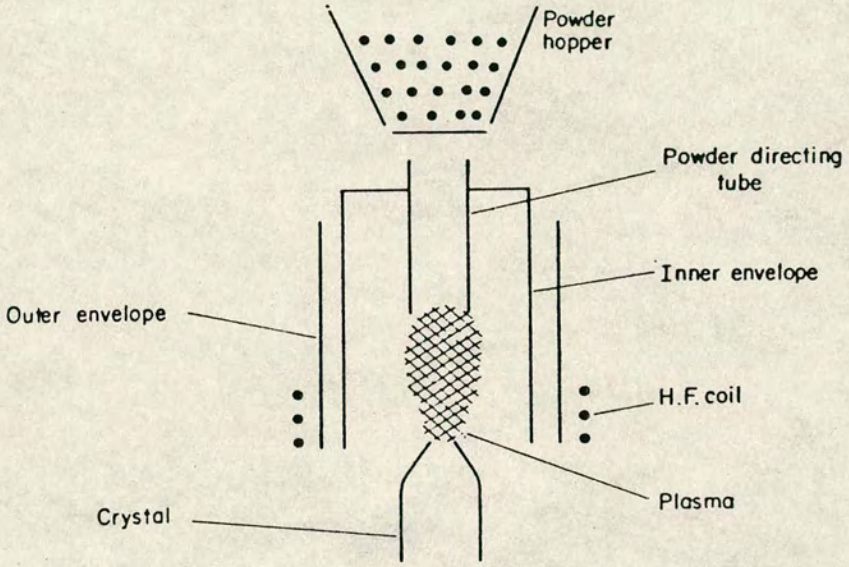

Fig. 4.4. A Verneuil apparatus using an open h.f. plasma torch.

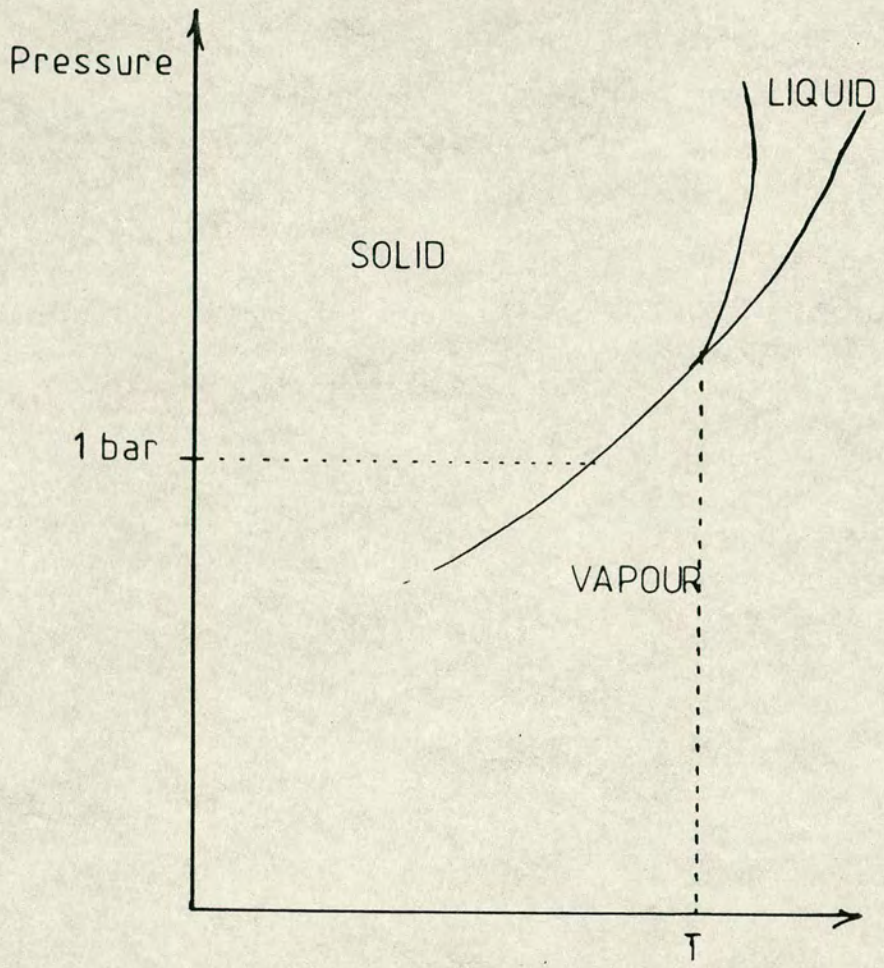

FIG. 4.5

Illustration of the phase diagram for element with their melting point above 1 bar (e.g. iodine)

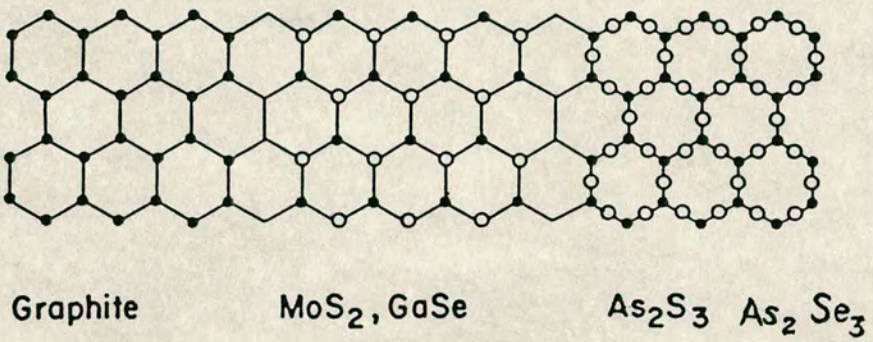

Figure (4.6)

Schematic bonding topology of the two-dimensionally-extended covalent networks which make up several classes of layer crystals.

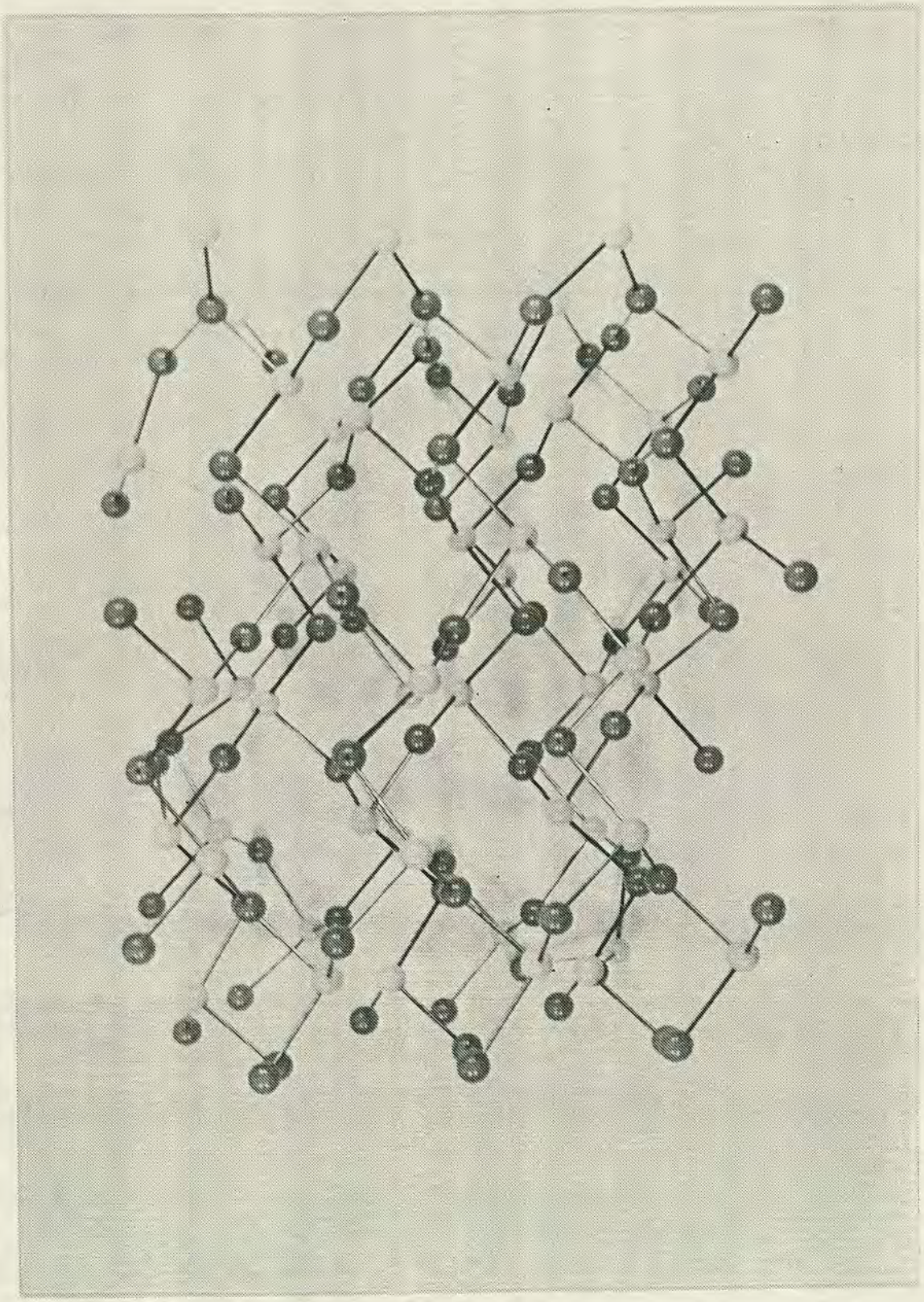

FIG.[4.7a]

Shows a view of the layers from above.

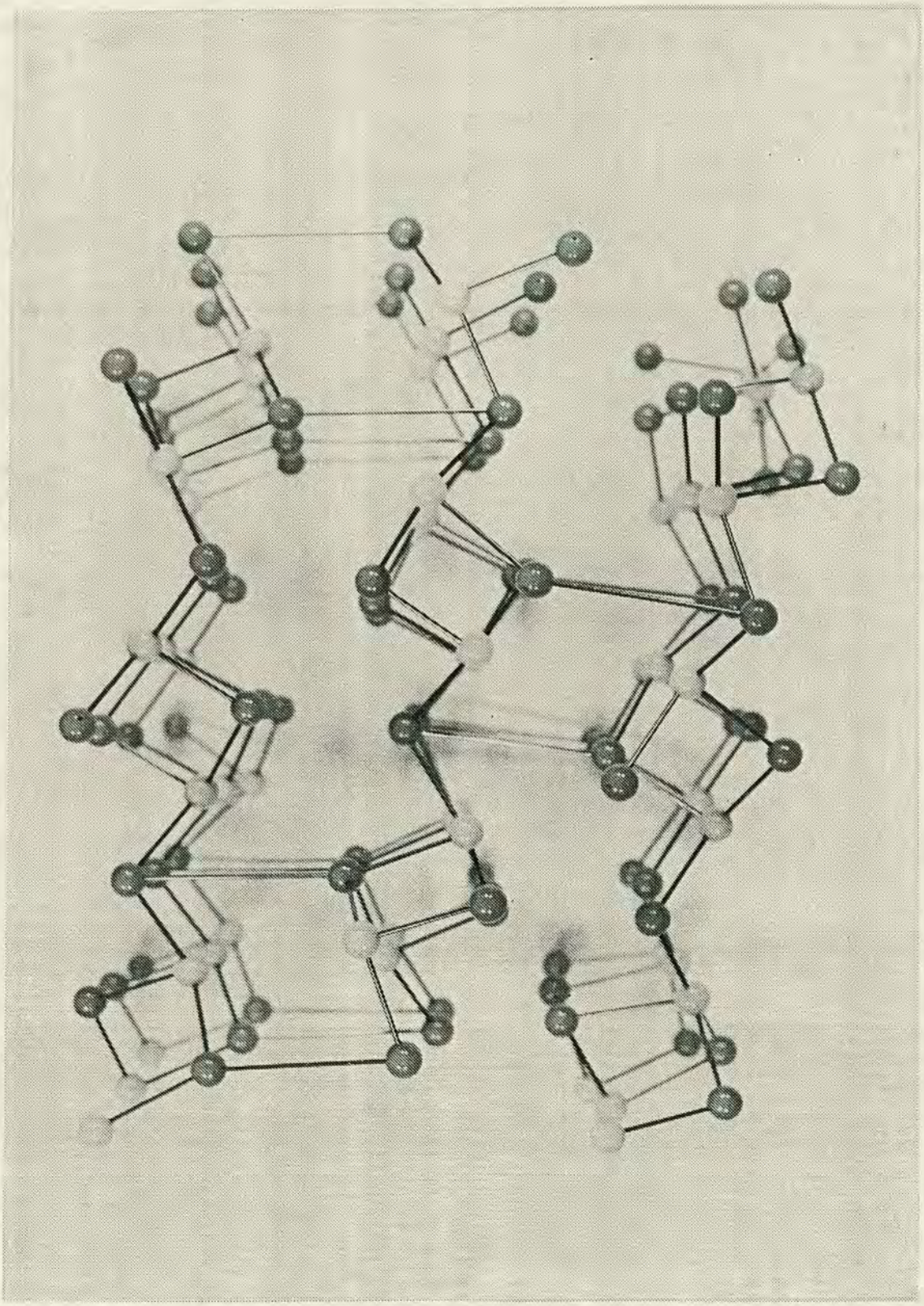

FIG. [4.7b]

Shows an edgewise view of the adjacent layers.

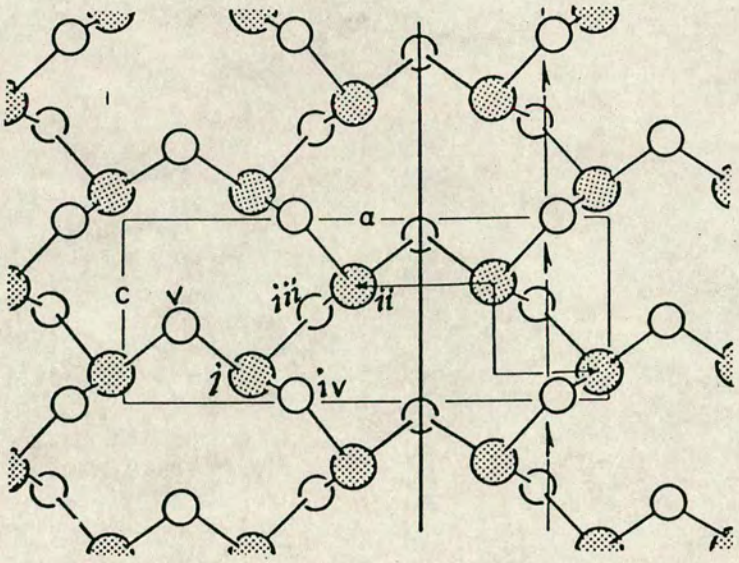

(A)

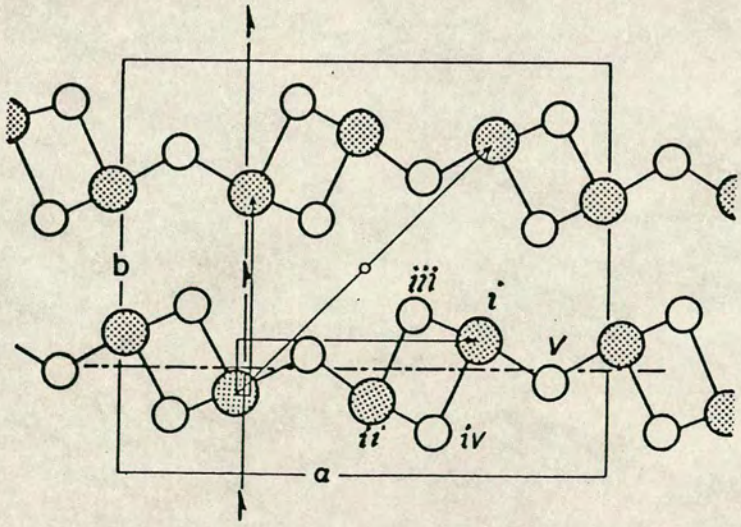

As Se

a = 12.053 Å ; b = 9.890 Å ; c = 4.277 Å

(B)

FIG.(4.8)

The orpiment structure. (A) Shows a view of a single layer from above. (B) Shows an edge-on view of the layer

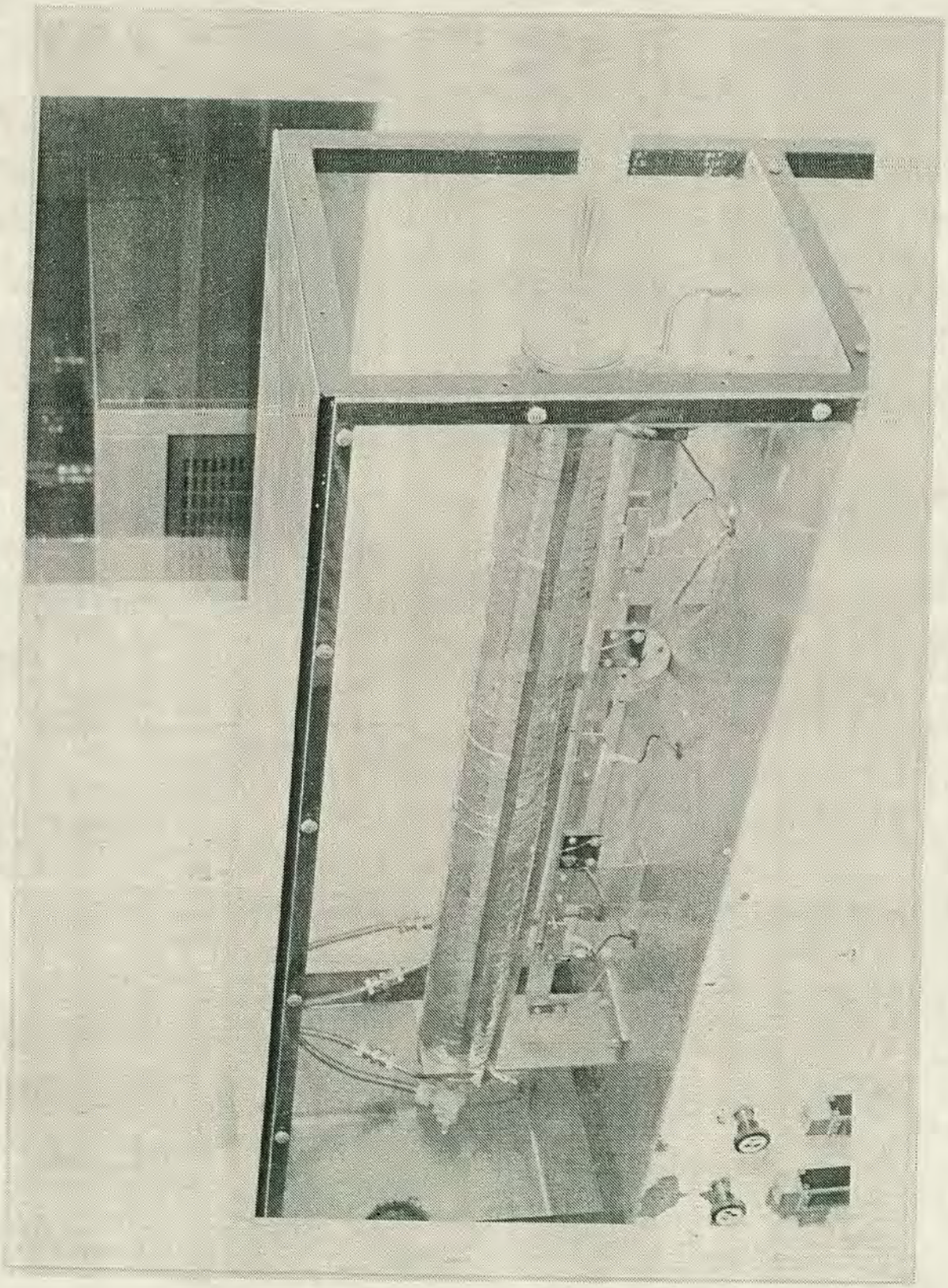

FIG. 4.9

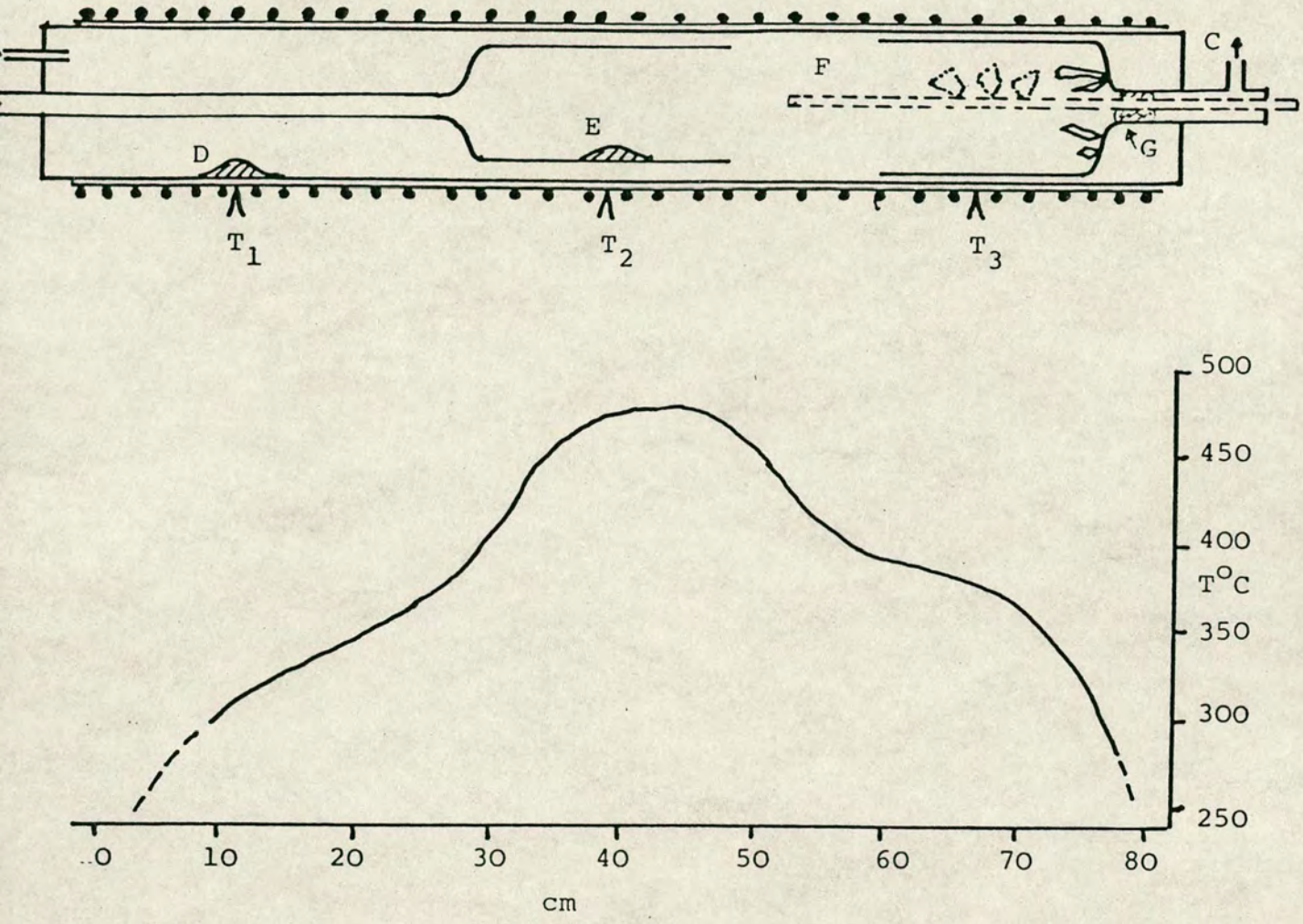

Figure (4.10) Diagram of the arrangement of glassware within the furnace. A,B are carrier gas inlets to zones 1 and 2, C is the outlet for waste carrier gas, D,E are quantities of source material (E only used in the present study), F is an axial pyrex rod used as a growth site in some experiments, G is a quartz wool plug used in some experiments, $T_{1,2,3}$ are control themocouples. Graph is temperature profile

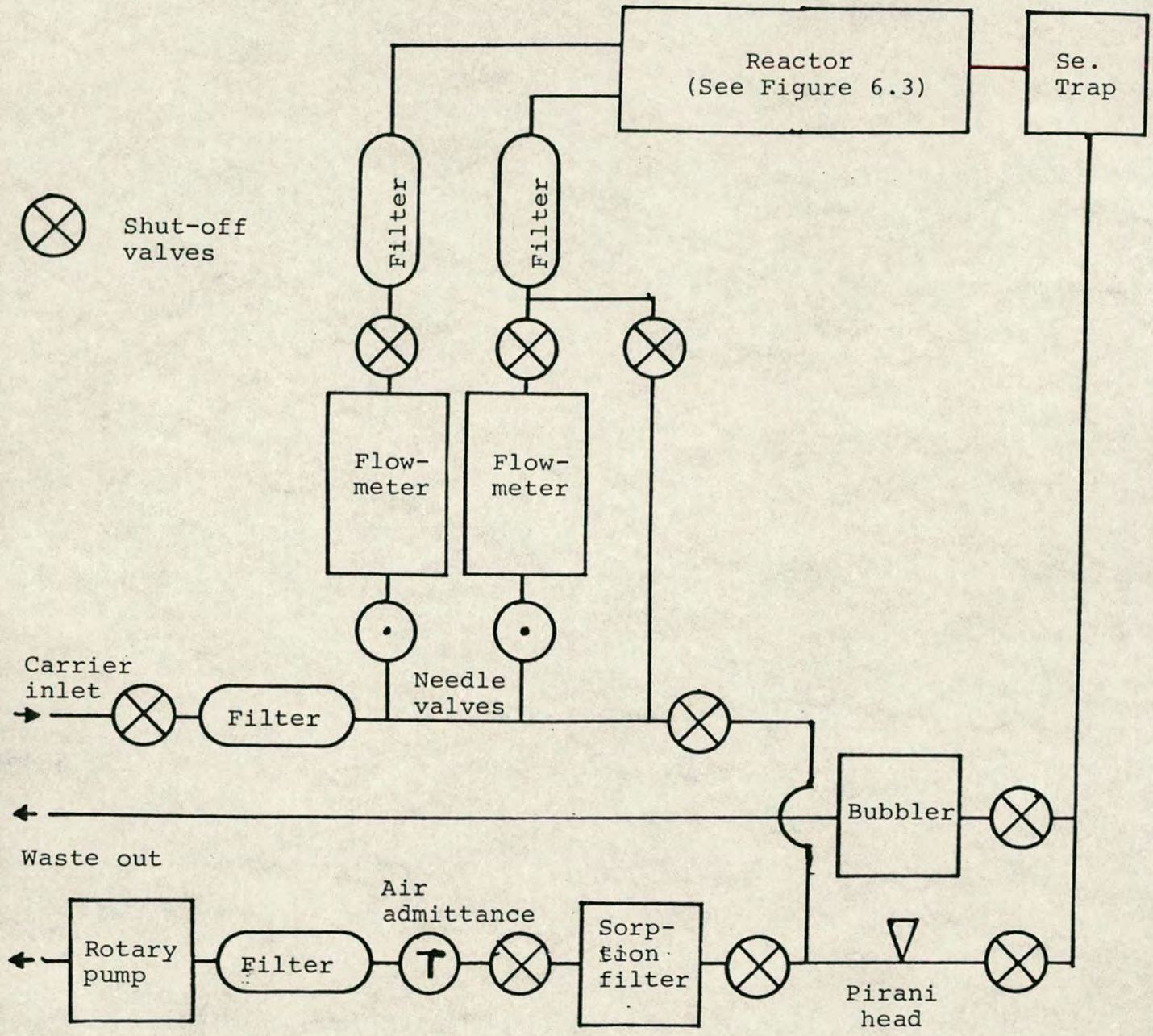

Figure (4.11) Diagram of the gas flow arrangement for the crystal growth apparatus.

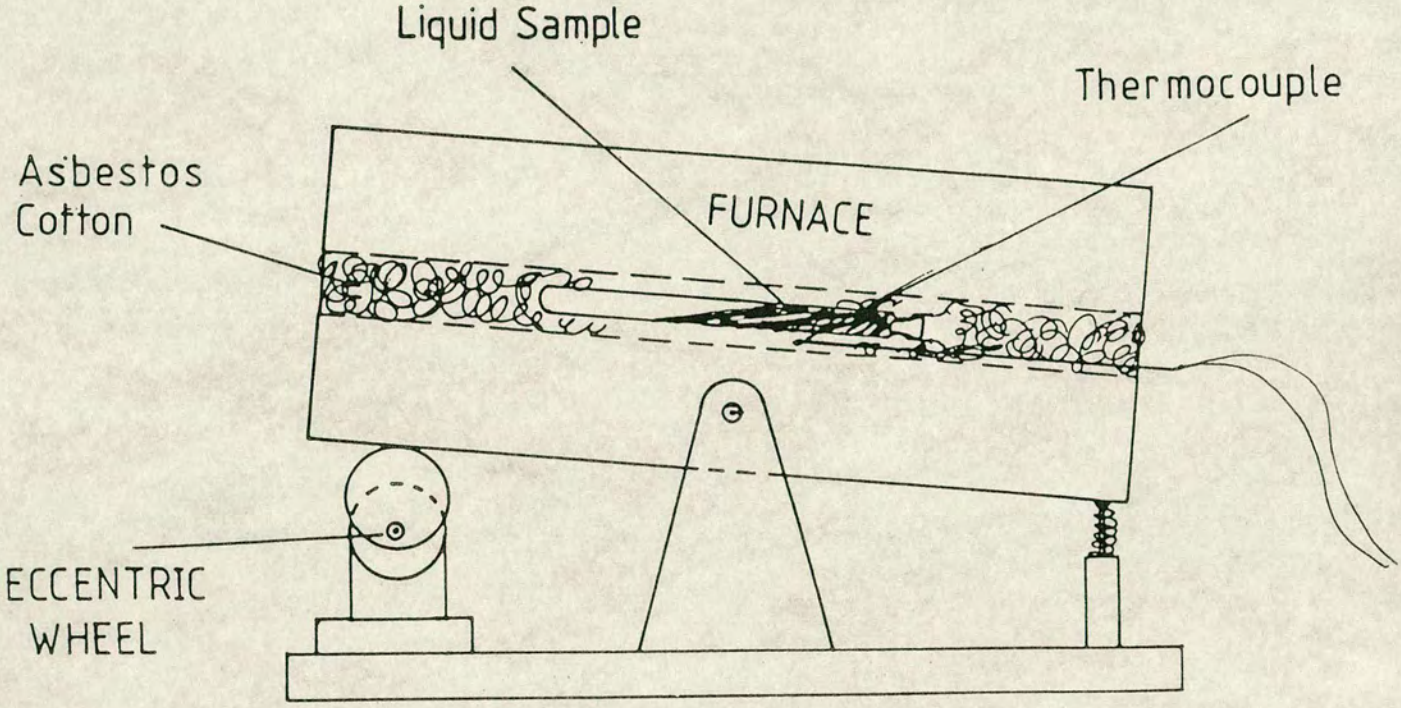

FIG.(5.1)

Rocking furnace

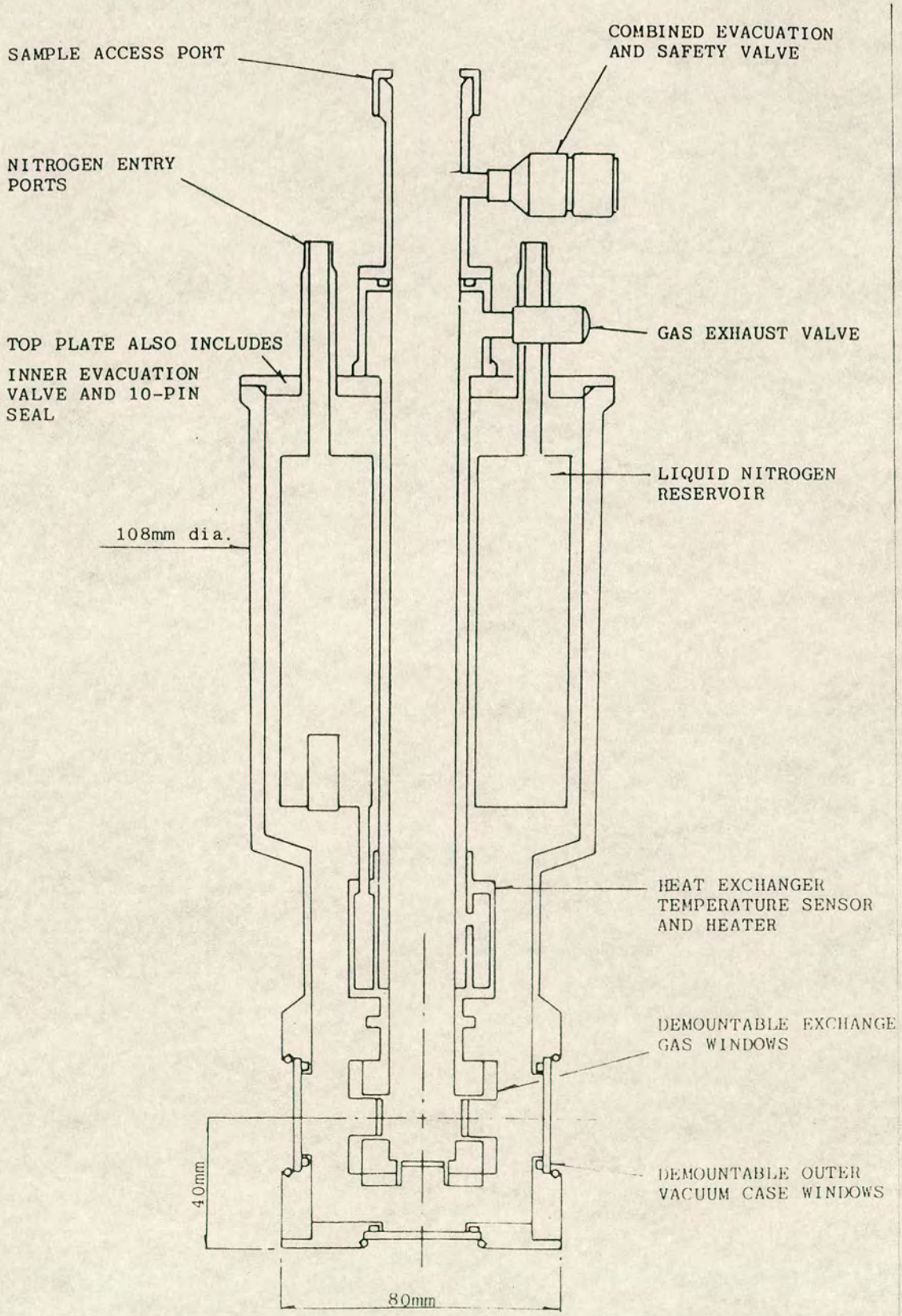

FIG.[5.2]

Schematic representaton of the Oxford Instrument DN1704 variable temperature liquid nitrogen cryostat

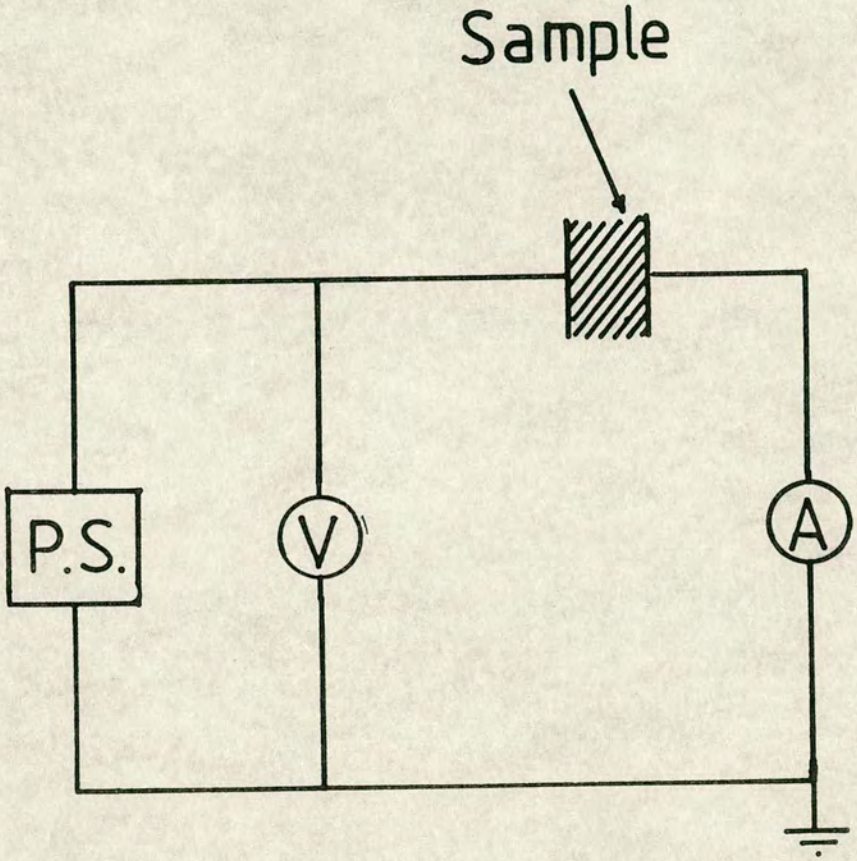

FIG. (5.3)

Circuit used for d.c. conductivity measurements

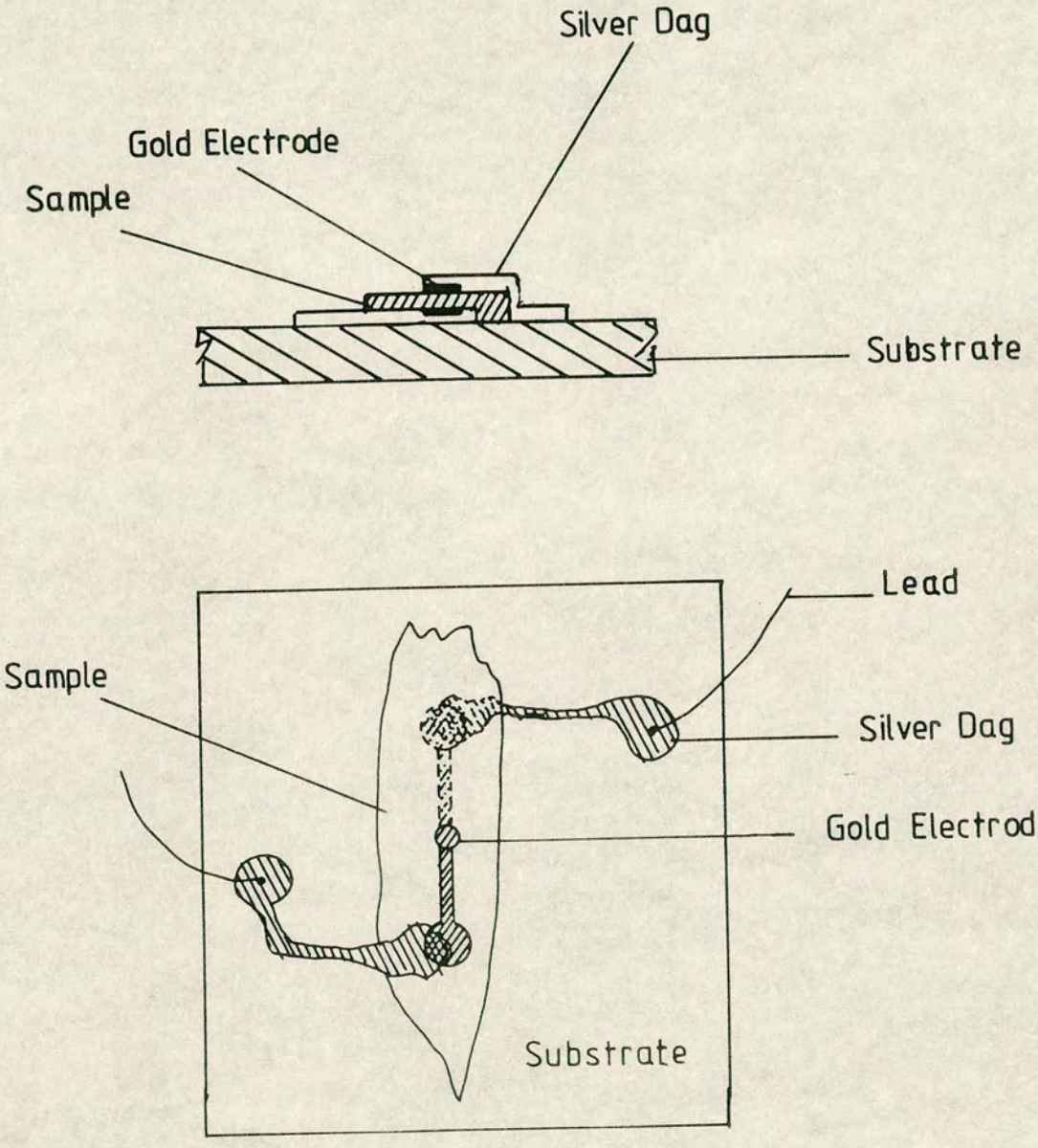

FIG.(5.4)

An illustration of the electrode connections to the sample

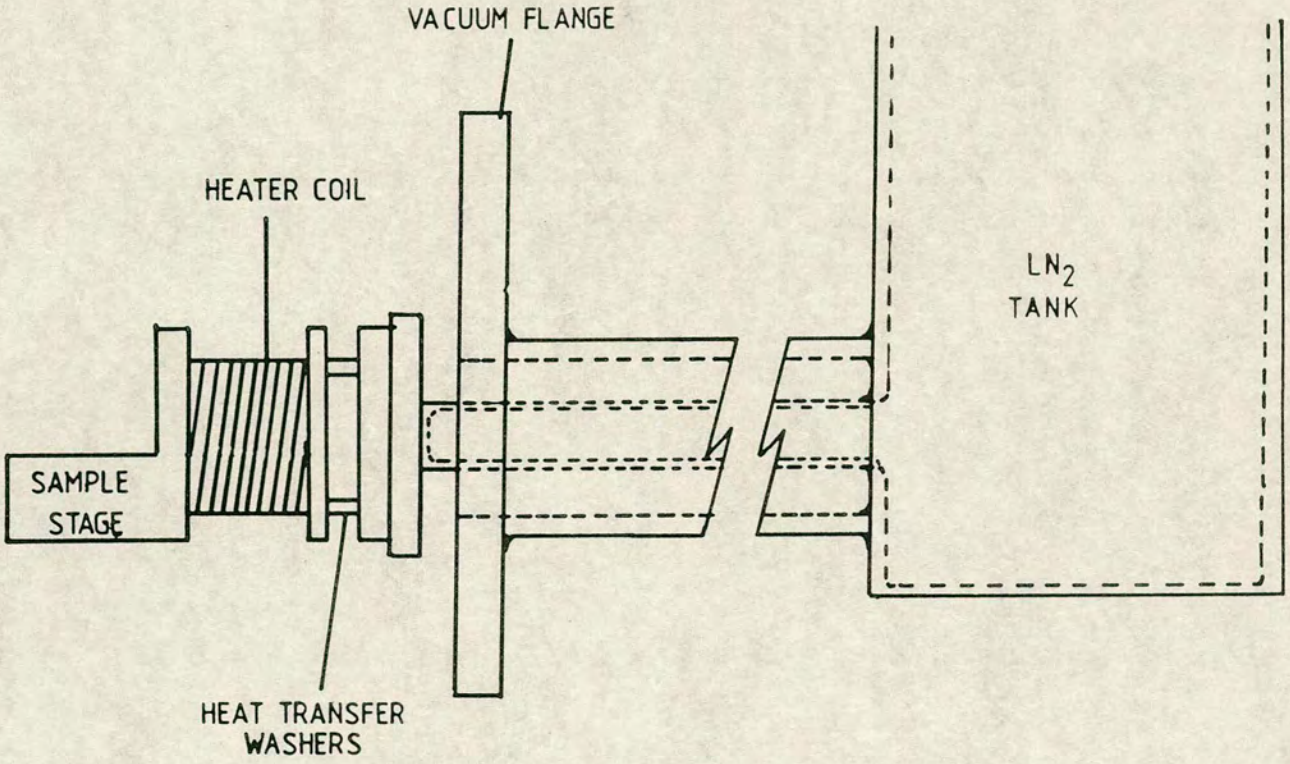

FIG.(5.5)

Drawing of cold-finger used for the thermopower measurements

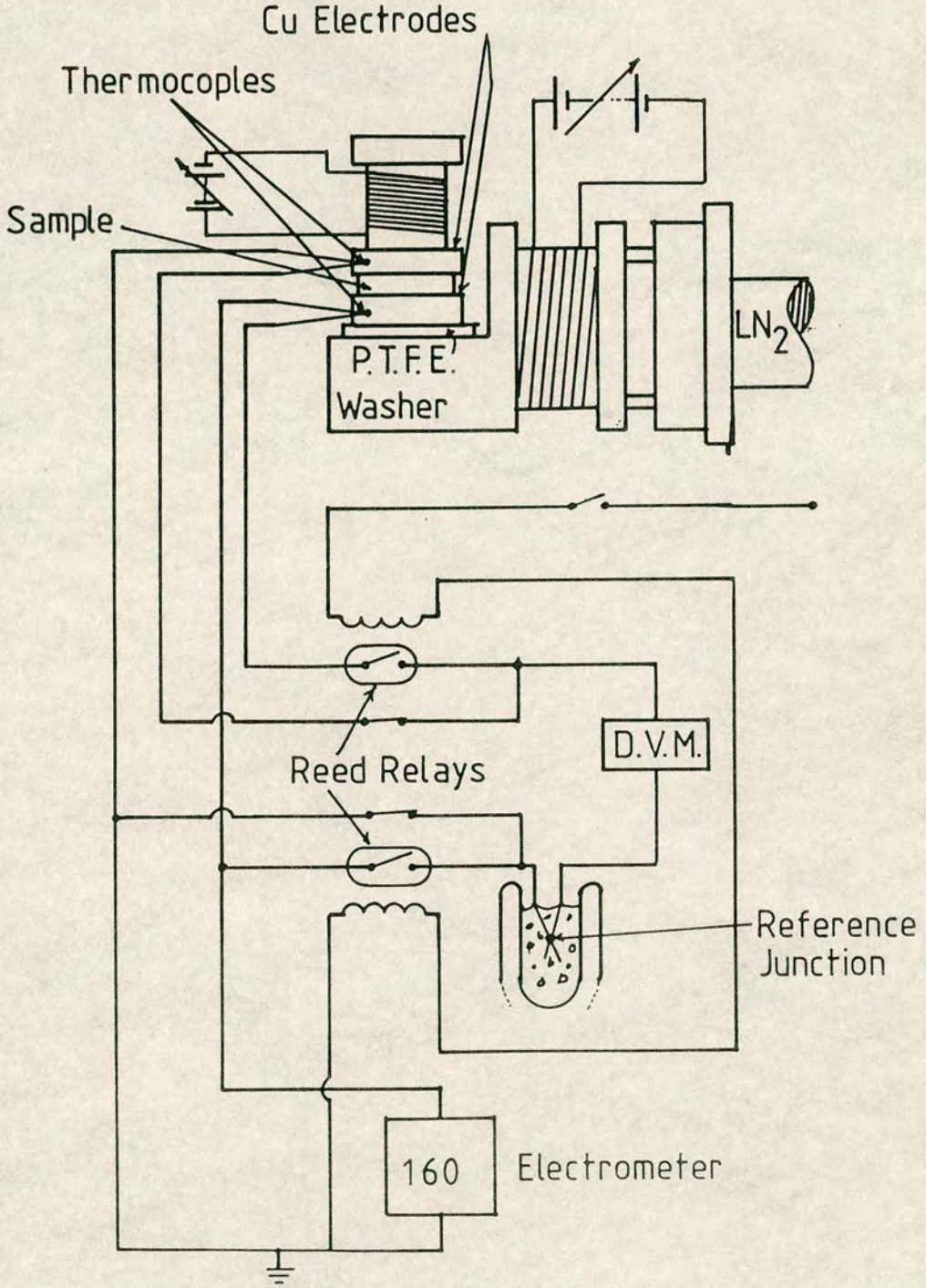

FIG.(5.6)

Schematic of the apparatus for the thermopower measurements

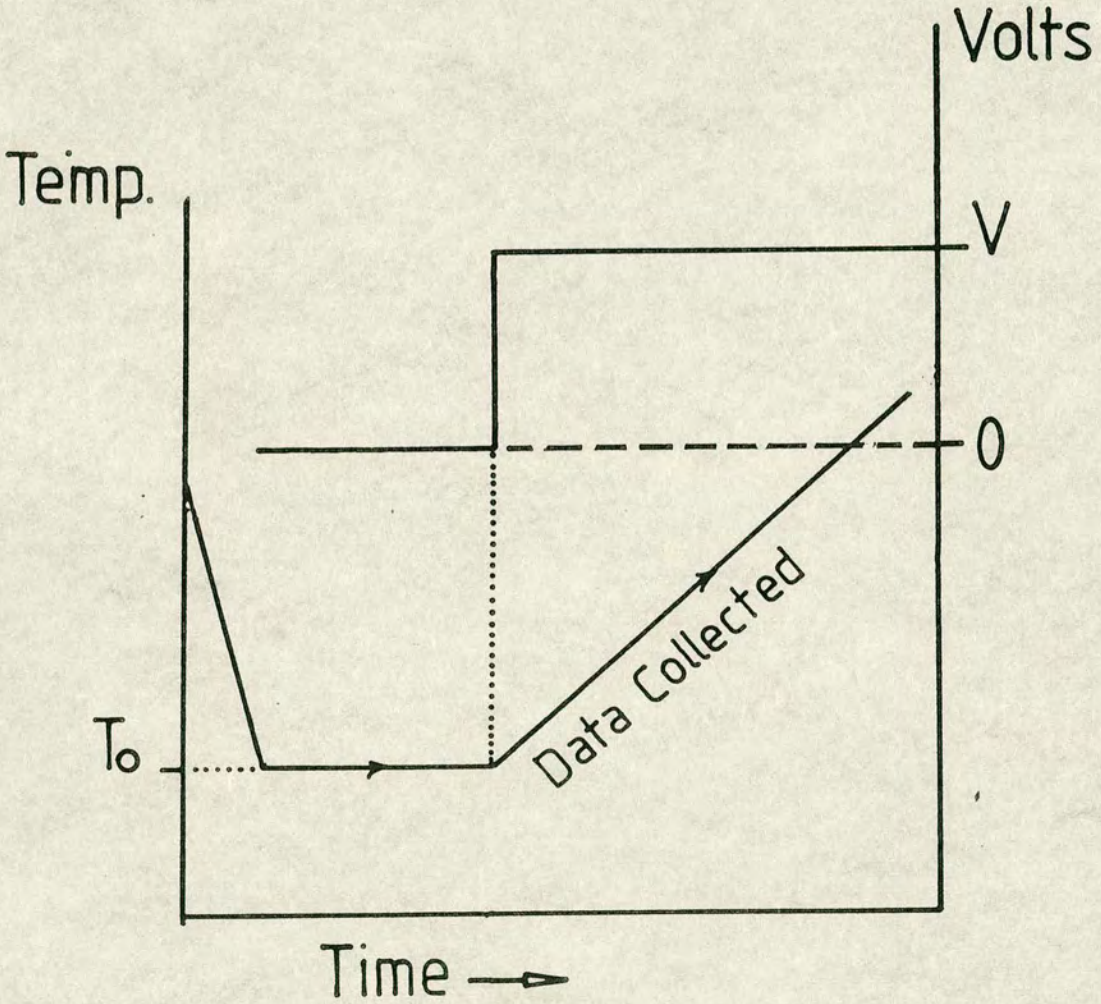

FIG.(5.7)

Experimental procedure

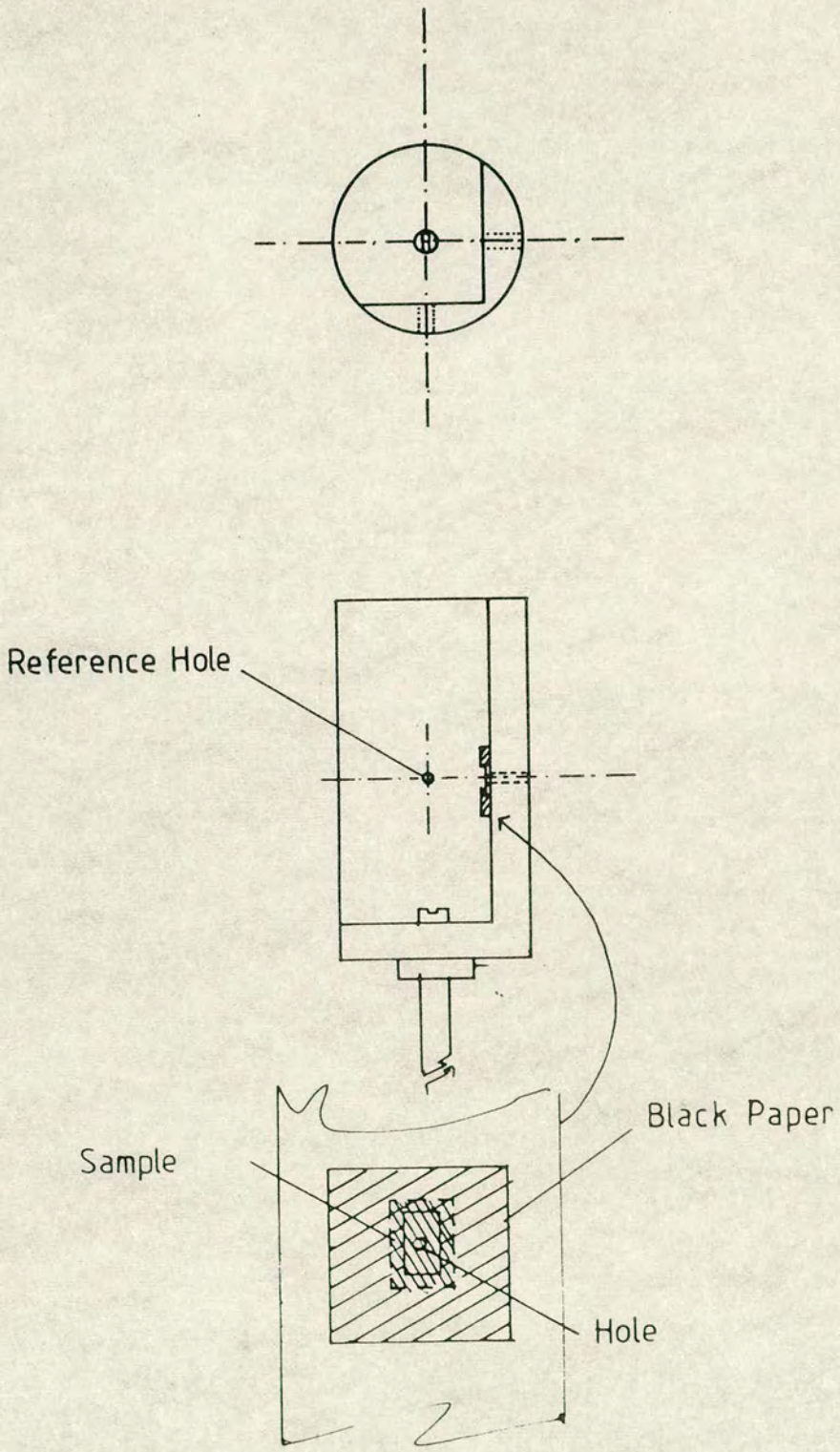

FIG.(5.8)

Illustration of the sample holder configuration

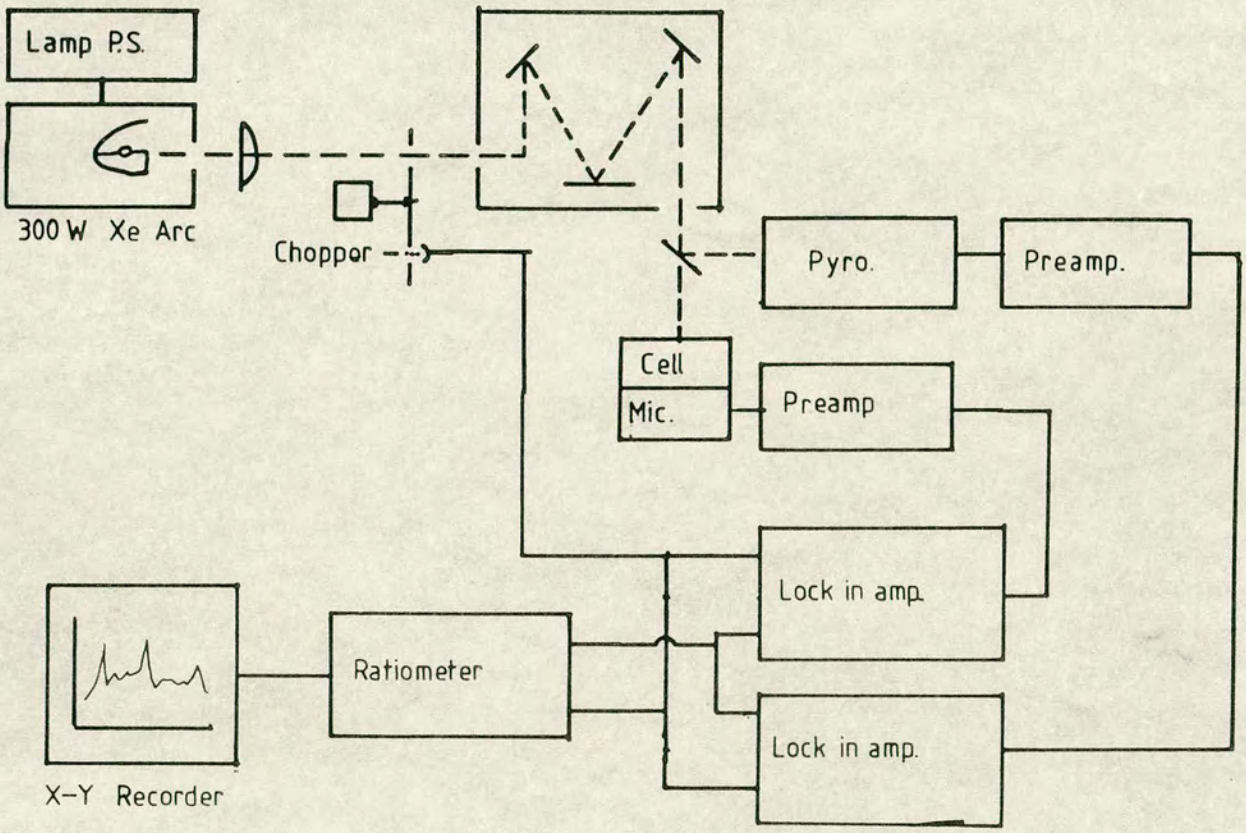

FIG. (5.9)

Schematic diagram of the EDT OAS400 photoacoustic spectroscopy

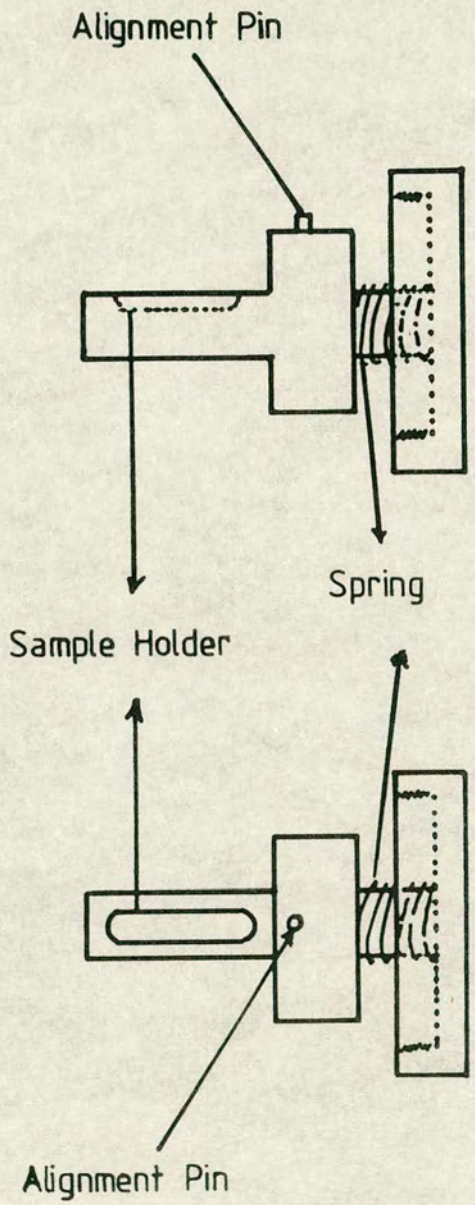

FIG. (5.10)

Sample holder of the EDT photoacoustic spectroscopy

SAMPLE	REFRACTIVE INDEX
As_2Se_3	4.57
$Cu_{.02}(As_{.4}Se_{.6})_{99.98}$	4.52
$Cu_{.1}(As_{.4}Sa_{.6})_{99.9}$	4.4
$Cu_{.17}(As_{.4}Se_{.6})_{99.83}$	3.51
$Ga_{.01}(As_{.4}Se_{.6})_{99.99}$	2.82
$Ga_{.12}(As_{.4}Se_{.6})_{99.88}$	2.13
$Ga_{.8}(As_{.4}Se_{.6})_{99.2}$	5.82

Table (6.1)

SAMPLE	FIGURE	Eo eV
As_2Se_3	6.19	1.22
As_2Se_3	6.20	1.1
$Cu_{.1}(As_{.4}Se_{.6})_{99.9}$	6.21	0.93

Table (6.2)

SAMPLE	NO.	FIGURE	TYPE OF PLOT
As_2Se_3	1	6.23a	I-V
a	2	6.23b	I-V
a	1,2	6.23c	σ vs 1000/T
$Cu_{.02}(As_{.4}Se_{.6})_{99.98}$	1	6.24a	I-V
a	2	6.24b	I-V
a	1,2	6.24c	σ vs 1000/T
$Cu_{.1}(As_{.4}Se_{.6})_{99.9}$	1	6.25a	I-V
a	2	6.25b	I-V
a	1,2	6.25c	σ vs 1000/T
$Cu_{.17}(As_{.4}Se_{.6})_{99.83}$	1	6.26a	I-V
a	2	6.26b	I-V
a	1,2	6.26c	σ vs 1000/T
$Ga_{.12}(As_{.4}Se_{.6})_{99.88}$	1	6.27a	I-V
a	1	6.27b	σ vs 1000/T

Table (6.3)

SAMPLE	NO.	Eσ eV	FIGURE
As_2Se_3	1	0.9	6.23c
a	1	0.89	6.23c
$Cu_{.02}(As_{.4}Se_{.6})_{99.98}$	1	0.89	6.24c
a	2	0.92	6.24c
$Cu_{.1}(As_{.4}Se_{.6})_{99.9}$	1	0.85	6.25c
a	2	0.85	6.25c
$Cu_{.17}(As_{.4}Se_{.6})_{99.83}$	1	0.87	6.26c
a	2	0.85	6.26c
$Ga_{.12}(As_{.4}Se_{.6})_{99.88}$	1	0.9	6.27b

Table (6.4)

CARRIER GAS	ACTIVATION ENERGY (eV)	TECHNIQUE
H_2 (9)	0.93 - 0.95	Close Tube
I (9)	1.1	. .
H_2 (10)	0.94 - 1.05	Close Tube
Ar+I (11)	0.77	Close Tube
N_2 (12)	0.95	Open Tube
N_2 (This project)	0.9	Open Tube

Table (6.5)

SAMPLE	FIGURE	a	b	c
As_2Se_3	6.44	80 °K	150 °K	295 °K
$Cu_{.02}(As_{.4}Se_{.6})_{99.98}$	6.45	80 °K	150 °K	295 °K
$Cu_{.1}(As_{.4}Se_{.6})_{99.9}$	6.46	80 °K	150 °K	295 °K
$Cu_{.17}(As_{.4}Se_{.6})_{99.83}$	6.47	80 °K	150 °K	295 °K
$Ga_{.12}(As_{.4}Se_{.6})_{99.88}$	6.48	80 °K	150 °K	295 °K
$Ga_{.8}(As_{.4}Se_{.6})_{99.2}$	6.49	80 °K	150 °K	296 °K

Table (6.6)

SAMPLE	E_{opt}(295 K)eV	E_{opt}(150 K)eV	E_{opt}(80 K)eV
As_2Se_3	1.82	1.92	1.98
$Cu_{.02}(As_{.4}Se_{.6})_{99.98}$	1.79	1.93	1.98
$Cu_{.1}(As_{.4}Se_{.6})_{99.9}$	1.80	1.93	1.98
$Cu_{.17}(As_{.4}Se_{.6})_{99.83}$	1.80	1.91	1.97
$Ga_{.12}(As_{.4}Se_{.6})_{99.88}$	1.79	1.92	1.96
$Ga_{.8}(As_{.4}Se_{.6})_{99.2}$	1.77	1.90	1.97

Table (6.7)

SAMPLE	E_{opt}(0 k)eV	γ eV.K^{-1}
As_2Se_3	2.04	7×10^{-4}
$Cu_{.02}(As_{.4}Se_{.6})_{99.98}$	2.06	9×10^{-4}
$Cu_{.1}(As_{.4}Se_{.6})_{99.9}$	2.05	8×10^{-4}
$Cu_{.17}(As_{.4}Se_{.6})_{99.83}$	2.03	8×10^{-4}
$Ga_{.12}(As_{.4}Se_{.6})_{99.88}$	2.03	8×10^{-4}
$Ga_{.8}(As_{.4}Se_{.6})_{99.2}$	2.04	9×10^{-4}

Table (6.8)

Shaw et al.	At T=77 °K	E_{opt}=2.03 eV
	At room Temperature	E_{opt}=1.82 eV
Althaus et al.	At T=10 °K	E_{opt}=2.00 eV
Kolomiets	At T=77 °K	E_{opt}=1.94 eV
Zallen et al.	At T=10 °K	E_{opt}=2.00 eV

SAMPLE	FIGURE	E_{opt} eV
As_2Se_3	6.51	1.83
$Cu_{.02}(As_{.4}Se_{.6})_{99.98}$	6.52	1.85
$Cu_{.1}(As_{.4}Se_{.6})_{99.9}$	6.53	1.82
$Cu_{.17}(As_{.4}Se_{.6})_{99.83}$	6.54	1.84
$Ga_{.01}(As_{.4}Se_{.6})_{99.99}$	6.55	1.86
$Ga_{.12}(As_{.4}Se_{.6})_{99.88}$	6.56	1.84
$Ga_{.8}(As_{.4}Se_{.6})_{99.2}$	6.57	1.83

Table (6.9)

SAMPLE	REALTIVE HEIGHT %
$Cu_{.02}(As_{.4}Se_{.6})_{99.98}$	+ 13%
$Cu_{.1}(As_{.4}Se_{.6})_{99.9}$	- 1.9%
$Cu_{.17}(As_{.4}Se_{.6})_{99.83}$	+ 12%
$Ga_{.01}(As_{.4}Se_{.6})_{99.99}$	+ 7%
$Ga_{.12}(As_{.4}Se_{.6})_{99.88}$	- 1%
$Ga_{.8}(As_{.4}Se_{.6})_{99.2}$	+ 10%

Table (6.10)

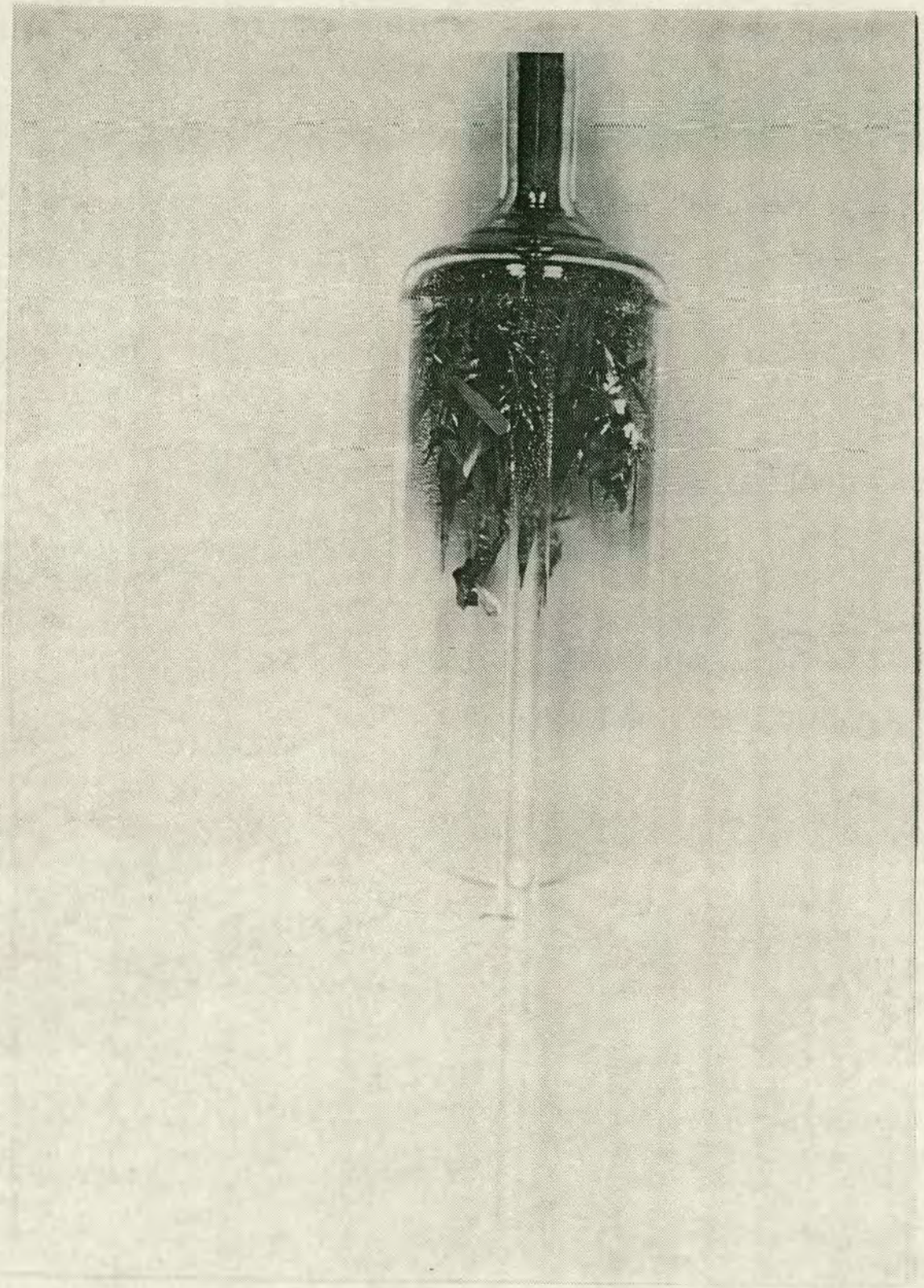

FIG. 6.1

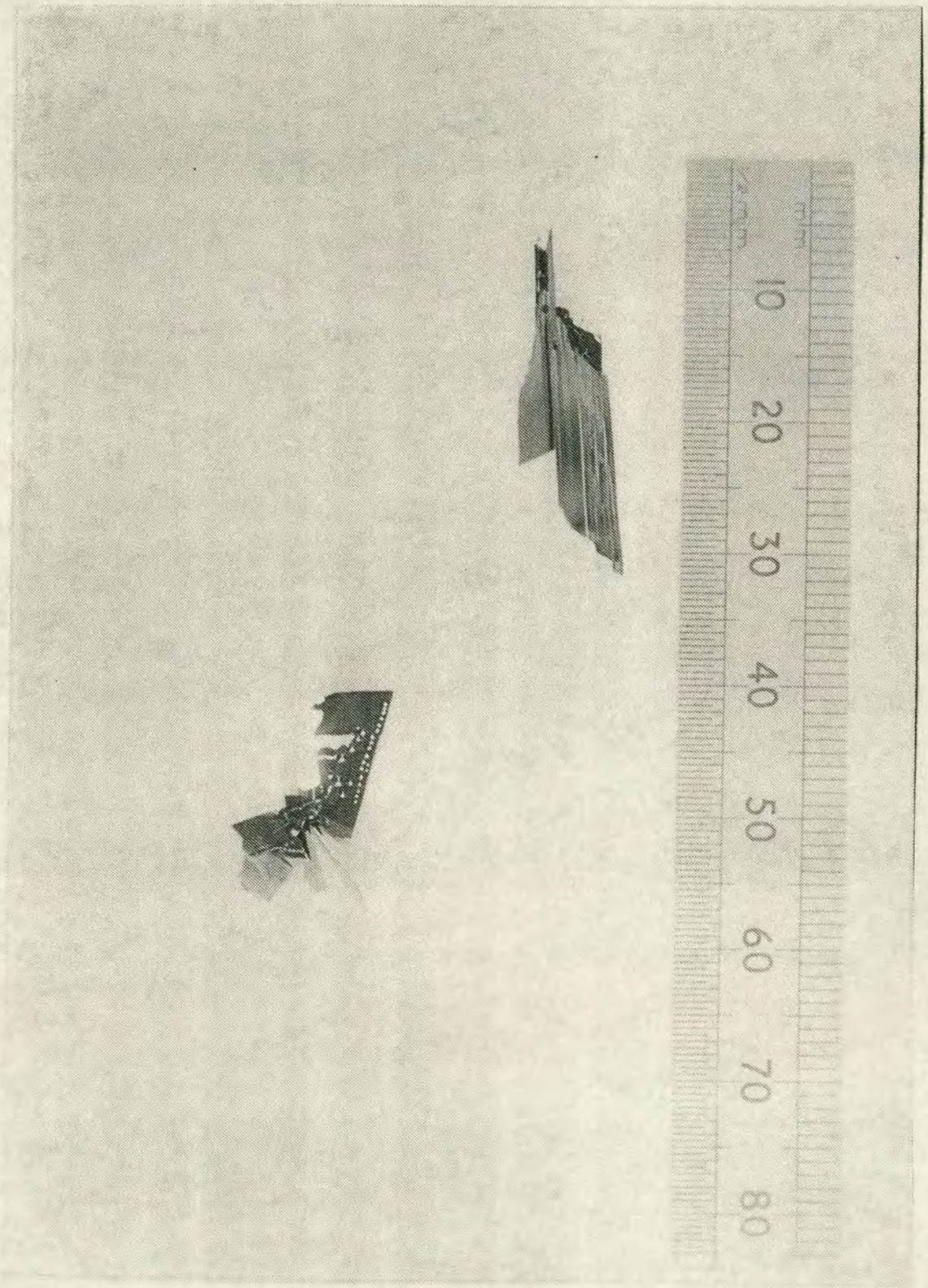

FIG. [6.2]

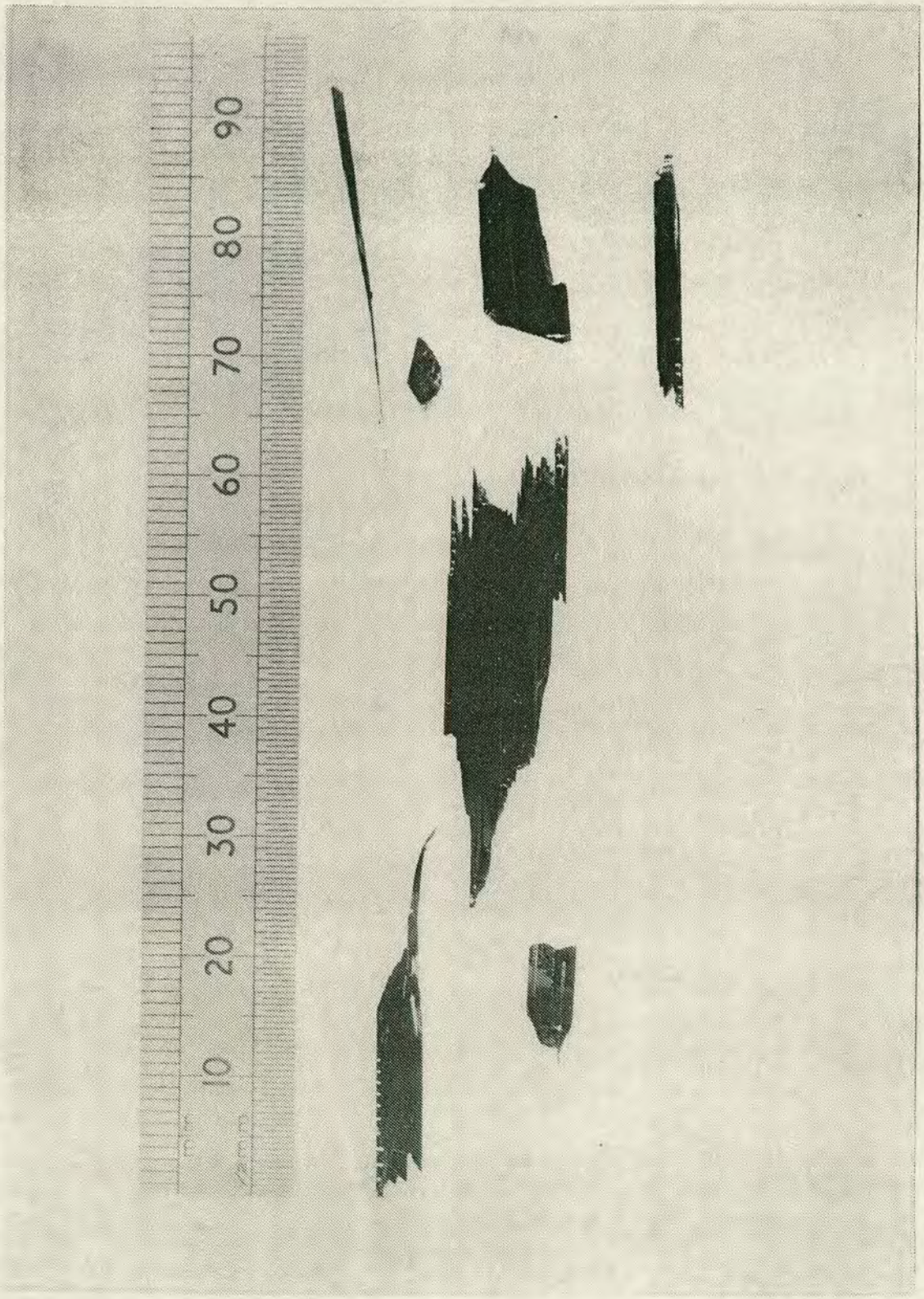

FIG. [6.3]

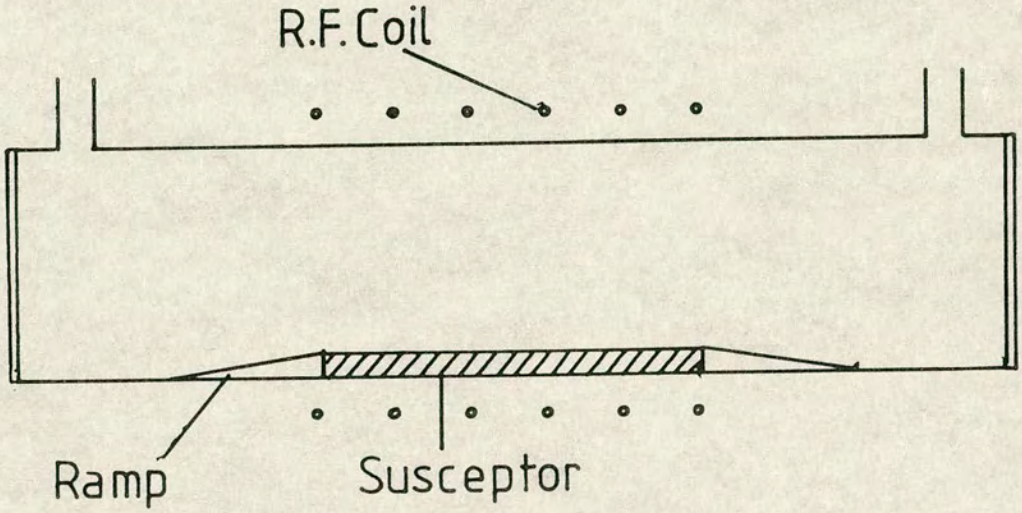

FIG. (6.4)

The reactor used by Giling

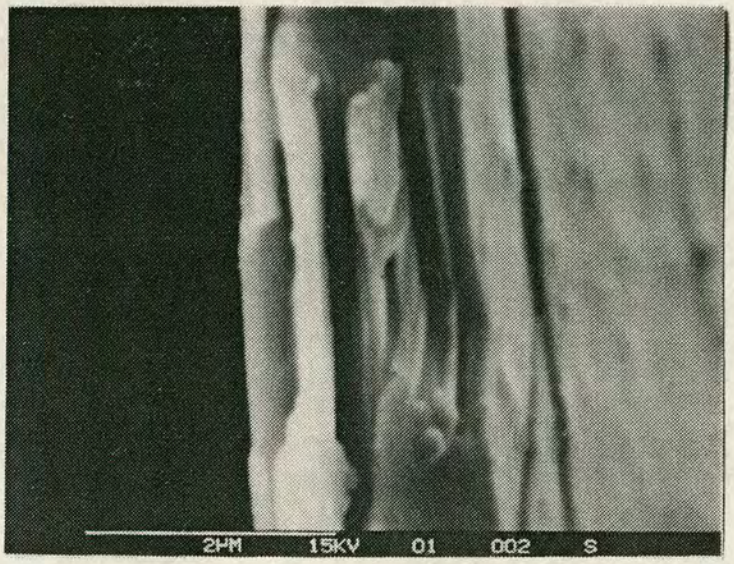

FIG. [6.5]

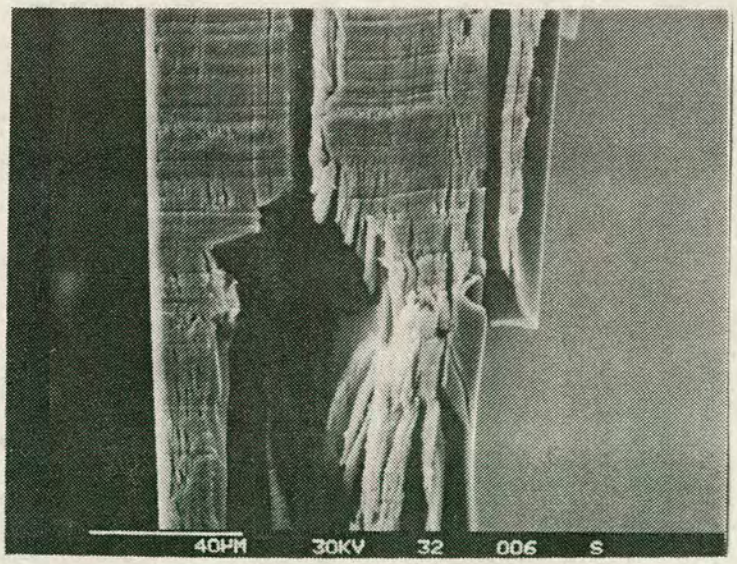

FIG. [6.6]

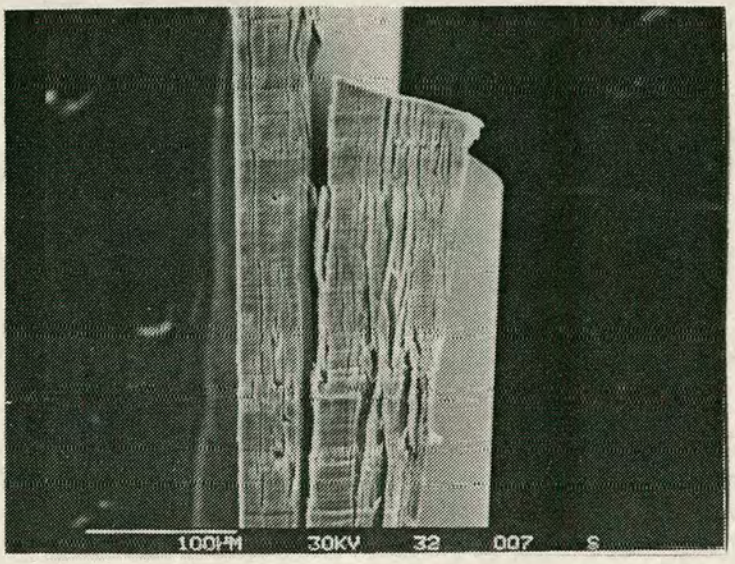

[FIG. 6.7]

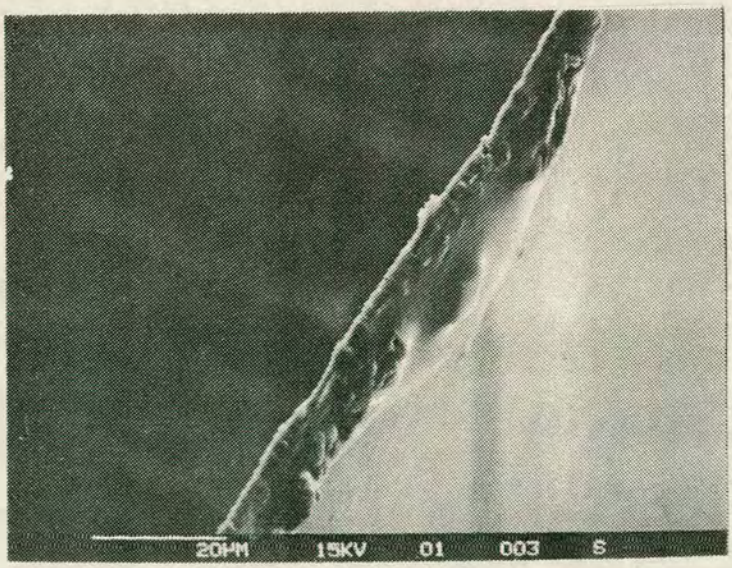

FIG. [6.8]

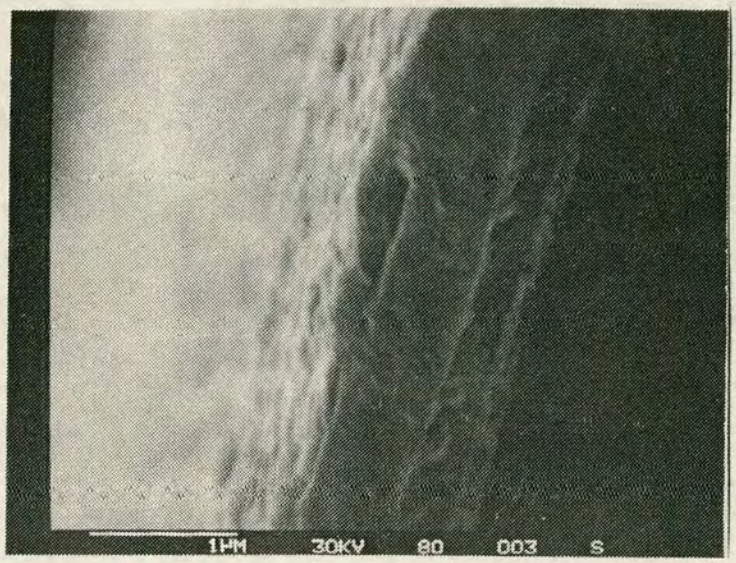

FIG. [6.9]

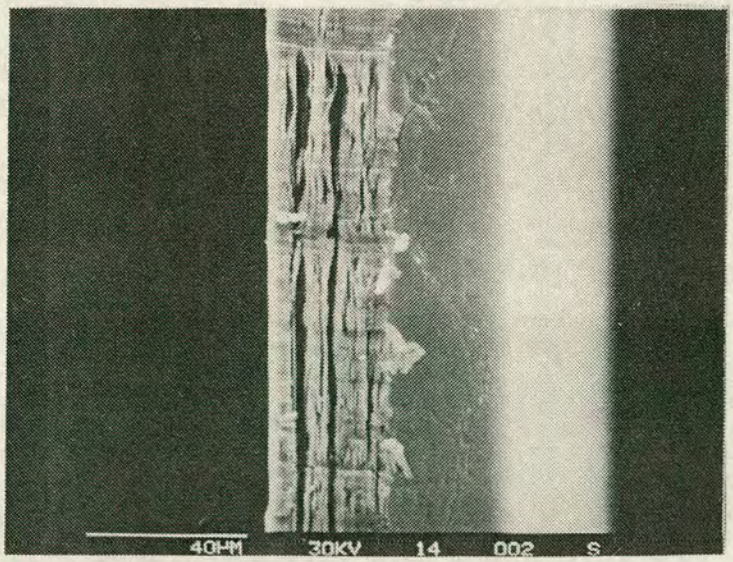

FIG. [6.10]

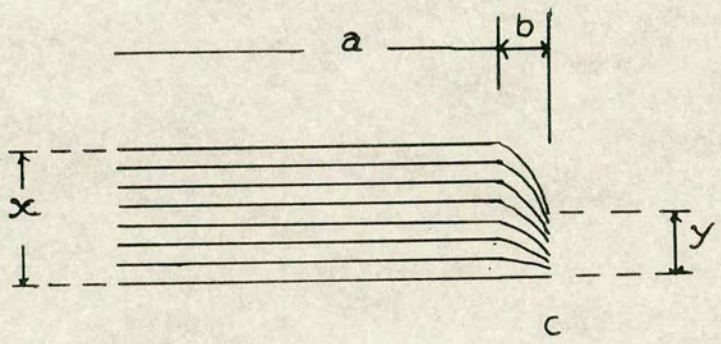

FIG. (6.11)

Schematic representation of the cross section at the edge of the crystal

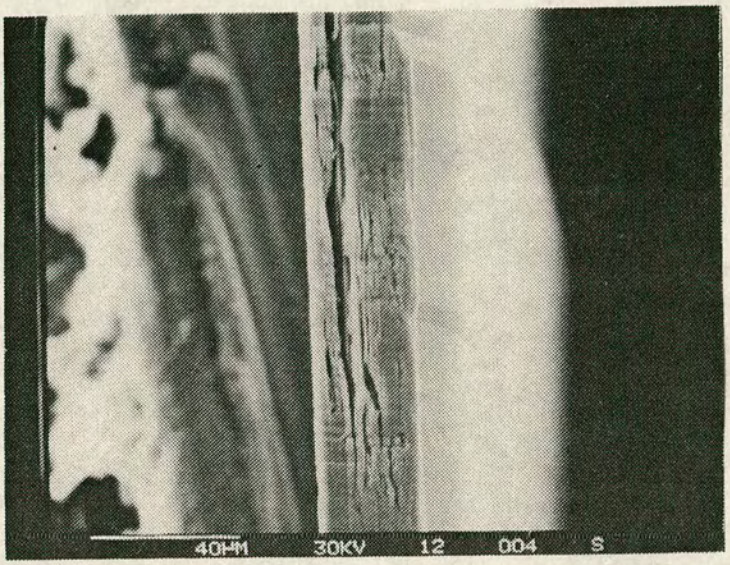

FIG. [6.12]

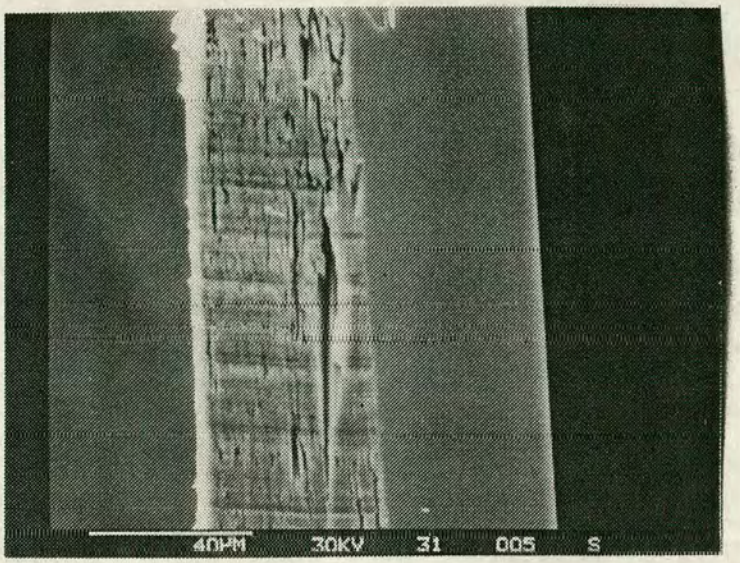

FIG. [6.13]

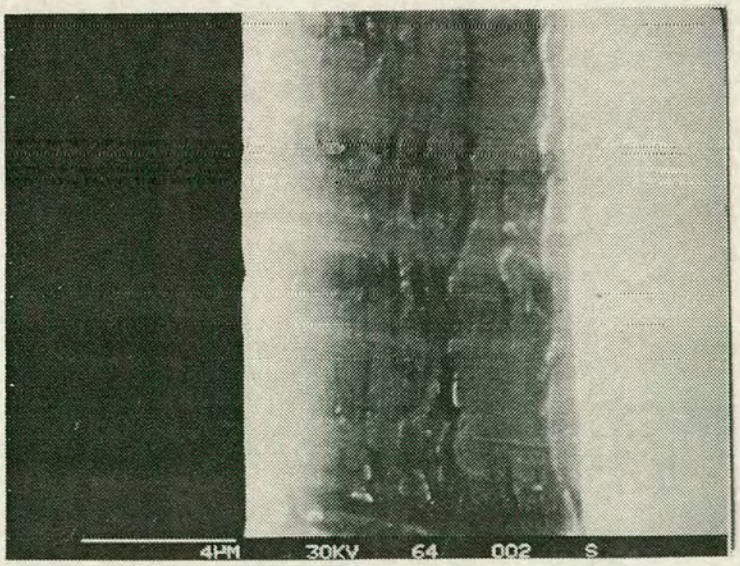

FIG. [6.14]

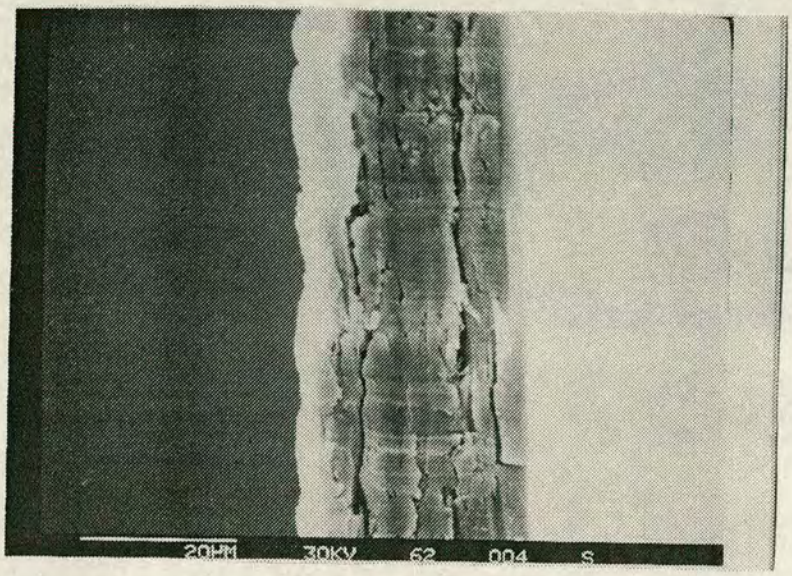

FIG.[6.15]

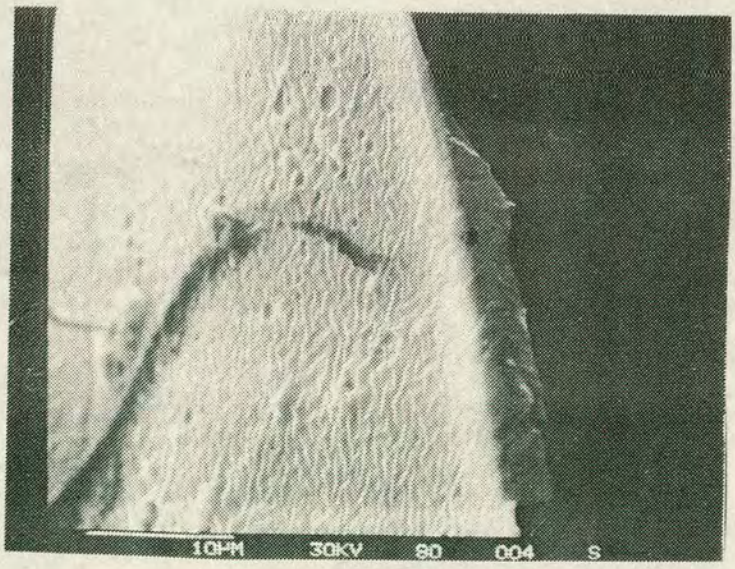

FIG.[6.16]

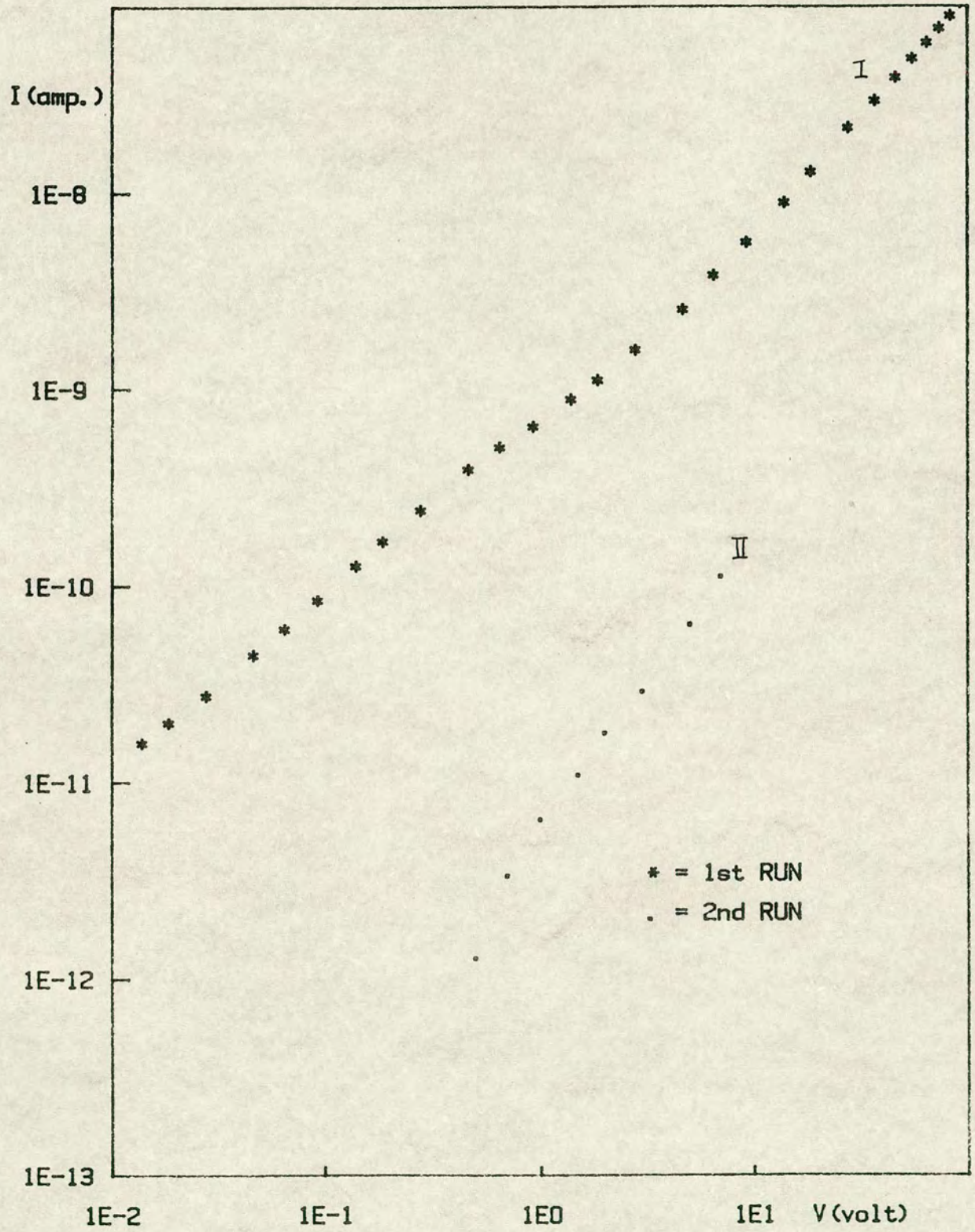

FIG.[6.17] : I-V CHARACTERISTIC OF PURE As2 Se3
AT TEMPERATURE = 400 K.

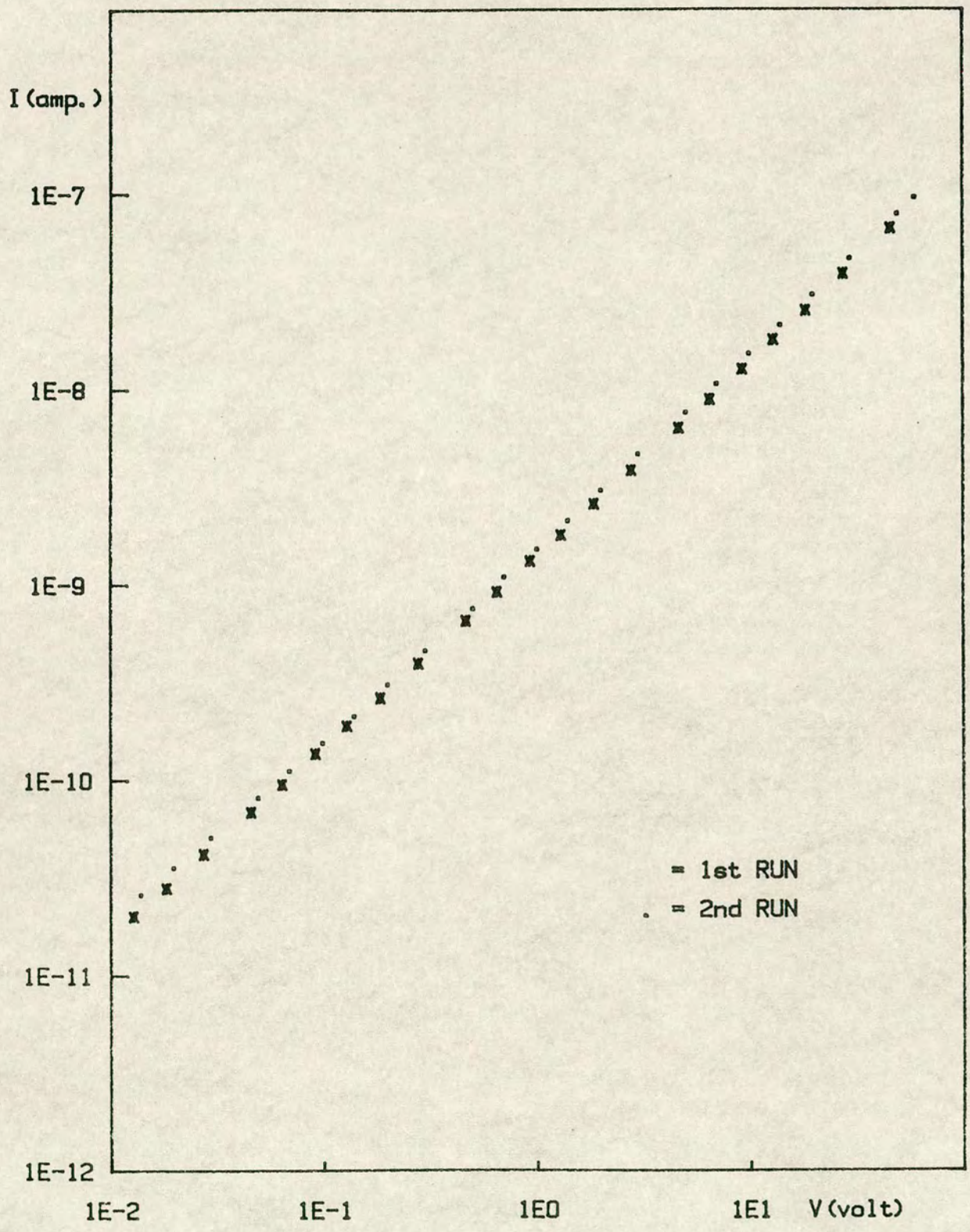

FIG. [6.18] : I-V CHARACTERISTIC OF Cu. 17 (As. 4 Se. 6) 99. 83
AT TEMPERATURE = 385 K.

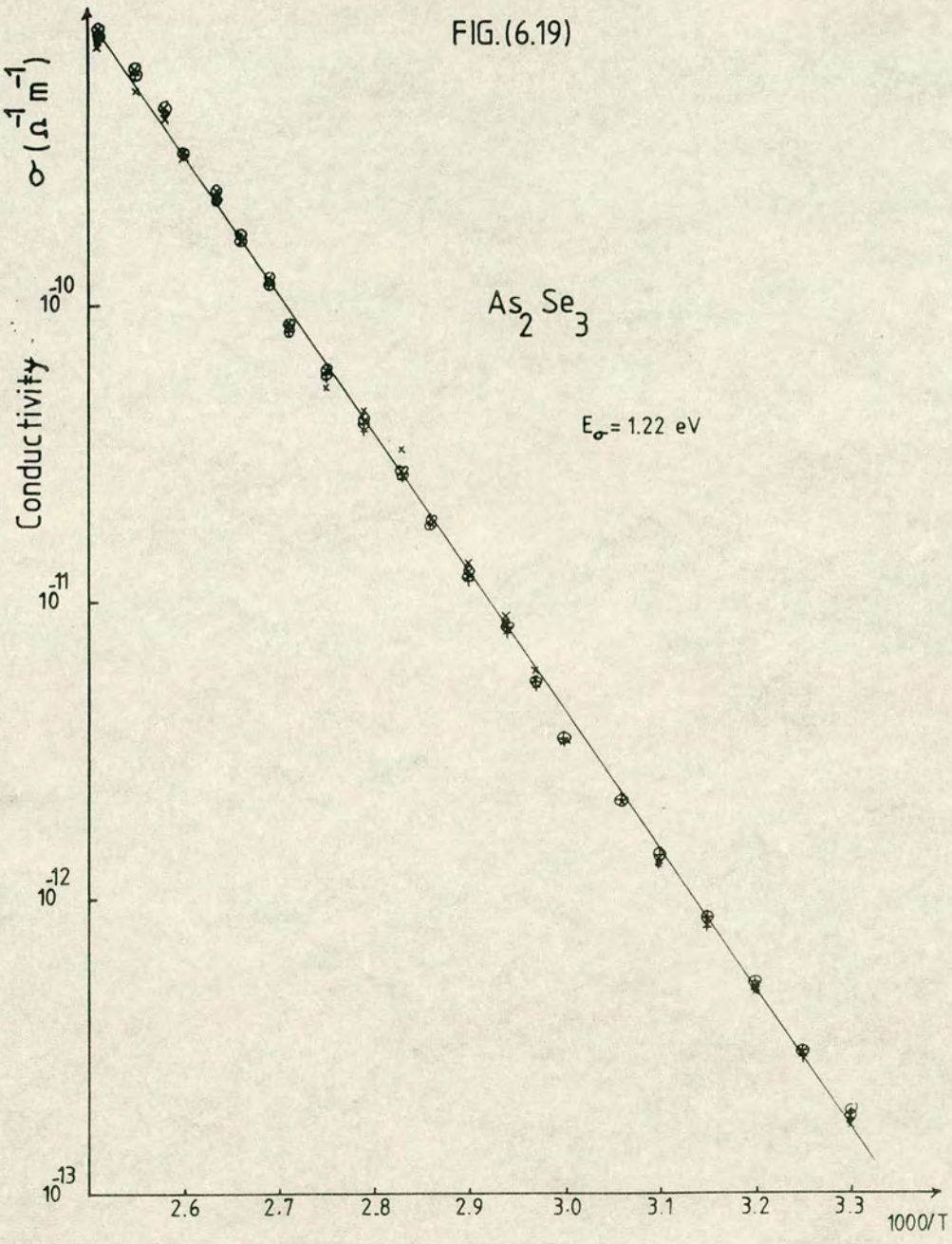

D.C. conductivity result using the first method for As_2Se_3 crystal

FIG.(6.20)

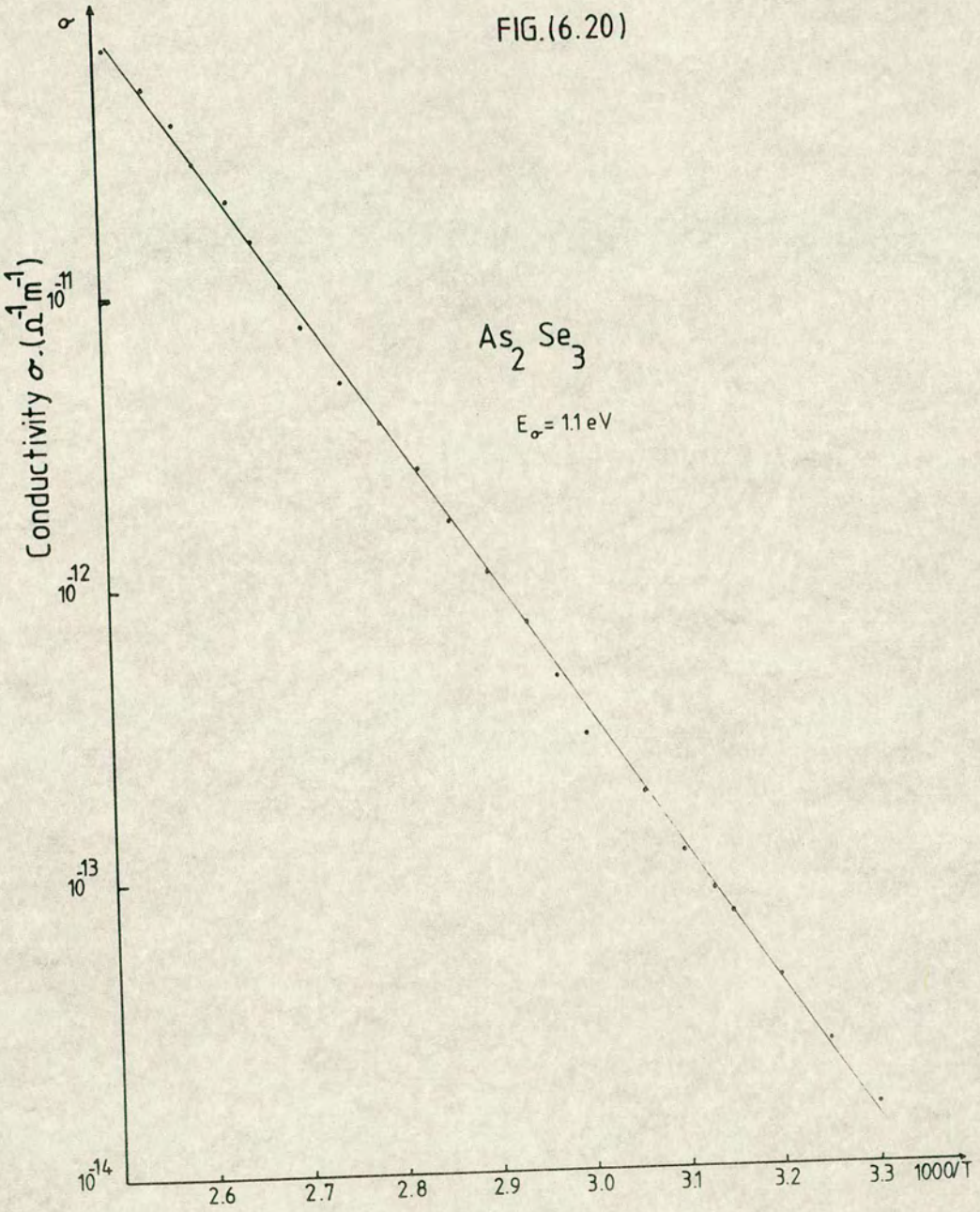

D.C. conductivity result using the first method for As_2Se_3 crystal

FIG.(6.21)

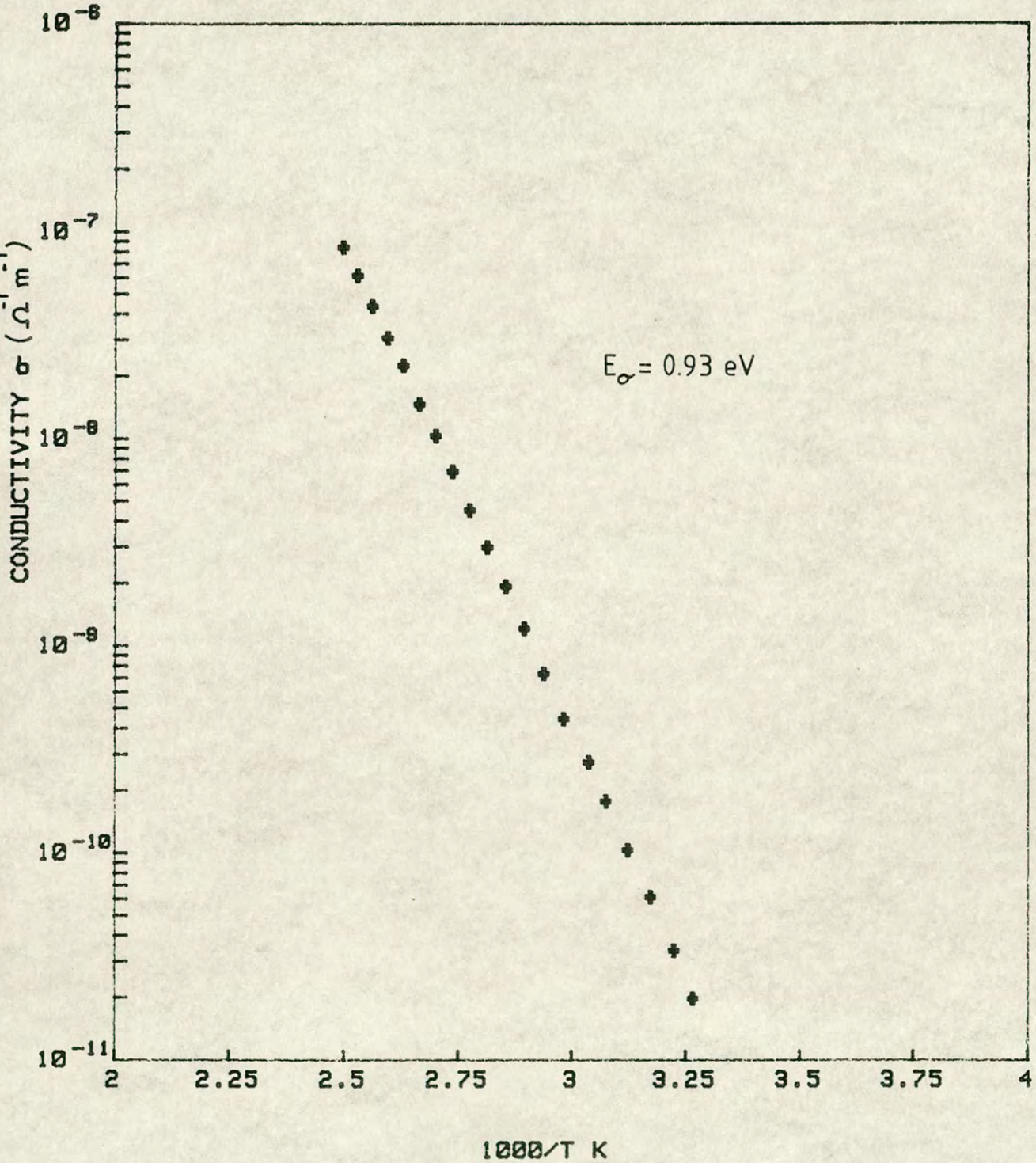

D.C. conductivity result using the first method for $Cu_{.1}(As_{.4}Se_{.6})_{99.9}$

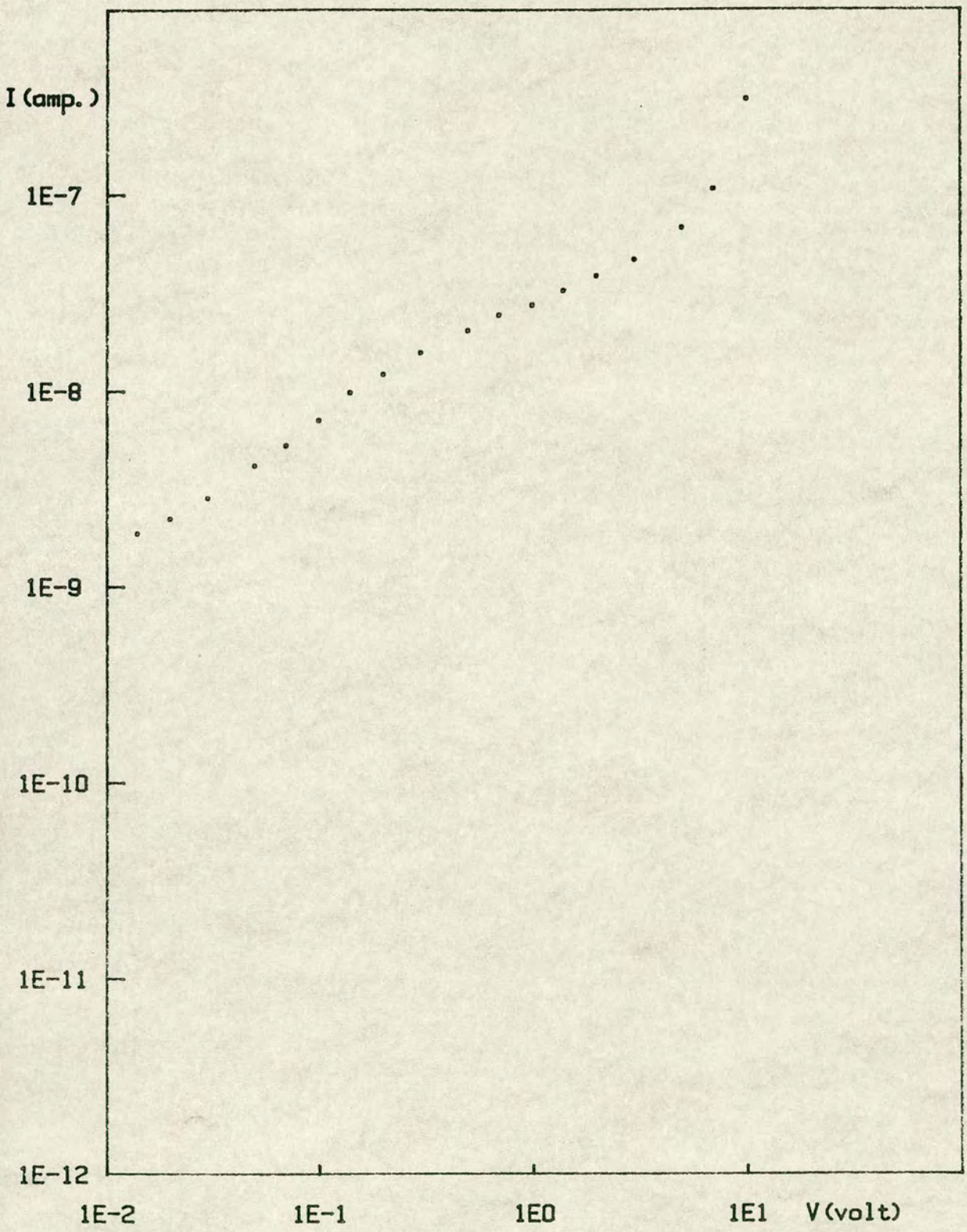

FIG. (6.22): I-V CHARACTERISTIC OF Ga.8(As.4 Sa.6)99.2
AT TEMPERATURE = 430 K.

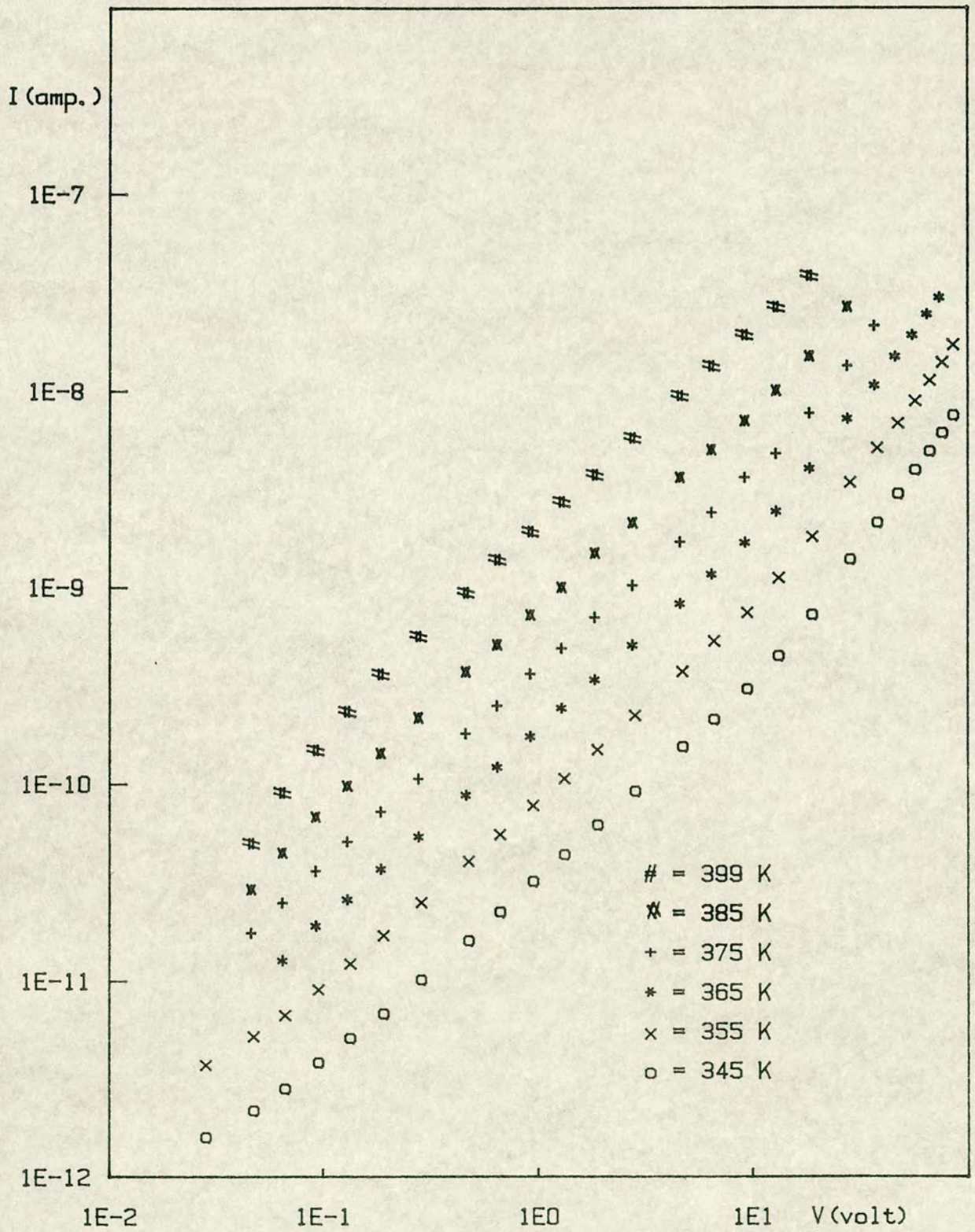

Fig. (6.23a): I-V Characterstic of pure As2 Se3 crystal.

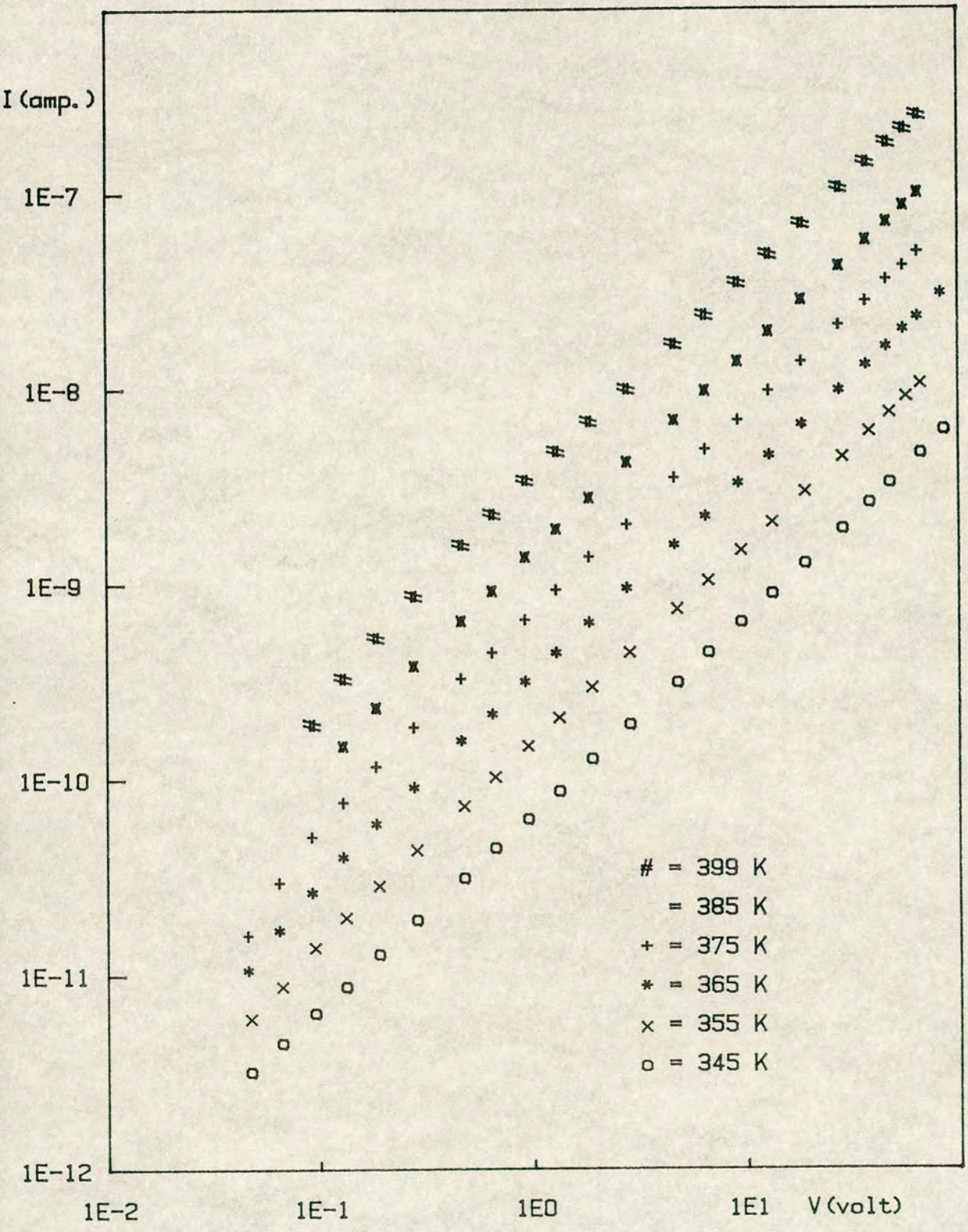

Fig.(6.23b): I-V Characterstic of pure As2 Se3 crystal.

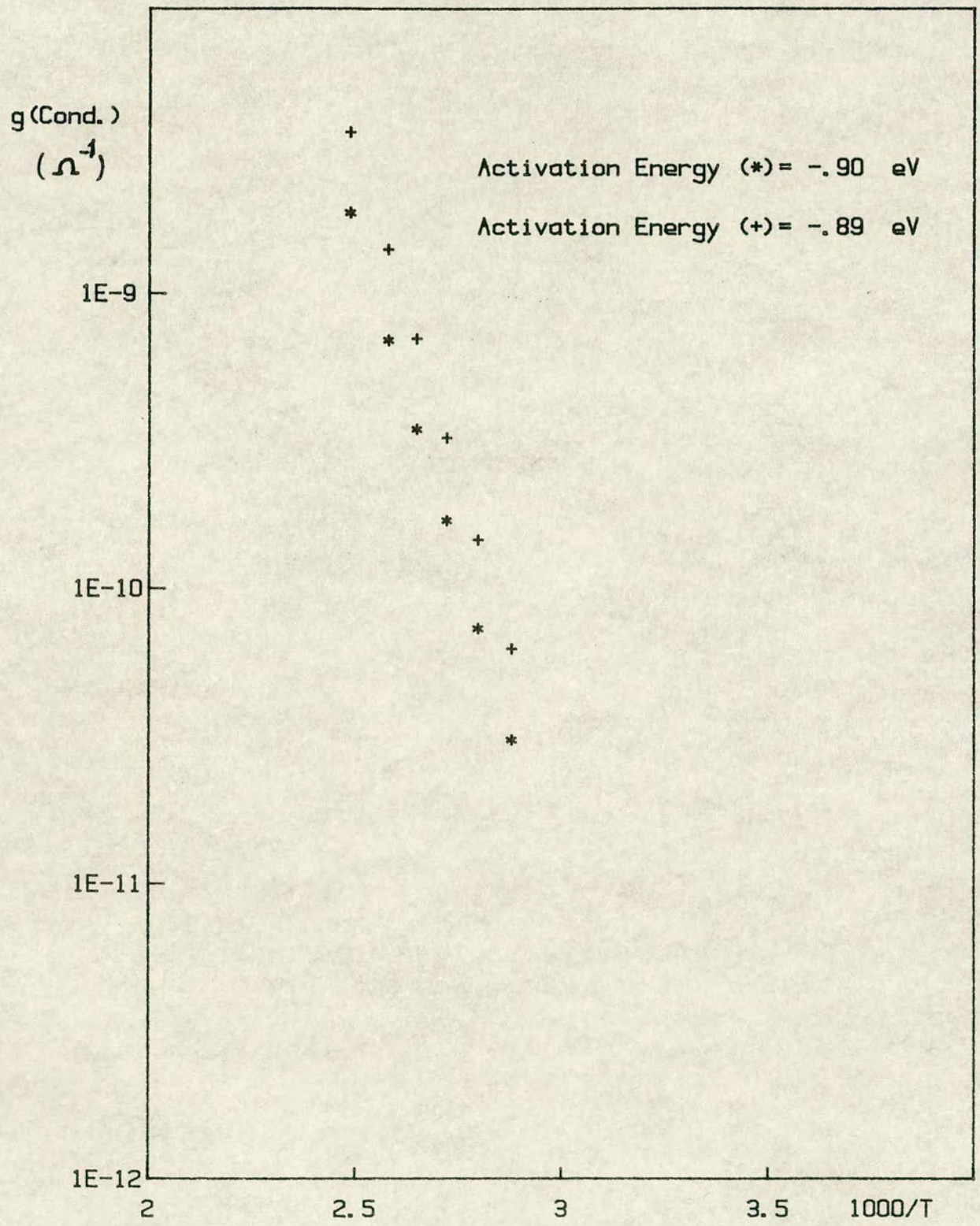

FIG.(6.23c): CONDUCTANCE VS 1/T FOR As2 Se3 FOR THE SAMPLES 1(*) 2(+)

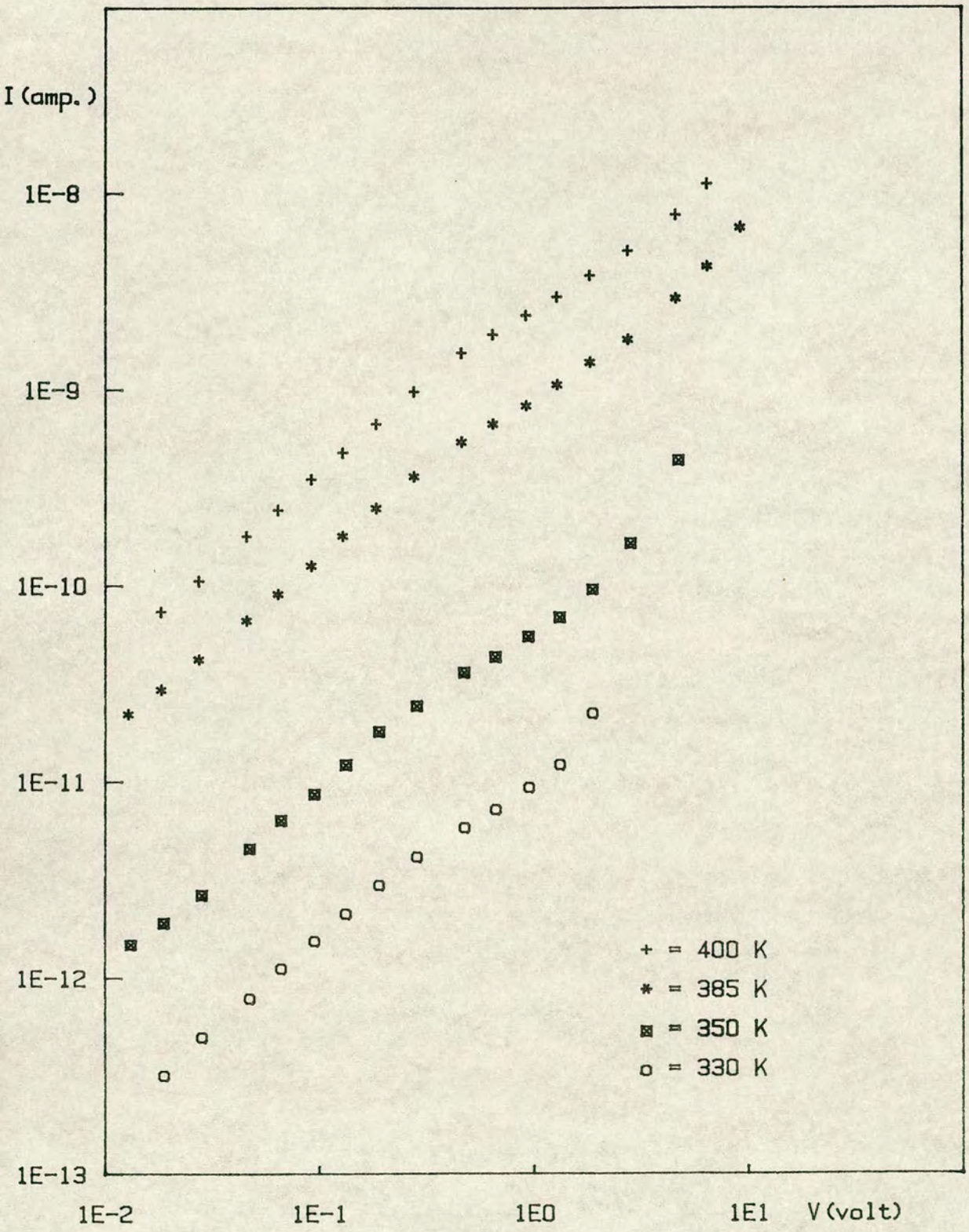

Fig.(6.24a): I-V Characterstic of As2 Se3 doped with 0.02 At.% of Cu at different temperatures.

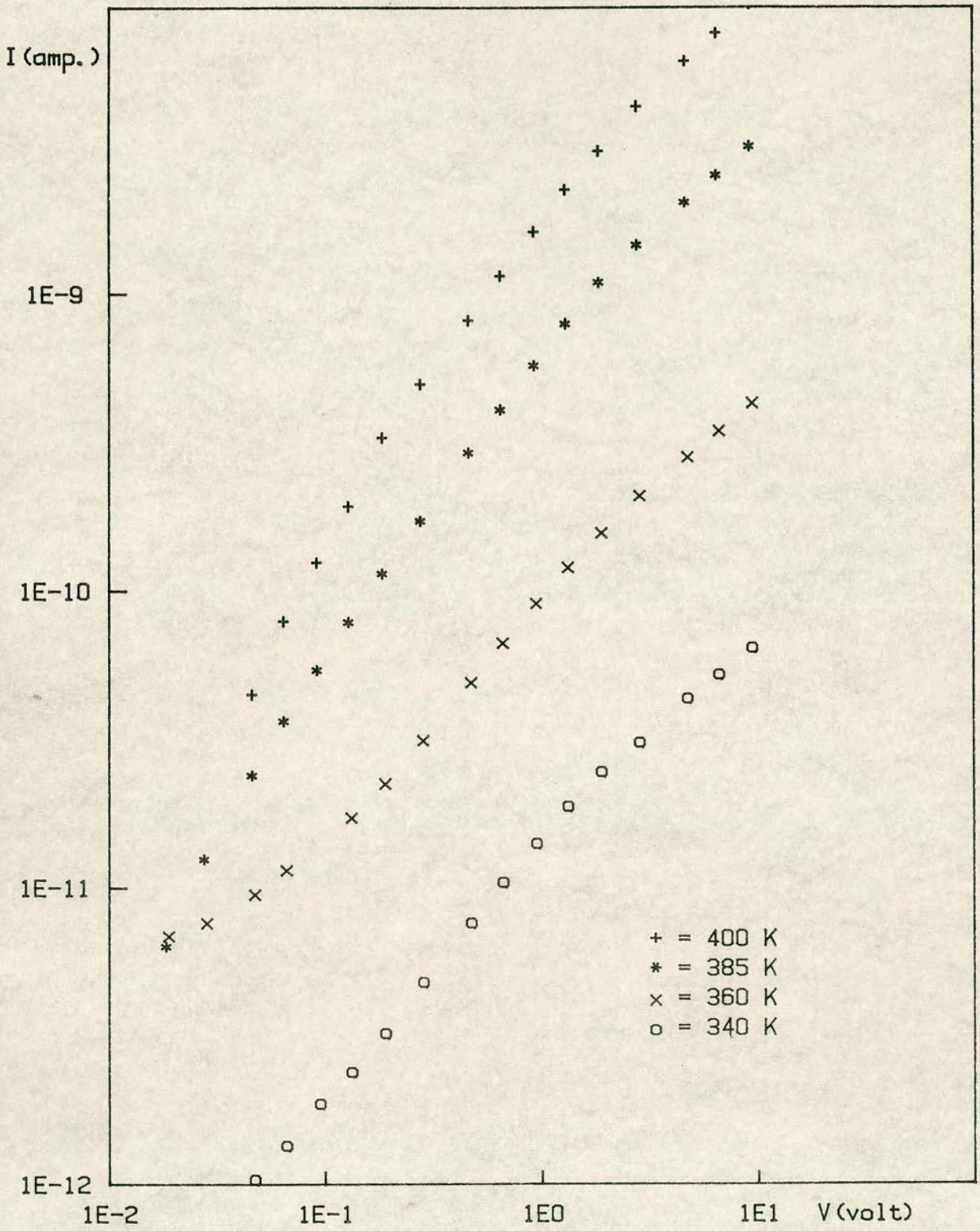

Fig.(6.24b): I-V Charachterstic of As2 Se3 doped with 0.02 At.% of Cu at different temperatures.

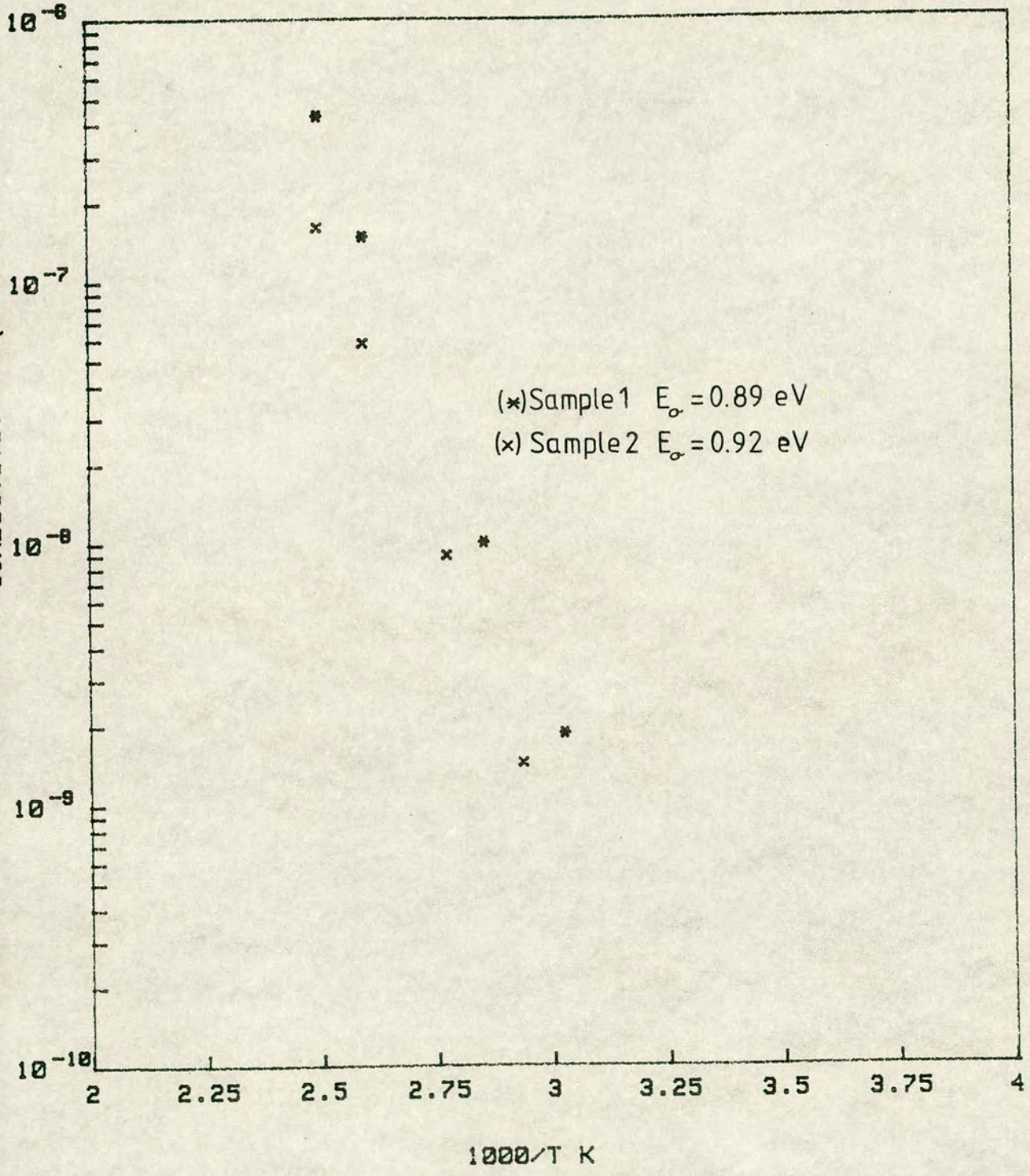

FIG.(6.24c)

Conductivity vs 1/T for $Cu_{.02}(As_{.4}Se_{.6})_{99.98}$

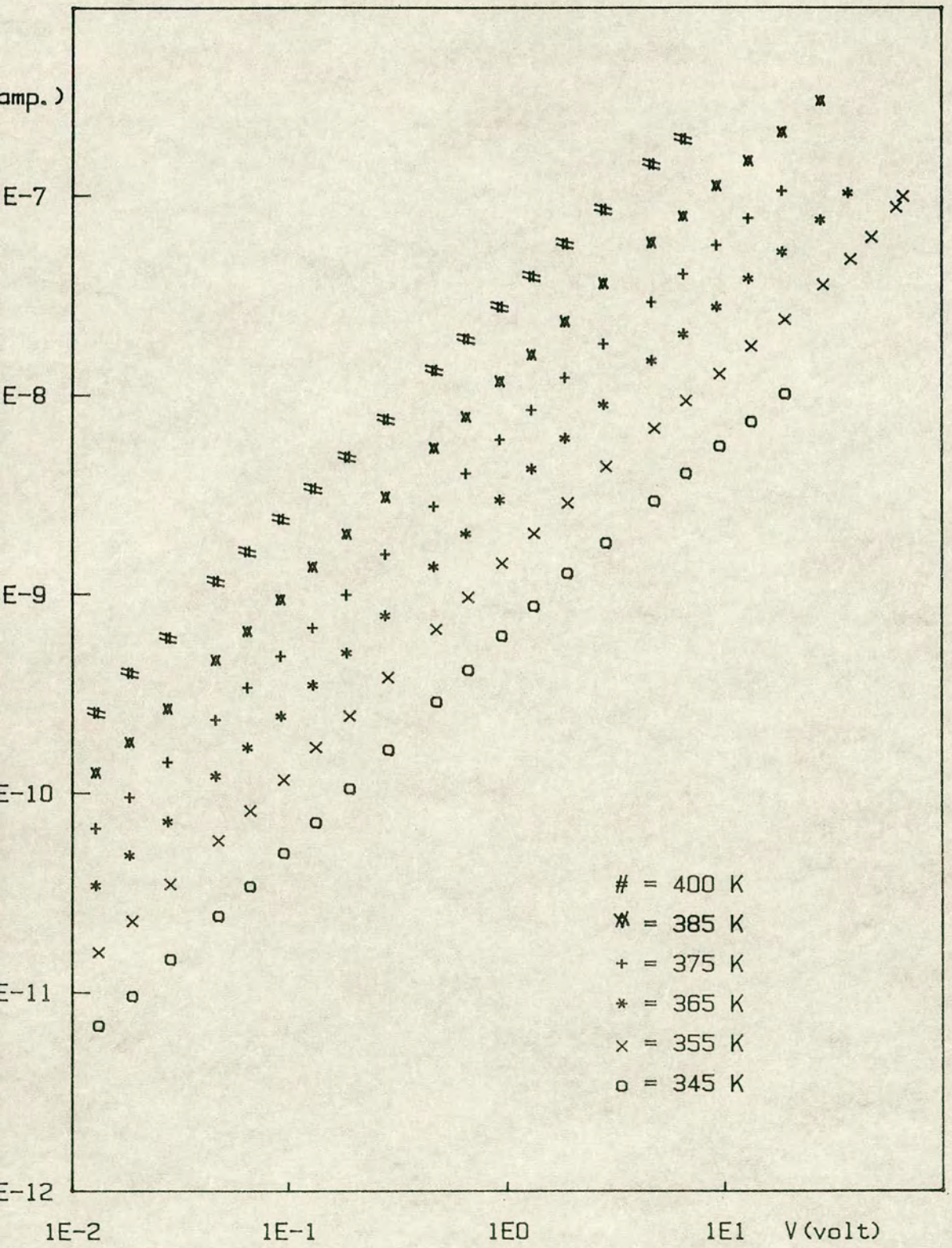

Fig.(6.25a): I-V Characterstic of As2 Se3 doped with 0.1 At.% of Cu at different temperatures.

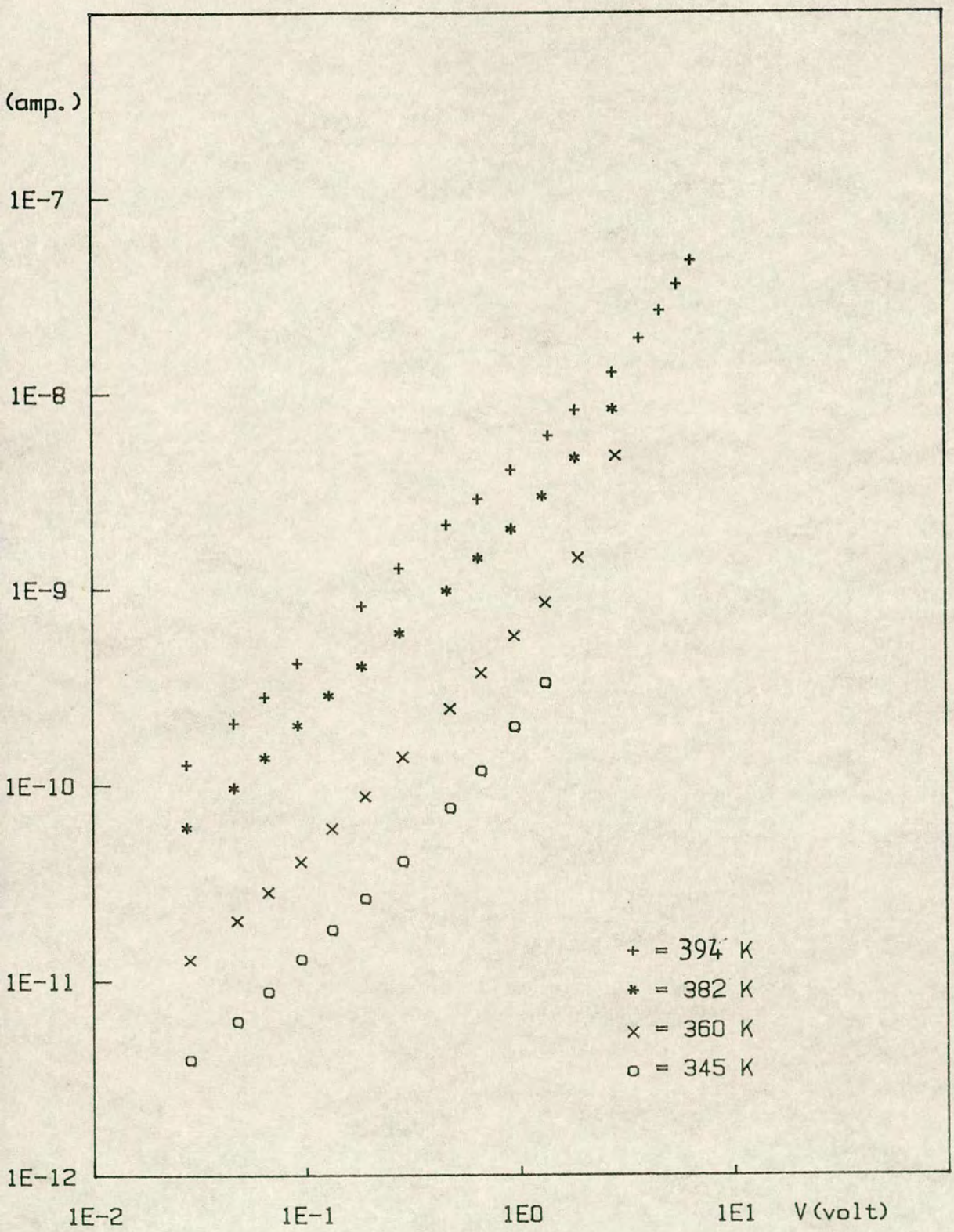

Fig.(6.25b) : I-V Characterstic of As2 Se3 doped with 0.1 At.% of Cu at different temperatures.

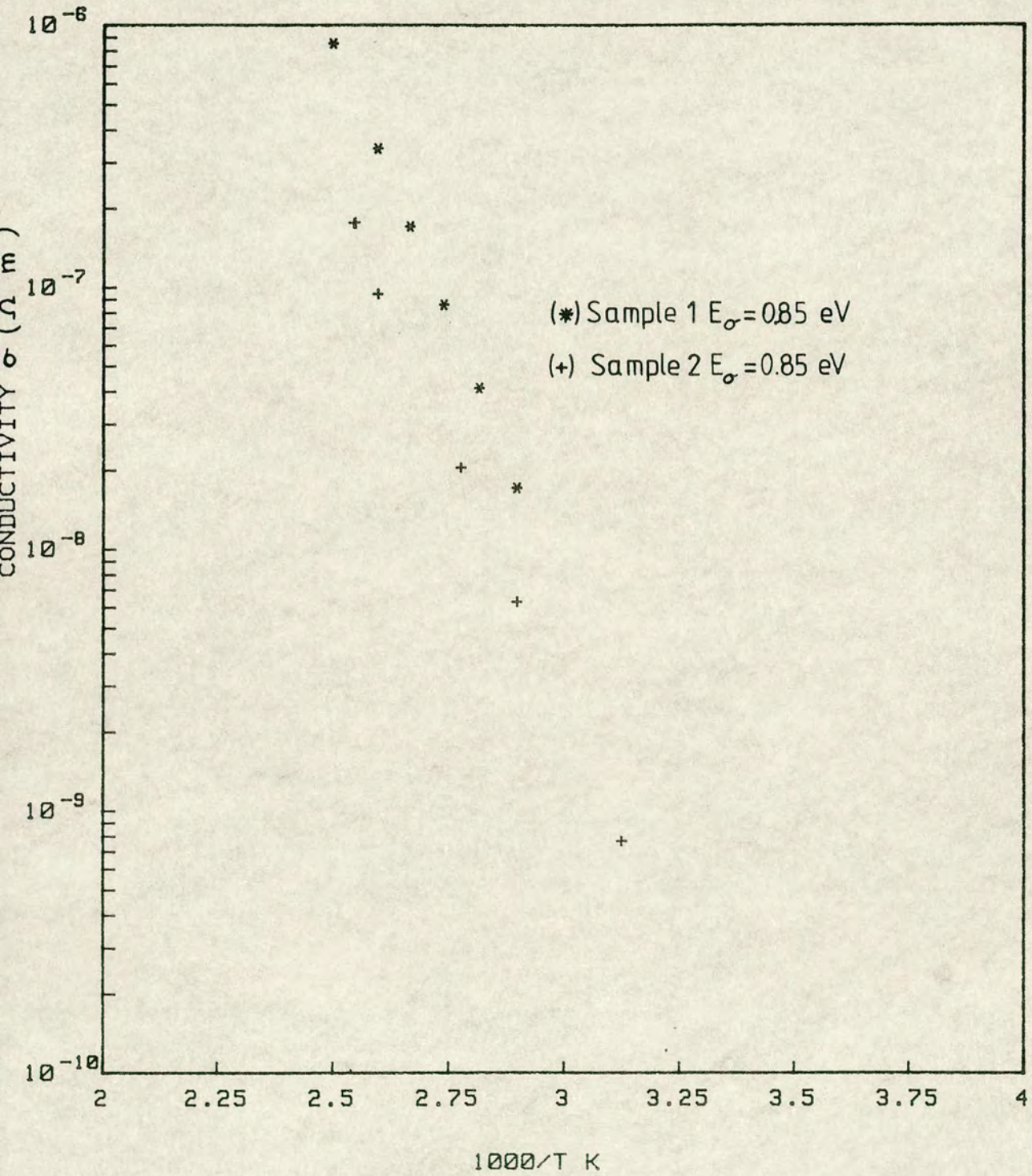

FIG.(6.25c)

Conductivity vs 1/T for $Cu_{.1}(As_{.4}Se_{.6})_{99.9}$

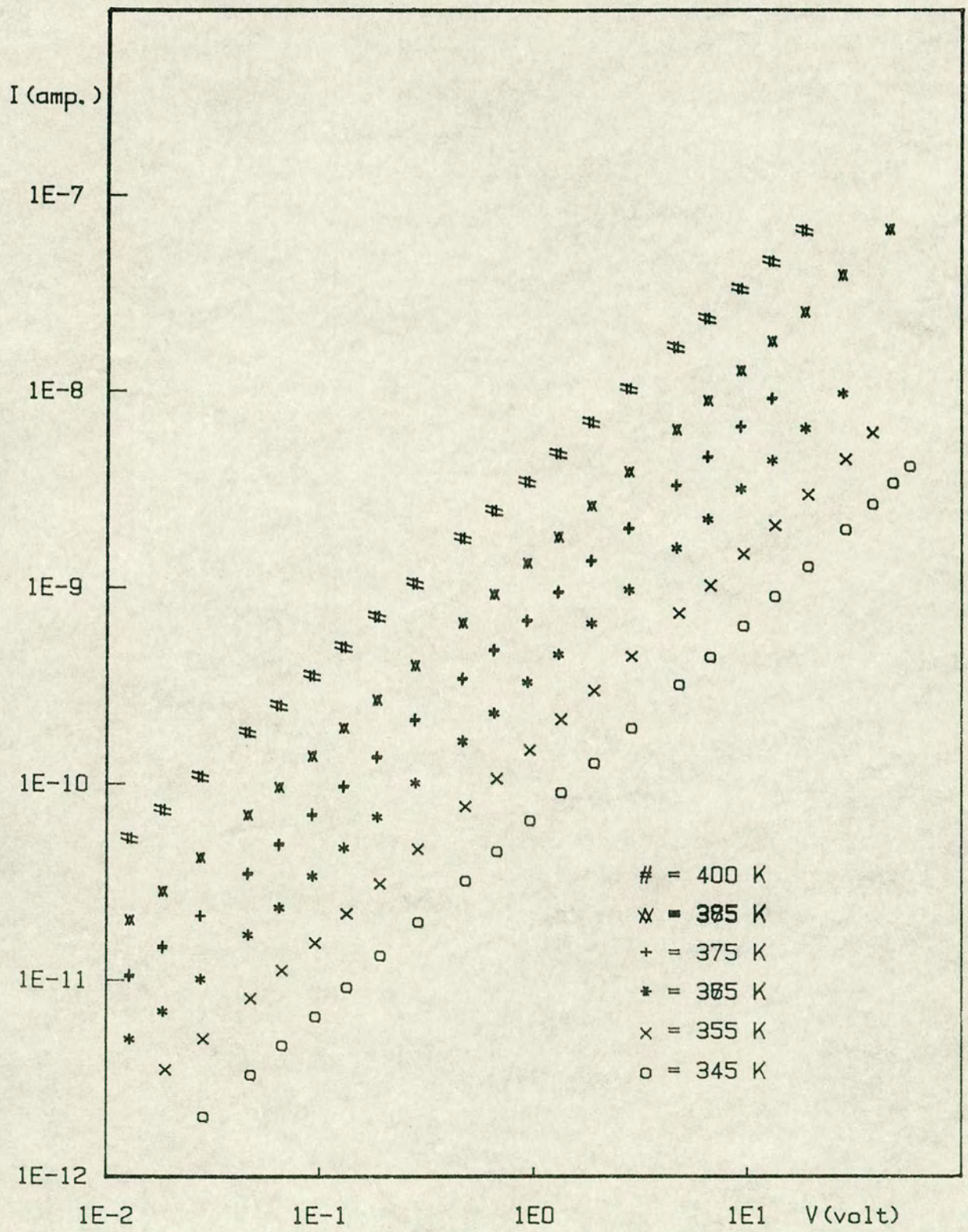

Fig.(6.26a): I-V Characterstic of As2 Se3 doped with 0.17 At.% of Cu at different temperatures.

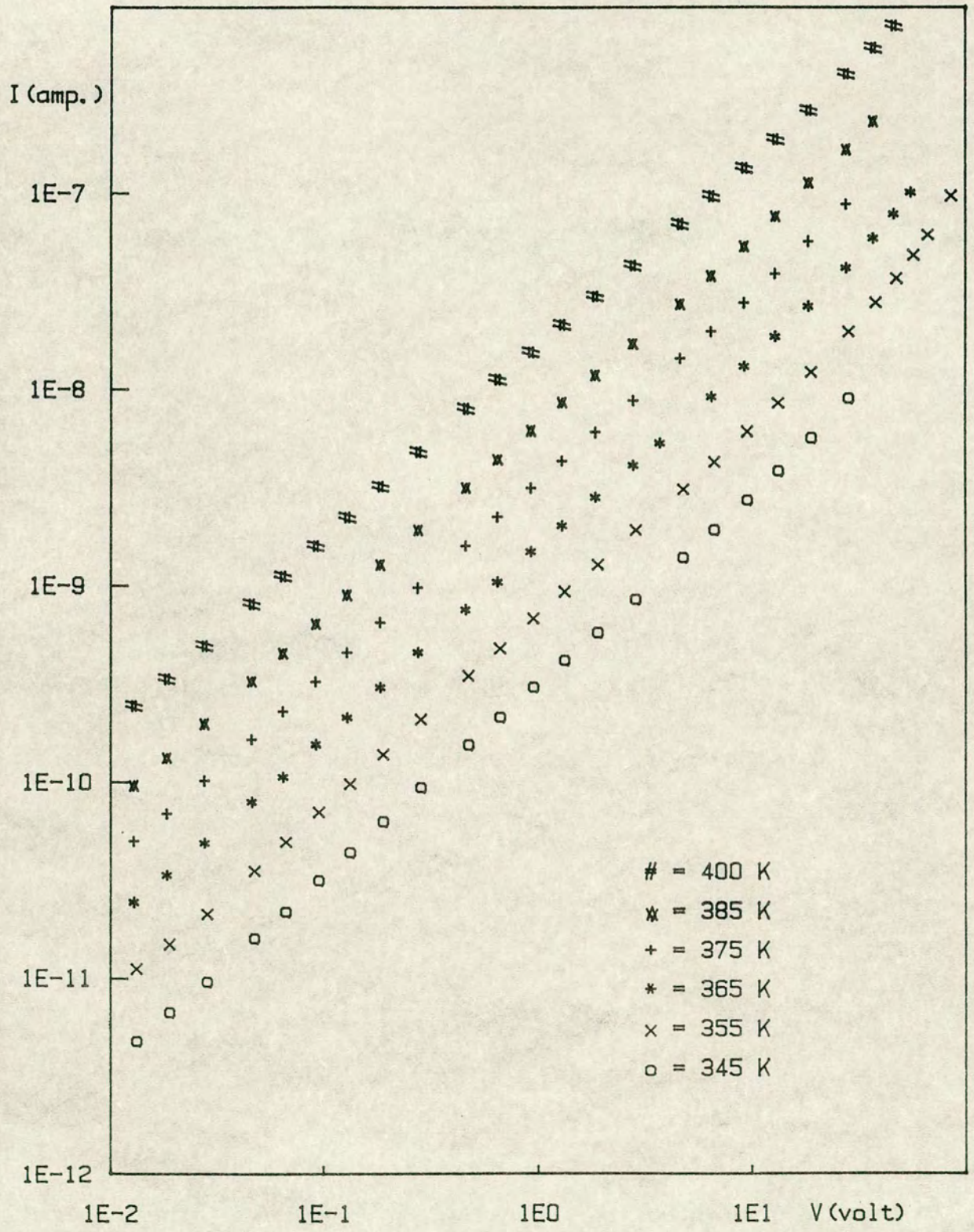

Fig.(6.26b): I-V Characterstic of As2 Se3 doped with 0.17 At.% of Cu at different temperatures.

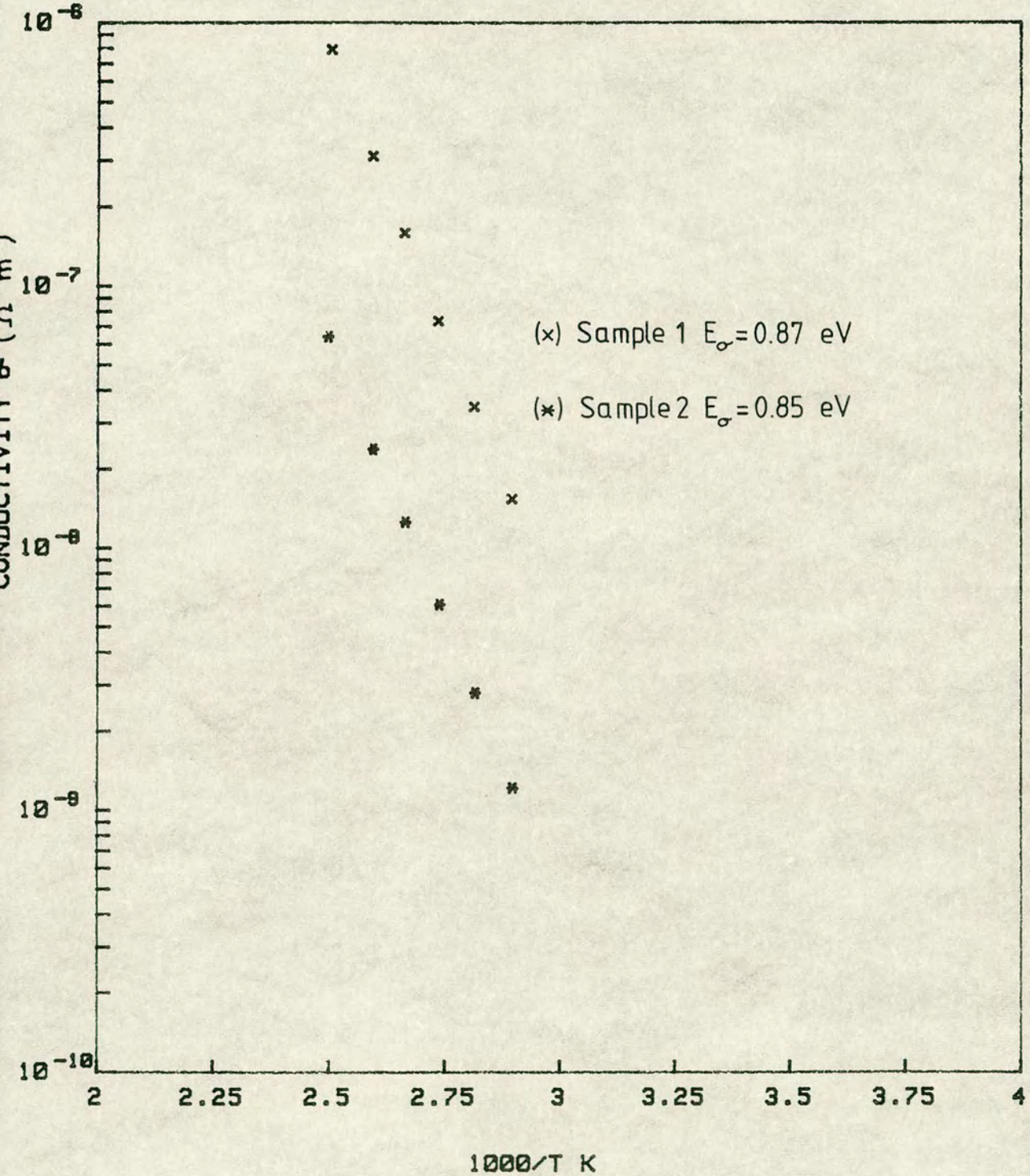

FIG. (6.26c)

Conductivity vs 1/T for $Cu_{.17}(As_{.4}Se_{.6})_{99.83}$

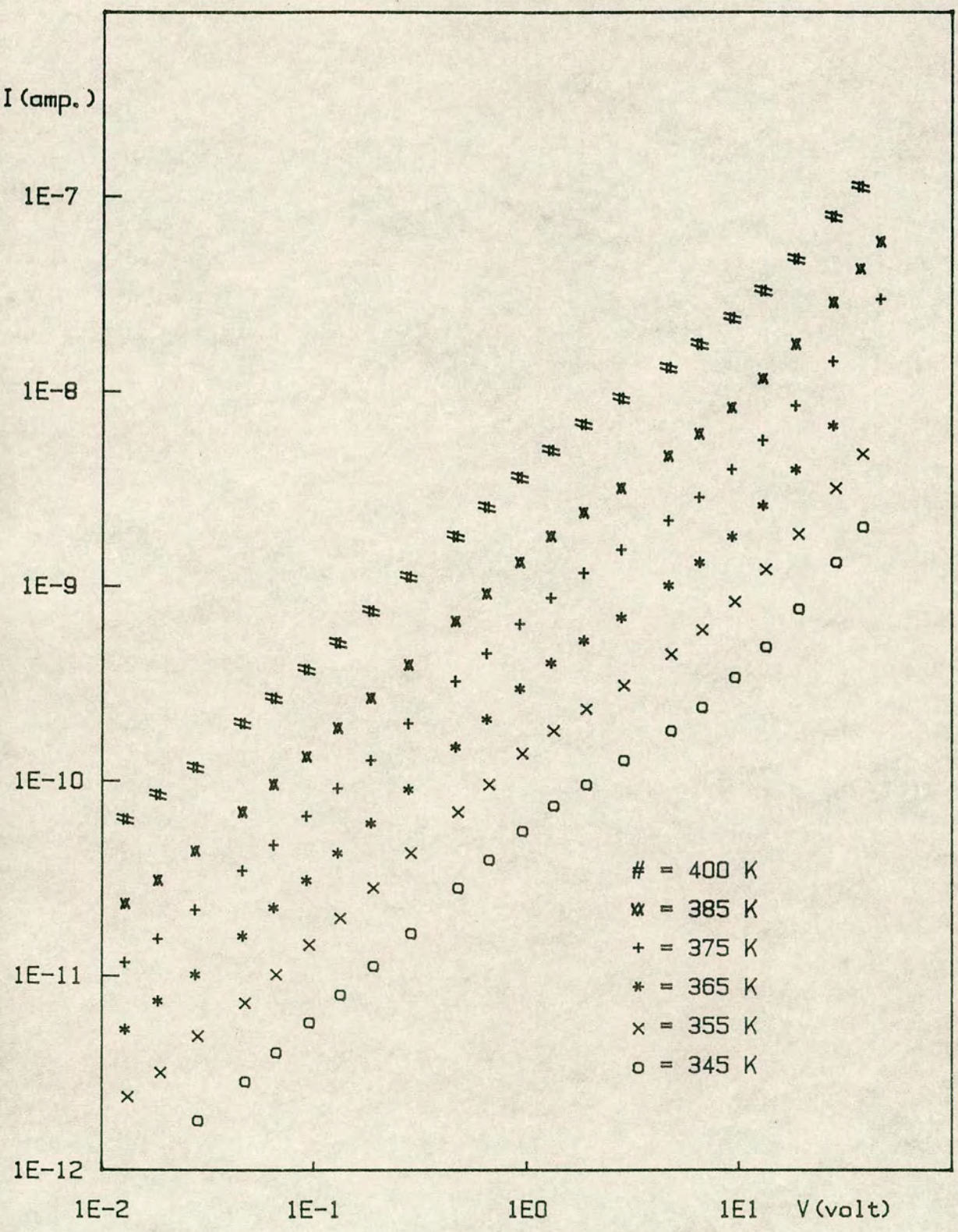

Fig.(6.27a): I-V Characterstic of As2 Se3 doped with 0.12 At.% of Ga at different temperatures.

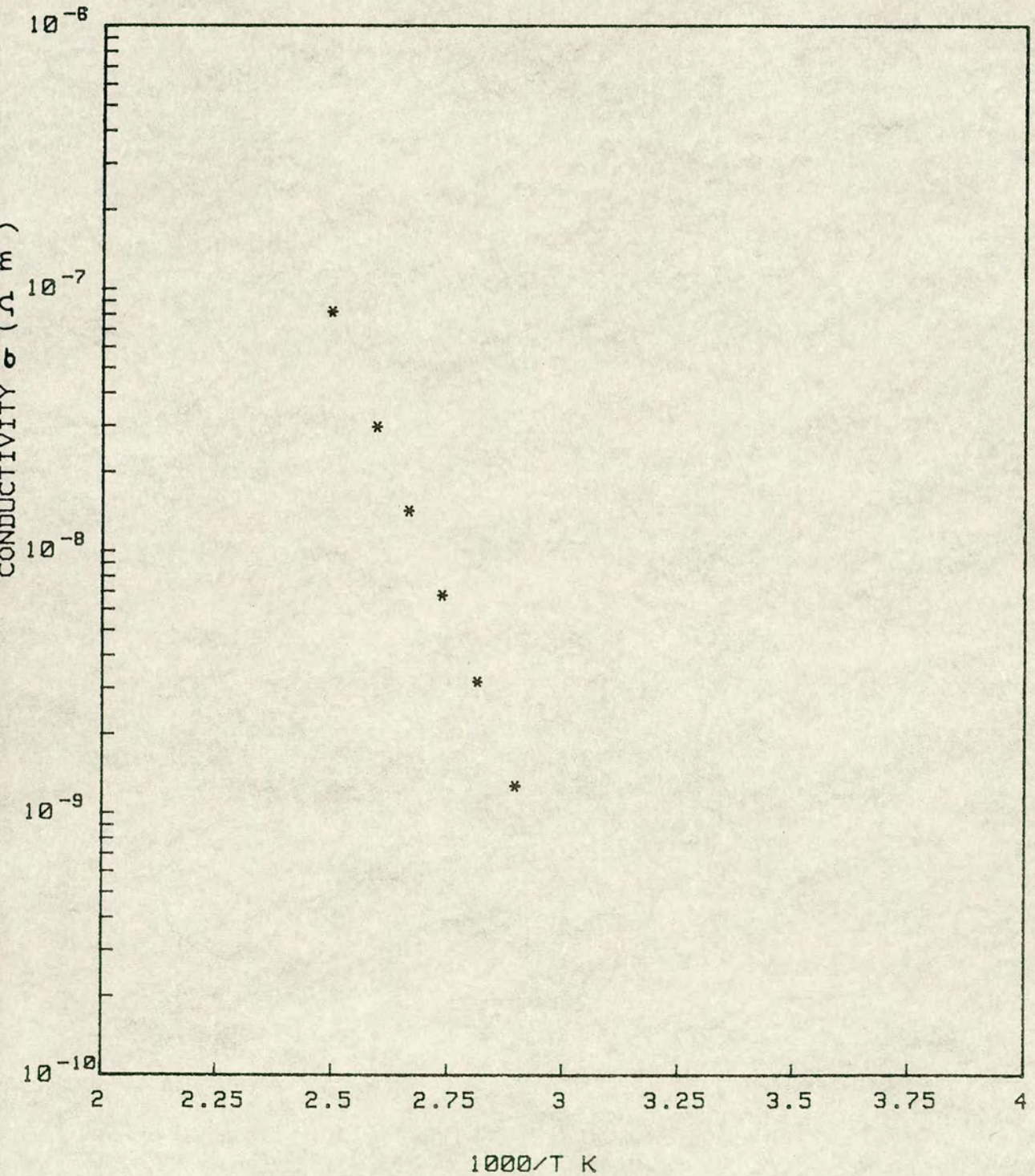

FIG.(6.27b)

Conductivity vs 1/T for $Ga_{.12}(As_{.4}Se_{.6})_{99.88}$

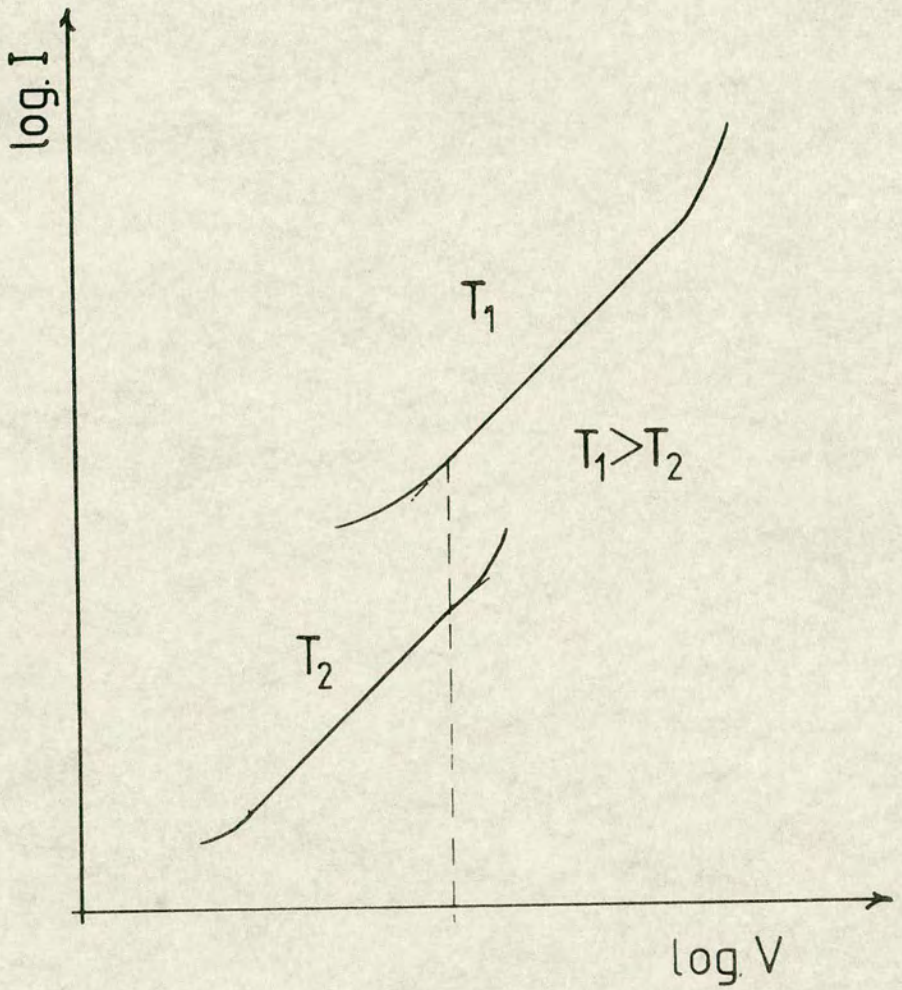

FIG.(6.28)

I-V characteristic at two different temperatures T_1 and T_2

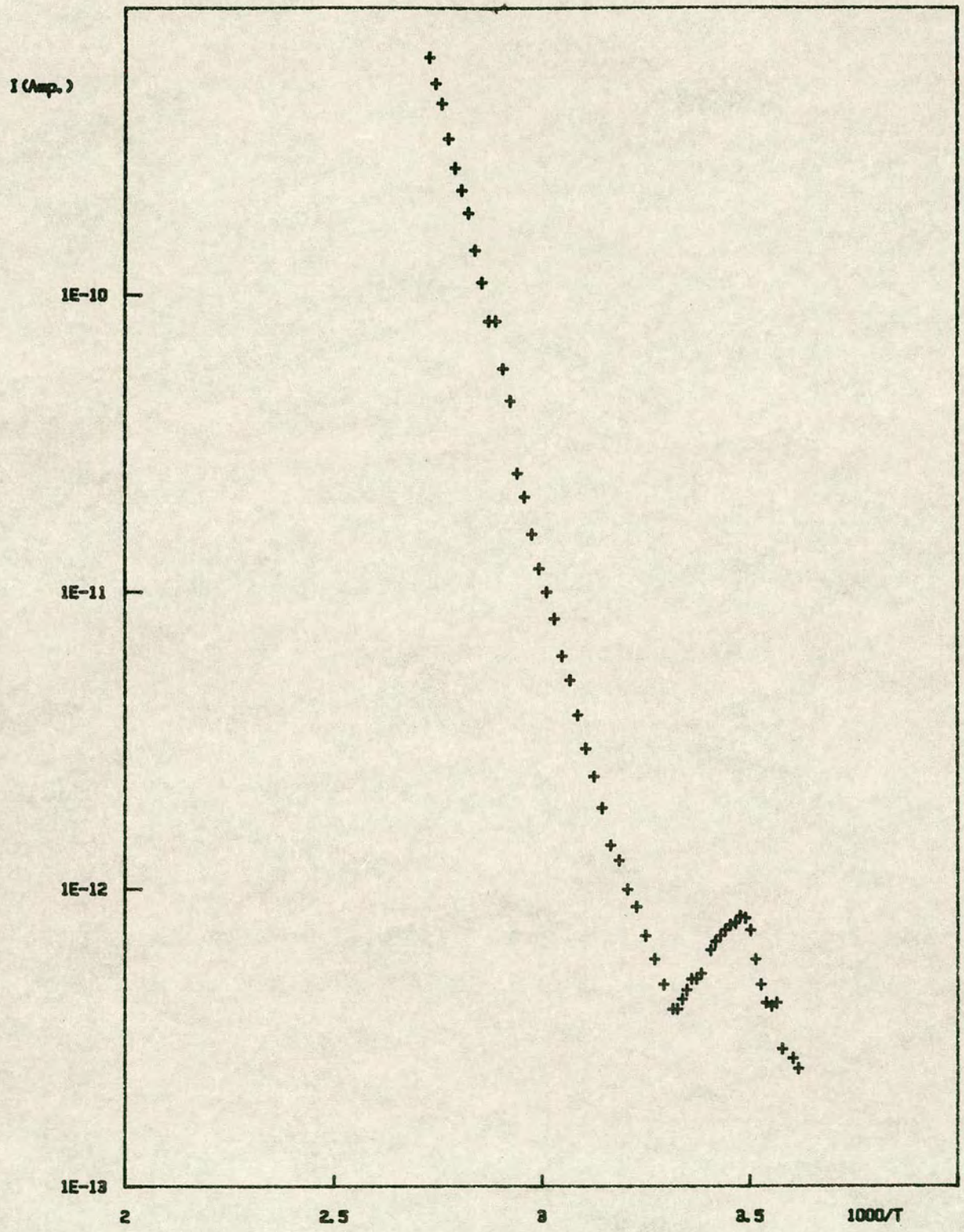

FIG. (6.29)

Thermally stimulated current with applied voltage = 10 V

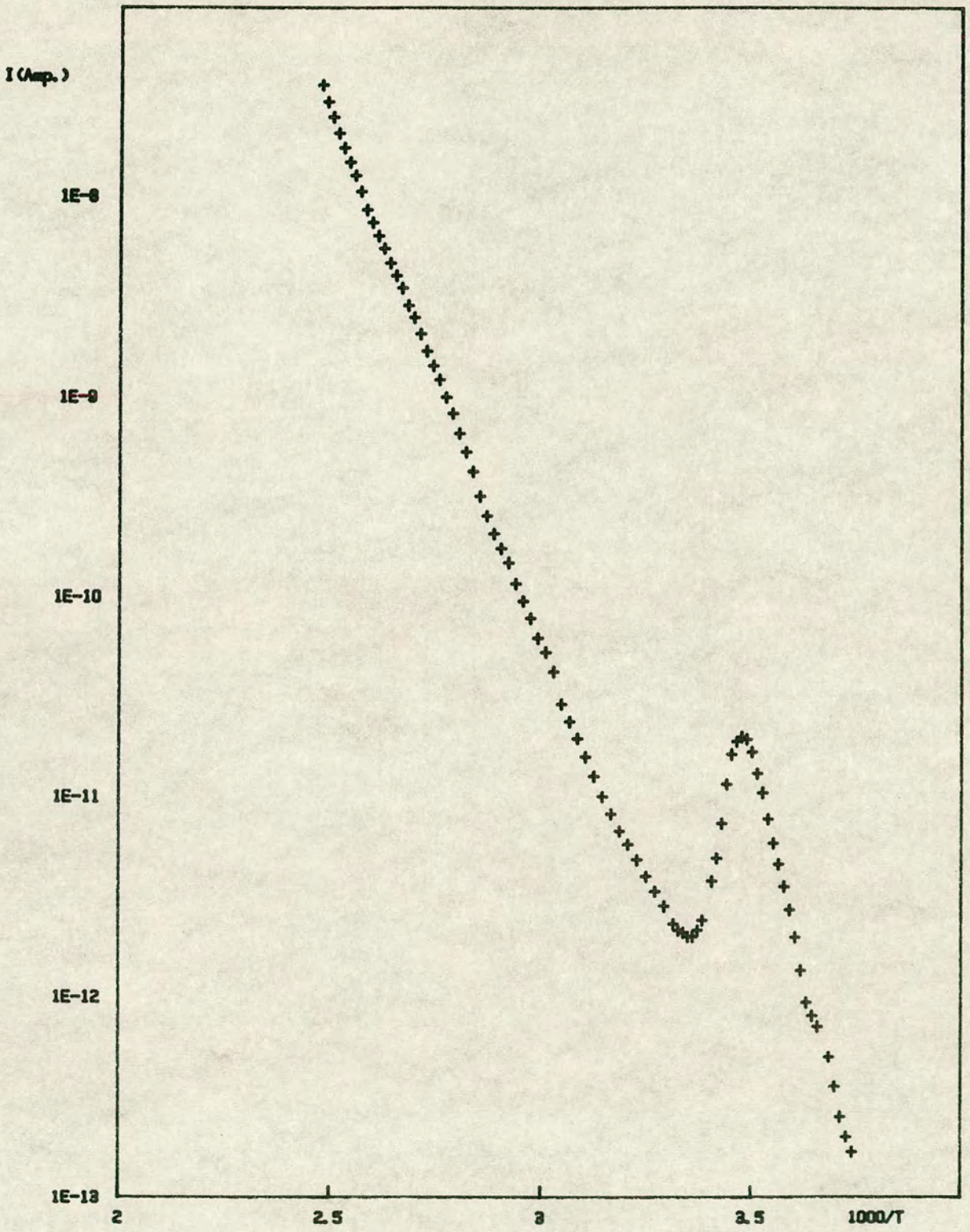

FIG. (6.30)

Thermally stimulated current with applied voltage = 20 V

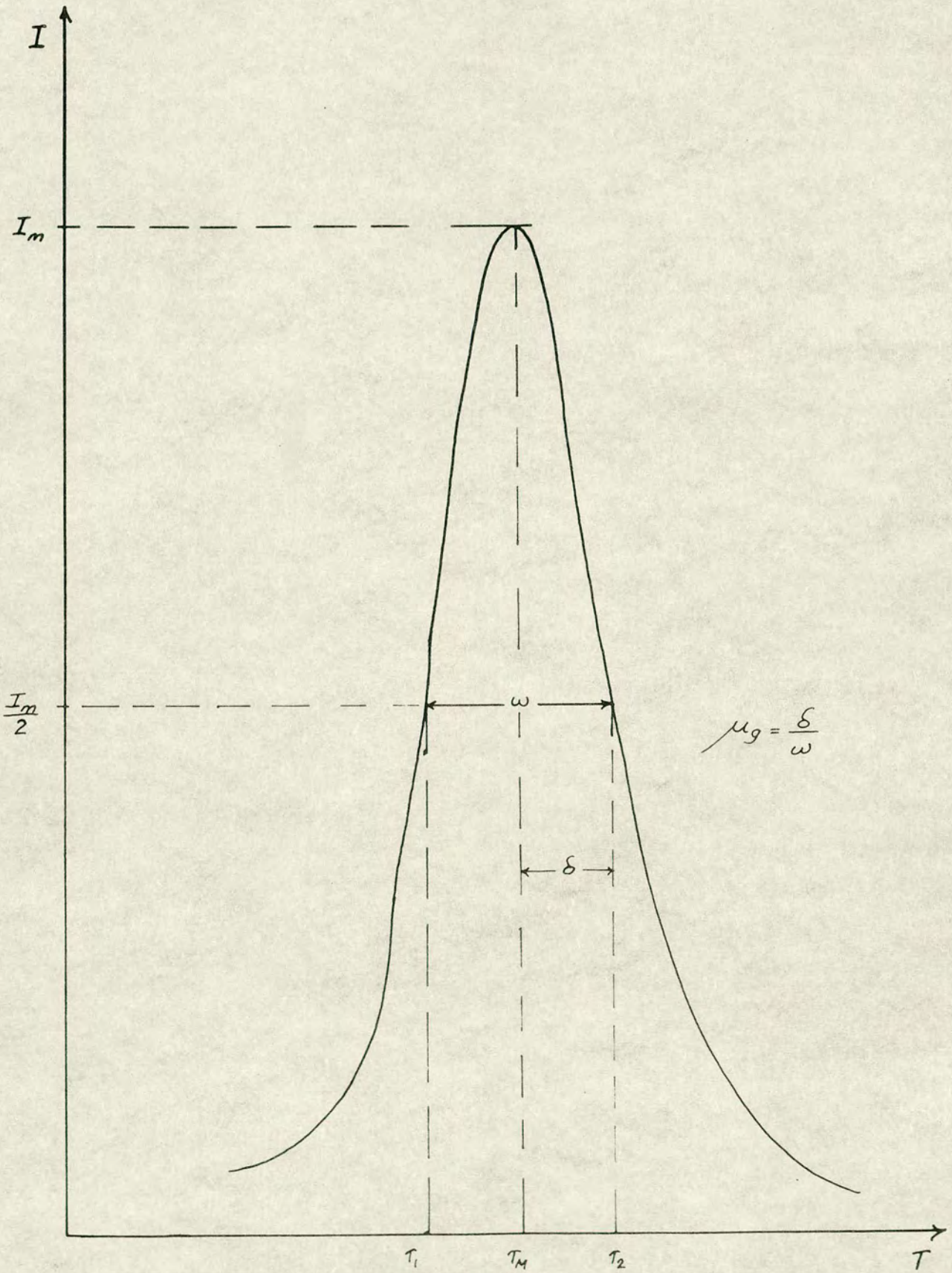

FIG. (6.31)

Method of determining the shape factor μ from the graph

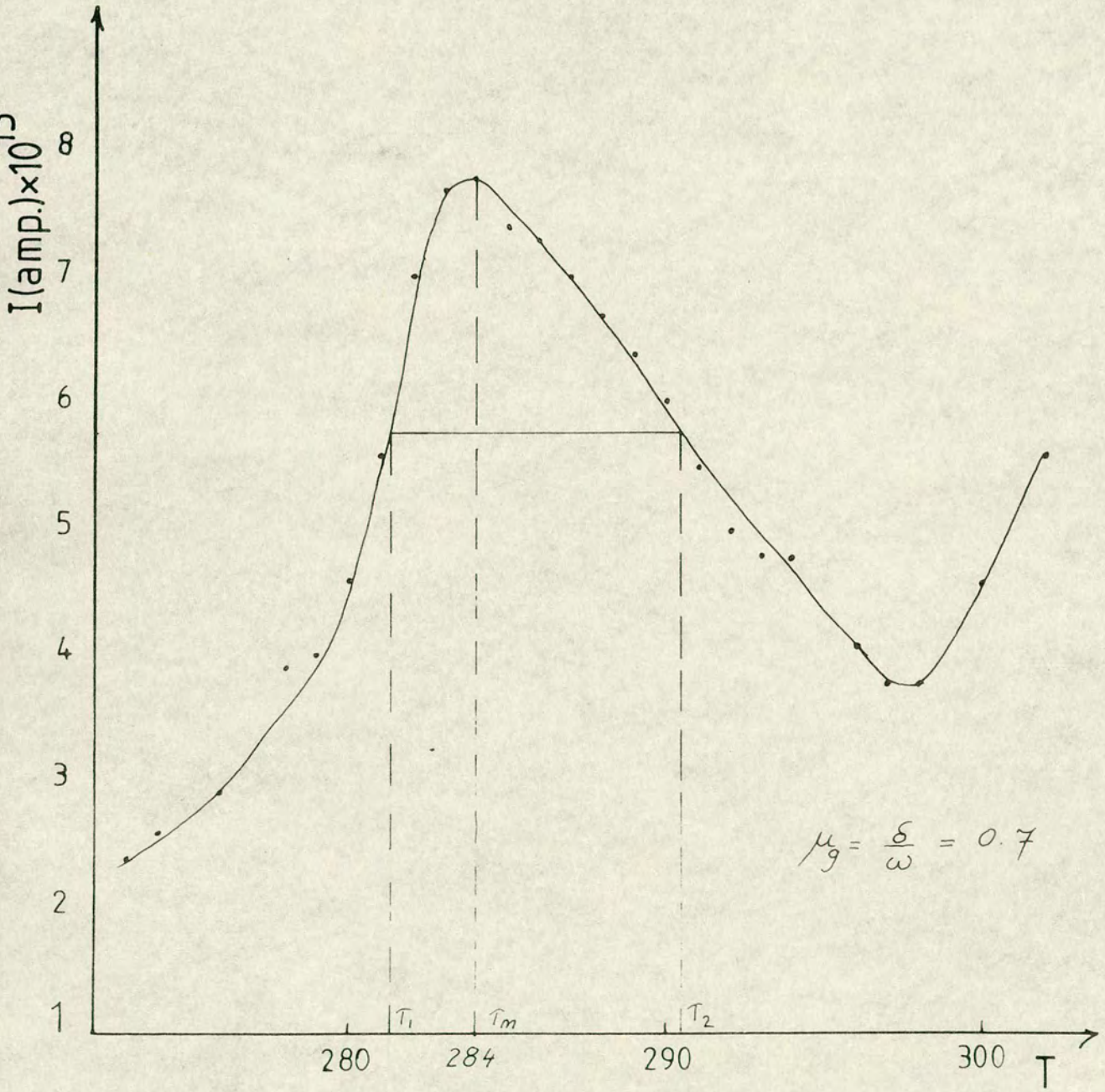

FIG.(6.32)

Linear plot of thermally stimulated current with applied voltage = 10 V

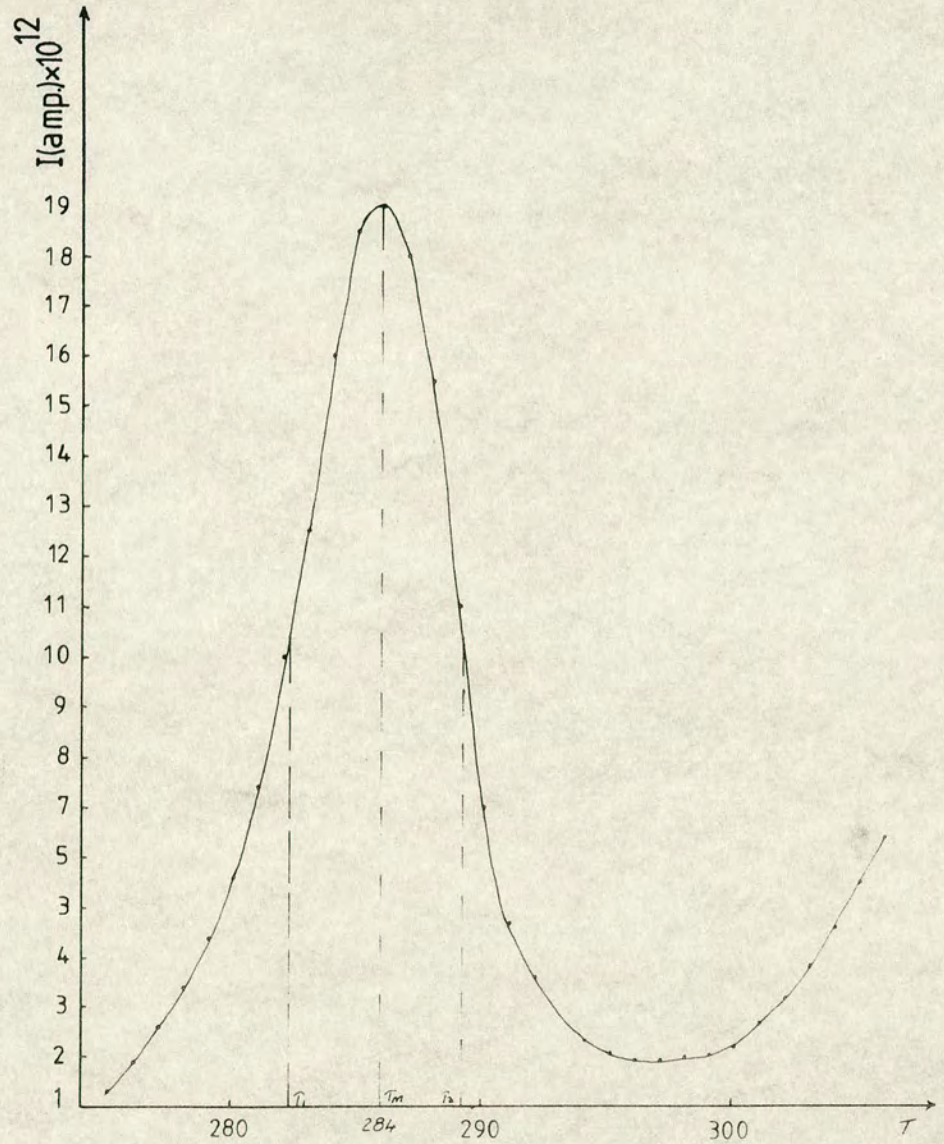

FIG. (6.33)

Linear plot of thermally stimulated current with applied voltage = 20 V

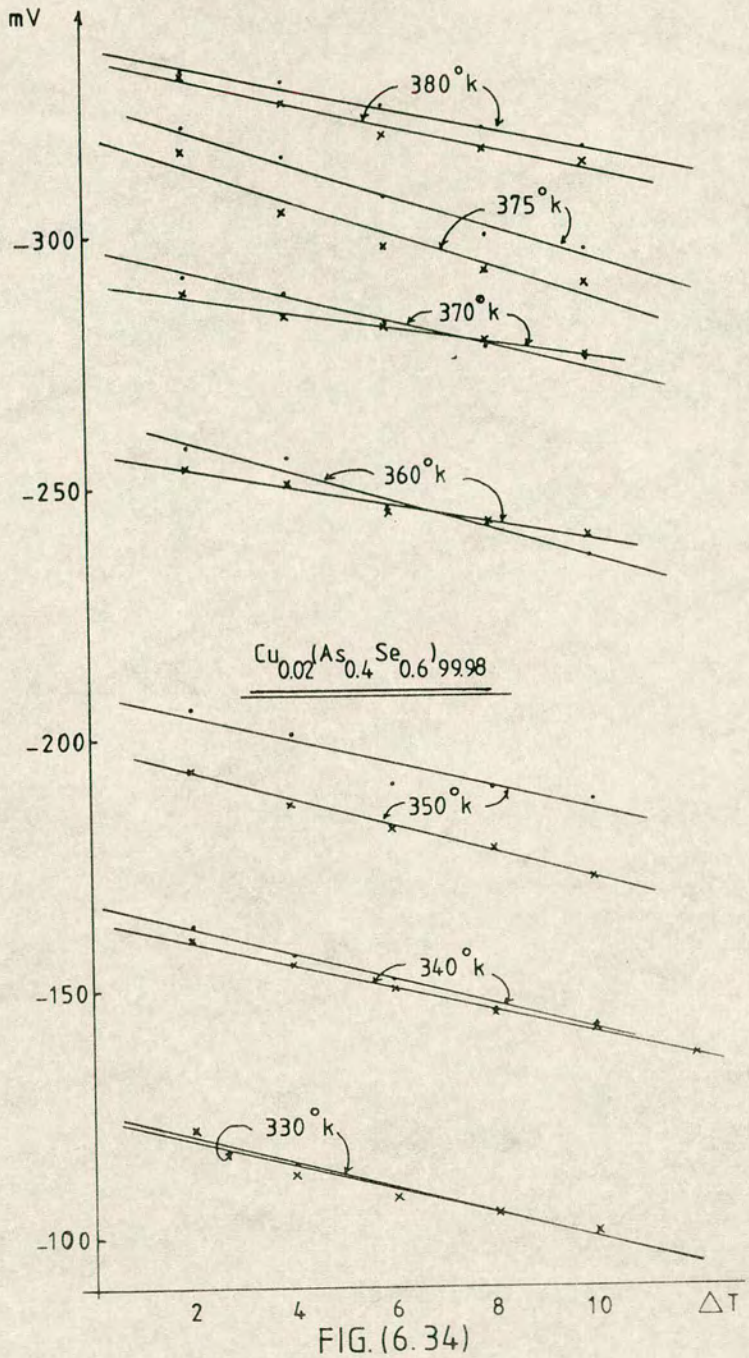

FIG. (6.34)

Thermvoltage vs ΔT for $Cu_{.02}(As_{.4}Se_{.6})_{99.98}$

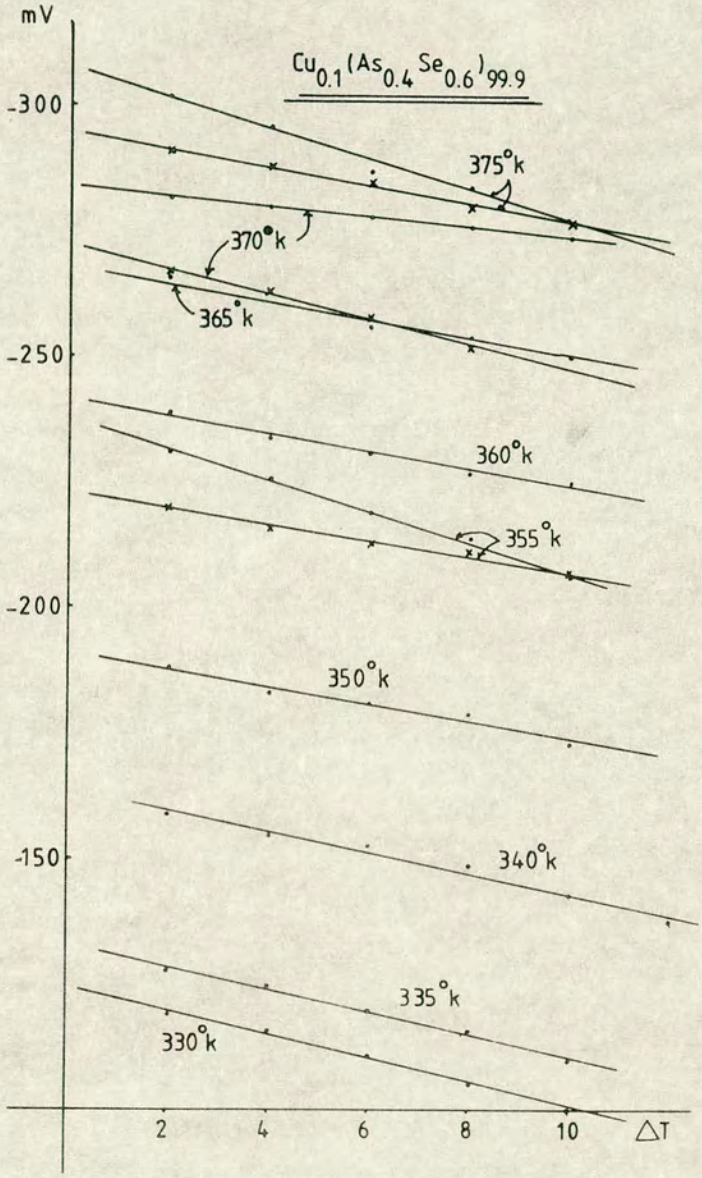

FIG. (6.35)

Thermovoltage vs ΔT for $Cu_{.1}(As_{.4}Se_{.6})_{99.9}$

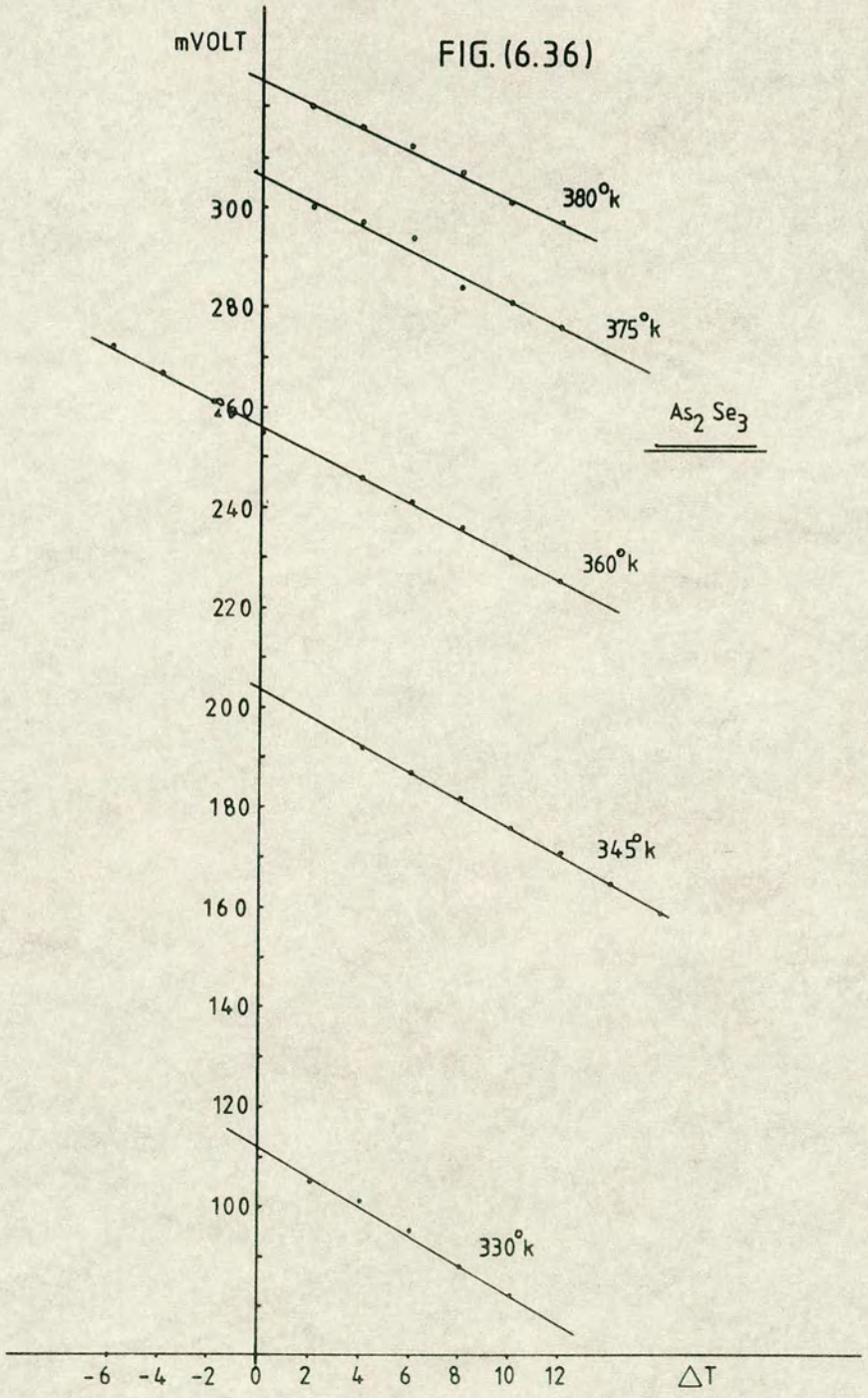

Thermovoltage vs ΔT for As_2Se_3

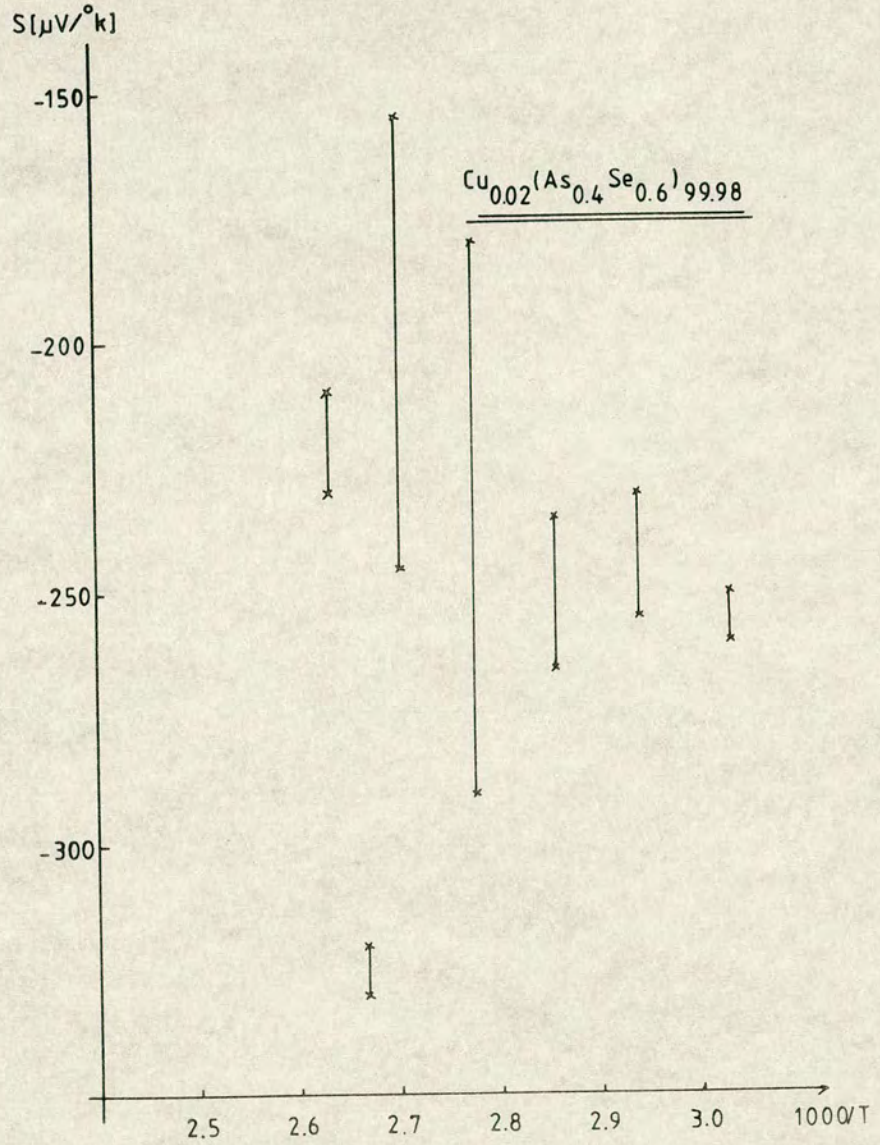

FIG. (6.37)

Thermopower vs 1/T for $Cu_{.02}(As_{.4}Se_{.6})_{99.98}$

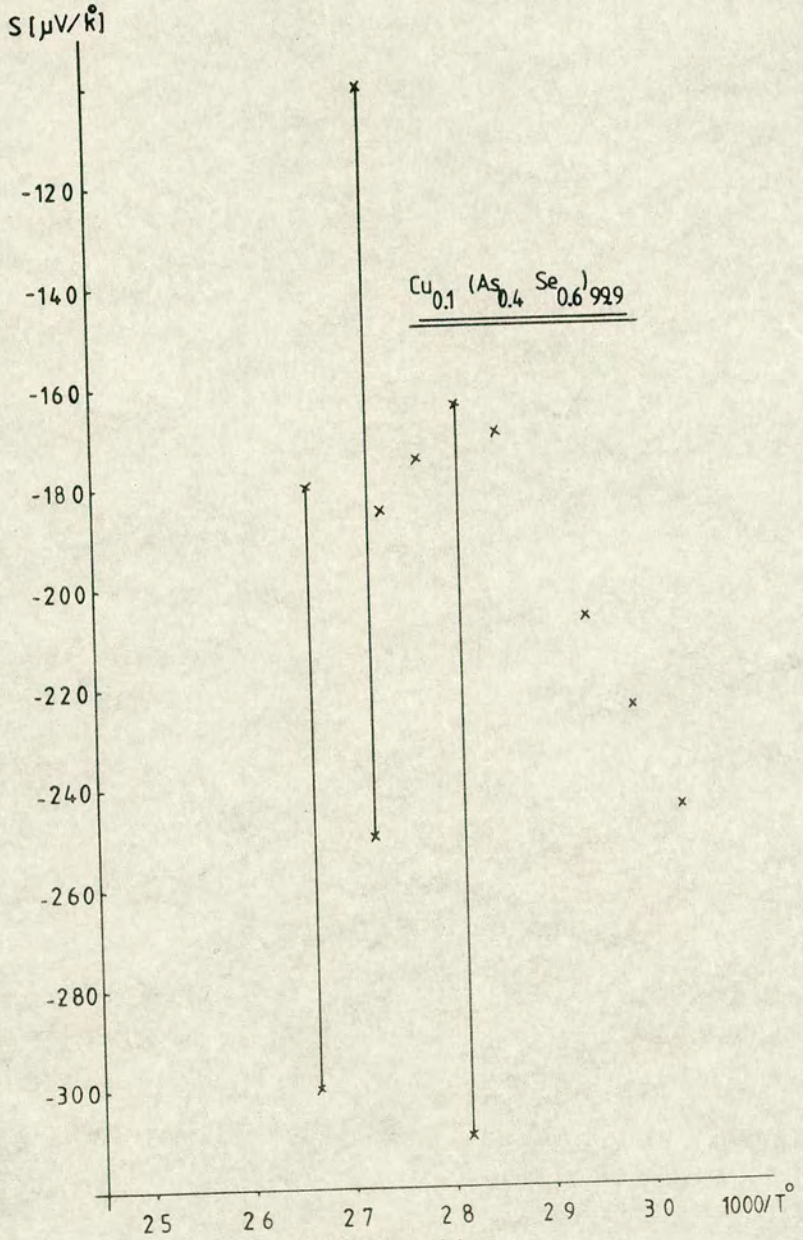

FIG.(6.38)

Thermopower vs 1/T for $Cu_{.1}(As_{.4}Se_{.6})_{99.9}$

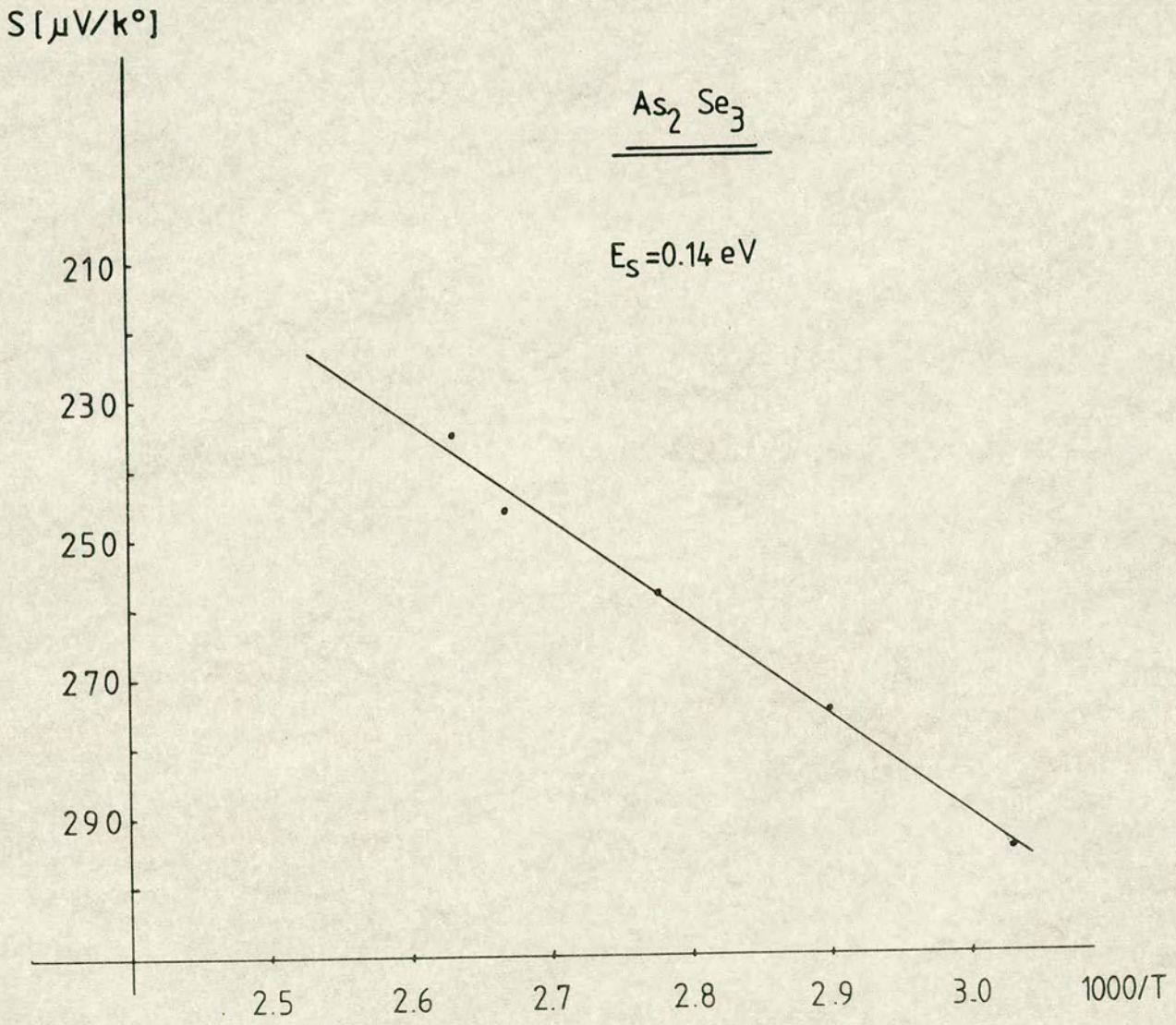

FIG. (6.39)

Thermopower vs 1/T for As_2Se_3

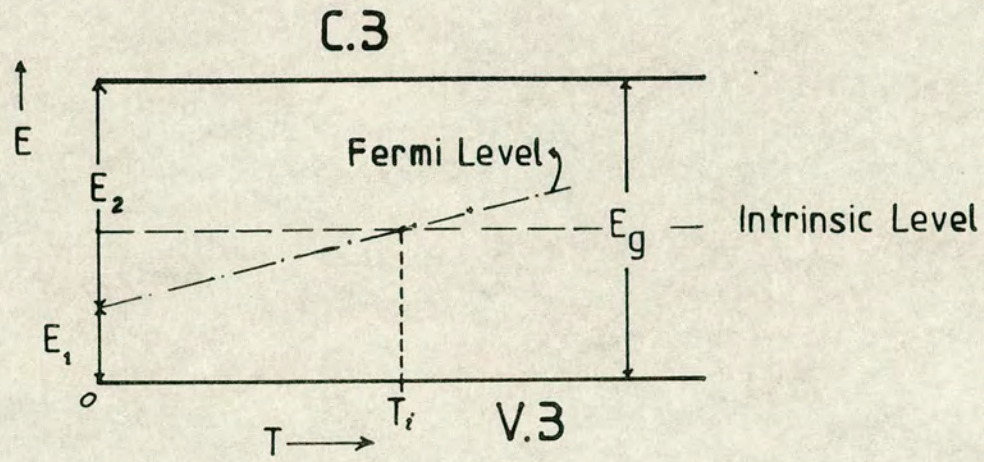

FIG. (6.40)

Illustrate the variation of the Fermi level to the band edge

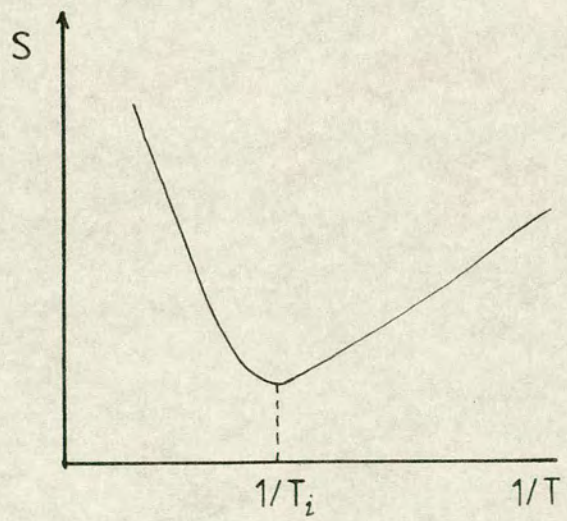

FIG. (6.41)

The suggested Seebeck coefficient plot according to Newman [24]

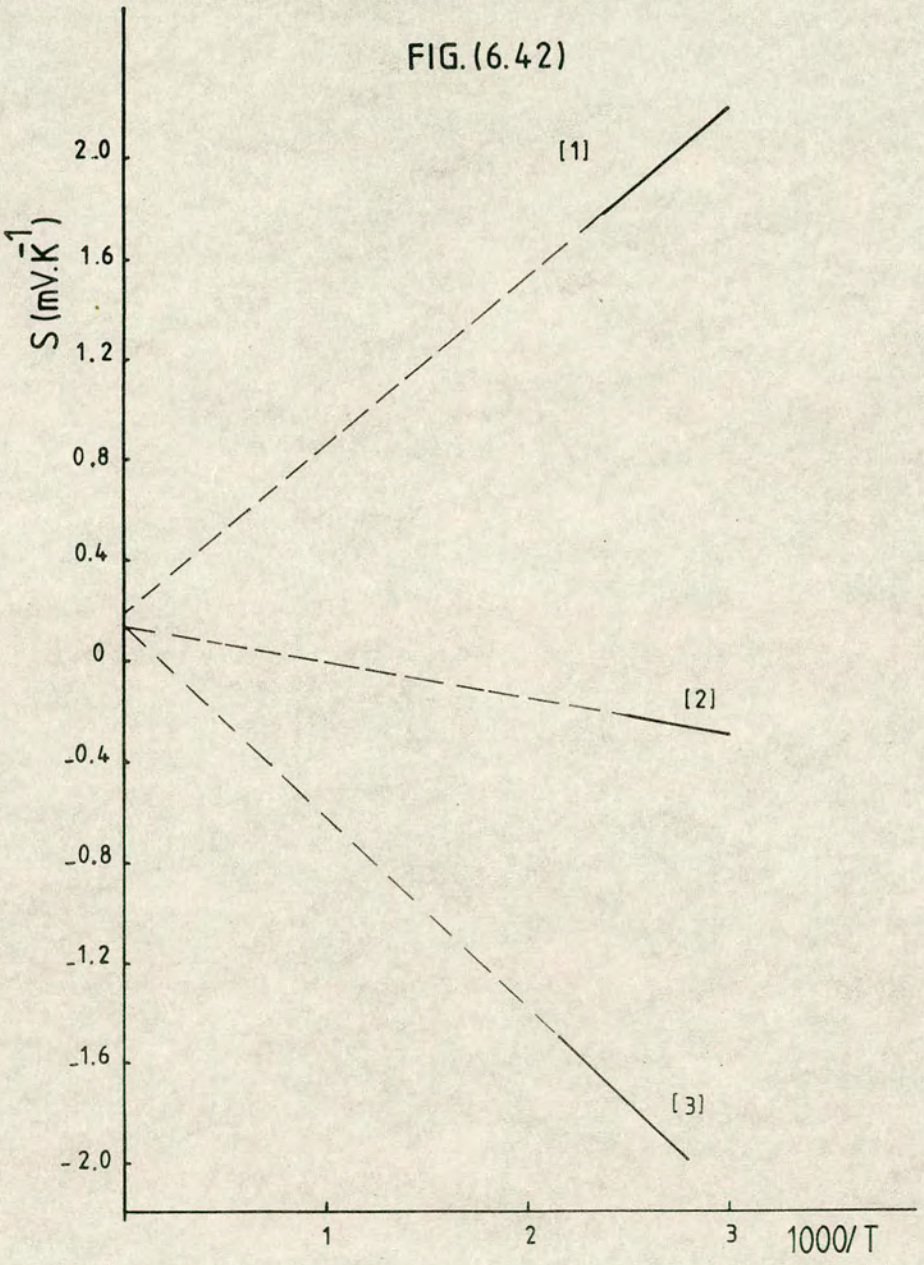

Thermopower plot. (1) Segear and Quinn [29], (2) This project and (3) Brunst and Weiser [11]

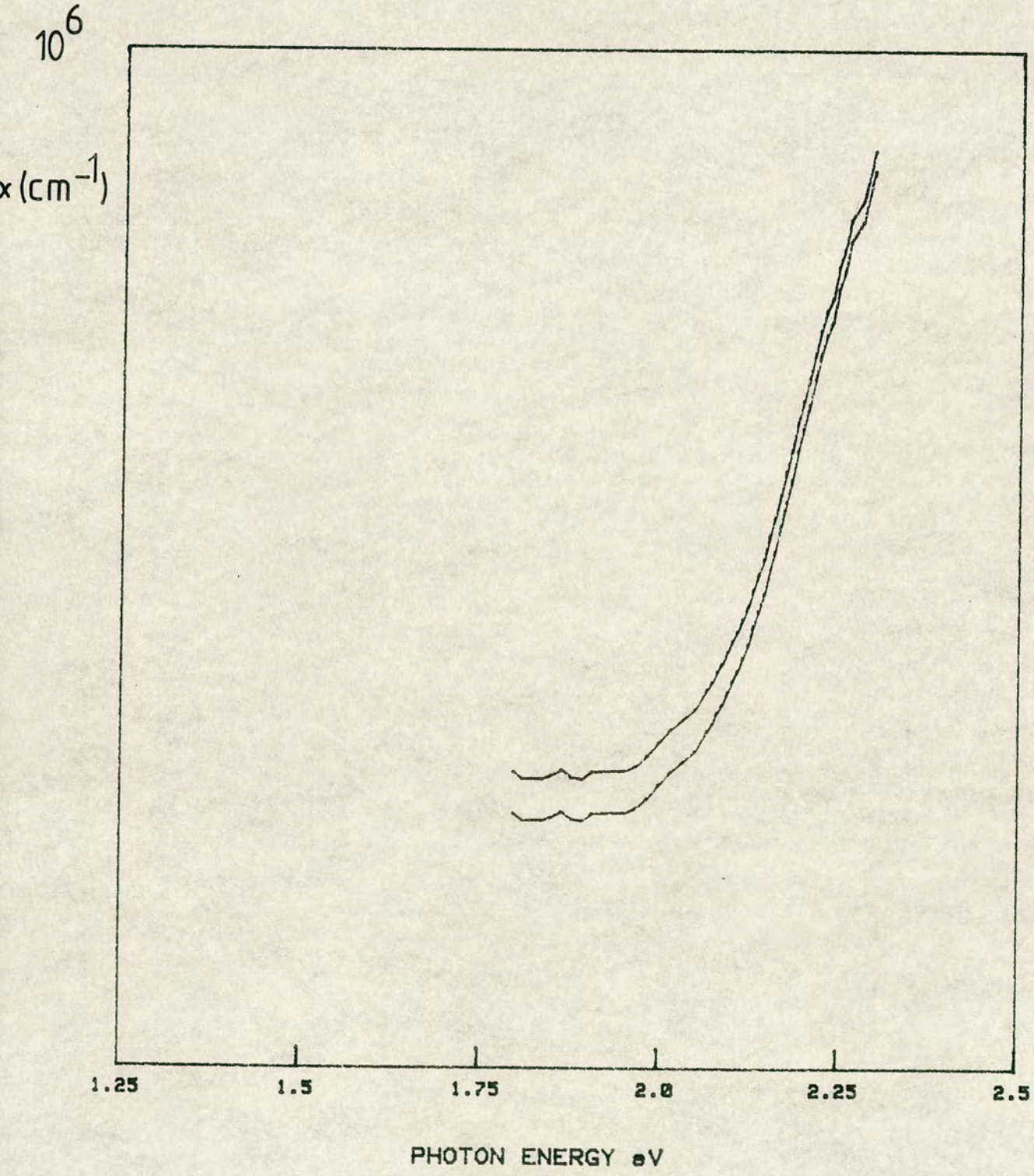

FIG. (6.43)

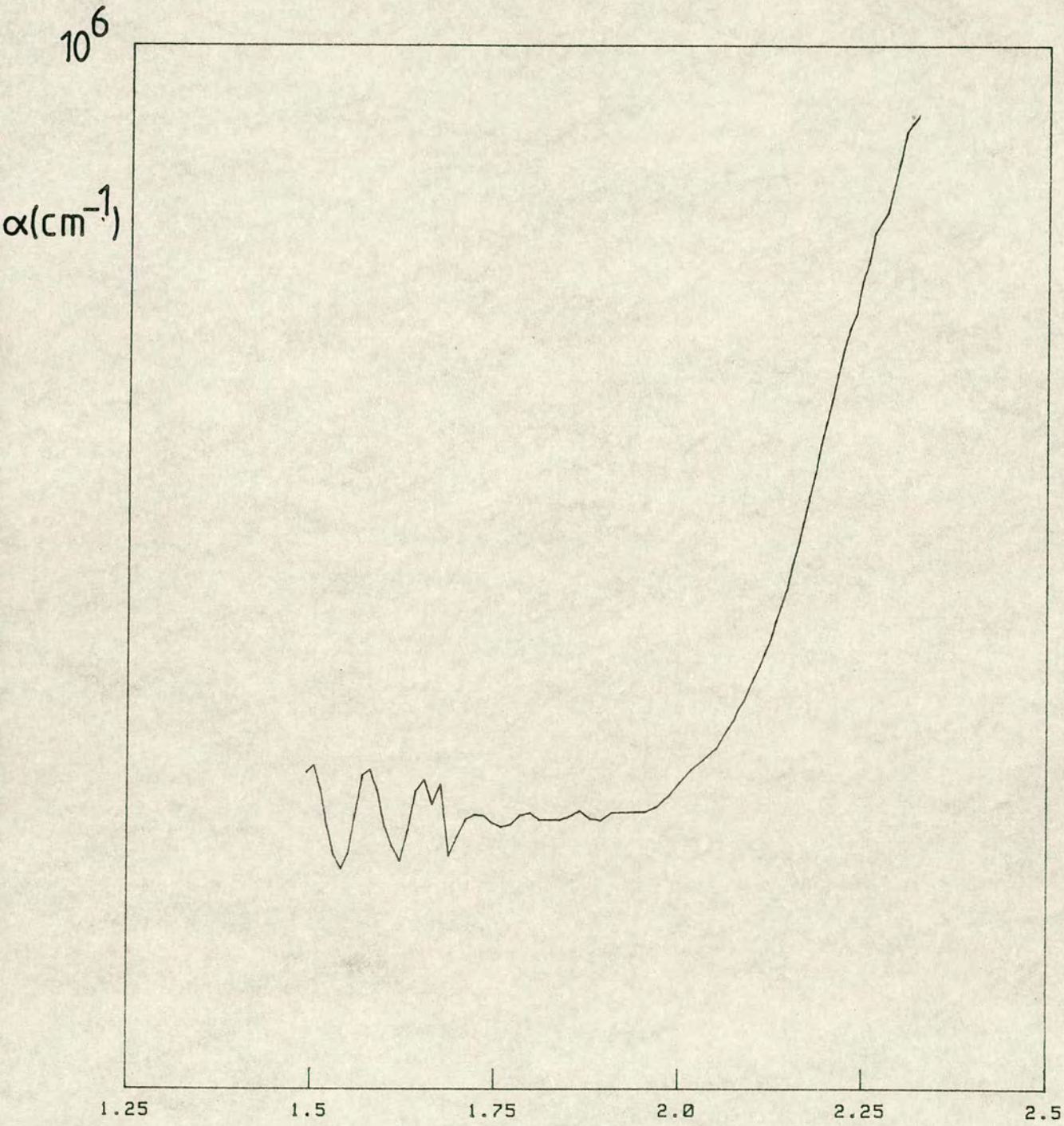

FIG. (6.44a)

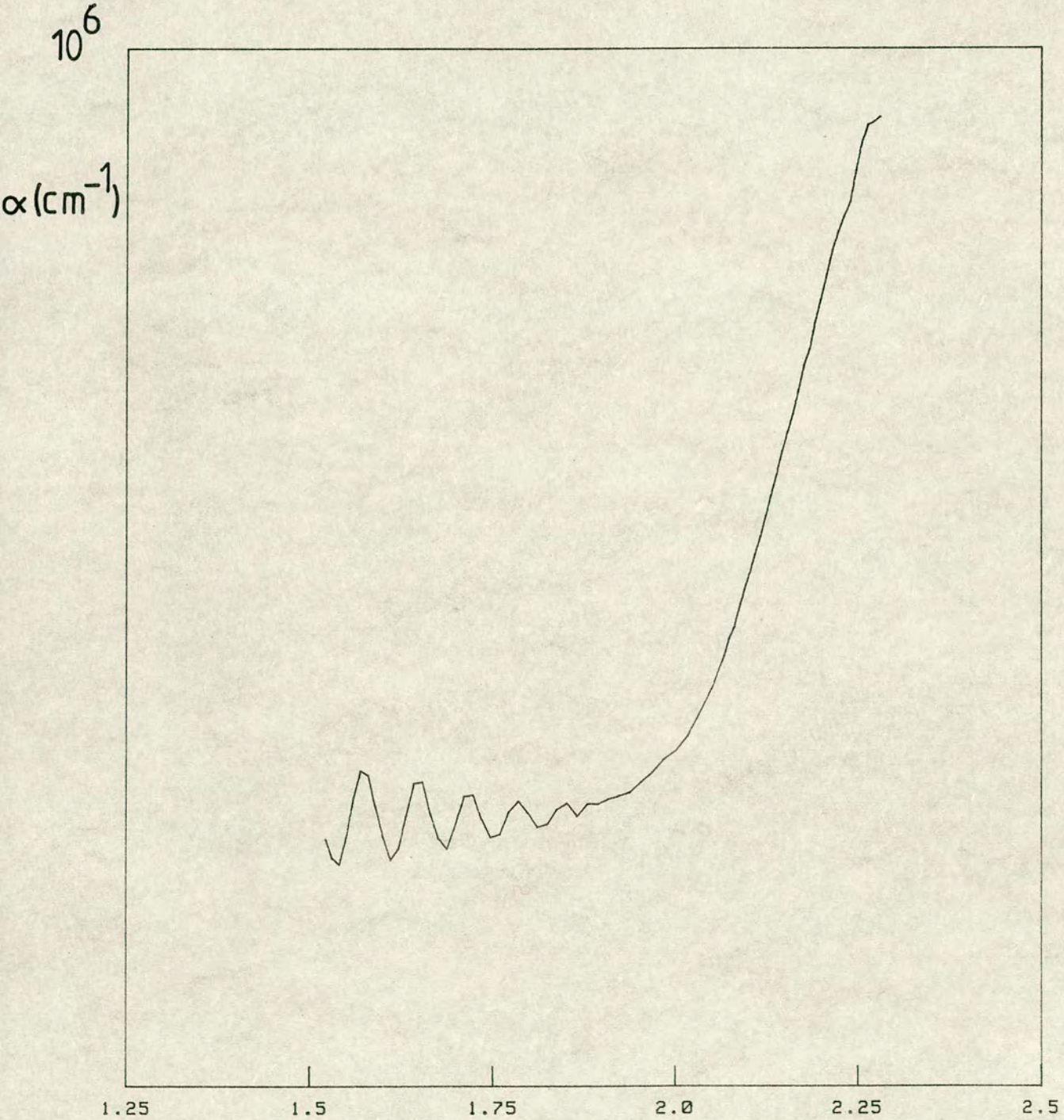

FIG.(6.44b)

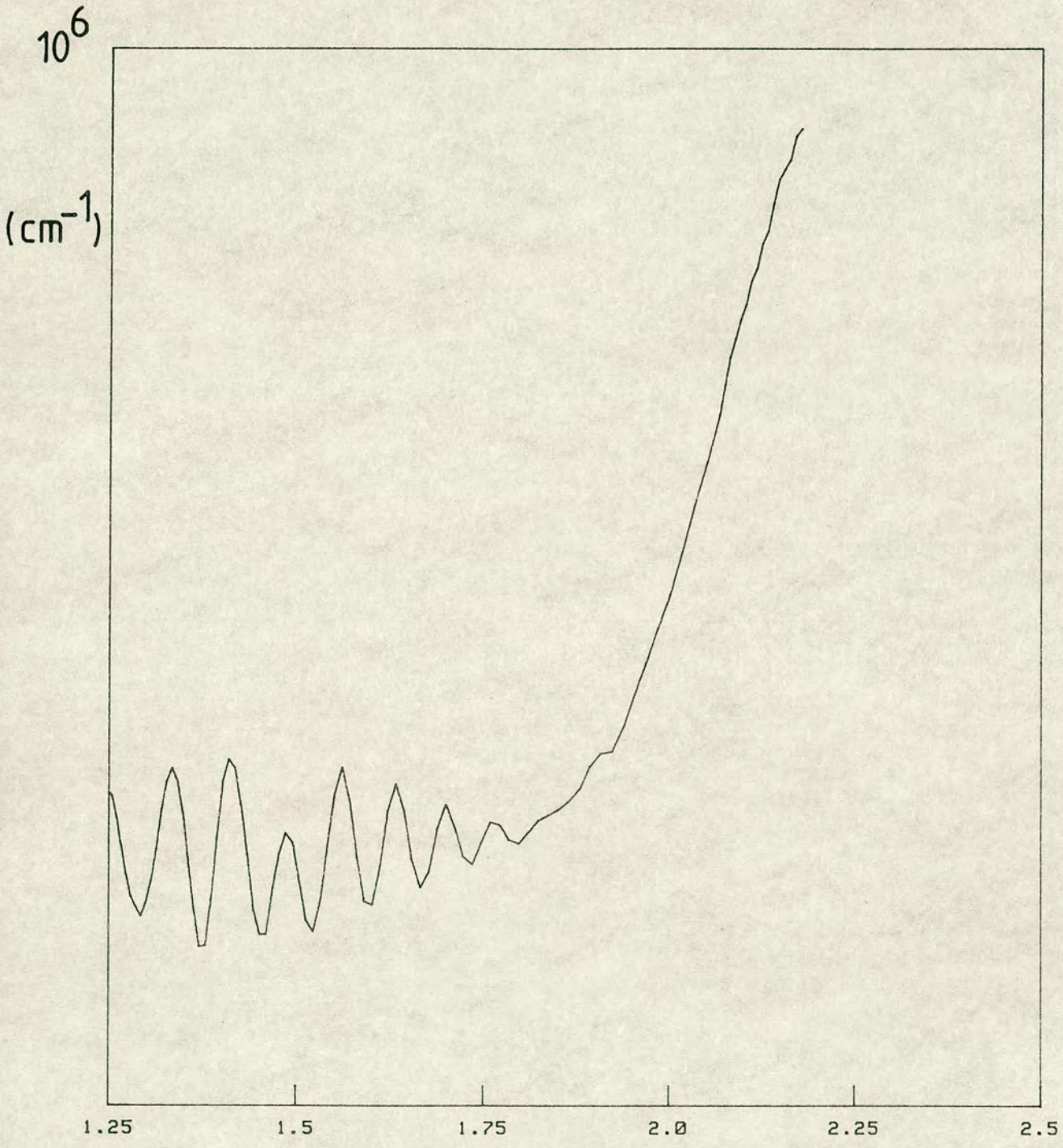

FIG.(6.44c)

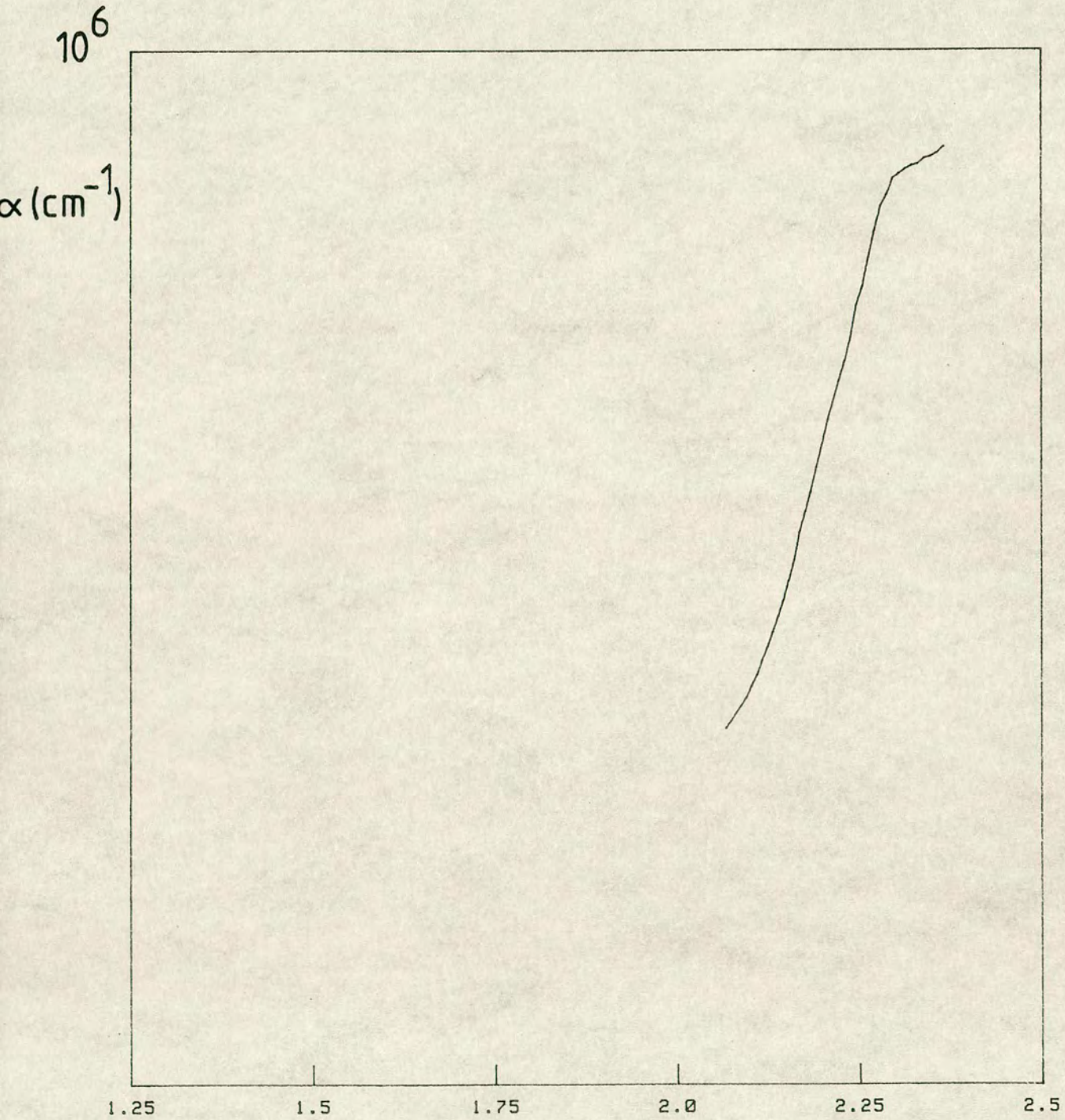

FIG.(6.45a)

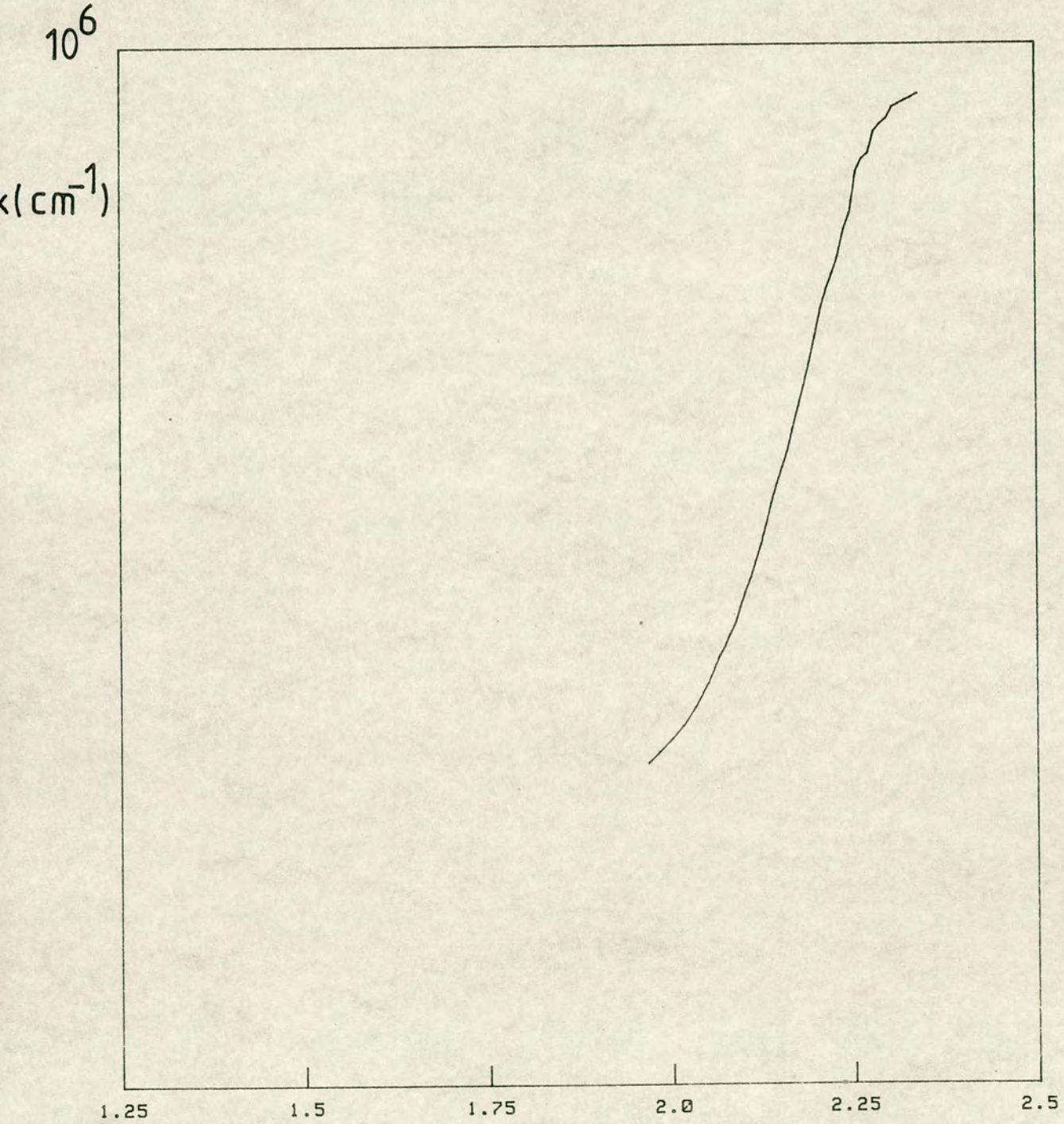

FIG.(6.45b)

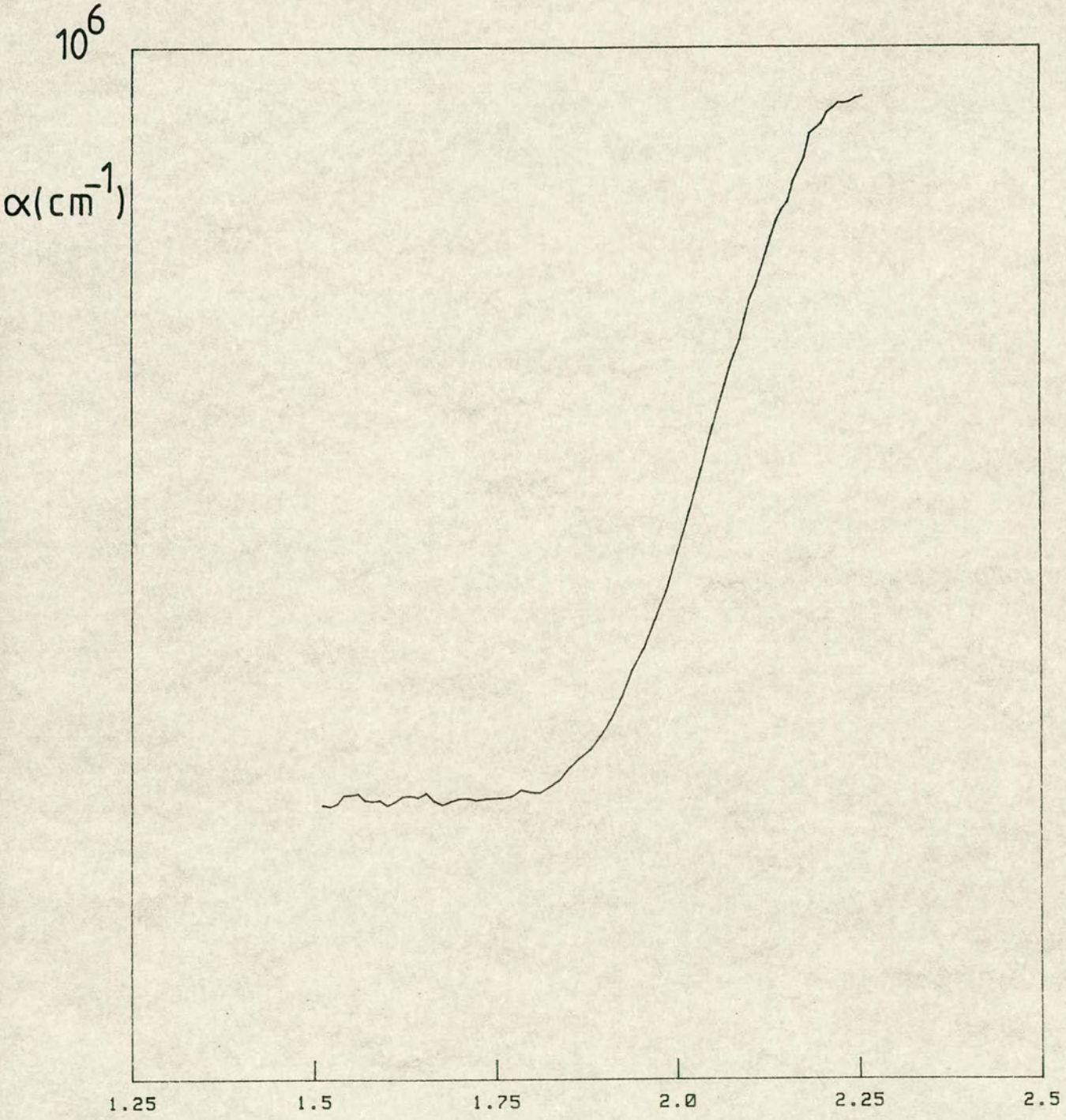

FIG.(6.45c)

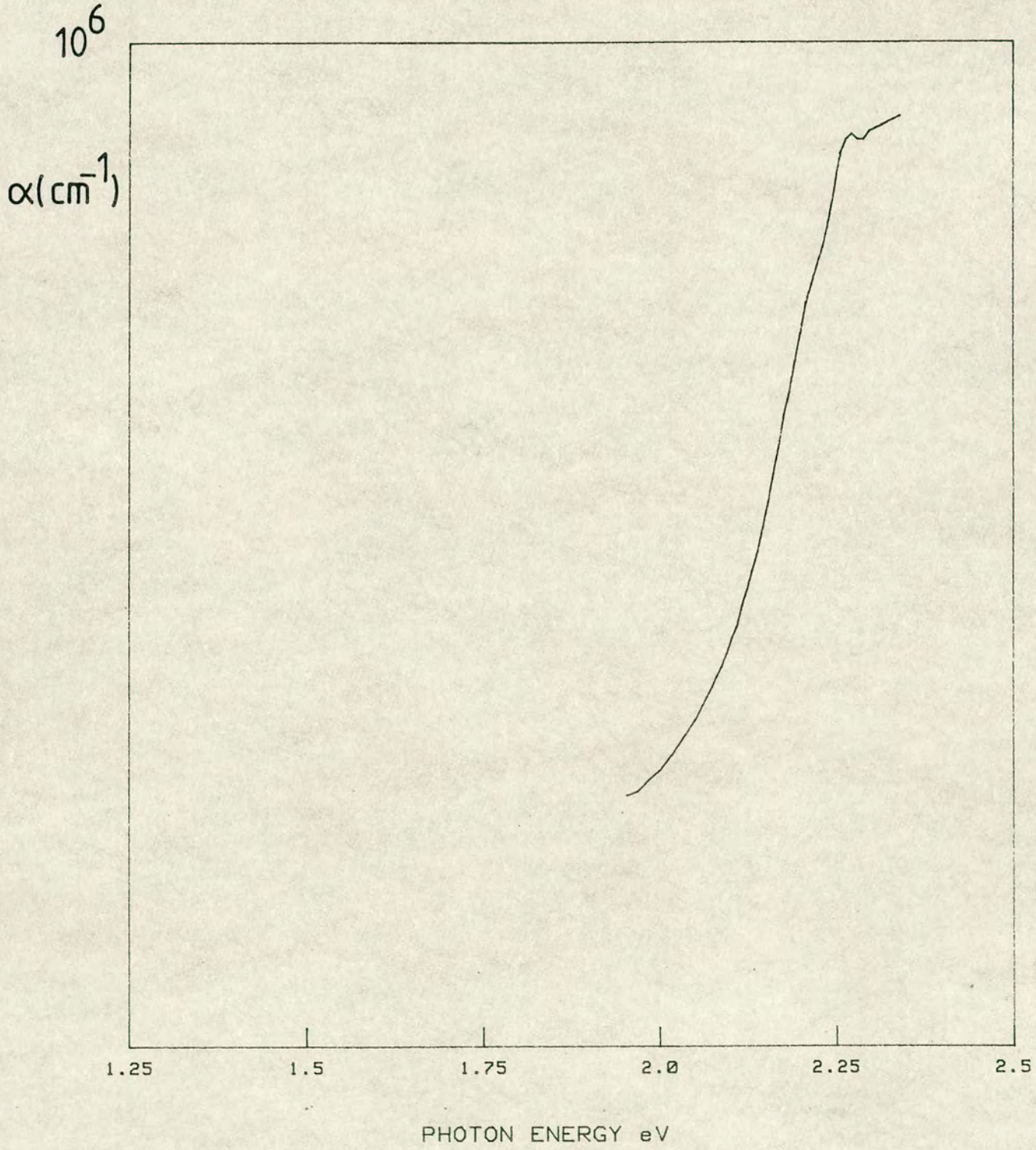

FIG.(6.46a)

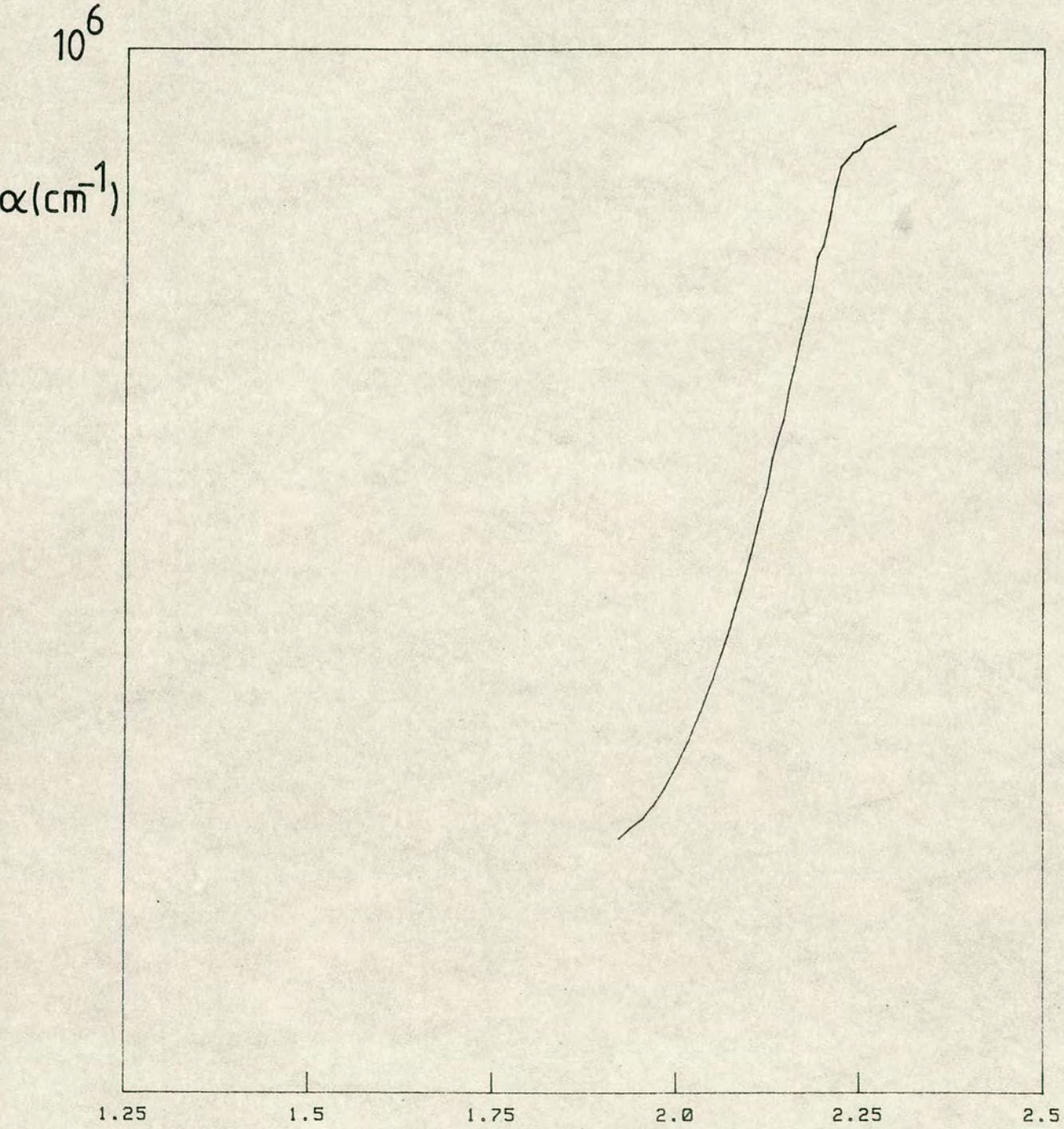

FIG.(6.46b)

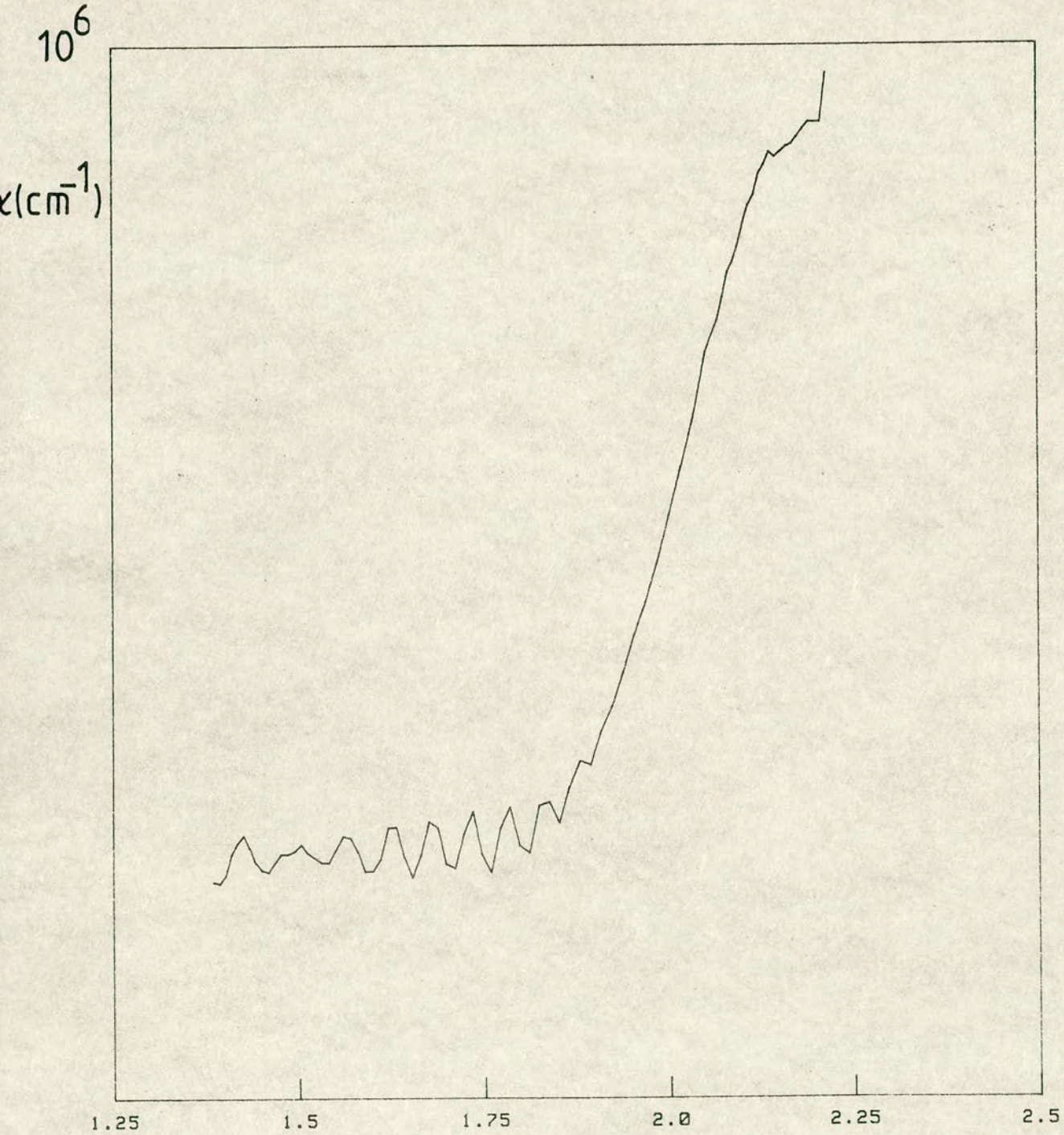

FIG.(6.46c)

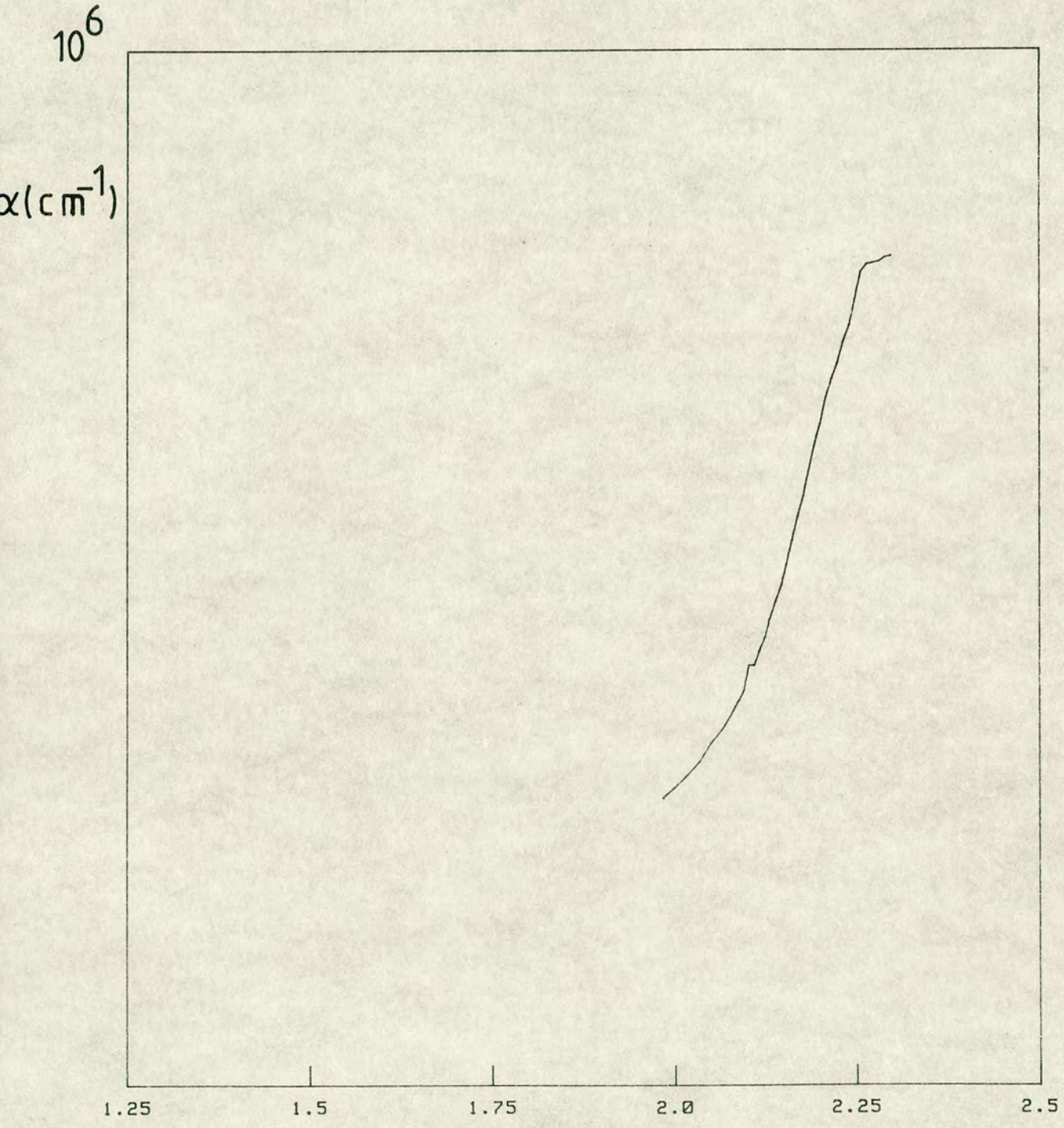

FIG.(6.47a)

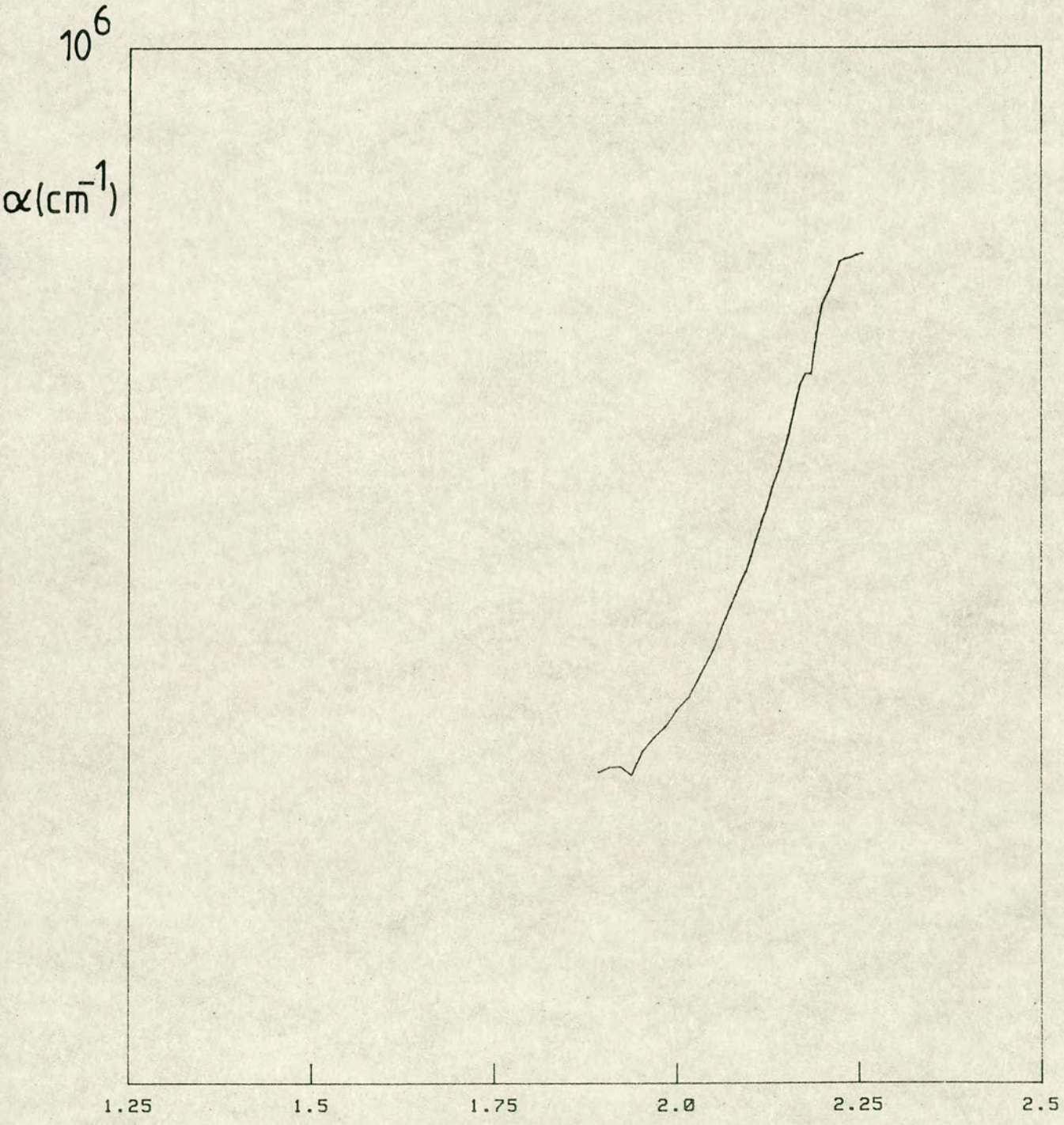

FIG.(6.47b)

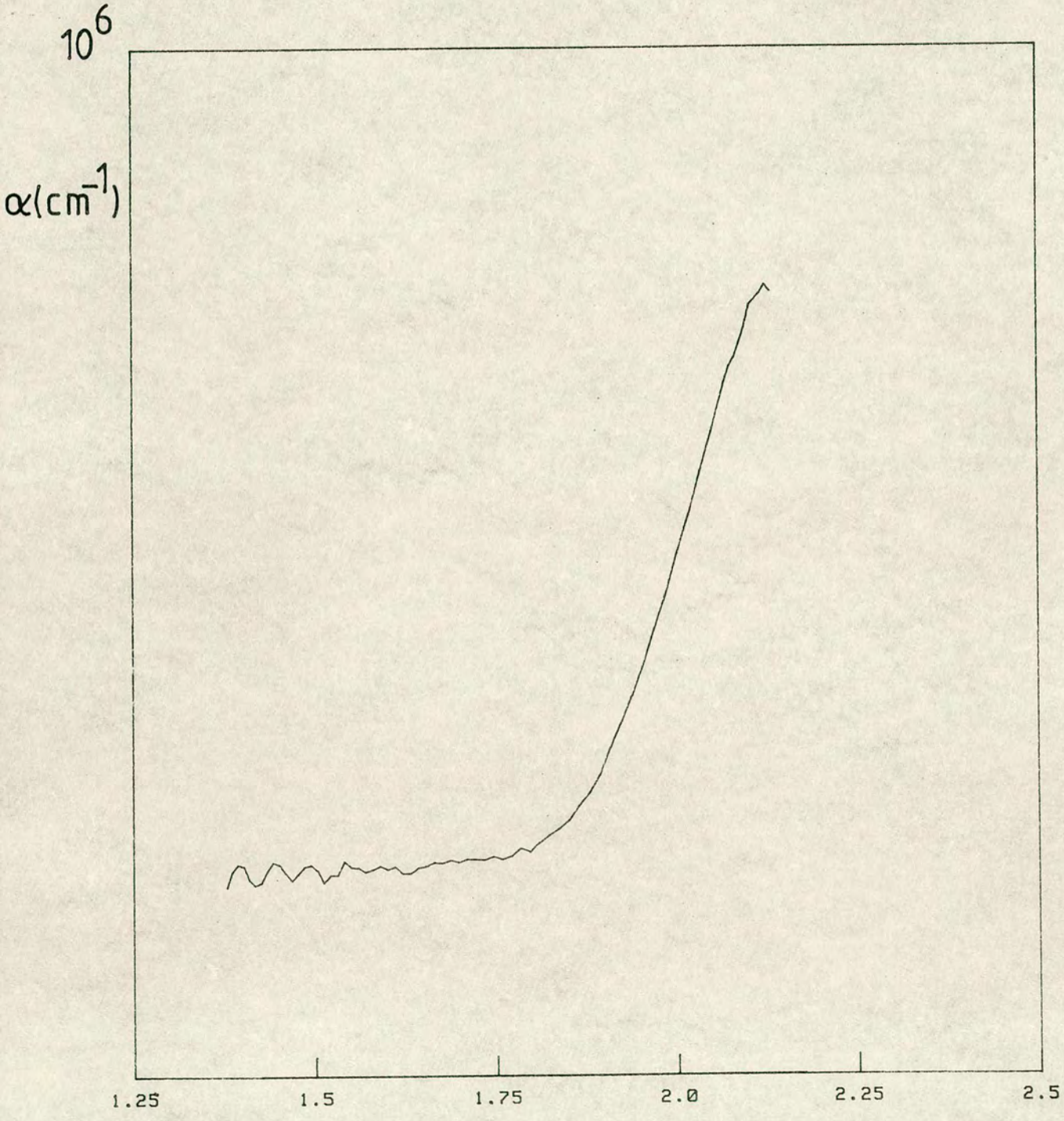

FIG.(6.47c)

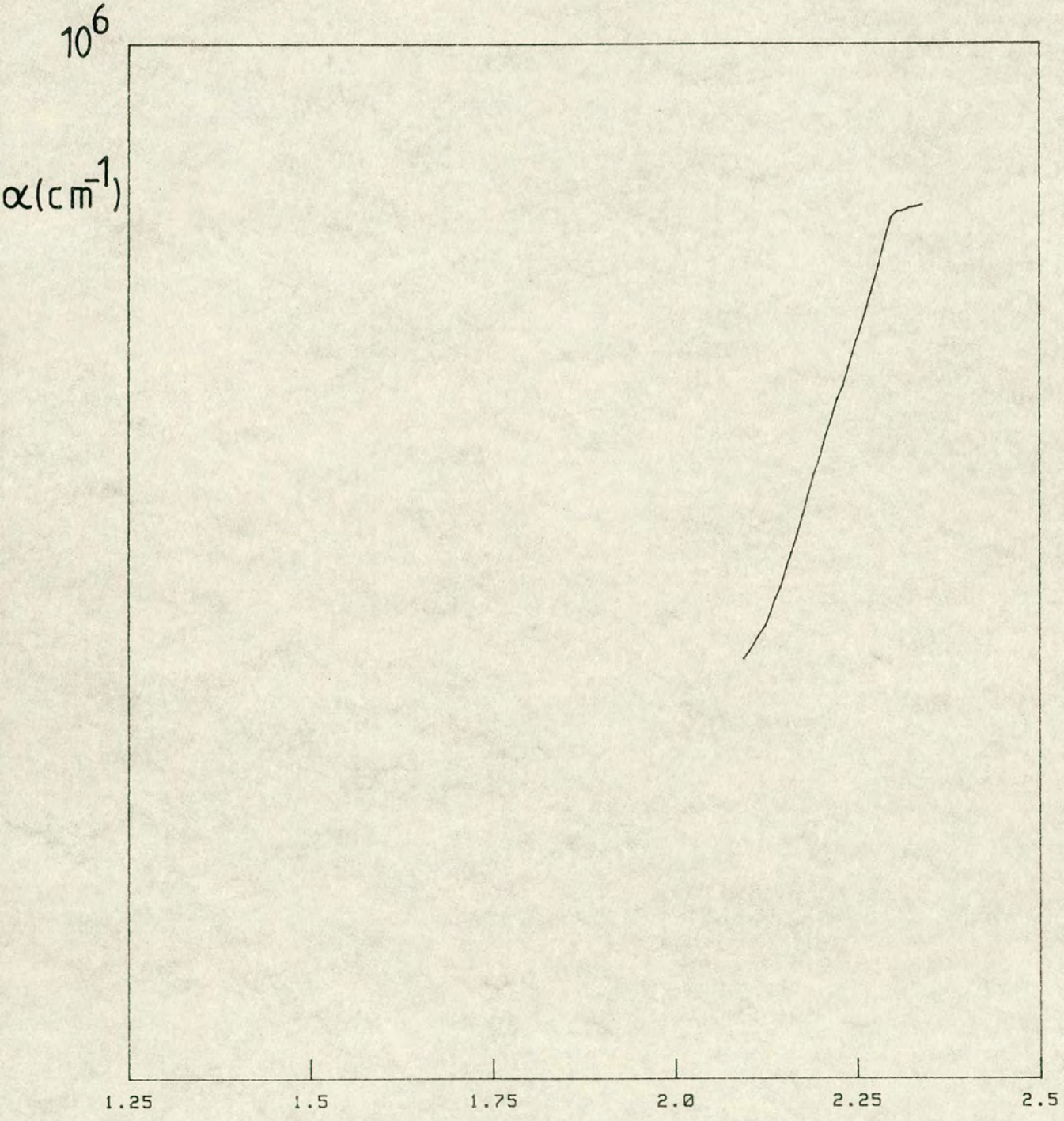

FIG.(6.48a)

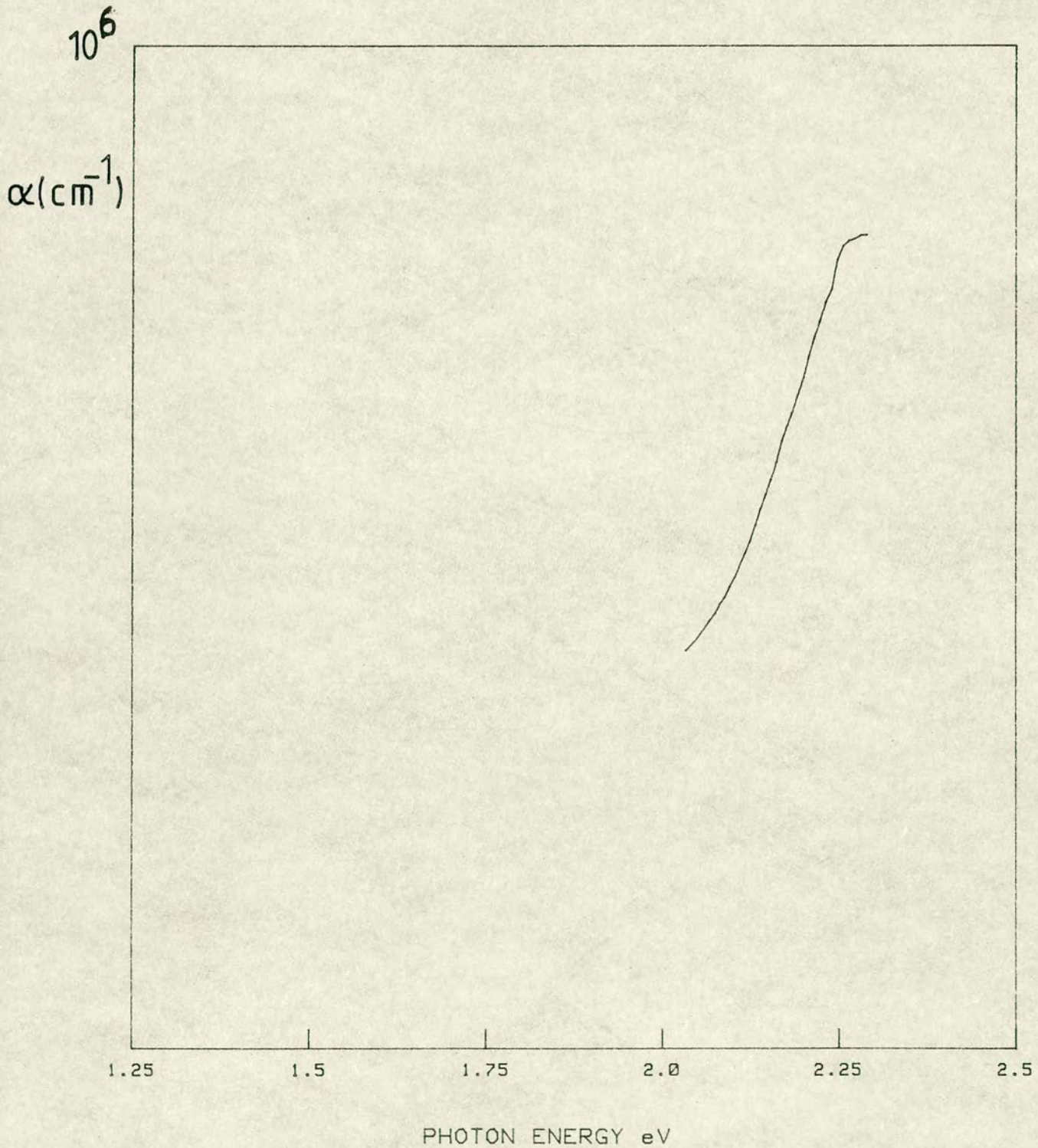

FIG.(6.48b)

FIG.(6.48c)

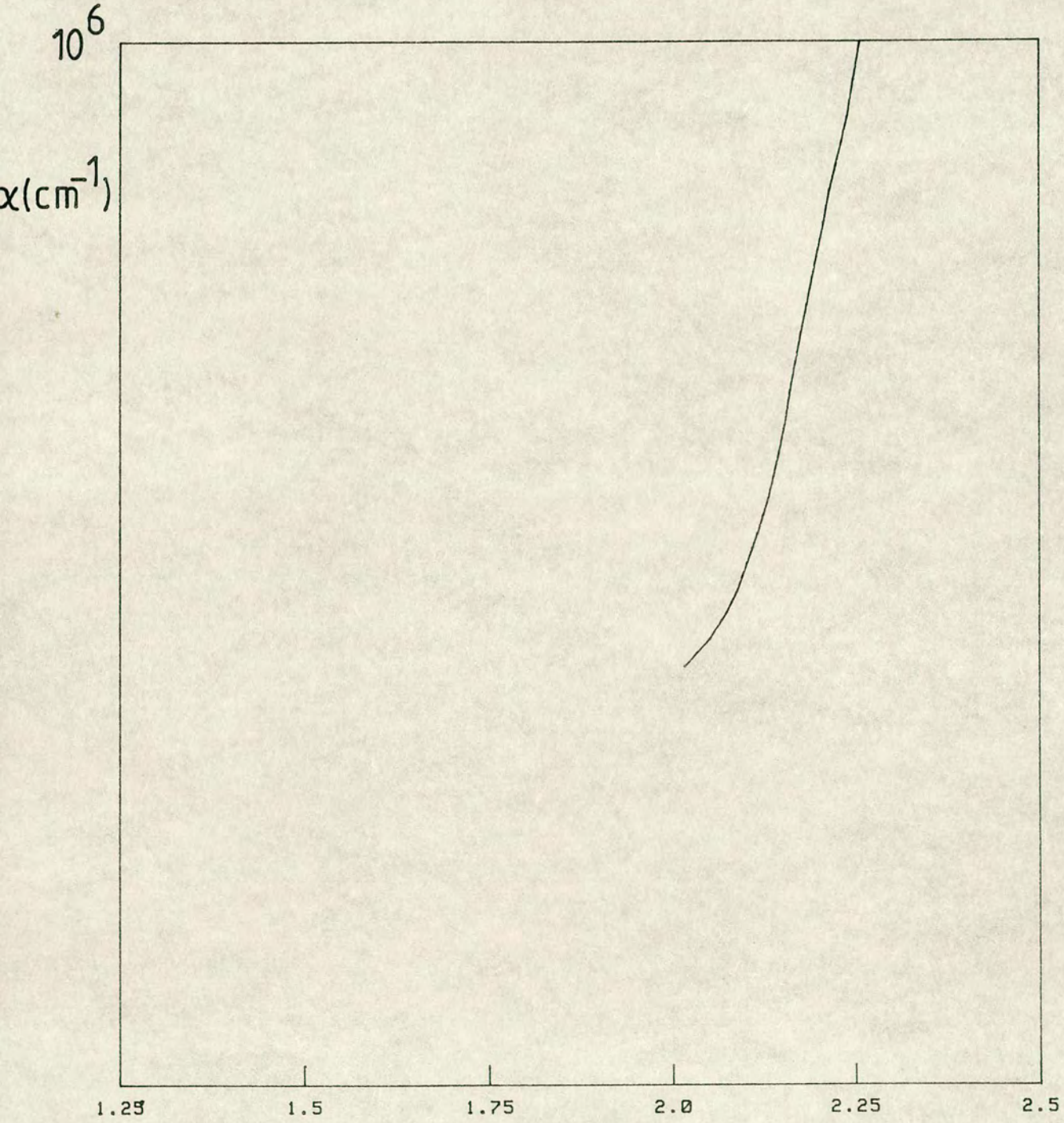

FIG.(6.49a)

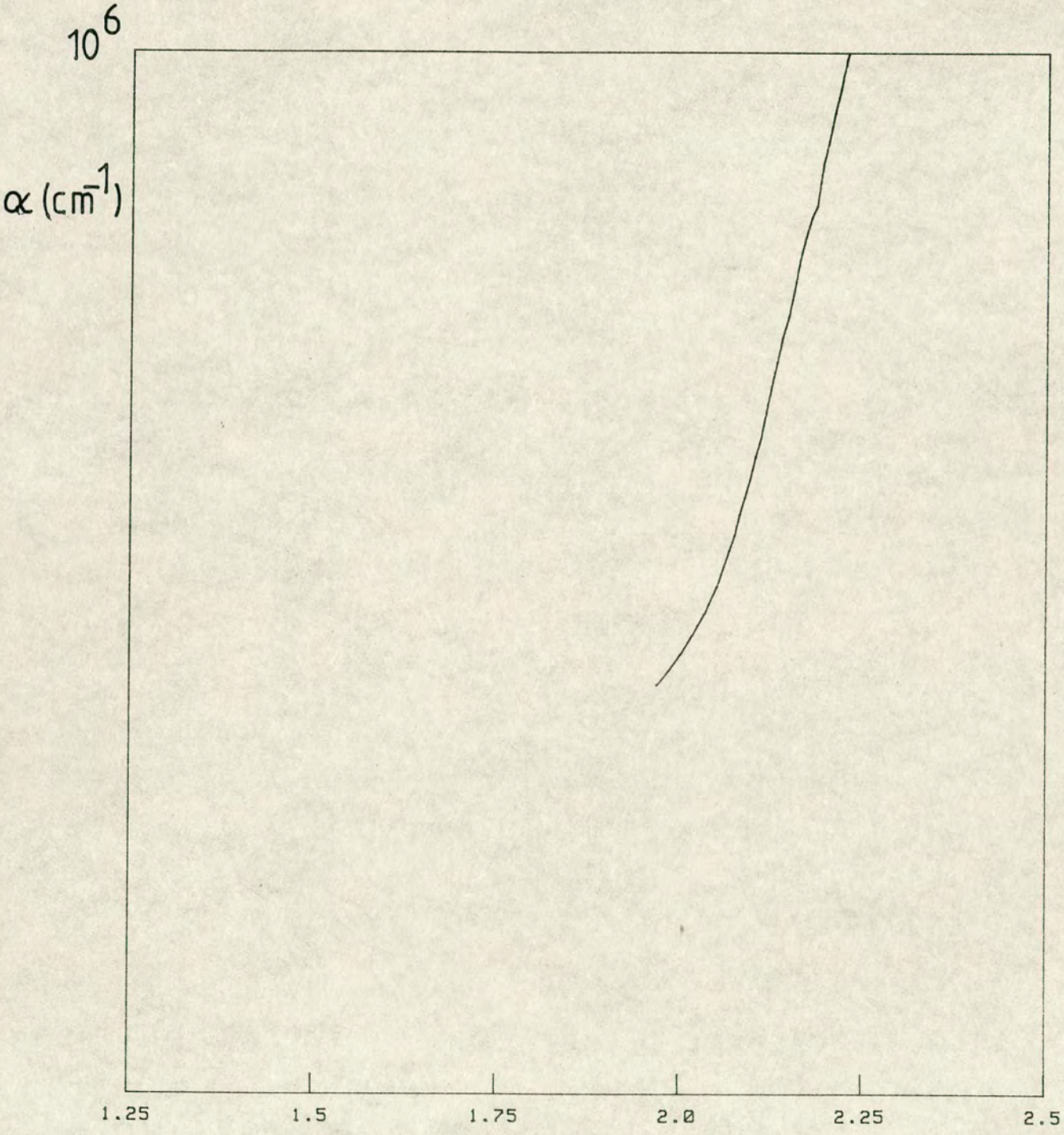

FIG.(6.49b)

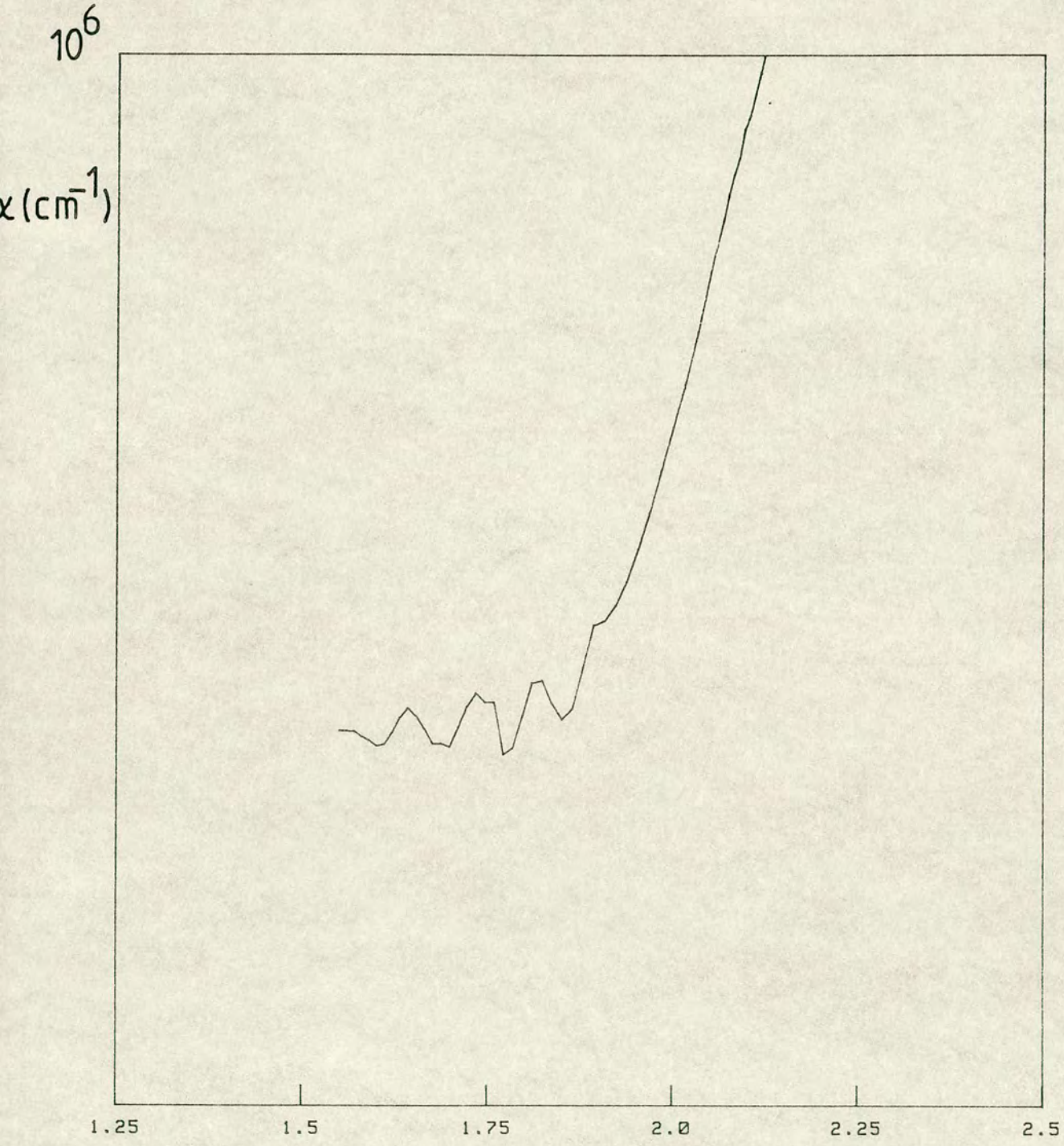

FIG.(6.49c)

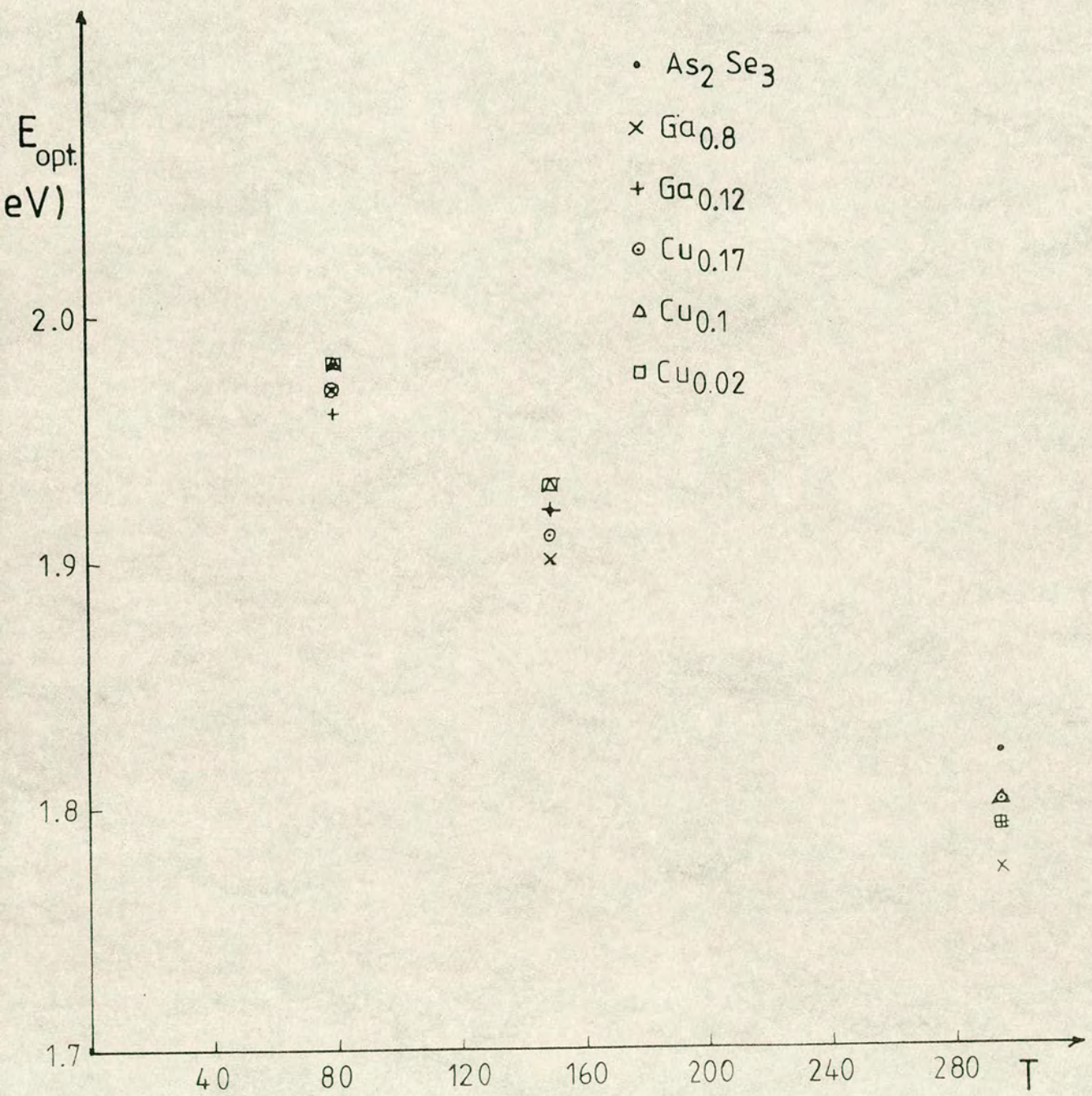
E opt. eV)
2.0
1.9
1.8
1.7
40
80
120
160
200
240
280
T
• As2 Se3
× Ga0.8
+ Ga0.12
⊙ Cu0.17
△ Cu0.1
□ Cu0.02

FIG. (6.50)

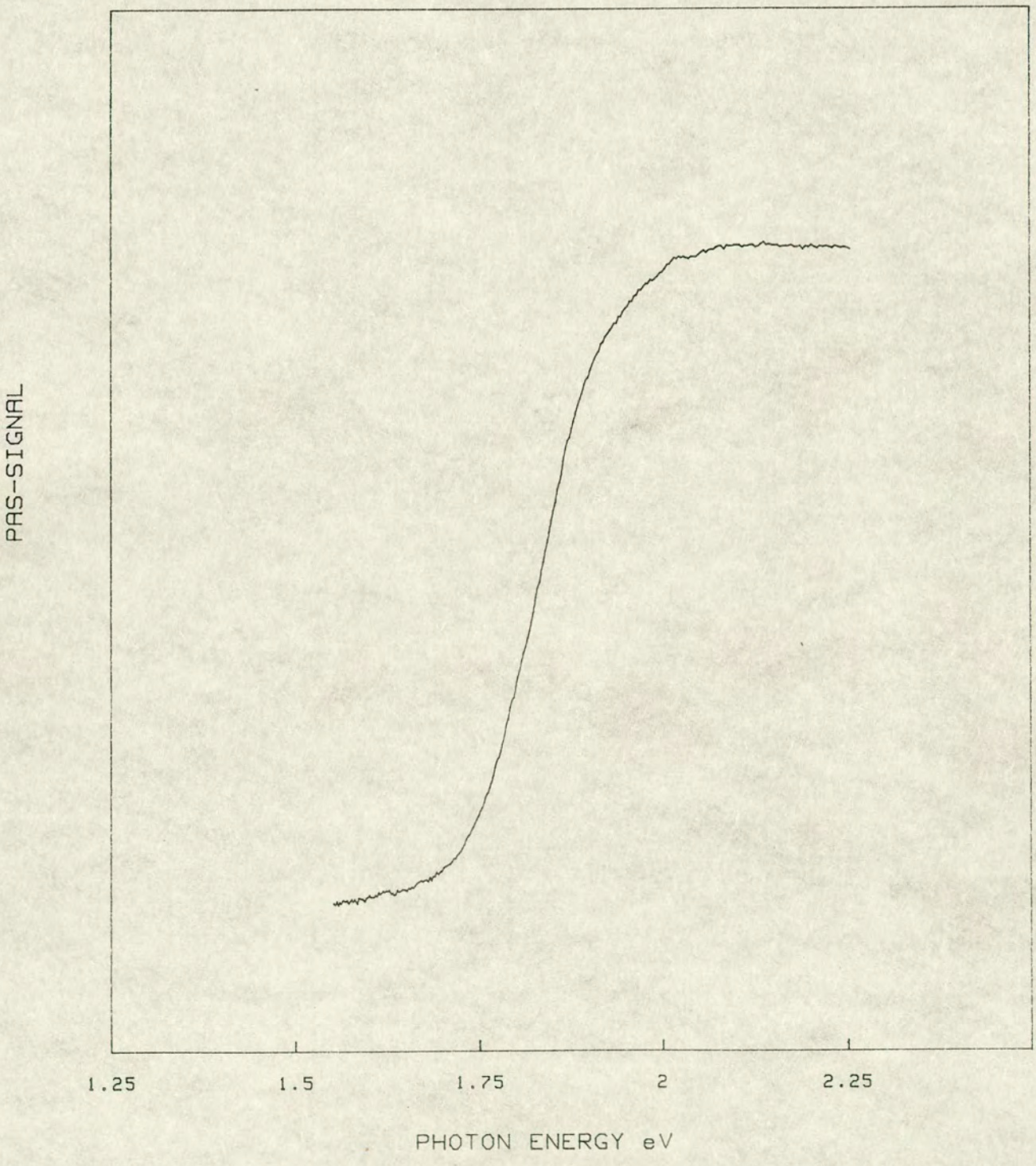

FIG.(6.51)

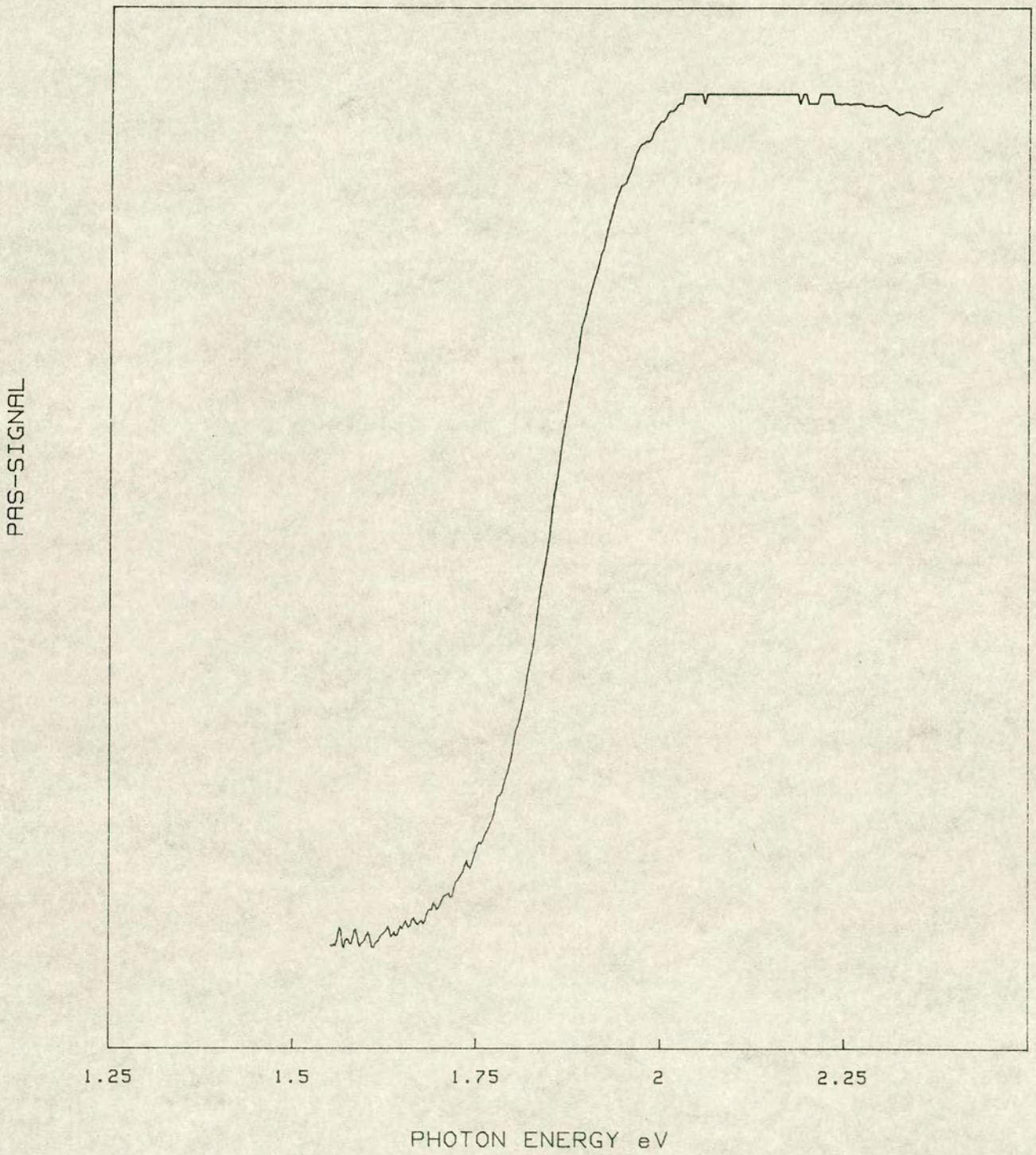

FIG.(6.52)

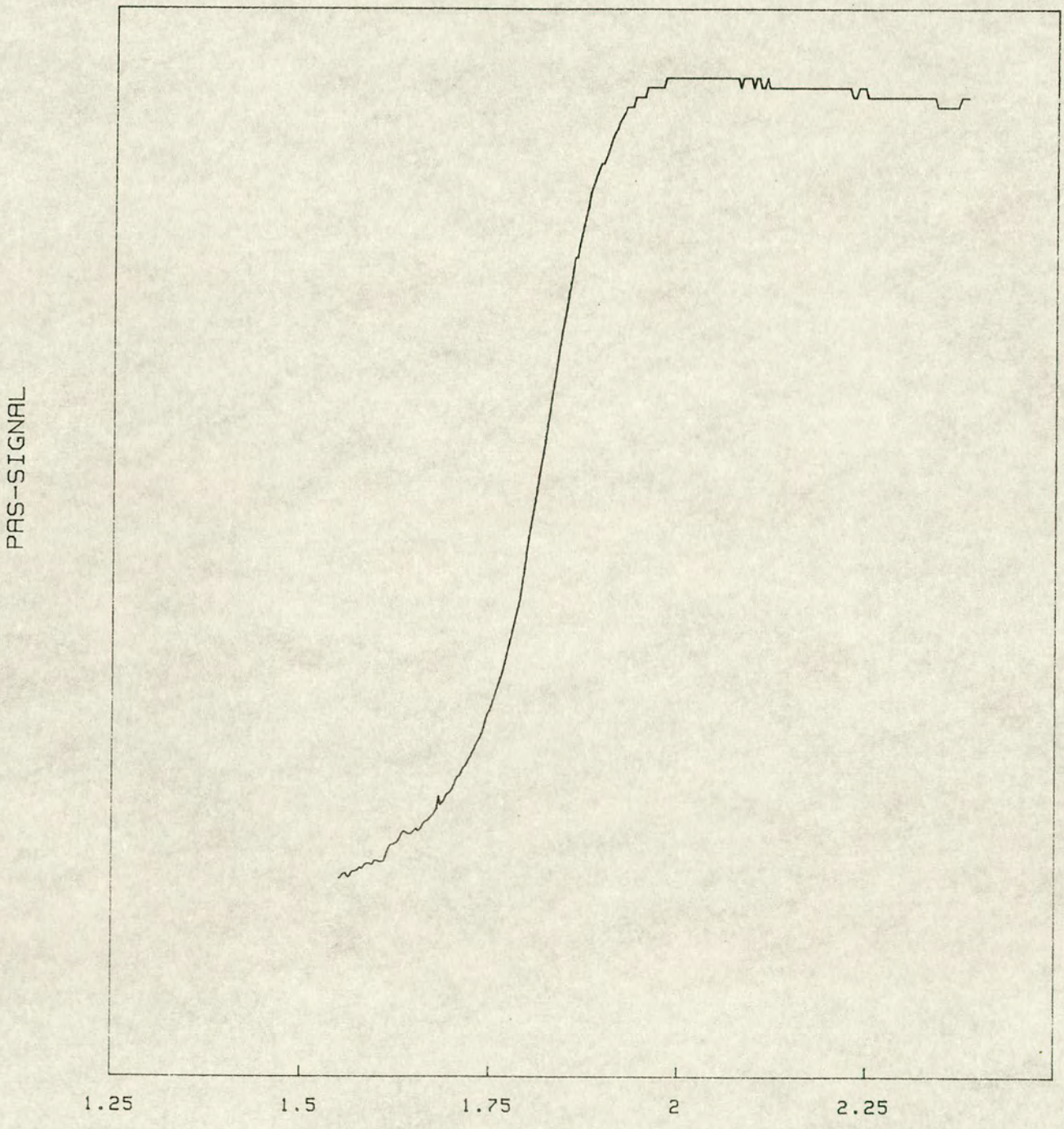

FIG.(6.53)

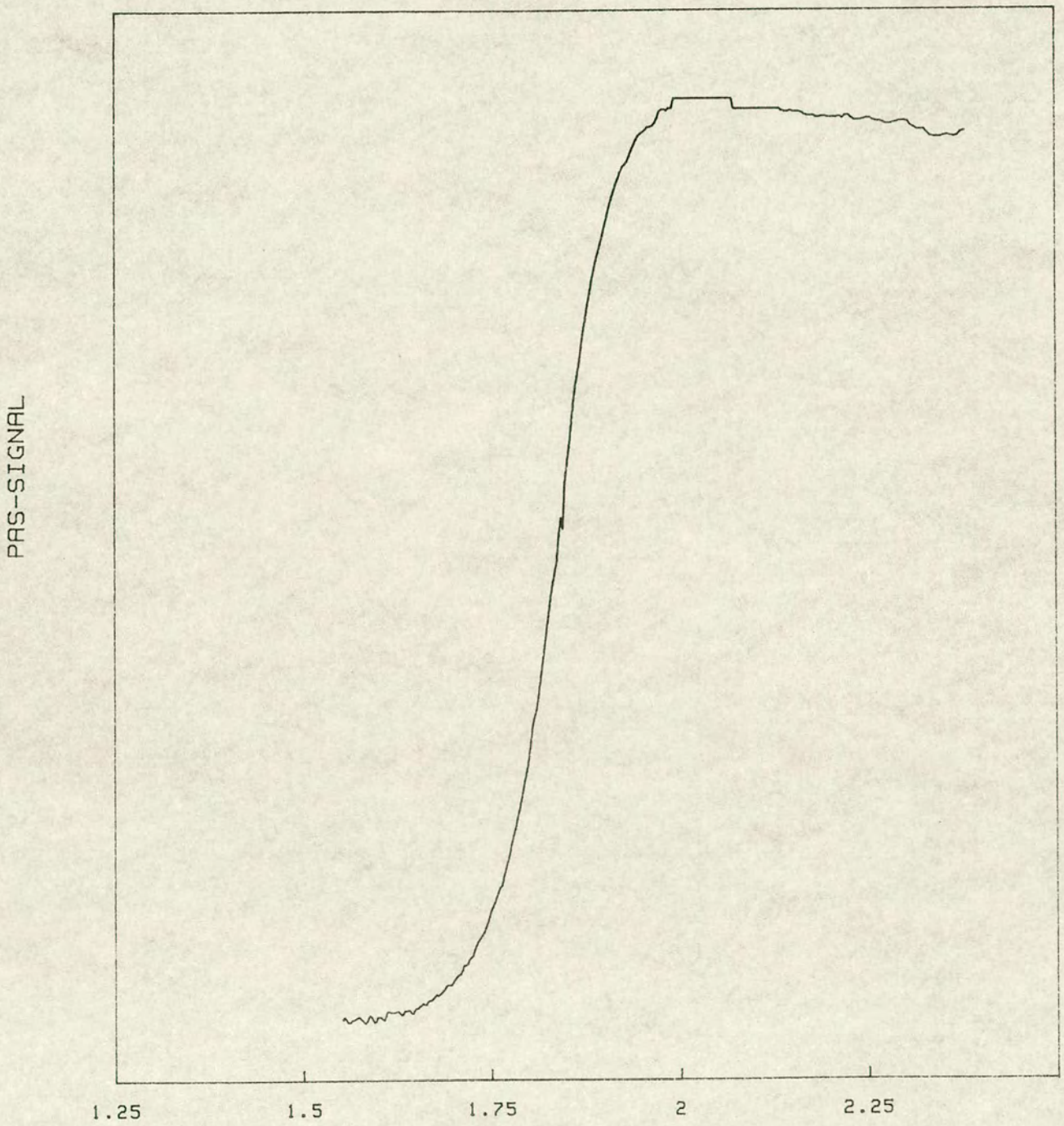

FIG.(6.54)

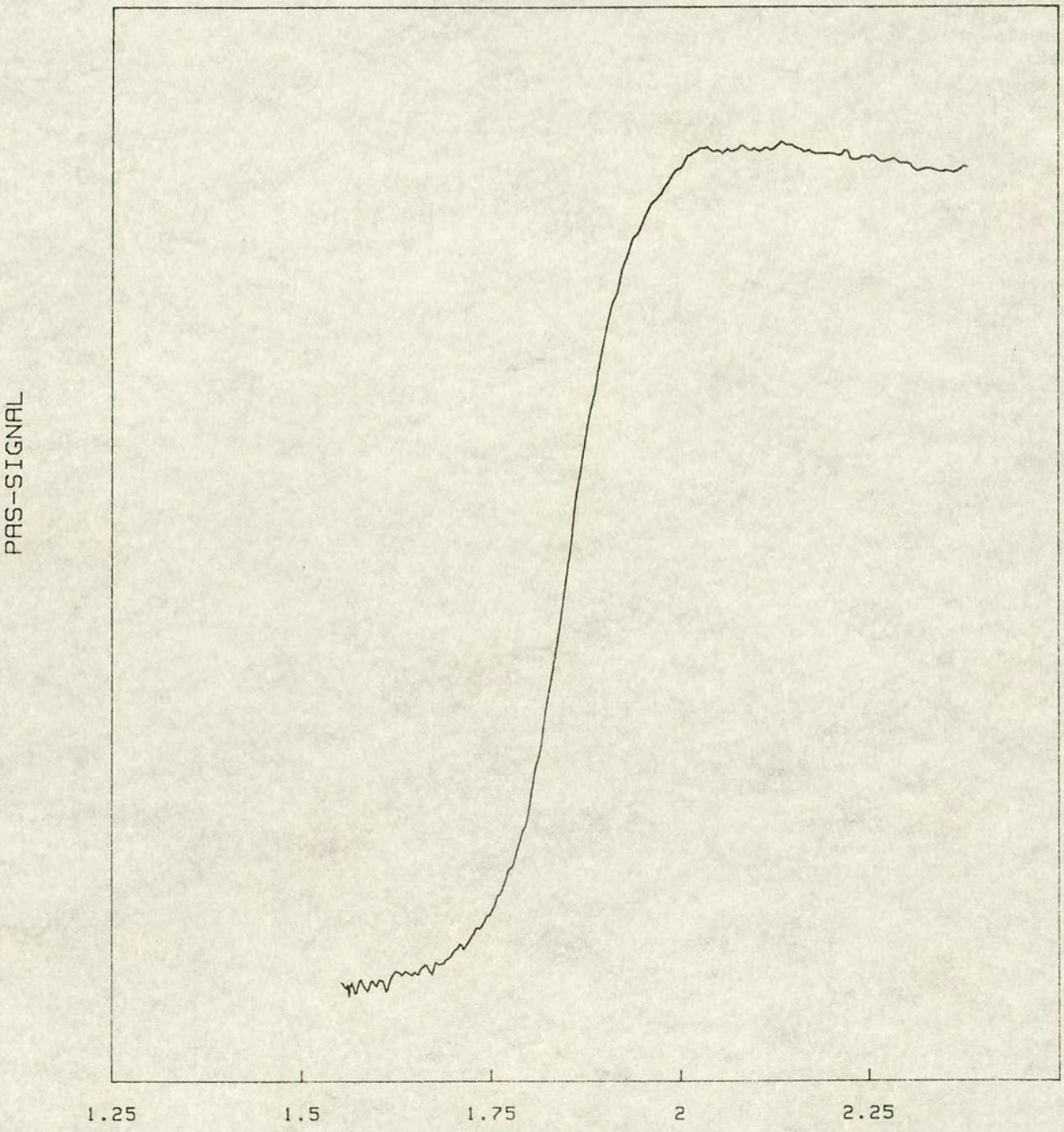

FIG.(6.55)

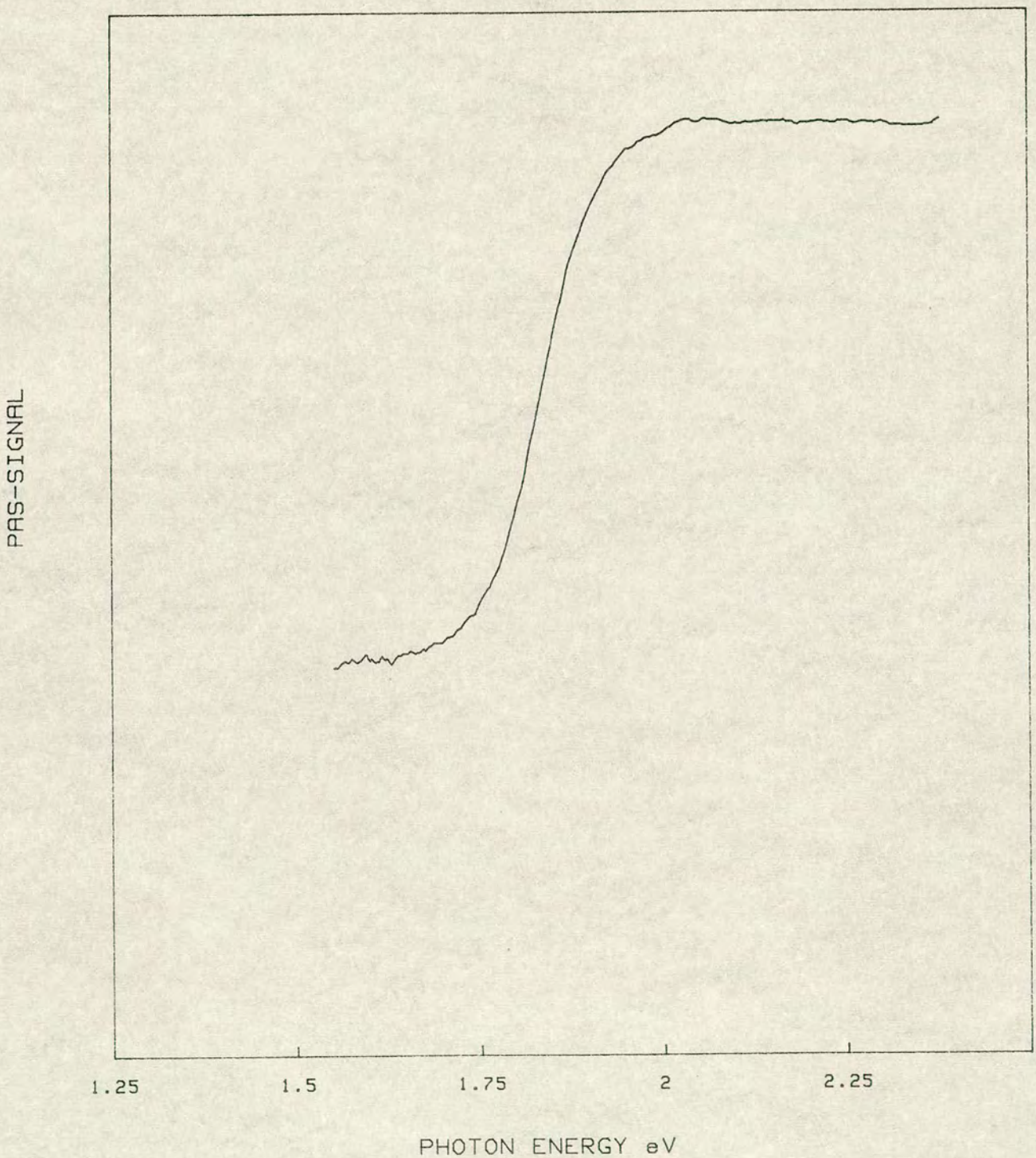

FIG.(6.56)

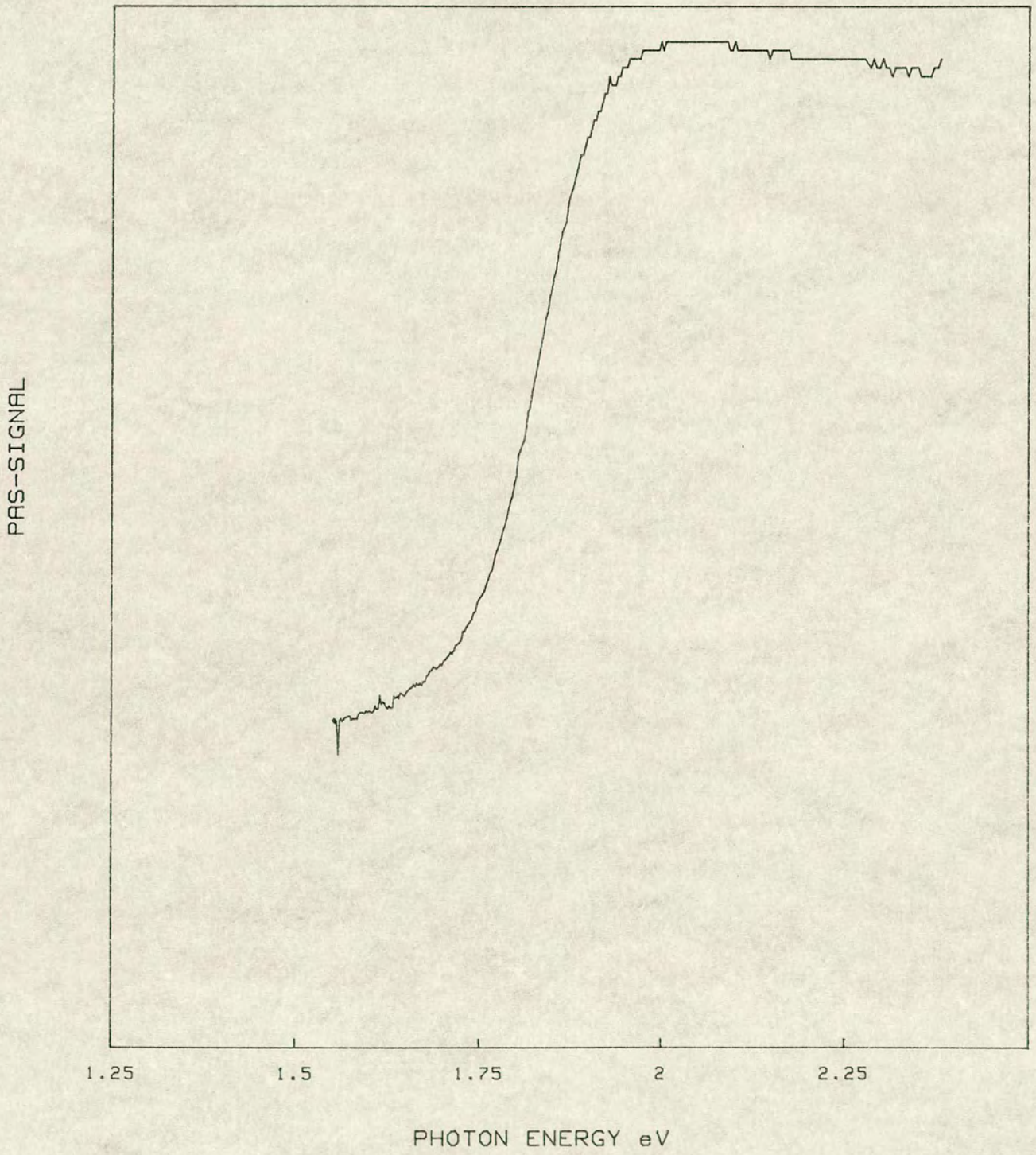

FIG.(6.57)

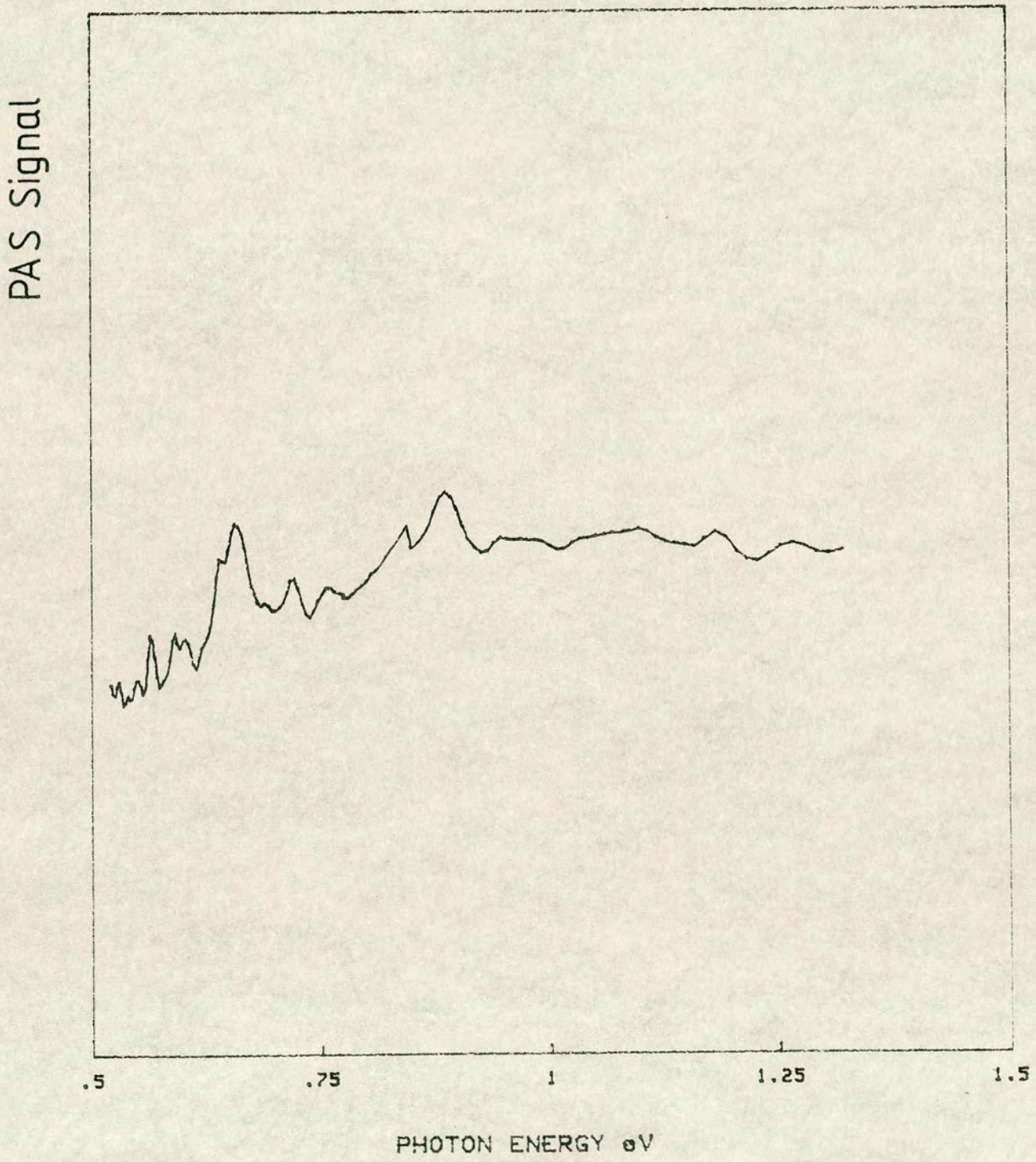

FIG. (6.58a)

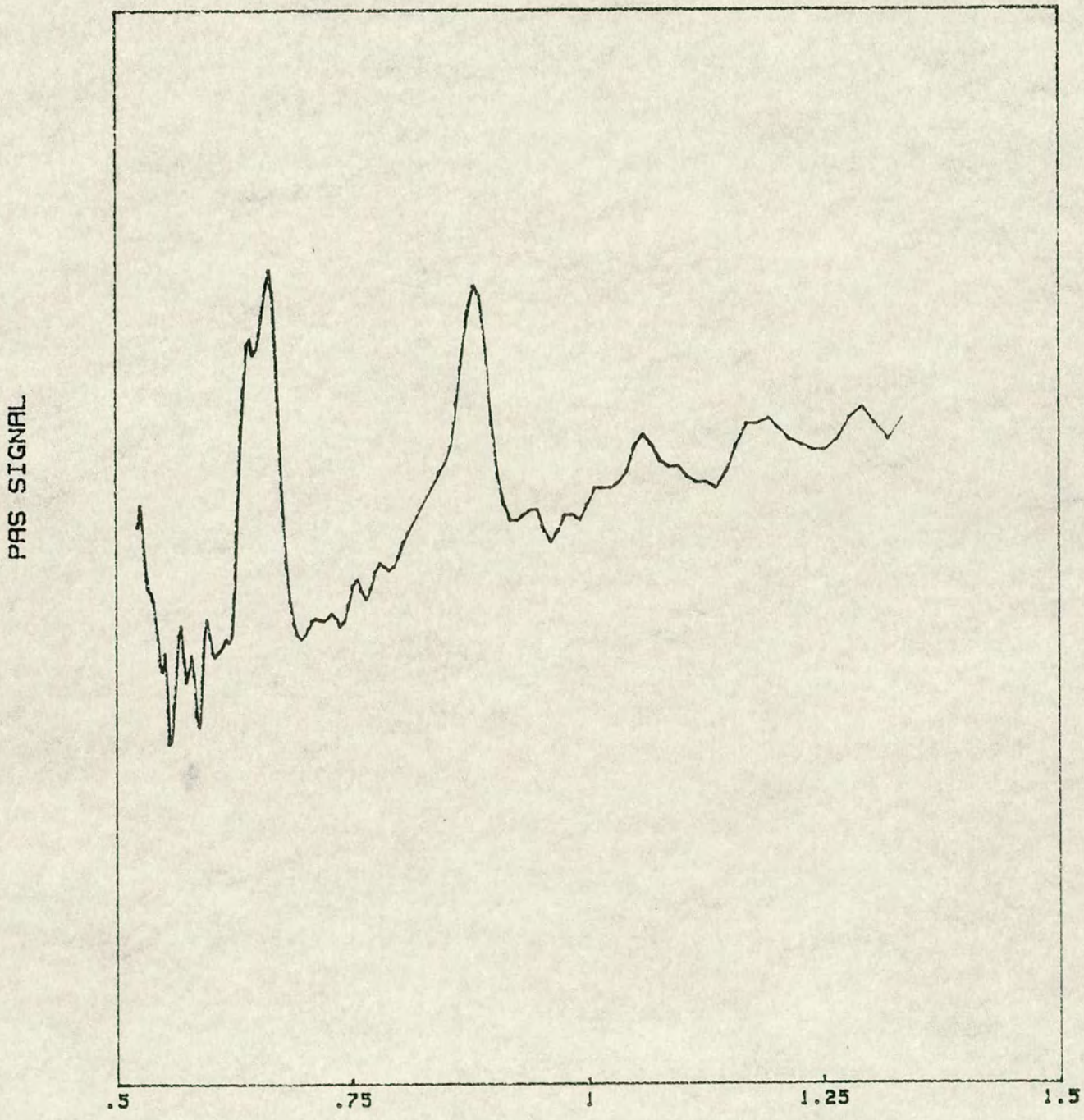

FIG. (6.58b)

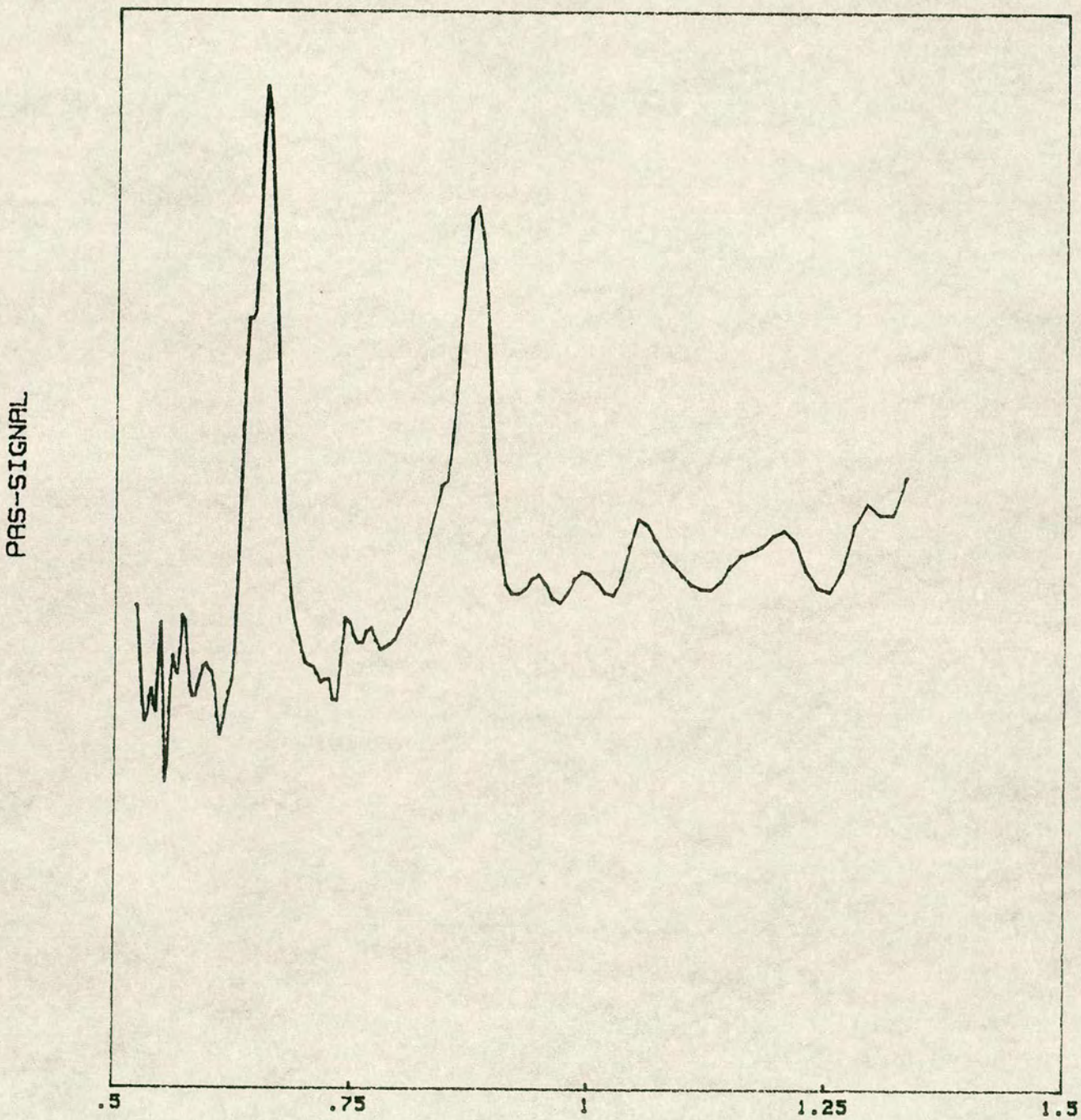

FIG. (6.59)

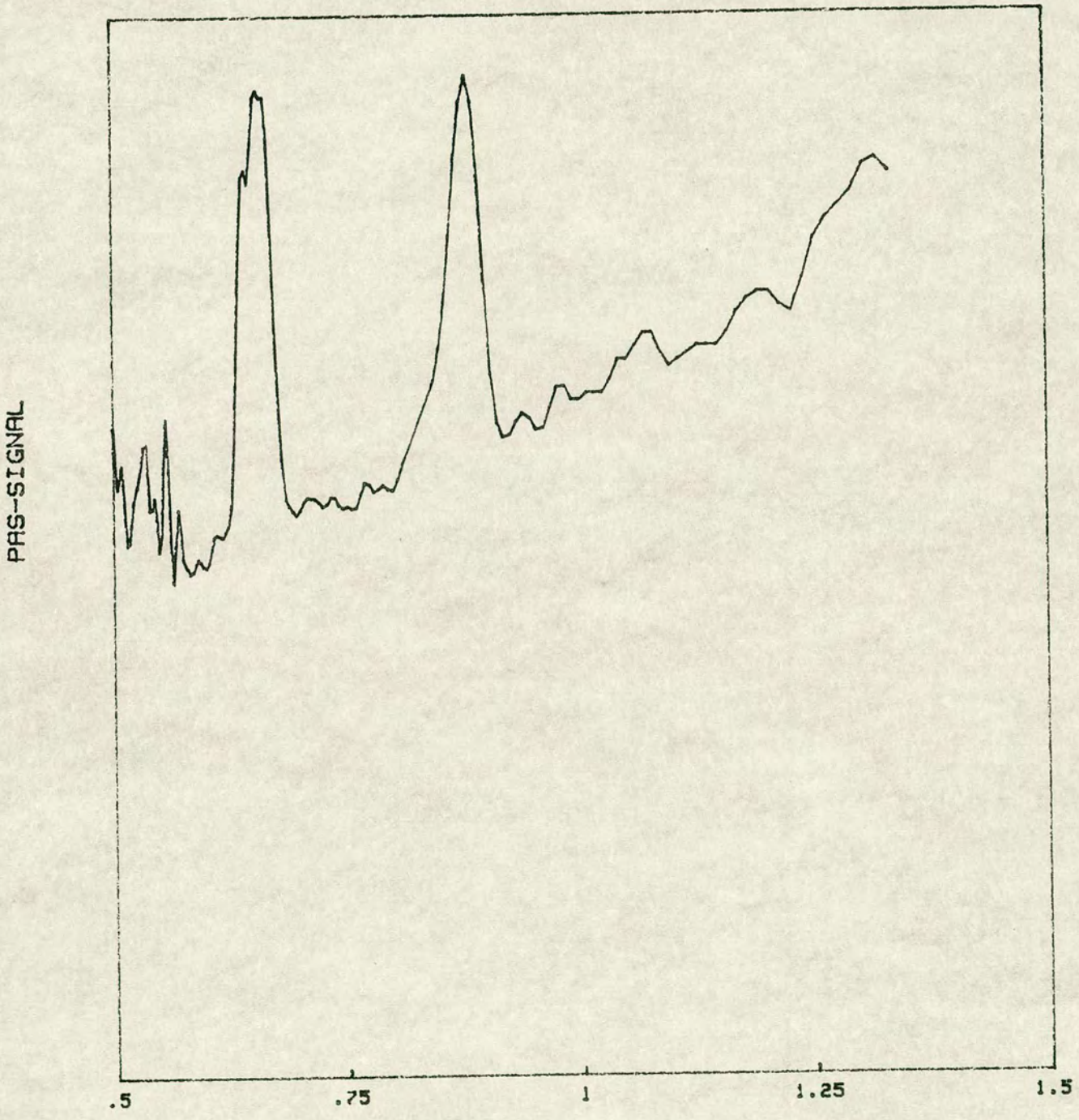

FIG. (6.60)

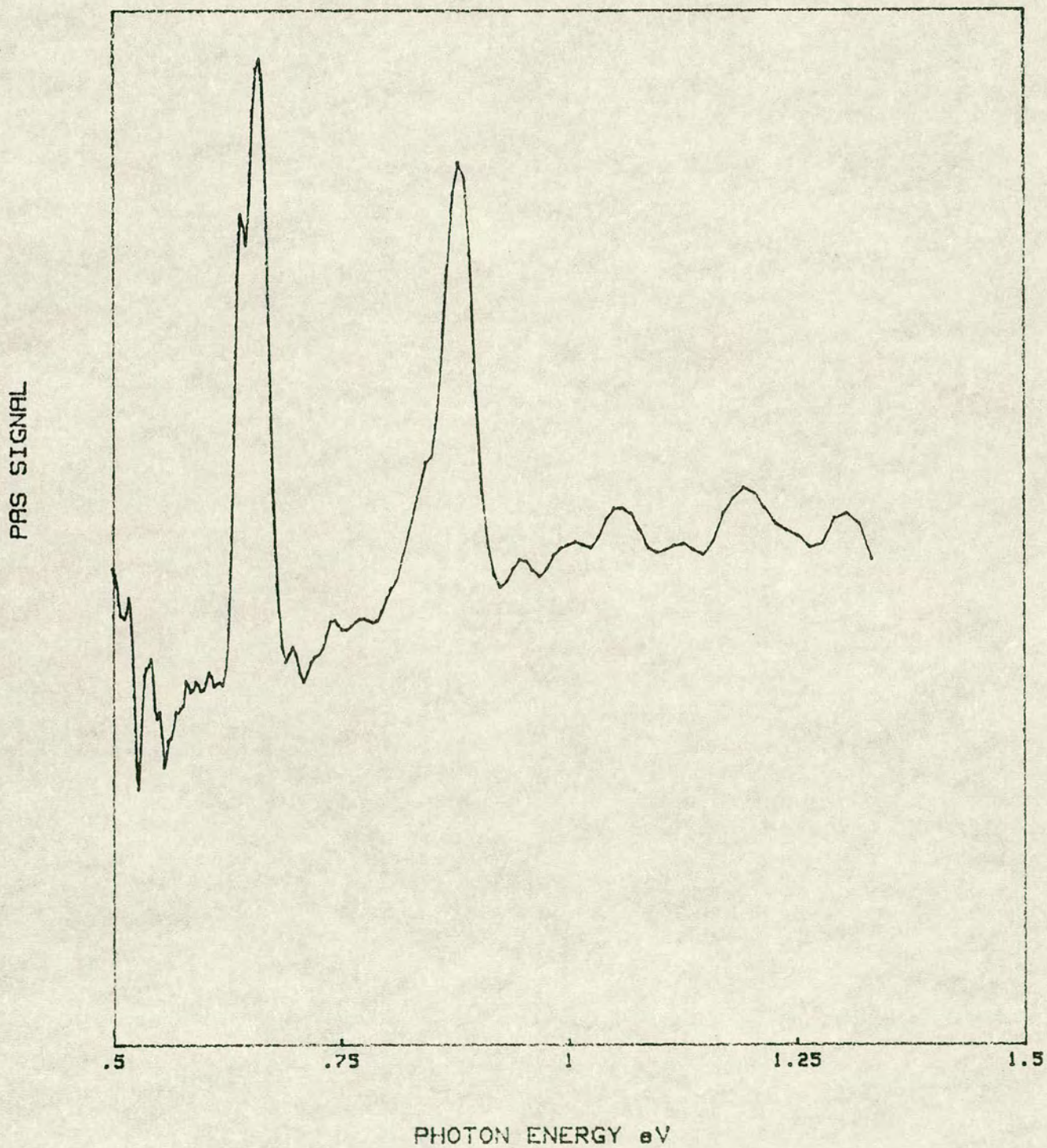

FIG. (6.61)

FIG. (6.62)

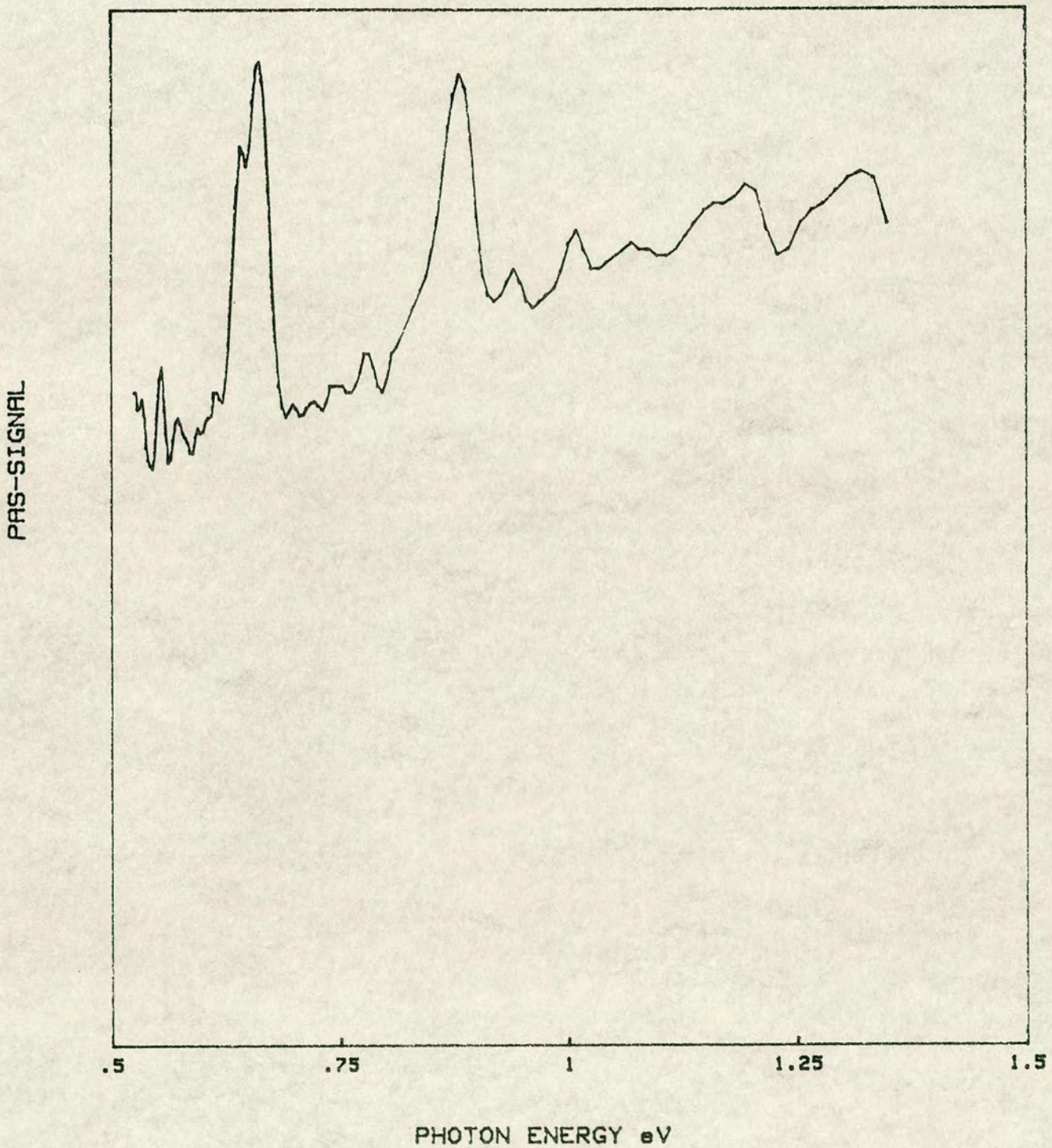

FIG. (6.63)

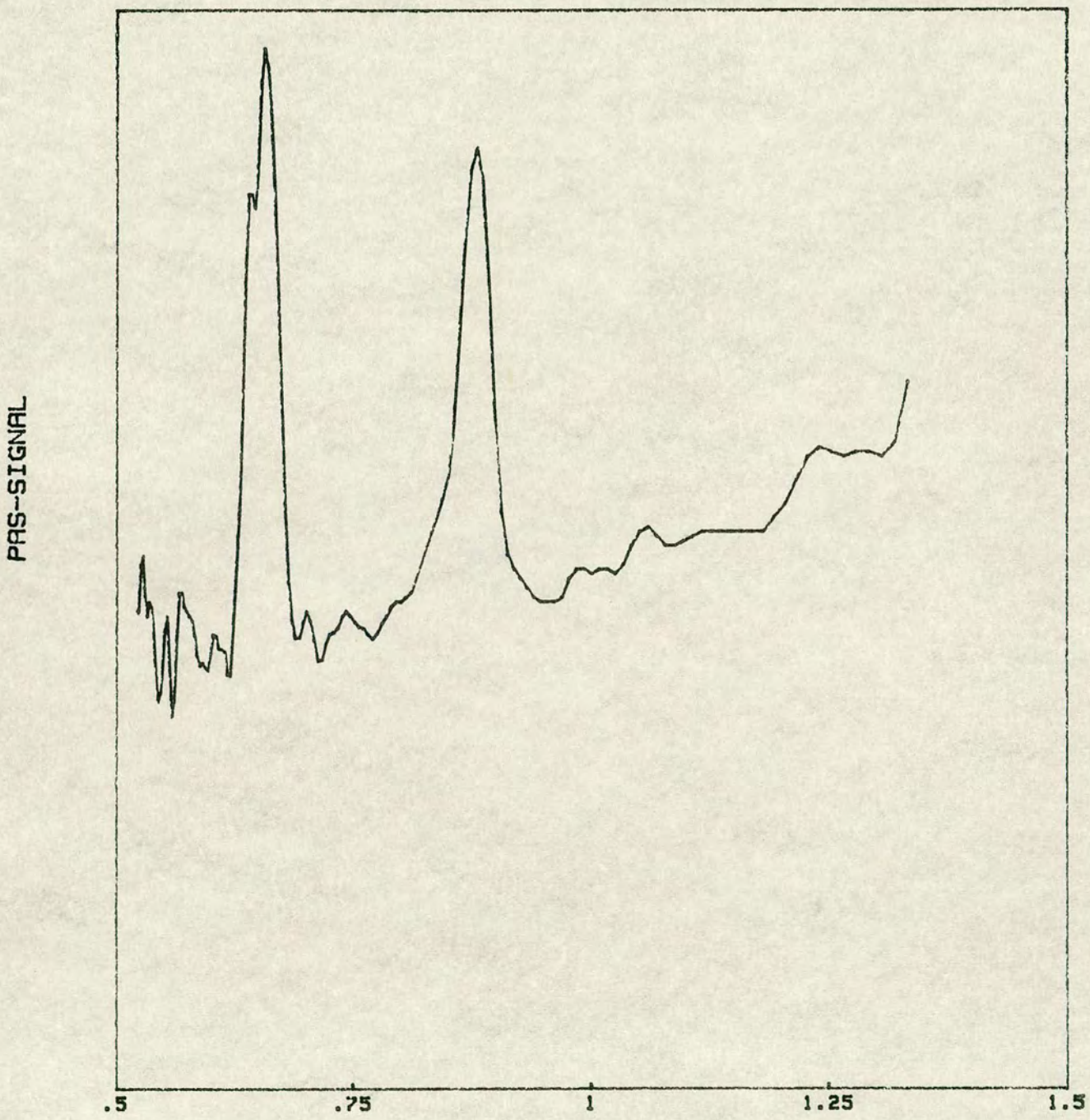

FIG. (6.64)

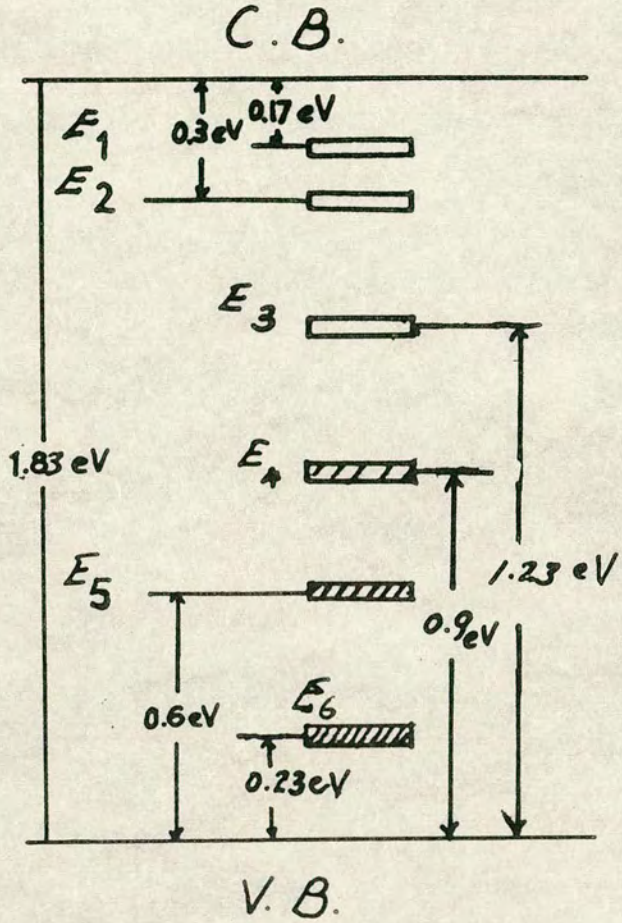

FIG. (6.65)

Band structure of crystalline As_2Se_3

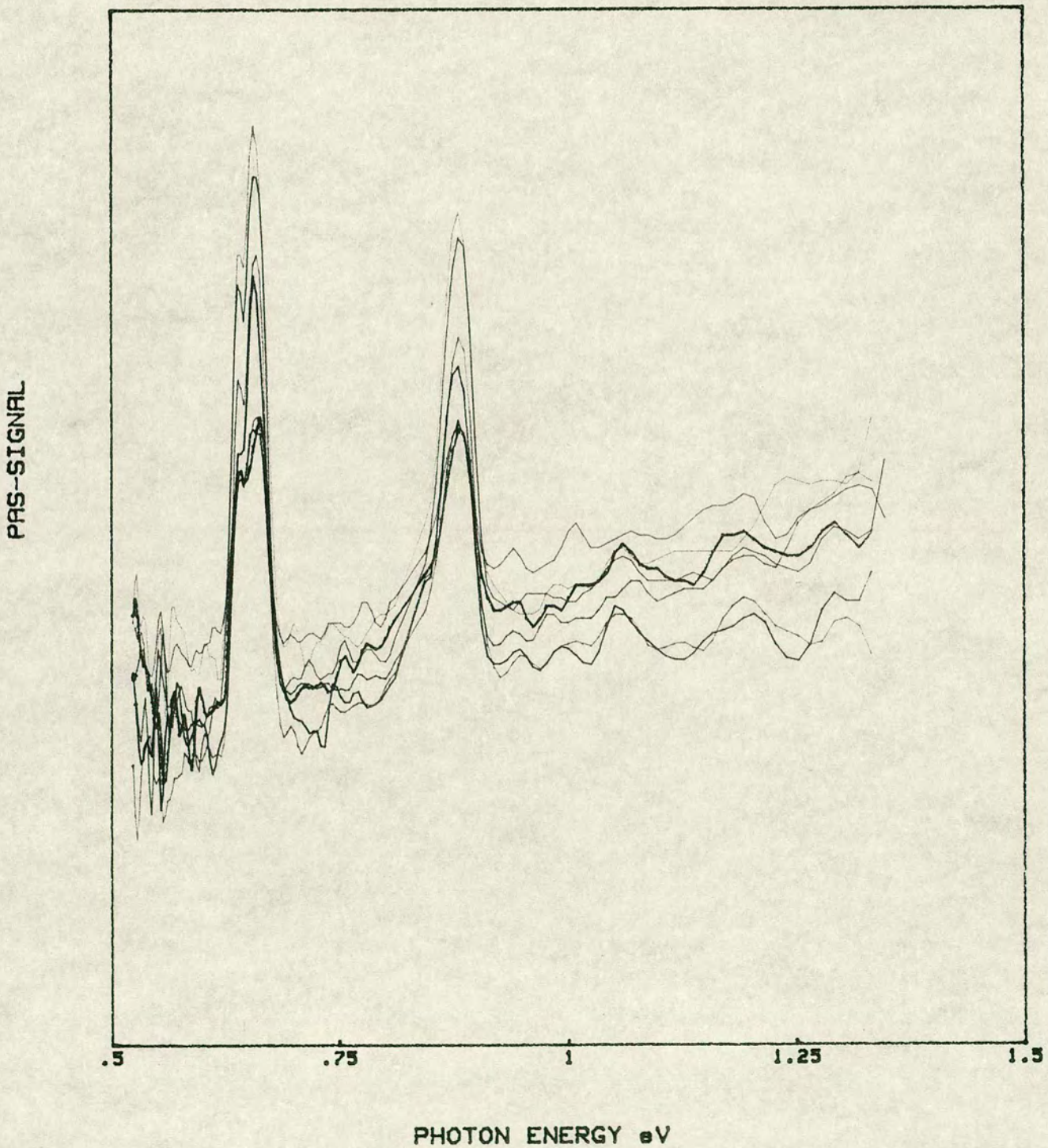

FIG. (6.66)

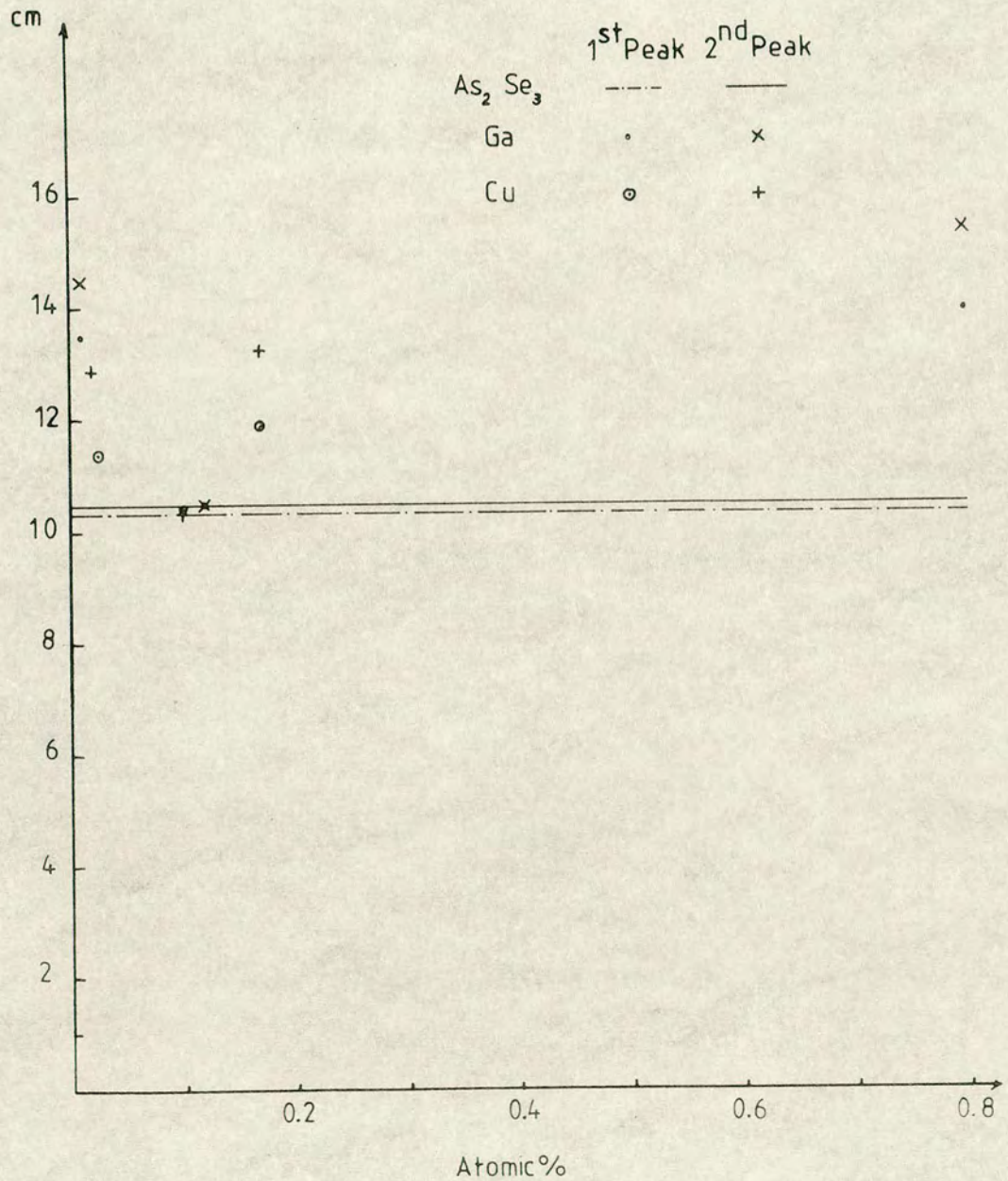

FIG. (6.67)

Plot of the PAS peaks height vs impurity concentration

DEFECT	ENERGY eV
P_2	1.6
P_1 (1)	1.6
C_3'''	1.55
C_2'	1.42
P_1 (2)	1.33
P_2'' (1)	0.9
P_3'	0.6
P_2'' (2)	0.32

C_3	1.36
C_2'	1.1
C_3'''	1.05
P_2' (1)	0.67
P_2' (2)	0.16
P_3'''	0.16

Table (7.1)

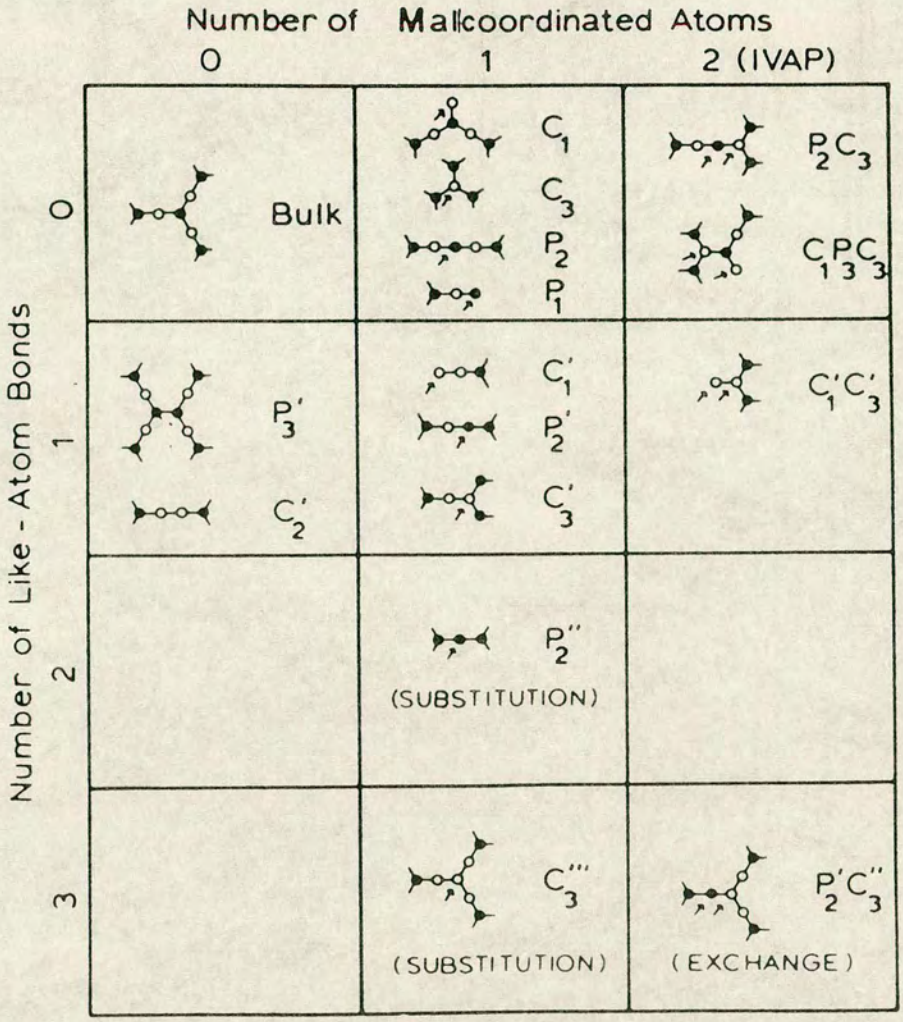

Defect topologies organized according to number of malcoordinated atoms (marked by arrows) and

FIG. [7.1]

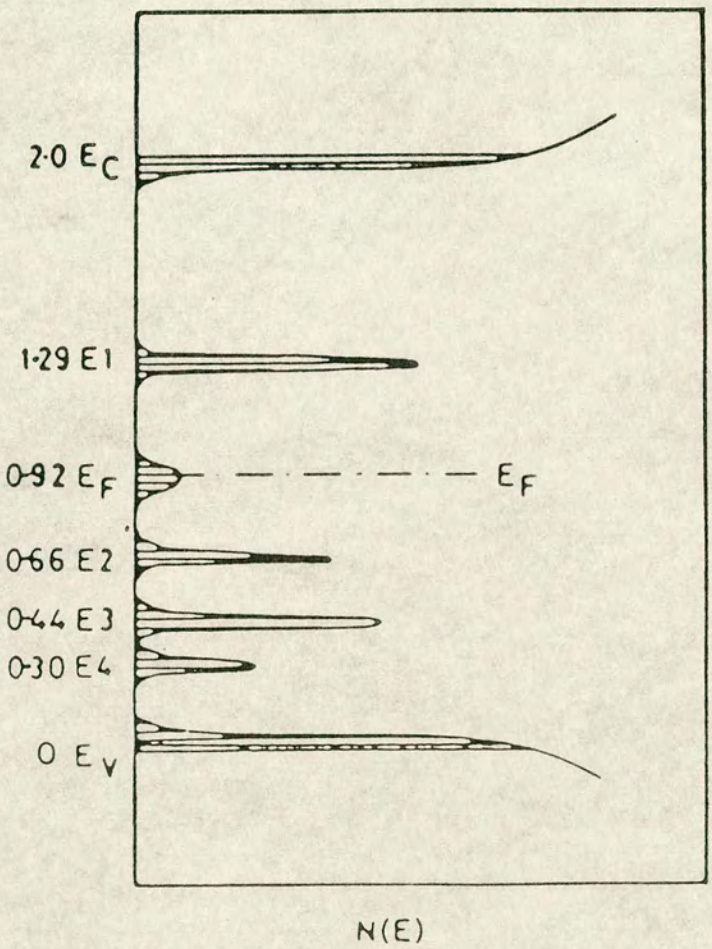

FIG. [7.2]

Band structure of amorphous As_2Se_3

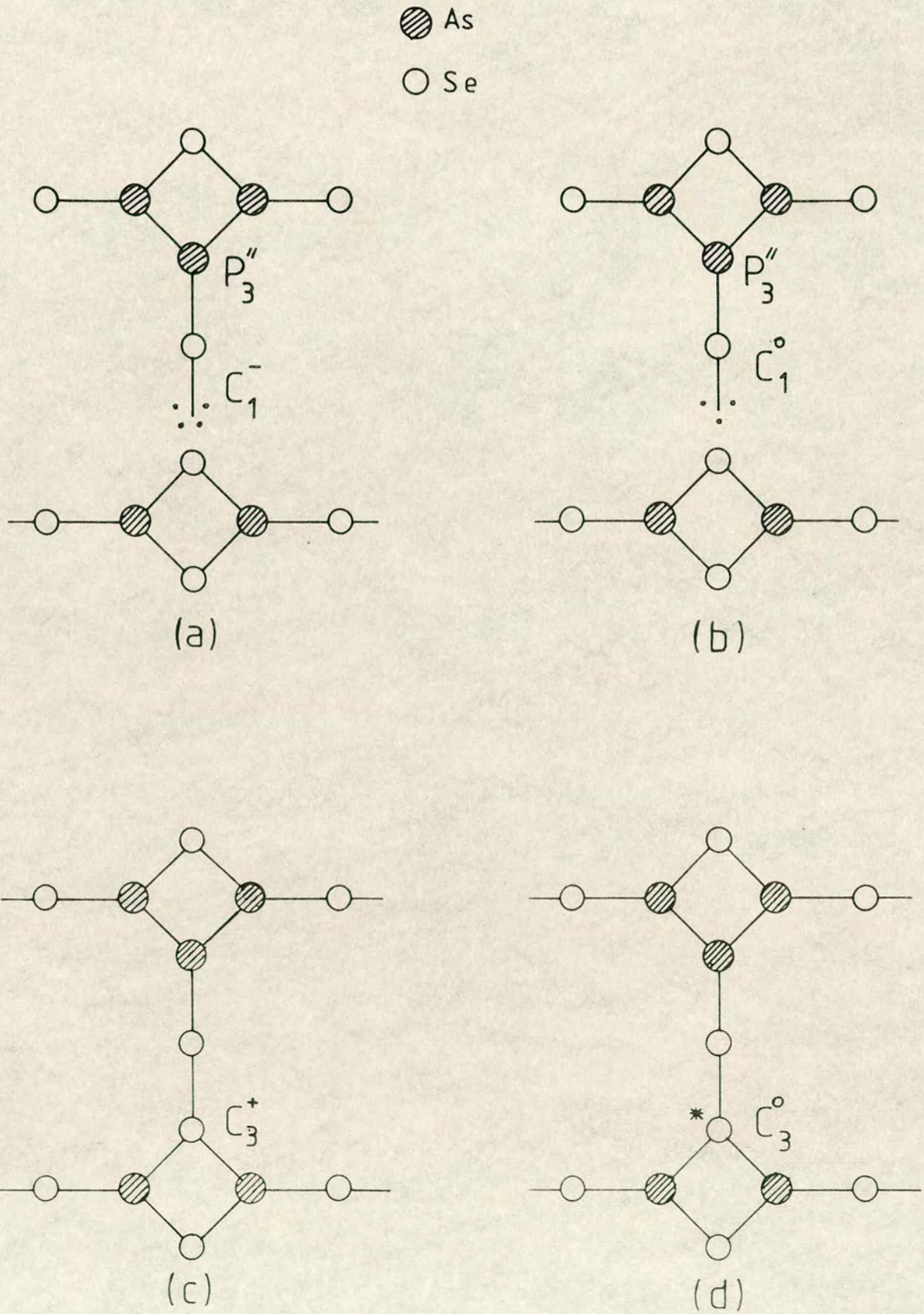

FIG. [7.3]

Illustration of the defects $P_3''C_1^-$ and $C_3'^+$